การจำลองพลศาสตร์ของไหลเชิงคำนวณของถังผสมแบบหัวฉีดปั๊มวน

COMPUTATIONAL FLUID DYNAMICS SIMULATIONS OF PUMP-AROUND JET MIXING TANKS

เอกราช บำรุงไทยชัยชาญ
EAKARACH BUMRUNGTHAICHAICHAN

วิทยานิพนธ์นี้สำหรับการศึกษาตามหลักสูตรปริญญาวิศวกรรมศาสตรดุษฎีบัณฑิต
สาขาวิชาวิศวกรรมเคมี
คณะวิศวกรรมศาสตร์
สถาบันเทคโนโลยีพระจอมเกล้าเจ้าคุณทหารลาดกระบัง
พ.ศ. 2562
KMITL-2019-EN-D-228-125

การจำลองพลศาสตร์ของไหลเชิงคำนวณของถังผสมแบบหัวฉีดปั๊มวน

COMPUTATIONAL FLUID DYNAMICS SIMULATIONS OF PUMP-AROUND JET MIXING TANKS

เอกราช บำรุงไทยชัยชาญ

EAKARACH BUMRUNGTHAICHAICHAN

วิทยานิพนธ์นี้สำหรับการศึกษาตามหลักสูตรปริญญาวิศวกรรมศาสตรดุษฎีบัณฑิต

สาขาวิชาวิศวกรรมเคมี

คณะวิศวกรรมศาสตร์

สถาบันเทคโนโลยีพระจอมเกล้าเจ้าคุณทหารลาดกระบัง

พ.ศ. 2562

KMITL-2019-EN-D-228-125

COMPUTATIONAL FLUID DYNAMICS SIMULATIONS OF PUMP-AROUND JET MIXING TANKS

EAKARACH BUMRUNGTHAICHAICHAN

A THESIS SUBMITTED IN FULFILLMENT
OF THE REQUIREMENT FOR THE DEGREE OF
DOCTOR OF ENGINEERING IN CHEMICAL ENGINEERING
FACULTY OF ENGINEERING
KING MONGKUT'S INSTITUTE OF TECHNOLOGY LADKRABANG
2019

KMITL-2019-EN-D-228-125

หัวข้อวิทยานิพนธ์ การจำลองพลศาสตร์ของไหลเชิงคำนวณของถังผสมแบบหัวฉีดปั๊มวน
นักศึกษา นายเอกราช บำรุงไทยชัยชาญ
รหัสประจำตัว 57601425
ปริญญา วิศวกรรมศาสตรดุษฎีบัณฑิต
สาขาวิชา วิศวกรรมเคมี
พ.ศ. 2562
อาจารย์ที่ปรึกษาวิทยานิพนธ์ ผศ.ดร.สันติ วัฒนานุสรณ์

บทคัดย่อ

วิทยานิพนธ์นี้ศึกษาการจำลองพลศาสตร์ของไหลเชิงคำนวณ (computational fluid dynamics; CFD (ซีเอฟดี)) ของถังผสมแบบหัวฉีดปั๊มวน แบบจำลองซีเอฟดีที่ครอบคลุมสำหรับถังผสมเปิดแบบหัวฉีดปั๊มวนที่ฉีดเข้าด้านข้างเอียง 45° (open 45° inclined side entry pump-around jet mixing tank) ถูกพัฒนาอย่างเหมาะสมด้วยความช่วยเหลือของดัชนีการลู่เข้าของกริด (grid convergence index; GCI (จีซีไอ)) กริดทรงหกหน้า (hexahedral grid) ที่จัดเรียงอย่างเหมาะสมถูกสร้างภายในถังผสม สมการนาเวียร์-สโตกส์เฉลี่ยเรย์โนลด์ แบบจำลองความปั่นป่วน realizable k-epsilon และสมการการถ่ายโอนองค์ประกอบ (species transport equations) ถูกใช้เพื่อจำลองสนามการไหล สนามความปั่นป่วน และสนามความเข้มข้นภายในถังผสมนี้ ตามลำดับ รูปแบบคู่ควบความดัน-ความเร็ว (pressure-velocity coupling scheme) รูปแบบการแยกเชิงพิกัด (spatial discretization scheme) และรูปแบบการแยกเชิงเวลา (temporal discretization scheme) คือ SIMPLE second order upwind และ first order implicit ตามลำดับ เวลาผสมสุทธิ (overall mixing time) ที่ถูกทำนายสำหรับความเร็วพ่นออกของเจ็ตที่แตกต่างกัน (2.2 - 11 เมตรต่อวินาที) ถูกสอบทวน (validate) ด้วยการเปรียบเทียบกับข้อมูลการทดลองก่อนหน้า ประเภทสภาวะขอบเขตที่แตกต่างกันถูกจำลองเพื่อให้ได้แบบจำลองซีเอฟดีที่เหมาะสมสำหรับการทำนายถังผสมแบบหัวฉีดปั๊มวน เนื่องจากการขาดสภาวะความปั่นป่วนแม่นตรง สภาวะขอบเขตของความปั่นป่วนขาเข้าจึงถูกจำลองเพื่อหาสาเหตุของความไม่สอดคล้องของโปรไฟล์ความเข้มข้นระหว่างแบบจำลองซีเอฟดีและข้อมูลการทดลอง นอกจากนี้ แบบจำลองซีเอฟดีปัจจุบันถูกนำมาเพื่อทำนายประสิทธิภาพการผสมของถังผสมแบบหัวฉีดที่ไม่เป็นวงกลม

ผลเฉลยลู่เข้าถูกทดสอบและยืนยันโดยการศึกษาความเป็นอิสระของกริด (grid independence study) และการวิเคราะห์จีซีไอ ตามลำดับ เวลาผสมที่ถูกทำนายมีความสอดคล้องเป็นอย่างดีกับการทดลอง โดยเฉพาะอย่างยิ่งความเร็วพ่นออกของเจ็ตเท่ากับ 4.4 - 11 เมตรต่อวินาที แต่อย่างไรก็ตาม ความไม่สอดคล้องระหว่างโปรไฟล์ความเข้มข้นที่ถูกทำนายและการทดลองยังคงถูกสังเกตได้ เพื่อศึกษาการผสมแบบบัลค์ (bulk mixing) ภายในถังผสมแบบหัวฉีด แบบจำลองซีเอฟดีปัจจุบันเป็นที่ยอมรับได้ จากการจำลองของสภาวะขอบเขตของความปั่นป่วนที่แตกต่างกัน ผลการทำนายชี้ว่าสาเหตุของความไม่สอดคล้องของโปรไฟล์ความเข้มข้นคือความไม่เหมาะสมของปริมาณ

การกระจายที่ปั่นป่วน (turbulent dispersion) ภายในถังผสมเนื่องจากความไม่เหมาะสมของสภาวะขอบเขตของความปั่นป่วนขาเข้า และการถ่ายโอนด้วยการพา (convective transport) ที่ถูกทำนายเกินจริงเนื่องจากสมมติฐานของผิวของของเหลวด้านบนแบบเรียบ

ในส่วนสุดท้าย ประสิทธิภาพการผสมของถังผสมแบบหัวฉีดวงรีและหัวฉีดจัตุรัสถูกจำลองและเปรียบเทียบกับผลที่ได้จากถังผสมแบบหัวฉีดวงกลมเพราะว่าเจ็ตที่ไม่เป็นวงกลมแบบอิสระ (free non-circular jet) แสดงการเหนี่ยวนำ (entrainment) ที่ดีกว่าเจ็ตวงกลม แต่อย่างไรก็ตาม ผลที่ถูกจำลองแสดงว่าเวลาผสมสุทธิที่ถูกทำนายโดยถังผสมแบบหัวฉีดวงกลมดีกว่าผลที่ถูกทำนายโดยถังผสมแบบหัวฉีดที่ไม่เป็นวงกลมเพราะว่าการหมุนของของไหล (rotation of fluid) สูงในบริเวณใกล้สนาม (near field region) ของเจ็ต และค่าสูงของพลังงานจลน์ของความปั่นป่วน (การผสมเนื่องจากความเร็วแกว่ง) ในบริเวณไกลสนาม (far field region) ของเจ็ต

Thesis	Computational Fluid Dynamics Simulations of Pump-Around Jet Mixing Tanks
Student	Mr. Eakarach Bumrungthaichaichan
Student ID.	57601425
Degree	Doctor of Engineering
Program	Chemical Engineering
Year	2019
Thesis Advisor	Asst. Prof. Dr. Santi Wattananusorn

ABSTRACT

This thesis studies the computational fluid dynamics (CFD) simulations of pump-around jet mixing tanks. The comprehensive CFD model for an open 45° inclined side entry pump-around jet mixing tank was properly developed with the help of grid convergence index (GCI). The hexahedral grids with appropriate arrangement were generated inside the jet mixing tank. The Reynolds-averaged Navier-Stokes equations, realizable k-epsilon turbulence model, and species transport equations were used to simulate flow, turbulence, and concentration fields inside this jet mixing tank, respectively. The pressure-velocity coupling, spatial discretization, and temporal discretization schemes respectively were SIMPLE, second order upwind, and first order implicit. The predicted overall mixing times for different jet discharge velocities (2.2 - 11 $m \cdot s^{-1}$) were validated by comparing with previous experimental data. The different boundary condition types were simulated to obtain a suitable CFD model for predicting pump-around jet mixing tank. Due to the absence of exact turbulence conditions, the inlet turbulence boundary conditions were also simulated to investigate the cause(s) of a discrepancy in concentration profiles between CFD model and experimental data. Further, the present CFD model was employed to predict the mixing performances of non-circular jet mixing tanks.

The converged solutions were tested and confirmed by grid independence study and GCI analysis, respectively. The predicted overall mixing times were in good agreement with experiment, especially for jet discharge velocities of 4.4 - 11 $m \cdot s^{-1}$. However, the discrepancy between predicted concentration profiles and experiments was still observed. In order to study bulk mixing inside jet mixing tank, the present CFD model was acceptable. From the simulations of different turbulence boundary conditions, the predicted results indicated that the reasons of discrepancy in

concentration profiles were the improper extent of turbulent dispersion inside the jet mixing tank due to the inappropriate inlet turbulence conditions and the overpredicted convective transport due to flat top liquid-surface assumption.

In last section, the mixing performance of elliptic and square jet mixing tanks were simulated and compared to that achieved by circular jet mixing tank because the free non-circular jets showed the better entrainment than circular jet. However, the simulated results revealed that the overall mixing time simulated by circular jet mixing tank was better than those predicted by non-circular jet mixing tanks because the high rotation of fluid in jet near field region and high value of turbulence kinetic energy (mixing due to velocity fluctuations) in far field region of jet.

Acknowledgements

During the course of this thesis, I have received the supports and assistance of many persons. I wish to acknowledge all of them.

First, I would like to express my deep gratitude to Assistant Professor Dr. Santi Wattananusorn, my thesis advisor, my teacher, my hero, and my elder brother, for his kind support, special discussion, and useful suggestions of the present research. I learned to understand various difficult topics in fluid mechanics and transport phenomena from him. I really appreciate him for giving me many great opportunities. I would also like to express my appreciation to my shared advisor Professor emeritus Dr ès sc. techn. Horst Stoff, Department of Mechanical Engineering, Ruhr-Universität Bochum, Germany, for his constructive suggestions and valuable knowledge of fluid mechanics.

I would like to offer my special thanks to Assistant Professor Dr. Apinan Namkanisorn and Assistant Professor Dr. Walairat Chandra-ambhorn for their help in English grammar checking, useful suggestions, and supports. Further, I would like to express my thanks to Associate Professor Dr. Prakob Kitchaiya and Associate Professor Dr. Benjapon Chalermsinsuwan for their supports, comments, and participation as my thesis committee.

I am very grateful to Associate Professor Dr. Anchaleeporn Waritswat Lothongkum for her helpful guidance and suggestions.

I am very thankful to Mr. Niwat Phoocharoen, my first CFD teacher, for his technical suggestions in computational fluid dynamics software.

I would like to thank my undergraduate teachers and support staffs at the Department of Chemical Engineering, Faculty of Engineering, King Mongkut's Institute of Technology Ladkrabang for their help, instruction, and valuable knowledge. Further, I would also like to thank King Mongkut's Institute of Technology Ladkrabang for place to perform the simulations.

I am particularly grateful for a research article given by Dr. Richard Grenville, Director of Mixing Technology at Philadelphia Mixing Solutions.

Special thanks to Mr. Nattawat Jaiklom for his important CFD information of jet mixing tank simulation.

Many thanks to all the members of computational fluid dynamics laboratory, Department of Chemical Engineering, Faculty of Engineering, King Mongkut's Institute of Technology Ladkrabang for their help, supports, and warm collaborations.

I wish to thank Mr. Ponkanut Chaloeyprach, my best friend, and his family for their help, supports, and good relationship.

Plenty of thanks to Miss Suthipa Pauekpong for her understanding and support in every situations.

Last but not least, I would like to express my special thank to my parents and my family for their love, supports, advice, and encouragement throughout my life. Moreover, I would like to dedicate this research to my late grandfather, who unfortunately did not stay in this world long enough to see his grandson become a doctor of engineering.

Eakarach Bumrungthaichaichan

Contents

page

Contents (continued)

page

Contents (continued)

Contents (continued)

Page

Contents (continued)

Page

List of Tables

List of Tables (continued)

List of Figures

List of Figures (continued)

Figure Page

List of Figures (continued)

Figure Page

Nomenclature

Alphabetical symbols

a	Coefficient of discretized equation
a_s	Swirl constant
a_u	Decay constant
$\mathbf{A}$	Surface area vector
b	Mass imbalance
c	Concentration
$\bar{c}$	Fully mixed concentration
C_μ	Empirical constant specified in the turbulence model
C_1, C_2, $C_{1\varepsilon}$, $C_{2\varepsilon}$, $C_{3\varepsilon}$	Constants for k-epsilon turbulence models
C_D	Constant for turbulence kinetic energy dissipation rate correlation
C_v	Constant for differential equation of eddy viscosity of RNGKE
d_j	Jet nozzle diameter
d_o	Tank outlet diameter
D	Tank diameter
D_e	Circular-equivalent diameter
D_h	Hydraulic diameter
$D_{i,m}$	Mass diffusion coefficient for species *i* in the mixture
D_t	Turbulent diffusivity
e	Relative error of numerical solutions
E	Total Energy
f	Numerical solution of key variable
f_{exact}	Exact value of key parameter
F_s	Safety factor

Nomenclature (continued)

G_b	Generation of turbulence kinetic energy due to buoyancy
G_k	Production of turbulence kinetic energy
h	Grid size
h_O	Outlet pipe height
H	Height of liquid
$\mathbf{i}$	Unit vector in x-direction
I	Turbulence intensity
$\mathbf{j}$	Unit vector in y-direction
k	Thermal conductivity or Turbulence kinetic energy
$\mathbf{k}$	Unit vector in z-direction
k_u	Constant for the Gaussian shape
l	Length scale
L_c	Characteristic length
N	Total number of computational cells
N_i	Number of grids for *i* grid level
p	Pressure or order of the discretization method
$\overline{p}$	Mean pressure
Pe	Peclet number
Q	Jet entrainment or rate of jet discharge
Q_0	Jet efflux rate
r	Radial distance or refinement factor
$r_{1/e}$, $r_{0.5}$	Jet half width
R	Convergence ratio
R^{ϕ}	Overall scaled residual

Nomenclature (continued)

Re	Reynolds number
Re_{crit}	Critical Reynolds number
Re_{D_h}	Hydraulic diameter based Reynolds number
Re_j	Jet Reynolds number
R_ε	Additional term due to interaction between turbulence dissipation and mean shear in ε-transport equation of RNGKE
s	Jet longitudinal distance or Jet streamwise distance
S	Modulus of the mean rate-of-strain tensor
S_E	Source term for energy equation
S_k	Source term for k-transport equation
$S_{M,i}$	Source term for momentum equation in i direction
S_ε	Source term for ε-transport equation
S_ϕ	Source term
Sc_t	Turbulent Schmidt number
t	Time
t_m	Mixing time
$t_{95\%}$	95% mixing time
$t_{99\%}$	99% mixing time
T	Temperature or Initial bulk liquid temperature
$\overline{T}$	Final mean temperature
u	Velocity in x-direction
$\overline{u}$	Mean velocity in x-direction or mean axial velocity
$\overline{u}_c$	Mean centerline axial velocity
u'	Fluctuation velocity in x-direction

Nomenclature (continued)

$\mathbf{U}$	Velocity vector
$\overline{\mathbf{U}}$	Mean velocity vector
U_b	Bulk mean velocity
U_j	Jet discharge velocity
U_{ref}	Reference velocity
v	Velocity in y-direction
$\overline{v}$	Mean velocity in y-direction
v'	Fluctuation velocity in y-direction
v_{avg}	Average velocity
V	Mixing tank volume
w	Velocity in z-direction
$\overline{w}$	Mean velocity in z-direction
w'	Fluctuation velocity in z-direction
x	Longitudinal distance of jet
x_0	Virtual original of the velocity
Y_i	Local mass fraction of species *i*
Y_M	Dilatation dissipation
ΔA_n	Area of the *n*-th cell
Δt	Time step size
ΔV_n	Volume of the *n*-th cell

Nomenclature (continued)

Greek symbols

α_k	Inverse effective Prandtl number for turbulence kinetic energy
α_ε	Inverse effective Prandtl number for turbulence kinetic energy dissipation rate
Γ_ϕ	Diffusivity
δ_{ij}	Krinecker delta
ε	Turbulence kinetic energy dissipation rate or difference in numerical solutions
θ	Nozzle angle
μ	Dynamic viscosity
μ_{eff}	Effective viscosity
μ_t	Turbulent viscosity or eddy viscosity
μ_{t0}	Eddy viscosity calculated without swirl modification
$\hat{v}$	The ratio of effective viscosity to dynamic viscosity
ν_t	Turbulent kinematic viscosity
ρ	Fluid density or previous iteration of p
σ_k	Turbulent Prandtl numbers for turbulence kinetic energy
σ_ε	Turbulent Prandtl numbers for turbulence kinetic energy dissipation rate
τ	Shear stress
ϕ	Universal independent variable
ϕ_f	Face value of scalar variable
$\overline{\phi}_f$	Arithmetic average of ϕ
φ	Instantaneous flow property

Nomenclature (continued)

$\overline{\varphi}$	Time average of flow property
φ'	Fluctuating property
φ_{rms}	Root mean square of fluctuations
ω	Relaxation factor
Ω	Characteristic swirl number

Abbreviations

AD	Axisymmetric type decay region
CD	Central difference or characteristic decay region
CJ	Circular jet
CS	Coherent structures
CFD	Computational fluid dynamics
DNS	Direct numerical simulation
EJ	Elliptic jet
FDM	Finite difference method
FEM	Finite element method
FOI	First order implicit
FOU	First order upwind
FVM	Finite volume method
GCI	Grid convergence index
LES	Large eddy simulation
PC	Potential core region
PDEs	Partial differential equations
PISO	Pressure-Implicit with Splitting of Operators

Nomenclature (continued)

PL	Power law
QUICK	Quadratic upwind interpolation for convective kinetics
rms	Root mean square
RANS	Reynolds-averaged Navier-Stokes equations
RKE	Realizable k-epsilon model
RNGKE	Renormalization group k-epsilon model
RSM	Reynolds stress model
RTD	Residence time distribution
SIMPLE	Semi-Implicit Method for Pressure-Linked Equations
SJ	Square jet
SKE	Standard k-epsilon model
SOI	Second order implicit
SOU	Second order upwind
TDR	Turbulence kinetic energy dissipation rate
TKE	Turbulence kinetic energy
UDF	User defined function
URF	Under relaxation factor
ZEF	Zone of established flow
ZFE	Zone of flow establishment

CHAPTER I

INTRODUCTION

1.1 Background and motivation

Jet mixing tank is one of the important mixing devices in chemical processes. This device uses the high velocity jet produced by the pump to create the liquid recirculation inside the vessel. Then, the different components in the tank are mixed. The jet mixer was originally used to mix the tetraethyl-lead fluid inside the large petroleum storage tank [1]. Further, this device is employed in various mixing applications because of its advantages. The advantages of the jet mixing tank are simple design (no additional structure support), low operating cost, no moving parts, and easy installation and maintenance.

Since 1940s, many researchers have been experimentally studied the jet mixing tanks. Most of the previous experimental works represented the overall mixing time correlations. Although there are many mixing time correlations but the universal mixing time correlation is still unavailable [2]. That is, these correlations can be only adopted to estimate the overall mixing time for the given parameters, i.e. the mixing time correlations are case specific. Furthermore, the details of fluid flow and mixing patterns inside this mixing device are not available. Hence, the computational fluid dynamics (CFD) technique is employed to resolve the limitations of experimental researches.

CFD is a method, which uses numerical methods and algorithms to solve the partial differential equations of fluid flow phenomena. This technique has been originally used in aerospace industry since 1960s [3]. Nowadays, CFD becomes an important engineering tool because it provides clear insight into various fluid flow phenomena and generates the large volume of results with low operating cost and time. Further, CFD is able to study the large systems or the systems under hazardous conditions. For jet mixing tanks, many previous works used the CFD to study the effects of tank configurations and operating conditions on jet mixing behavior. Although there are many previous works related to numerical investigation of jet mixing tanks, however, the comprehensive modeling of jet mixing tank was not presented and used [2]. Further, the discretization errors of the previous CFD models

were not reported. Hence, the development of comprehensive CFD model for jet mixing tank and other parametric studies, e.g. non-circular jet nozzle geometries, are still the challenging topics worthwhile for further study.

1.2 Objectives of the research

There are three main objectives of this research. The first is to develop the comprehensive CFD model for predicting the mixing performance (overall mixing time) inside an open 45° inclined side entry pump-around jet mixing tank. The second is to address the discrepancy in concentration profiles between CFD simulation and experiment and/or to represent the cause(s) of this shortfall. The last objective is to predict the mixing performances of non-circular pump-around jet mixing tanks by using the present CFD model.

1.3 Scope of the research

- The solid model and hexahedral grids are created by GAMBIT 2.4.6 with the help of domain decomposition technique.

- The flow and turbulence fields inside the jet mixing tank are calculated by steady state Reynolds-averaged Navier-Stokes equations of ANSYS FLUENT 14.5 together with k-epsilon turbulence model. The concentration distribution is computed by unsteady state species transport equations.

- The converged solutions are obtained by conventional grid independence study and grid convergence index method. In addition, the predicted overall mixing times and concentration profiles are validated by comparing with previous literature.

- The effects of boundary condition types and inlet turbulence boundary conditions on mixing behavior are investigated to achieve the comprehensive CFD model for pump-around jet mixing tank and to describe the discrepancy in concentration profiles between CFD simulation and experiment.

- The mixing and flow phenomena of circular and non-circular pump-around jet mixing tanks having the same flow area, mass flow rate, and Reynolds number are investigated and compared.

1.4 Benefits of the research

The present CFD research is proposed to show the CFD modeling guideline for jet mixing tank and to explain the discrepancy in concentration profiles between CFD model and experimental data. Further, the understanding of circular and non-circular jet mixing tanks may be useful for the jet nozzle configuration selections in different flow situations.

1.5 Outline of the thesis

This thesis is distinguished into eight chapters. Chapter I represents the introduction of the present thesis as mentioned previously. Chapter II shows the fundamentals of computational fluid dynamics, turbulence and its modeling, and general CFD procedure. Chapter III introduces the phenomena of jets and jet mixing tanks. Further, the previous experimental and CFD researches of jet mixing tanks are summarized and reported. Chapter IV shows the descriptions of the present CFD model for an open 45° inclined side entry pump-around jet mixing tank. In addition, the reliability of the present CFD model is also represented. Chapter V presents the grid independence study and grid convergence index analysis of the present CFD model. Moreover, the model validation is also reported. Chapter VI illustrates the effects of boundary condition types and turbulence boundary conditions on CFD simulation of pump-around jet mixing tank. The reasons of the discrepancy in concentration profiles between CFD model and experiment are also given. Chapter VII shows the comparison of mixing performance and flow phenomena between circular and non-circular jet mixing tanks. Chapter VIII summarizes the conclusions of this research and recommendation for the future work.

CHAPTER II

COMPUTATIONAL FLUID DYNAMICS

Chapter II represents the fundamentals of computational fluid dynamics (CFD), including introduction to computational fluid dynamics, CFD processes, viscous fluid flow governing equations and history, turbulence and its modeling, solver theory, solution methods, and CFD study.

2.1 Introduction to computational fluid dynamics

Computational fluid dynamics (CFD) is a scientific tool, which combines fluid mechanics, numerical method, and computer science to investigate various fluid flow phenomena. Meaning that, CFD is a tool that uses to solve the partial differential equations of fluid flow with the help of numerical methods and algorithms. The numerical method is used to solve fluid flow problems because of the difficulty in solving the non-linearity of fluid flow equations, e.g. turbulence, chemical reaction, etc. The early version of numerical prediction role was published by Richardson in 1911 [4]. This numerical method was applied to the irregular body problems. The solutions were achieved by hand calculations with human computers (2,000 operations per week) [5]. Later, the numerical solutions can be done by using computer alone due to the development in computer performance. The earliest computer simulation for fluid flow was proposed by Fromm and Harlow in 1963 [6]. The numerical study performed by computer is called “computer experiment” [7]. Over 50 years, the CFD techniques were developed to achieve the accurate and reliable results for various flow problems. Nowadays, CFD becomes a famous scientific and engineering tools because it produces a huge volume of results with inexpensive operating cost. And it clearly represents the deep insight into various fluid flow phenomena. Moreover, CFD can also be applied to study and analyze the heat transfer and chemical reaction problems. CFD has been adopted in a wide range of industrial and non-industrial application areas. Some examples are:

- Aeronautical engineering: lift and drag predictions for aircraft

- Biomedical engineering: air flow through human airways

- Environmental engineering: prediction of pollutant distribution

- Chemical engineering: fluid flow prediction in chemical equipment

- Civil engineering: fluid flow pass a building

- Mechanical engineering: prediction of heat transfer inside heat exchanger

2.2 How does CFD work?

Generally, CFD process contains three main steps, including pre-processing, solver, and post-processing [3]. The details of three different steps can be described as the following:

2.2.1 Pre-processing

This stage consists of the input of fluid flow problem to a CFD program, such as computational domain specification, grid generation, physical and chemical phenomena selection, definition of material properties, specification of boundary conditions, etc.

2.2.2 Solver

For conventional CFD code, there are three common numerical solution techniques, including finite difference method (FDM), finite element method (FEM), and finite volume method (FVM). Generally, the solver performs the following processes:

- Approximation of unknown variables by using simple functions.

- Discretization of the governing equations by substituting the approximations into the partial differential equations (PDEs) to achieve the algebraic equations.

- Solving the algebraic equations to obtain the numerical solutions.

The differences between these three different numerical techniques are the approximation of flow variables and the discretization process. The details of these numerical techniques are mentioned as the follows:

2.2.2.1 Finite difference method (FDM)

FDM is the oldest numerical technique. It describes the unknown variables (ϕ) by means of node points of grid lines. The derivatives of ϕ are usually

approximated by using Taylor series expansions. Those approximated derivatives are replaced in the governing equations to get the algebraic equations at each grid points. The first successful case of FDM is the numerical solutions of low speed flow pass a cylinder reported by Thom [8].

2.2.2.2 Finite element method (FEM)

FEM is one of the famous numerical techniques. It is originally developed for structural mechanics. Later, in middle to late 1970s, it is also used to solving fluid flow problems. FEM use simple piecewise functions to explain the local variations of unknown ϕ. The exact solution ϕ satisfies the governing equation. If the piecewise approximation functions of ϕ are replaced into the equation it will not satisfy the governing equation and the residual is adopted to identify the errors. To reduce the errors, the residuals are multiple by a set of weighting function and integrating. Finally, a set of algebraic equations is obtained. In the past, the Galerkin finite element method (GFEM) was successfully applied to solve the self adjoint PDEs problems, e.g. solid mechanics, heat transfer, etc. However, GFEM failed to predict the fluid flow problems, which are non-self adjoint PDEs (Navier-Stokes equations). So, the FEM should be modified and developed to solve fluid flow phenomena, e.g. least-squares finite element method (LSFEM) [9], Discontinuous GFEM [10].

2.2.2.3 Finite volume method (FVM)

FVM was developed as a special formula of FDM. A set of algebraic equations for fluid flow problem is obtained by integrating the governing equations over all finite control volumes and replacing the finite difference approximations for the terms in the integrated governing equations. The first well known FVM work was published by Evans and Harlow [11]. Nowadays, FVM becomes a favorite numerical solution technique for fluid flow problems because of its advantages, such as low memory usage, low computational time, the physical quantities conserve even on the large grid size, etc.

2.2.3 Post-processing

Post-processing is a process for representing the numerical solutions. The numerical results can be shown in a different aspects, such as computational geometry and grid displays, graph, contour plots, vector plots, 2D and 3D surface plot, video clips, etc.

2.3 Governing equations of viscous fluid flow

Over two century or so, many researchers attempted to develop the governing equations for fluid flow. The first well known equation for fluid flow is Bernoulli's equation, which was introduced by Bernoulli in his treatise "Hydrodynamica, sive De viribus et motibus fluidorum commentarii" in 1738 [12]. This equation is formed by considering the conservation of energy. However, there are four assumptions, including steady state, incompressible fluid, frictionless, and no influence of work. Later, in 1755, Euler represented the differential equation for fluid flow (published in 1757), which is commonly known as Euler's equation [13]. In Euler's equation, the effect of viscosity is also negligible.

The effect of fluid viscosity was originally taken into fluid flow equations as reported by Navier in 1822 [14]. Further, in 1845, Stokes also showed the viscous fluid flow equations [15]. According to these contributions, the governing equations for viscous fluid flow, which is called "Navier-Stokes equations", are achieved. Generally, the equations for fluid flow are governed by three fundamental physical laws, including the mass conservation law, the second Newton's law of motion, and the first law of thermodynamics.

2.3.1 Continuity equation

The mass conservation law states that mass may be neither created nor destroyed. The continuity equation or mass conservation equation for unsteady state compressible fluid flow for Cartesian coordinates is given by

$$\frac{\partial \rho}{\partial t}+\frac{\partial}{\partial x}(\rho u)+\frac{\partial}{\partial y}(\rho v)+\frac{\partial}{\partial z}(\rho w)=0 \tag{2.1}$$

or

$$\frac{\partial \rho}{\partial t}+\nabla\cdot(\rho \mathbf{U})=\mathbf{0} \tag{2.2}$$

where ρ is fluid density. t is time. u, v, and w are velocity components in x, y, and z axes, respectively. $\mathbf{U}$ is the velocity vector ($\mathbf{U} = u\mathbf{i} + v\mathbf{j} + w\mathbf{k}$). Further, $\mathbf{i}$, $\mathbf{j}$, and $\mathbf{k}$ are the unit vectors along x, y, and z axes, respectively.

2.3.2 Momentum equations

The Newton's second law of motion states that the time rate of change of momentum for a system is equal to the net force acting on the system and takes place in the direction of the net force. The momentum equations for Cartesian coordinates can be written as:

x-component:

$$\rho\frac{Du}{Dt}=\frac{\partial}{\partial t}(\rho u)+\nabla\cdot(\rho u\mathbf{U})=-\frac{\partial p}{\partial x}+\frac{\partial\tau_{xx}}{\partial x}+\frac{\partial\tau_{yx}}{\partial y}+\frac{\partial\tau_{zx}}{\partial z}+S_{Mx} \tag{2.3}$$

y-component:

$$\rho\frac{Dv}{Dt}=\frac{\partial}{\partial t}(\rho v)+\nabla\cdot(\rho v\mathbf{U})=-\frac{\partial p}{\partial y}+\frac{\partial\tau_{xy}}{\partial x}+\frac{\partial\tau_{yy}}{\partial y}+\frac{\partial\tau_{zy}}{\partial z}+S_{My} \tag{2.4}$$

z-component:

$$\rho\frac{Dw}{Dt}=\frac{\partial}{\partial t}(\rho w)+\nabla\cdot(\rho w\mathbf{U})=-\frac{\partial p}{\partial z}+\frac{\partial\tau_{xz}}{\partial x}+\frac{\partial\tau_{yz}}{\partial y}+\frac{\partial\tau_{zz}}{\partial z}+S_{Mz} \tag{2.5}$$

where p is pressure. τ is shear stress. S_{Mx}, S_{My}, and S_{Mz} are momentum source terms for x, y, and z components, respectively.

2.3.3 Energy equation

The first law of thermodynamics states that if a system is carried through a cycle, the total heat added to a system from its surroundings is proportional to the work done by system on its surroundings. The energy equation in term of total energy (E) for Cartesian coordinates is given by

$$\begin{aligned}\rho\frac{DE}{Dt}=&-\frac{\partial(up)}{\partial x}-\frac{\partial(vp)}{\partial y}-\frac{\partial(wp)}{\partial z}+\frac{\partial}{\partial x}\left(k\frac{\partial T}{\partial x}\right)+\frac{\partial}{\partial y}\left(k\frac{\partial T}{\partial y}\right)+\frac{\partial}{\partial z}\left(k\frac{\partial T}{\partial z}\right)\\&+\frac{\partial(u\tau_{xx})}{\partial x}+\frac{\partial(u\tau_{yx})}{\partial y}+\frac{\partial(u\tau_{zx})}{\partial z}+\frac{\partial(v\tau_{xy})}{\partial x}+\frac{\partial(v\tau_{yy})}{\partial y}+\frac{\partial(v\tau_{zy})}{\partial z}\\&+\frac{\partial(w\tau_{xz})}{\partial x}+\frac{\partial(w\tau_{yz})}{\partial y}+\frac{\partial(w\tau_{zz})}{\partial z}+S_E\end{aligned} \tag{2.6}$$

where k is thermal conductivity. S_E is energy source term. Equations (2.1) - (2.6) are called "Navier-Stokes equations for compressible fluid".

2.4 Turbulence and its modeling

There are three general flow regions, including laminar, transition, and turbulent regions. The flow region is generally identified by considering the ratio between inertia force to viscous force. The idea of this ratio was originally proposed by Stokes in 1851 [16]. However, Sommerfeld named the dimensionless ratio as Reynolds number [17] because it was frequently used by Reynolds [18]. So, the Reynolds number (Re) is commonly defined as a ratio of inertia force ($\rho v_{avg}^2 L_c^2$) to viscous force ($\mu v_{avg} L_c$), where v_{avg} is average velocity, μ is dynamic viscosity, and L_c is characteristic length. In fluid flow experiments, the fluid flow with Reynolds number below the critical Reynolds number (Re_{crit}) is called "laminar flow". For laminar flow, the flow is smooth and fluid layers slide past each other in an orderly pattern.

For turbulent flow, the Reynolds number of fluid system is higher than the critical value. The turbulent flow is a flow characterized by chaotic property changes. It also includes rapid variations of flow properties in space and time (unsteady state), rapid mixing due to diffusivity, three-dimensional flow, rotational flow structures (turbulent eddies, including small and large eddies), and high Reynolds number (not for all flow situations). Generally, for turbulent flow, the kinetic energy is converted into heat due to viscous shear stresses. This process is called "dissipative". Another important characteristic of turbulent flow is irregularity (randomness), which makes the deterministic approach to turbulence problems impossible. Then, the statistical approach is usually used to describe the turbulence in fluid.

There are three common routes to solve turbulent flow problems. First, direct numerical simulation (DNS) directly resolves all turbulent eddy scales. However, it requires a powerful computing facility due to small grid size, e.g. supercomputer. So, to reduce this requirement, the large turbulent eddies are only resolved while the small eddies are modeled. The second method is called "large eddy simulation (LES)". In engineering applications, the effects of fluctuations on mean flow are only considered, meaning that the details of turbulent fluctuations are not resolved. The last method is called "Reynolds-averaged Navier-Stokes equations (RANS)" or "Time-averaged Navier-Stokes equations" [19].

2.4.1 Reynolds equations

As mentioned earlier, the statistical approach is adopted to solve the turbulent flow problems due to the random characteristic of turbulent flow. The

instantaneous flow property (φ) is decomposed into time average of flow property ($\overline{\varphi}$) and fluctuating property (φ') as depicted in Equation (2.7).

$$\varphi(t) = \overline{\varphi} + \varphi'(t) \tag{2.7}$$

This process is known as Reynolds decomposition. The time average of flow property and its fluctuation can be defined as shown in Equations (2.8) and (2.9), respectively.

$$\overline{\varphi} = \frac{1}{\Delta t}\int_{0}^{\Delta t} \varphi(t)dt \tag{2.8}$$

$$\overline{\varphi'} = \frac{1}{\Delta t}\int_{0}^{\Delta t} \varphi'(t)dt \approx 0 \tag{2.9}$$

The root mean square (rms) of the fluctuations is given by

$$\varphi_{rms} = \sqrt{\overline{(\varphi')^2}} = \left[\frac{1}{\Delta t}\int_{0}^{\Delta t} (\varphi')^2\, dt\right]^{1/2} \tag{2.10}$$

Further, the turbulence kinetic energy per unit mass (k) can be defined as:

$$k = \frac{1}{2}\left(\overline{u'^2} + \overline{v'^2} + \overline{w'^2}\right) \tag{2.11}$$

The turbulence intensity (I) is linked to the turbulence kinetic energy and reference velocity (U_{ref}) as follows:

$$I = \frac{\sqrt{\frac{2}{3}k}}{U_{ref}} \tag{2.12}$$

The effects of fluctuations on mean flow can be determined by using the Reynolds decompositions of flow properties (pressure, velocity vector, and three velocity components) and applying time average of flow properties and their fluctuations as depicted in Equations (2.8) and (2.9).

The continuity equation of compressible fluid for Cartesian coordinates can be written as:

$$\frac{\partial \rho}{\partial t} + \frac{\partial}{\partial x}\left(\rho\overline{u}\right) + \frac{\partial}{\partial y}\left(\rho\overline{v}\right) + \frac{\partial}{\partial z}\left(\rho\overline{w}\right) = 0 \tag{2.13}$$

or

$$\frac{\partial \rho}{\partial t} + \nabla \cdot \left(\rho\overline{\mathbf{U}}\right) = 0 \tag{2.14}$$

Further, the turbulent flow equations of compressible fluid for Cartesian coordinates are given by

x-component:

$$\frac{\partial}{\partial t}(\rho\bar{u})+\frac{\partial}{\partial x}(\rho\bar{u}^2)+\frac{\partial}{\partial y}(\rho\bar{u}\bar{v})+\frac{\partial}{\partial z}(\rho\bar{u}\bar{w})=-\frac{\partial\bar{p}}{\partial x}+\mu\frac{\partial^2\bar{u}}{\partial x^2}+\mu\frac{\partial^2\bar{u}}{\partial y^2}+\mu\frac{\partial^2\bar{u}}{\partial z^2}$$

$$+\left[-\frac{\partial}{\partial x}\left(\rho\overline{(u')^2}\right)-\frac{\partial}{\partial y}\left(\rho\overline{u'v'}\right)-\frac{\partial}{\partial z}\left(\rho\overline{u'w'}\right)\right]+S_{Mx} \tag{2.15}$$

or $$\frac{\partial}{\partial t}(\rho\bar{u})+\nabla\cdot\left(\rho\bar{u}\bar{\mathbf{U}}\right)=-\frac{\partial\bar{p}}{\partial x}+\mu\nabla^2\bar{u}$$

$$+\left[-\frac{\partial}{\partial x}\left(\rho\overline{(u')^2}\right)-\frac{\partial}{\partial y}\left(\rho\overline{u'v'}\right)-\frac{\partial}{\partial z}\left(\rho\overline{u'w'}\right)\right]+S_{Mx} \tag{2.16}$$

y-component:

$$\frac{\partial}{\partial t}(\rho\bar{v})+\frac{\partial}{\partial x}(\rho\bar{v}\bar{u})+\frac{\partial}{\partial y}(\rho\bar{v}^2)+\frac{\partial}{\partial z}(\rho\bar{v}\bar{w})=-\frac{\partial\bar{p}}{\partial y}+\mu\frac{\partial^2\bar{v}}{\partial x^2}+\mu\frac{\partial^2\bar{v}}{\partial y^2}+\mu\frac{\partial^2\bar{v}}{\partial z^2}$$

$$+\left[-\frac{\partial}{\partial x}\left(\rho\overline{u'v'}\right)-\frac{\partial}{\partial y}\left(\rho\overline{(v')^2}\right)-\frac{\partial}{\partial z}\left(\rho\overline{v'w'}\right)\right]+S_{My} \tag{2.17}$$

or $$\frac{\partial}{\partial t}(\rho\bar{v})+\nabla\cdot\left(\rho\bar{v}\bar{\mathbf{U}}\right)=-\frac{\partial\bar{p}}{\partial y}+\mu\nabla^2\bar{v}$$

$$+\left[-\frac{\partial}{\partial x}\left(\rho\overline{u'v'}\right)-\frac{\partial}{\partial y}\left(\rho\overline{(v')^2}\right)-\frac{\partial}{\partial z}\left(\rho\overline{v'w'}\right)\right]+S_{My} \tag{2.18}$$

z-component:

$$\frac{\partial}{\partial t}(\rho\bar{w})+\frac{\partial}{\partial x}(\rho\bar{w}\bar{u})+\frac{\partial}{\partial y}(\rho\bar{w}\bar{v})+\frac{\partial}{\partial z}(\rho\bar{w}^2)=-\frac{\partial\bar{p}}{\partial z}+\mu\frac{\partial^2\bar{w}}{\partial x^2}+\mu\frac{\partial^2\bar{w}}{\partial y^2}+\mu\frac{\partial^2\bar{w}}{\partial z^2}$$

$$+\left[-\frac{\partial}{\partial x}\left(\rho\overline{u'w'}\right)-\frac{\partial}{\partial y}\left(\rho\overline{v'w'}\right)-\frac{\partial}{\partial z}\left(\rho\overline{(w')^2}\right)\right]+S_{Mz} \tag{2.19}$$

or $$\frac{\partial}{\partial t}(\rho\bar{w})+\nabla\cdot\left(\rho\bar{w}\bar{\mathbf{U}}\right)=-\frac{\partial\bar{p}}{\partial z}+\mu\nabla^2\bar{w}$$

$$+\left[-\frac{\partial}{\partial x}\left(\rho\overline{u'w'}\right)-\frac{\partial}{\partial y}\left(\rho\overline{v'w'}\right)-\frac{\partial}{\partial z}\left(\rho\overline{(w')^2}\right)\right]+S_{Mz} \tag{2.20}$$

Equations (2.15) - (2.20) are called “Reynolds equations”. The additional terms in the brackets as shown in Equations (2.15) - (2.20) are extra turbulent stresses, which

describe the diffusive nature of turbulence [20]. Further, these extra turbulent stresses are generally called as “Reynolds stresses”.

In 1877, Boussinesq postulated that the Reynolds stresses (momentum transfer due to turbulent eddies) can be modeled by eddy viscosity or turbulent viscosity (μ_t). The Boussinesq assumption showed that the Reynolds stress tensor is proportional to the mean deformation rate (strain rate) and can be written as [21]:

$$\tau_{ij} = -\rho\overline{u_i' u_j'} = \mu_t\left(\frac{\partial \overline{u}_i}{\partial x_j} + \frac{\partial \overline{u}_j}{\partial x_i} - \frac{2}{3}\frac{\partial \overline{u}_k}{\partial x_k}\delta_{ij}\right) - \frac{2}{3}\rho k\delta_{ij} \tag{2.21}$$

where u_i' and u_j' are fluctuation velocities for i and j directions. $\overline{u}_i$, $\overline{u}_j$, and $\overline{u}_k$ respectively are mean velocities for i, j, and k directions. Further, δ_{ij} is Kronecker delta. It can be seen that Equation (2.21) is similar to the Newton’s law of viscosity.

According to Boussinesq hypothesis, Equations (2.16), (2.18), and (2.20) can be written as:

x-component:

$$\frac{\partial}{\partial t}(\rho\overline{u}) + \nabla\cdot\left(\rho\overline{u}\overline{\mathbf{U}}\right) = -\frac{\partial \overline{p}}{\partial x} + \mu_{eff}\nabla^2\overline{u} + S_{Mx} \tag{2.22}$$

y-component:

$$\frac{\partial}{\partial t}(\rho\overline{v}) + \nabla\cdot\left(\rho\overline{v}\overline{\mathbf{U}}\right) = -\frac{\partial \overline{p}}{\partial y} + \mu_{eff}\nabla^2\overline{v} + S_{My} \tag{2.23}$$

z-component:

$$\frac{\partial}{\partial t}(\rho\overline{w}) + \nabla\cdot\left(\rho\overline{w}\overline{\mathbf{U}}\right) = -\frac{\partial \overline{p}}{\partial z} + \mu_{eff}\nabla^2\overline{w} + S_{Mz} \tag{2.24}$$

where μ_{eff} is an effective viscosity coefficient ($\mu_{eff} = \mu + \mu_t$).

According to Equations (2.22) - (2.24), it can be observed that the extra parameter is eddy viscosity. In order to obtain this viscosity, the additional model is required. It is called “turbulence model”. Over 90 years, the various turbulence models were developed. These models can be categorized into four types [22], including algebraic (zero-equation) models, one-equation models, two-equation models, and second order closure models. Among of these turbulence model types, the two-equation models become the famous turbulence models because of their accuracy, time efficiency, etc. There are various two-equation models, such as k-

omega model, k-epsilon model, etc. The k-epsilon turbulence model is widely used in many engineering applications. The details of this model are described below.

2.4.2 k-epsilon turbulence model

The form of k-epsilon model was first introduced by Harlow and Nakayama [23]. This model includes two extra transport equations, including transport equation of turbulence kinetic energy (k) and transport equation of dissipation rate of turbulence kinetic energy (ε). The exact k-epsilon equations contain many unmeasurable terms [24]. Later, Launder and Spalding [25] represented the more practical k-epsilon model in 1972. Nowadays, there are three common versions of k-epsilon model, including standard k-epsilon model (SKE), renormalization group k-epsilon model (RNGKE), and realizable k-epsilon model (RKE). The transport equations of these three versions can be represented by using a general Reynolds average equation as shown in Equation (2.25). Moreover, the details of variables for three k-epsilon models and their model constants are shown in Table 2.1 and Table 2.2, respectively.

$$\frac{\partial(\rho\phi)}{\partial t}+\frac{\partial(\rho\bar{u}_i\phi)}{\partial x_i}=\frac{\partial}{\partial x_j}\left[\Gamma_\phi\frac{\partial\phi}{\partial x_j}\right]+S_\phi \tag{2.25}$$

where Γ_ϕ is diffusion coefficient for ϕ. S_ϕ is source of ϕ per unit volume.

Table 2.1 The details of variables for three different versions of k-epsilon model [26]

Model	Transport equation	ϕ	Γ_ϕ	S_ϕ
SKE	k-transport equation	k	$\mu+\frac{\mu_t}{\sigma_k}$	$G_k+G_b-\rho\varepsilon-Y_M+S_k$
	ε-transport equation	ε	$\mu+\frac{\mu_t}{\sigma_\varepsilon}$	$C_{1\varepsilon}\frac{\varepsilon}{k}(G_k+C_{3\varepsilon}G_b)-C_{2\varepsilon}\rho\frac{\varepsilon^2}{k}+S_\varepsilon$
RNGKE	k-transport equation	k	$\alpha_k\mu_{eff}$	$G_k+G_b-\rho\varepsilon-Y_M+S_k$
	ε-transport equation	ε	$\alpha_\varepsilon\mu_{eff}$	$C_{1\varepsilon}\frac{\varepsilon}{k}(G_k+C_{3\varepsilon}G_b)-C_{2\varepsilon}\rho\frac{\varepsilon^2}{k}-R_\varepsilon+S_\varepsilon$
RKE	k-transport equation	k	$\mu+\frac{\mu_t}{\sigma_k}$	$G_k+G_b-\rho\varepsilon-Y_M+S_k$
	ε-transport equation	ε	$\mu+\frac{\mu_t}{\sigma_\varepsilon}$	$\rho C_1 S\varepsilon-\rho C_2\frac{\varepsilon^2}{k+\sqrt{\nu\varepsilon}}+C_{1\varepsilon}\frac{\varepsilon}{k}C_{3\varepsilon}G_b+S_\varepsilon$

Table 2.2 The model constants for three different versions of k-epsilon model [26]

Model	$C_{1\varepsilon}$	$C_{2\varepsilon}$	C_μ	σ_k	σ_ε	C_1	C_2
SKE	1.44	1.92	0.09	1.0	1.3	-	-
RNGKE	1.42	1.68	0.0845	-	-	-	-
RKE	1.44	-	$\left[A_0 + A_S \frac{kU^*}{\varepsilon}\right]^{-1}$	1.0	1.2	$\max\left[0.43, \frac{\eta}{\eta+5}\right]$	1.9

Generally, the eddy viscosity for three versions of k-epsilon model can be evaluated by using the correlation as shown in Equation (2.26).

$$\mu_t = \rho C_\mu \frac{k^2}{\varepsilon} \tag{2.26}$$

Moreover, for RNGKE, the differential equation for eddy viscosity obtained by scale elimination procedure in RNG theory is given by

$$d\left(\frac{\rho^2 k}{\sqrt{\varepsilon\mu}}\right) = 1.72 \frac{\hat{\nu}}{\sqrt{\hat{\nu}^3 - 1 + C_\nu}} d\hat{\nu} \tag{2.27}$$

where $\hat{\nu} = \mu_{eff} / \mu$ and $C_\nu \approx 100$. Equation (2.27) is used for accounting the low-Reynolds number effects. For swirl flow, the eddy viscosity of RNGKE is calculated by using the correlation as represented in Equation (2.28).

$$\mu_t = \mu_{t0} f\left(a_s, \Omega, \frac{k}{\varepsilon}\right) \tag{2.28}$$

where μ_{t0} is eddy viscosity calculated without the swirl modification by using Equation (2.26) or Equation (2.27). Ω is a characteristic swirl number. a_s is swirl constant.

2.5 Solver theory

In this thesis, the finite volume method CFD code is adopted to study fluid flow inside jet mixing tank due to its advantages. The important details of this numerical technique are represented in this section.

2.5.1 Discretization of the domain

Discretization of the domain or grid generation is a process that break a computational domain into a set of computational cells by using grids or meshes. There are various grid types, such as quadrilateral (2D), triangle (2D), tetrahedron (3D), hexahedron (3D), etc. The selection of grid is an important step for CFD researchers because it has a significant impact on convergence rate, computational time, and solution accuracy. Generally, the quadrilateral and hexahedral cells should be respectively adopted to two- and three-dimensional domains because these grid types can eliminate or reduce the truncation error and numerical diffusion [27]. Numerical diffusion is a numerical error of an increase in diffusion coefficient, meaning that the viscosity, thermal conductivity, and diffusion coefficient are higher than the actual values for momentum, energy, and mass transfer problems [28].

For FVM, the details for two- and three-dimensional grids are easily illustrated by considering the quadrilateral and hexahedral grids. The computational grids include node, cell center, and cell face as depicted in Figure 2.1.

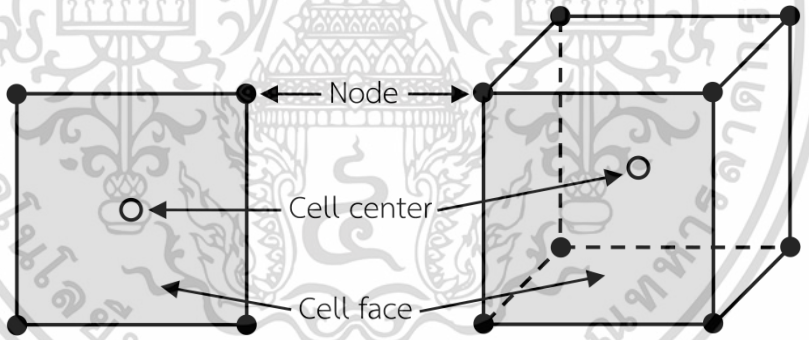

Figure 2.1 Grid details for FVM: node (black filled dot); cell center (no filled dot); cell face (gray color)

2.5.2 Discretization of transport equation

The discretization of general transport equation by finite volume method can be achieved by integrating the transport equation over a control volume (V) as shown in Equation (2.29) [26].

$$\frac{\partial}{\partial t}\int_V \rho\phi dV + \oint_A \rho\phi \mathbf{U}\cdot d\mathbf{A} = \oint \Gamma_\phi \nabla\phi \cdot d\mathbf{A} + \int_V S_\phi dV \tag{2.29}$$

where $\mathbf{A}$ is surface area vector. Equation (2.29) is applied to each cell in computational domain. The two dimensional triangular cell as shown in Figure 2.2 is used to illustrate the example of discretization of transport equation. For a given cell, the discretized transport equation is given by

$$\frac{\partial \rho \phi}{\partial t} V + \sum_{f}^{N_{faces}} \rho_f \mathbf{U}_f \phi_f \cdot \mathbf{A}_f = \sum_{f}^{N_{faces}} \Gamma_\phi \nabla \phi_f \cdot \mathbf{A}_f + S_\phi V \tag{2.30}$$

where N_{faces} is number of faces enclosing cell. ϕ_f is value of ϕ convected through face f. $\rho_f \mathbf{U}_f \cdot \mathbf{A}_f$ is mass flux through the face. $\mathbf{A}_f$ is area of face f. $\nabla \phi_f$ is gradient of ϕ at face f. The unsteady term as shown in the first term on left-hand side of Equation (2.30) is defined in temporal discretization.

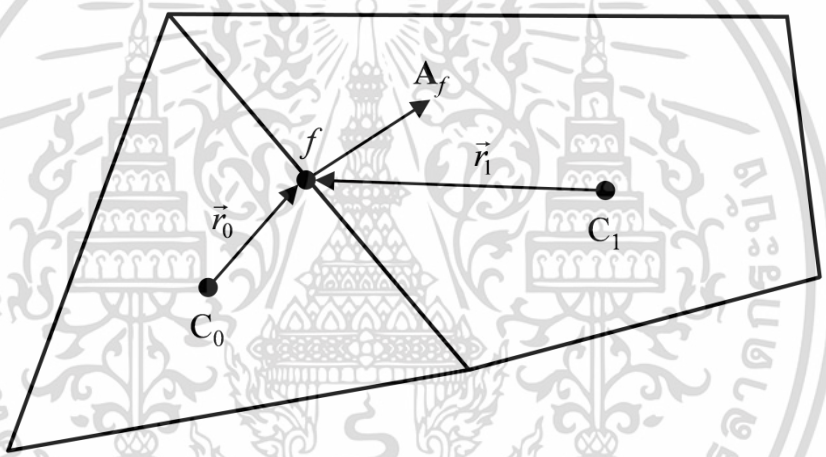

Figure 2.2 Example of grid used to illustrate the discretization of transport equation

2.5.3 Spatial discretization

Typically, the discrete values of scalar variable (ϕ) are stored at cell center. However, the convection terms in the discrete governing equation require the face values of scalar variable (ϕ_f), which can be interpolated by using cell center values. The common discretization schemes for FVM are central difference (CD), power law (PL), first order upwind (FOU), second order upwind (SOU), quadratic upwind interpolation for convective kinetics (QUICK), Third order MUSCL. It is a good practice to test the different spatial discretization schemes before other studies. The general spatial discretization schemes for FVM can be explained by considering the one-dimensional control volume as illustrated in Figure 2.3. The ϕ value of face e (ϕ_e) for different discretization schemes can be expressed as shown in Table 2.3.

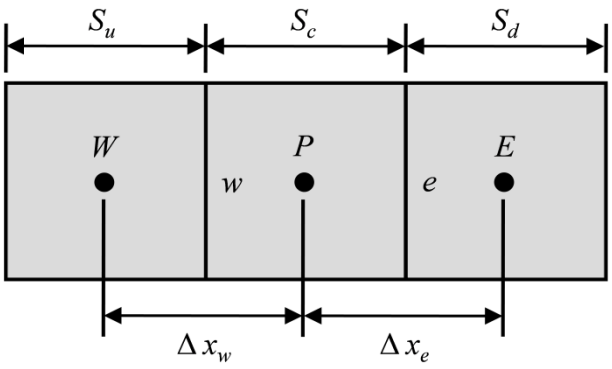

Figure 2.3 Schematic of one-dimensional control volume

Table 2.3 The details for common discretization schemes [26, 29]

Scheme	ϕ_e	General description
CD	$\frac{S_d}{S_c+S_d}\phi_P+\frac{S_c}{S_c+S_d}\phi_E$	This scheme is suitable when diffusion dominates. This scheme is recommended for LES.
PL	$\phi_P-\frac{(1-0.1\mathrm{Pe})}{\mathrm{Pe}}(\phi_E-\phi_P)$	It is good for intermediate values of Peclet number ($\mathrm{Pe}=\rho uL/\Gamma$). For high Pe, it is similar to FOU.
FOU	ϕ_P	Good when diffusion dominates and the flow is aligned with the grid.
SOU	$\phi_P+\left(\frac{\phi_P-\phi_W}{S_u+S_c}\right)S_c$	It is valid for full range of Peclet numbers. Further, this scheme is more accurate than FOU.
QUICK	$\phi_P+\frac{7}{8}\left(\frac{\phi_P-\phi_W}{S_u+S_c}\right)S_c+\frac{1}{8}\left(\frac{\phi_E-\phi_P}{S_c+S_d}\right)S_c$	Similar to SOU, but restricted to quadrilateral and hexahedral grids.
Third order MUSCL	$\theta\phi_{e,\mathrm{CD}}+(1-\theta)\phi_{e,\mathrm{SOU}}$	It improves the accuracy for all grids because it reduces the numerical diffusion.

2.5.4 Temporal discretization

For transient simulation, the fluid flow governing equations are discretised in both space and time. The temporal discretization includes the integration of every

term in differential equations over the time step Δt. The integration of the transient terms can be demonstrated as shown below [26].

The expression for time derivative of variable ϕ is given by

$$\frac{\partial \phi}{\partial t} = F(\phi) \tag{2.31}$$

where F is a function incorporates any spatial discretization. The first-order accuracy and second-order accuracy of the temporal discretizations obtained by backward differences are written as shown in Equations (2.32) and (2.33), respectively.

$$\frac{\phi^{n+1} - \phi^{n}}{\Delta t} = F(\phi) \tag{2.32}$$

$$\frac{3\phi^{n+1} - 4\phi^{n} + \phi^{n-1}}{2\Delta t} = F(\phi) \tag{2.33}$$

where n-1, n, and n+1 respectively are the values at previous time level (t-Δt), current time level (t), and next time level (t+Δt). For implicit time integration, the $F(\phi)$ is evaluated at the future time level as:

$$\frac{\phi^{n+1} - \phi^{n}}{\Delta t} = F\left(\phi^{n+1}\right) \tag{2.34}$$

The ϕ^{n+1} at a given cell is related to the ϕ^{n+1} in the neighboring cells through $F(\phi^{n+1})$ as:

$$\phi^{n+1} = \phi^{n} + \Delta t F\left(\phi^{n+1}\right) \tag{2.35}$$

This implicit method can be iteratively solved at each time level before solving the future time step. The advantage of this method is that it is stable with regardless of time step size.

2.5.5 Gradient and derivative evaluations

The gradient of scalar variable ϕ ($\nabla\phi$) is employed to discretize the diffusion and convection terms in the governing equations. There are three common methods to evaluate the gradient [26], including Green-Gauss cell-based, Green-Gauss node-based, and least squares cell-based. For irregular cells, the accuracy of least-squares cell-based is comparable to the accuracy of Green-Gauss node-based method. And Green-Gauss cell-based method shows less accuracy. Further, for computation, the least-squares cell-based is less expensive than Green-Gauss node-

based. Thus, the least squares cell-based method is commonly used to evaluate the gradient. The formulas of these three different methods can be summarized as shown in Table 2.4.

Table 2.4 Summary of gradient evaluations [26]

Method	Formula
Green-Gauss cell-based	$(\nabla\phi)_{c0} = \frac{1}{V}\sum_f \bar{\phi}_f \vec{A}_f$ where $\bar{\phi}_f = \frac{\phi_{c0} + \phi_{c1}}{2}$ [a,b]
Green-Gauss node-based	$(\nabla\phi)_{c0} = \frac{1}{V}\sum_f \bar{\phi}_f \vec{A}_f$ where $\bar{\phi}_f = \frac{1}{N_f}\sum_n^{N_f} \bar{\phi}_n$ [a,c]
least squares cell-based	$(\nabla\phi)_{c0} \cdot \Delta r_i = (\phi_{ci} - \phi_{c0})$ [b,d]

[a] V is volume. $\bar{\phi}_f$ is arithmetic average of ϕ.

[b] $c0$, $c1$, and ci respectively are cell 0, cell 1, and cell i.

[c] N_f is number of nodes on face.

[d] r_i is distance between center of cell 0 and center of cell i.

2.6 Solution methods

Generally, the velocity field is unknown and it is also related to other variables. Thus, the proper method to achieve the correct solutions is required. This section presents the solution methods, including algorithms and convergence criterion.

2.6.1 Algorithms

Typically, there are two important problems during the calculation process [3], including (i) The convective terms in momentum equations are non-linear quantities and (ii) There is no transport equation for pressure. In order to solve these problems, the iterative method is conducted. Further, the new equation for pressure is derived by using momentum equations and continuity equation, which commonly known as pressure correction equation. There are many algorithms for CFD. The most famous CFD algorithm is SIMPLE algorithm. So, in this part, the SIMPLE algorithm is introduced. Further, the PISO algorithm, which is commonly used as the algorithm for transient flow problems, is also presented.

2.6.1.1 SIMPLE

SIMPLE stands for Semi-Implicit Method for Pressure-Linked Equations. It was firstly introduced by Patankar and Spalding in 1972 [30]. This algorithm is a guess-and-correct procedure for the pressure calculation on staggered grid agreement [3]. The pressure correction equation of SIMPLE algorithm is formed by continuity and momentum equations. The pressure correction equation is shown in Equation (2.36). Further, the calculation procedure of SIMPLE can be illustrated as shown in Figure 2.4.

$$a_{I,J}p'_{I,J} = \sum a_{nb}p'_{nb} + b'_{I,J} \tag{2.36}$$

where a is coefficient and $a_{I,J} = \sum a_{nb}$. b' is mass imbalance.

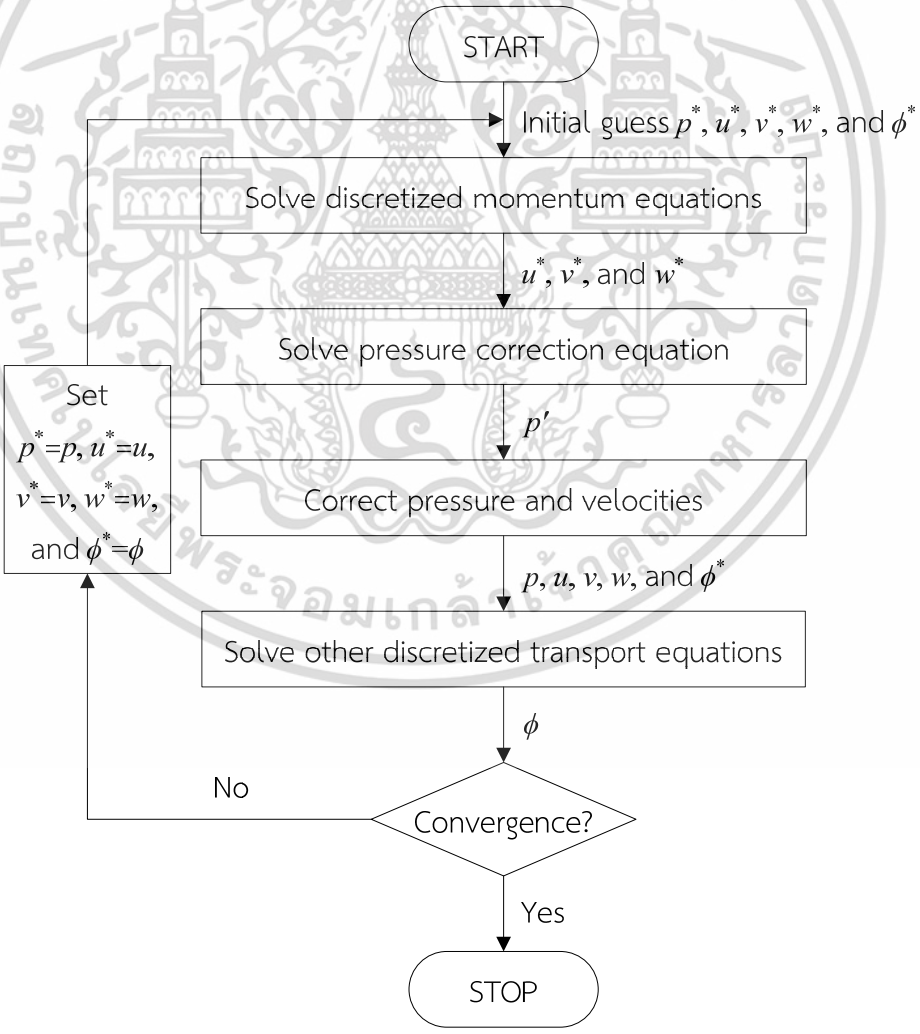

Figure 2.4 Procedure of SIMPLE algorithm [3]

2.6.1.2 PISO

PISO stands for Pressure-Implicit with Splitting of Operators, which is based on the higher degree of pressure and velocity correction relation. PISO is one of the SIMPLE algorithm family. Moreover, this algorithm is recommended for transient calculation because it provides the stable calculation with the larger time step size and under relaxation factor (URF) of unity [31]. For small time step size, it increases the computational expense, so the SIMPLE should be used instead. The calculation procedure can be demonstrated in Figure 2.5.

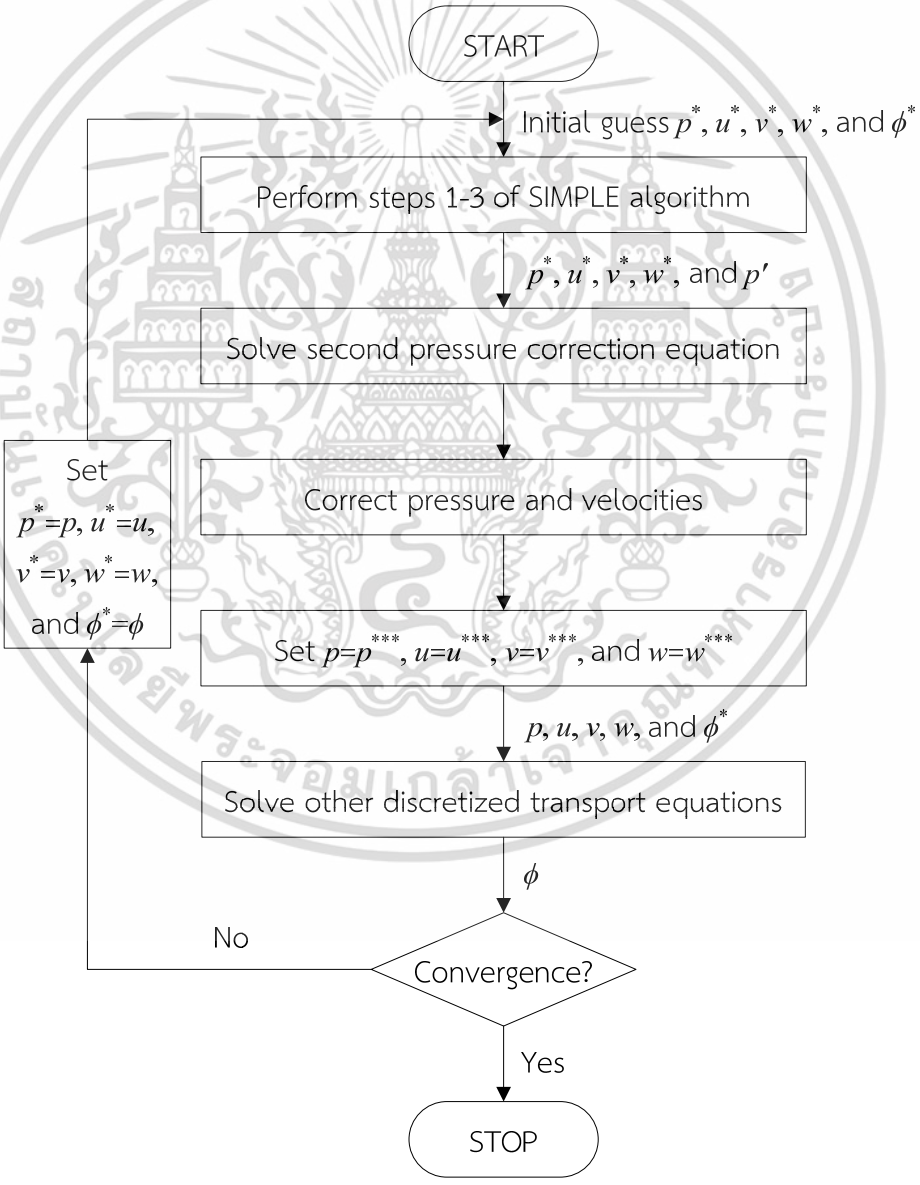

Figure 2.5 Procedure of PISO algorithm [3]

2.6.2 Convergence criterion

For iterative calculation, the process is repeatedly calculated until the changes in variables become small as compared to the previous iteration. So, the solutions can be considered as the converged solutions. At convergence, the mass, momentum, and other variables should be balance. At least, the solutions of all variables should be obeyed the specified tolerance. Furthermore, the solutions are no longer changes with increasing the iterations. For CFD, there are many different routes to consider the solution convergence. The popular convergence criteria is residual (R), which measures the imbalance of conservation equations. The residual is usually scaled by the local value of the variable ϕ, which is called "scaled residual". The overall scaled residual for variable ϕ can be written as shown in Equation (2.37) [29].

$$R^{\phi} = \frac{\sum_{all\ cells} \left| a_P \phi_P - \sum_{nb} a_{nb} \phi_{nb} - b \right|}{\sum_{all\ cells} |a_P \phi_P|} \tag{2.37}$$

Generally, the scale residuals for CFD should be less than 10^{-3} or 10^{-4}. For energy equation, the scaled residual should be lower than 10^{-6}. When the scaled residuals are used to consider the convergence, it is a good practice to consider the following suggestions.

- If the residuals reach the specified levels but are still falling down, the obtained simulated solutions may not be converged.

- If the residuals never meet the specified criterion and are no longer decreasing but the other solution monitors, e.g. the monitor of velocity at specified location, are also no longer changes, the simulated results are converged.

- The residuals are not the solutions. So, the low residuals do not confirm that the obtained results are correct. Further, the high residuals do not automatically show the wrong solutions.

- For higher discritization schemes, the residuals may be higher as compared to the first order discretization scheme. It does not mean that the first order scheme is better.

2.7 CFD study

There are three general steps for studying fluid dynamics by using CFD, including grid independent solution study, validation, and prediction. In this section, the details of three important steps are represented as follows:

2.7.1 Grid independent solution study

Grid independent solution study is the first important step for CFD study. The grid independent solution is defined as the solutions that are invariant or show small variation with increasing the number of grids. In other words, the solutions are independent on the influence of grid. Thus, the grid independent solution must be achieved before considering the calculated results.

2.7.2 Validation

Validation is the second process of CFD study that presents the reliability of the CFD model. There are five important definitions, which are used to describe this process, including model, modeling, simulation, verification, and validation. The American Institute of Aeronautics and Astronautics (AIAA) clearly defined these five terms in 1998 [32] as follows:

"Model: A representation of a physical system or process intended to enhance our ability to understand, predict, or control its behavior."

"Modeling: The process of construction or modification of a model."

"Simulation: The exercise or use of a model. (That is, a model is used in a simulation.)"

"Verification: The process of determining that a model implementation accurately represents the developer's conceptual description of the model and the solution to the model."

"Validation: The process of determining the degree to which a model is an accurate representation of the real world from the perspective of the intended uses of the model."

Generally, there are two model types, including conceptual model and computational model (computerized model). The conceptual model is achieved by observations and analysis of the physical system. It includes information, mathematical

modeling data, and mathematical equations which explain the system or process. In CFD, the governing equations are conceptual model. The computational model is a computer program which is used to implement a conceptual model, e.g. CFD code.

According to these definitions, for convenience, the verification can be considered as a process that shows the fidelity of computational model to the conceptual model. Further, the validation is a process which presents the accuracy of computational model to the real world, e.g. experiment.

In CFD, typically, the validation can be directly obtained by comparing the simulated flow properties, such as velocity, temperature, etc., at specified locations with the experimental data. Furthermore, the indirect data (overall process variables) can also be used for comparison, such as cyclone collection efficiency, overall mixing time for mixing tank, production yield for chemical reactor, etc.

2.7.3 Prediction

The last stage of CFD study is prediction, which is a process to investigate the effects of variable parameters. The results of this step are commonly used and analyzed to develop the performance of the processes. So, the correct solutions or tendencies should be achieved. That is, if the model shows the error between simulation and experiment but it exhibits the similar tendency as compared to the experiment. Such simulated data can be used to develop the process. In contrast, if the model represent the accurate results for some conditions but the tendency between simulation and experiment is not similar. In this case, the simulated results can only be used to develop process for a specific condition or may not be employed to develop the process. So, the CFD researchers must ensure that the simulated results show the similar tendency as compared to experiment before making the analysis or discussion.

CHAPTER III

JET AND JET MIXING TANK

Chapter III explains the fundamentals of jet flow and jet mixing tank. Further, the previous experimental and CFD studies of jet mixing tanks are also reviewed and represented.

3.1 Jet

Jet is one of the most important free shear flows, which there is no wall effect on the flow. Jet is started from the jet nozzle exit plane. As the jet issues into a stationary fluid or slow-moving fluid, it will entrain the surrounding fluid and spread in the radial direction along the downstream distance until the jet reaches the point where viscous effect will dissipate the energy and lead to the death of the jet. Typically, the jet mixing is insignificant at the distance above 400 jet diameters [33].

Jet can be classified as laminar jet or turbulent jet by considering the jet Reynolds number (Re_j), which is commonly defined as shown in Equation (3.1).

$$\mathrm{Re}_j = \frac{\rho d_j U_j}{\mu} \tag{3.1}$$

where d_j is jet nozzle diameter and U_j is jet inlet velocity or jet discharge velocity. The laminar jet is the jet flow with the jet Reynolds number below about 100. For fully turbulent jet, the jet Reynolds number is above about 1,000-2,000 [33].

Generally, jet is produced by a continuous source of momentum. Further, the intrusion of fluid can also be generated by buoyancy source. The various types of intrusion for two different injection types, including continuous and intermittent injections, can be summarized as shown in Table. 3.1.

The appearance of jet and plume are similar. However, the mixing mechanisms of these flows are different [35]. The mixing of the jet is directly related to the inertia of the turbulent eddies. For the plume, the mixing is dominated by the inertia due to the buoyant force. Jets can be observed in various applications, such as jet reactor,

combustion chamber, jet mixing tank, etc. In this thesis, the turbulent round jet is only mentioned because the considered system is related to this type of flow.

Table 3.1 Types of fluid intrusions into another fluid [34]

Source	Continuous injection	Intermittent injection
Momentum	Jet	Puff
Buoyancy	Plume	Thermal
Momentum and buoyancy	Buoyant jet (forced plume)	Buoyant puff

3.2 Fluid dynamics of turbulent round jet

The jet consists of three distinguished layers, including centerline layer, shear layer, and outer layer [36], as shown in Figure 3.1. In jet shear layer, the mixing process involves bulk mixing and small scales mixing [37]. The bulk mixing and small scales mixing are respectively driven by large scale coherent structures (CS) and turbulent velocity fluctuations.

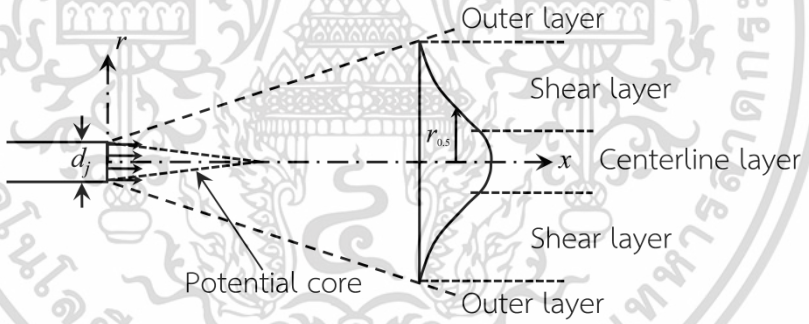

Figure 3.1 Details of jet layers [36]

In the jet shear layer near nozzle exit, the jet flow produces rolling up of a vortex fairly close to the nozzle exit. The cause of vortex roll up formation is due to the Kelvin-Helmholtz instability. Later, the vortices are paired to create a single vortex with greater strength, which is called “vortex pairing”. A short distance further downstream, the three-dimensional disturbances cause the vortices to become highly distorted and less distinct. Then, the flow breaks down and generates a large number of small scale eddies. Finally, the flow undergoes rapidly from transition to the fully turbulent regime [3]. This transition in a jet flow can be illustrated in Figure 3.2.

In turbulent round jet, there are two different regions, including zone of flow establishment (ZFE) and zone of established flow (ZEF) [38], as shown in Figure 3.3. In ZFE, the mean centerline axial velocity ($\overline{u}_c$) is equal to jet discharge velocity and the turbulent mixing has not penetrated into the jet center. This zone is also known as the potential core region, which will appear only for the jet issuing from the contraction nozzle (uniform velocity profile) [36]. The potential core is usually observed within $0 \leq x/d_j \leq 6$ [39] and found to decrease as the jet Reynolds number increased [38]. For ZEF, the mixing penetrates into jet centerline and the mean centerline axial velocity is found to decrease with increasing longitudinal distance (x). The transverse velocity profiles of this region show Gaussian distribution.

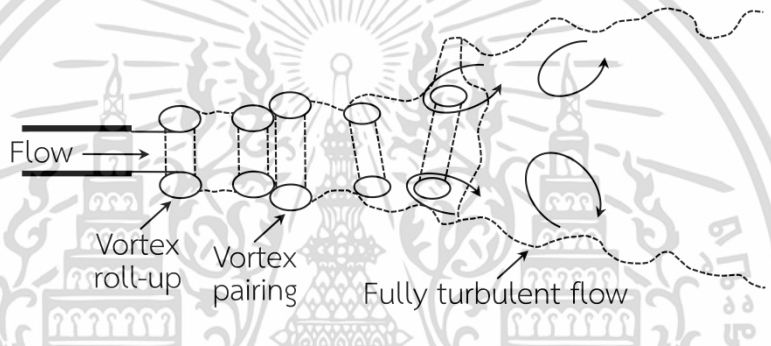

Figure 3.2 Transition in a jet flow [3, 36]

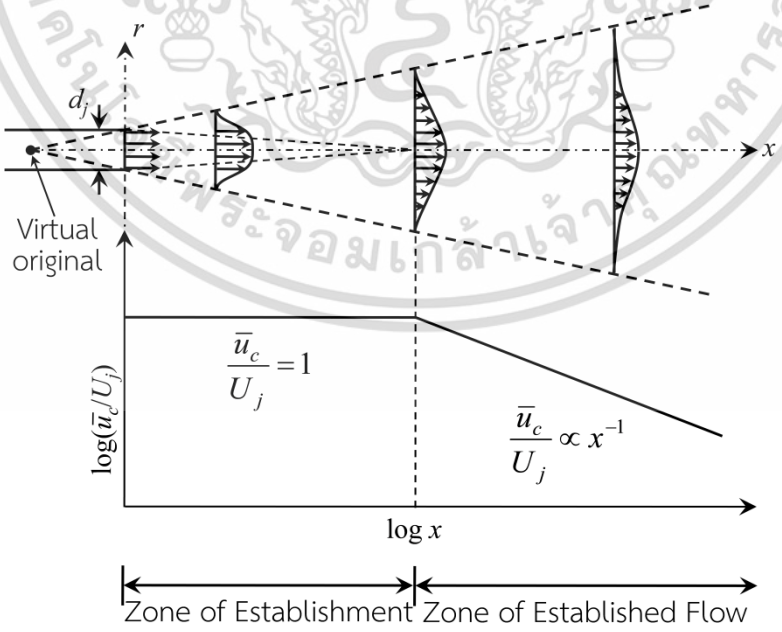

Figure 3.3 Schematic of axis-symmetric turbulent round jet

Further, the turbulent round jet may be separated into three regions [40], including near-field, intermediate-field, and far-field. The near-field region or potential core region is generally found within $0 \leq x/d_j \leq 6$ as mentioned earlier. The intermediate-field is located within $6 < x/d_j < 30$. For far-field region, the fully-developed or self-similarity region is observed at approximately $x/d_j \geq 30$. In turbulent flow, the self-similarity is a condition that the velocity profiles for different sections show similar shapes when they are scaled by using proper scale factors, that depend only on one of variables [41, 42]. Further, the self-preservation is a condition which is similar to self-similarity but it is not only valid for velocity but also other quantities, such as turbulence quantities, cross correlations, etc. [41]. Although the difference between self-similarity and self-preservation were clearly explained by Gartshore [41], however, some researchers used these terms in similar fashion [42-44]. For turbulent round jet, Wygnanski and Fiedler [45] showed the self-preservation of jet at 70 nozzle diameters downstream.

Many studies represented the Gaussian profile of axis-symmetric turbulent round jet as shown in Equation (3.2) [46-48].

$$\frac{\overline{u}}{\overline{u}_c} = \exp\left[-k_u\left(\frac{r}{x}\right)^2\right] \tag{3.2}$$

where k_u is a constant for the Gaussian shape, which varies from 55 to 100, and r is the radial distance from jet centerline. Further, in ZEF, the decay of mean centerline velocity along the jet centerline is represented in Equation (3.3) [46, 47].

$$\frac{\overline{u}_c}{U_j} = a_u\left(\frac{x - x_0}{d_j}\right)^{-1} \tag{3.3}$$

where a_u is the decay constant and x_0 is a virtual original of the velocity. George [42] stated that both a_u and x_0 might be dependent on exit conditions. Hongwei [48] suggested that many researchers assumed that the virtual original was zero because it was much smaller than the longitudinal distance.

The jet boundaries (jet nominal boundaries) are usually defined as the outer edges where the mean axial velocity ($\overline{u}$) is equal to 1/e of the mean centerline axial velocity [38]. The jet width is found to increase with increasing the longitudinal jet distance as the surrounding fluid is entrained into jet stream. According to this jet boundary, the jet half width ($r_{1/e}$) is a distance from the centerline to the point where mean axial velocity is 1/e of the mean centerline axial velocity ($0.3679\overline{u}_c$). Further,

the jet half width can also defined as a radial distance where the mean axial velocity is equal to a half of mean centerline axial velocity ($0.5\bar{u}_c$) [49, 50], which is denoted by $r_{0.5}$. These two different jet half width definitions are commonly known as velocity half width. Further, the concentration profiles can also be employed to determine the jet half width, which is known as concentration half width [43].

Generally, jets spread linearly in ZEF. So, the spreading rate of jet (S) is constant [51]. The spreading rate can be obtained by using two different velocity half width. For $r_{1/e}$, the experimental results of Papanicolaou and List [52] and Hongwei [48] showed that the jet spreading rate ($dr_{1/e}/dx$) were 0.107 and 0.105, respectively. For $r_{0.5}$, the jet spreading rate ($dr_{0.5}/dx$) experimentally achieved by Panchapakesan and Lumley [53] was 0.096. Further, the jet spreading rate of Hussein et al. [47] obtained by hot-wire data and laser-Doppler data were 0.102 and 0.094, respectively.

3.3 Correlations for turbulent round jet

For turbulent round jet, the correlations of the mean centerline axial velocity, radial profile of mean axial velocity, and jet entrainment are described as follows:

3.3.1 Mean centerline axial velocity

The mean centerline axial velocity of round jet can be evaluated by using the correlation of Davies [54] as shown in Equation (3.4).

$$\bar{u}_c = 6.4\frac{d_j U_j}{x}, \text{ for } \frac{x}{d_j} > 6.4 \tag{3.4}$$

3.3.2 Radial profile of mean axial velocity

For radial distribution of mean axial velocity, Schlichting [55] represented analytical correlation as shown in Equation (3.5).

$$\bar{u} = \frac{3}{8\pi}\frac{K}{\nu_0 x}\frac{1}{\left[1+\frac{1}{4}\eta^2\right]^2} \tag{3.5}$$

where $\eta = \frac{1}{4}\sqrt{\frac{3}{\pi}}\frac{K^{1/2}}{\nu_0}\frac{r}{x}$, $K^{1/2} = 1.59 b_{1/2}\bar{u}_c$, $\nu_0 = 0.0256 b_{1/2}\bar{u}_c$, $b_{1/2} = 0.0848x$, and $\bar{u}_c = 7.31\frac{d_j U_j}{x}$.

Further, Davies [54] also showed the radial profile of mean axial velocity as shown in Equation (3.6).

$$\log_{10}\left[\frac{\overline{u}_c}{\overline{u}}\right] = 40\left[\frac{r}{x}\right]^2, \text{ for } 7 < \frac{x}{d_j} < 100 \tag{3.6}$$

The radial profiles of mean axial velocity obtained by two different correlations are shown in Figure 3.4. The mean axial velocity and radial distance are represented in dimensionless forms. The dimensionless mean axial velocity is defined as a ratio of mean axial velocity to mean centerline axial velocity. Further, the dimensionless radial distance is defined as a ratio of jet radial distance to jet half width ($r_{0.5}$).

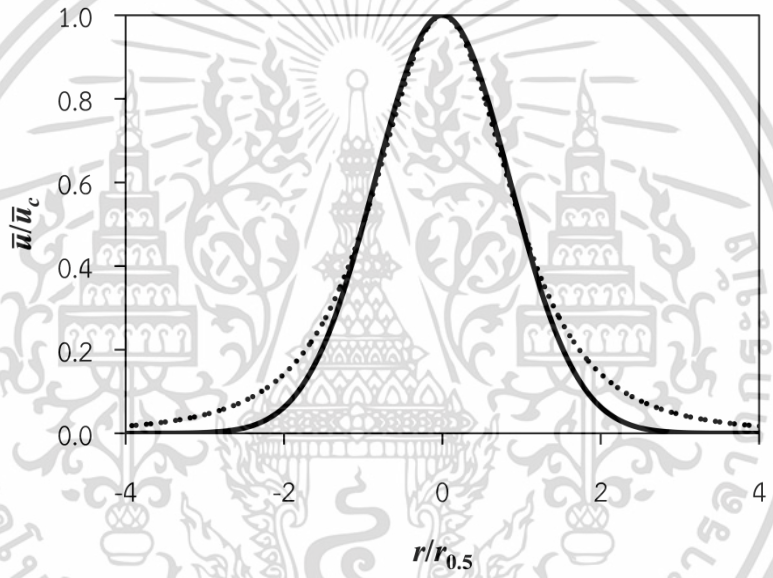

Figure 3.4 Radial profiles of jet axial velocity for two different correlations: —— Davies [54]; ····· Schlichting [55]

3.3.3 Jet entrainment

The entrainment is another interesting phenomena of jet flow, that the jet induces the surrounding fluid into its stream. Albertson et al. [56] reported that, for round free jet, the entrainments of two different jet regions are not identical. For ZFE, the correlation for jet entrainment can be written as:

$$\frac{Q}{Q_0} = 1 + 0.083\frac{x}{d_j} + 0.0128\left[\frac{x}{d_j}\right]^2, \text{ for } \frac{x}{d_j} \le 6.2 \tag{3.7}$$

where Q and Q_0 are jet entrainment and jet efflux rates, respectively. Moreover, the correlation for jet entrainment in ZEF is given by

$$\frac{Q}{Q_0} = 0.32\frac{x}{d_j}, \quad \text{for} \quad \frac{x}{d_j} > 6.2 \tag{3.8}$$

3.4 Jet mixing tank

Fluid mixing is one of the important topics in chemical processes. The mixing in tank can be achieved by using two common mixing devices, including impeller stirred tank and jet mixing tank. The jet mixing tanks exhibit the shorter mixing time as compared to the conventional stirred tanks [1, 57]. Jet mixing tank was firstly proposed by Fossett and Prosser [1]. Their jet mixing tank work was originated from a practical war-time problem of the secure mixing system of tetraethyl-lead fluid in 4,000 tons underground petroleum storage tanks.

In jet mixing tanks, the liquid is drawn into a pump, which is used to produce high liquid velocity jet. The liquid jet discharges through a nozzle into the tank. Then, the jet entrains the surrounding liquid and creates the liquid circulation inside the tank. Finally, the different components inside the tank are mixed. There are three general jet mixing tank geometries as shown in Figure 3.5. Figures 3.5(a) and 3.5(b) show the batch jet mixing tanks. The difference between these tanks is only the injection positions of liquid B. In Figure 3.5(a), liquid B is directly added into the tank. For another batch jet mixing tank, liquid B is injected in to the recycle line as shown in Figure 3.5(b). The last geometry of jet mixing tank is the continuous jet mixing tank, which liquids A and B are directly added into the tank, as shown in Figure 3.5(c).

The jet mixing tanks are widely used in various chemical processes because they are cheaper and easier to install. They also do not require the additional structure supports. Moreover, they are easier to maintenance due to the absence of moving parts. According to these advantages, the jet mixing tanks are commonly employed in various applications, such as blending the inhibitor to stop runaway reactions [58, 59], emergency cooling systems [60], mixing in hydrocarbon and LNG storage tanks [1, 61], jet reactors [62, 63], acid mixing [64], etc.

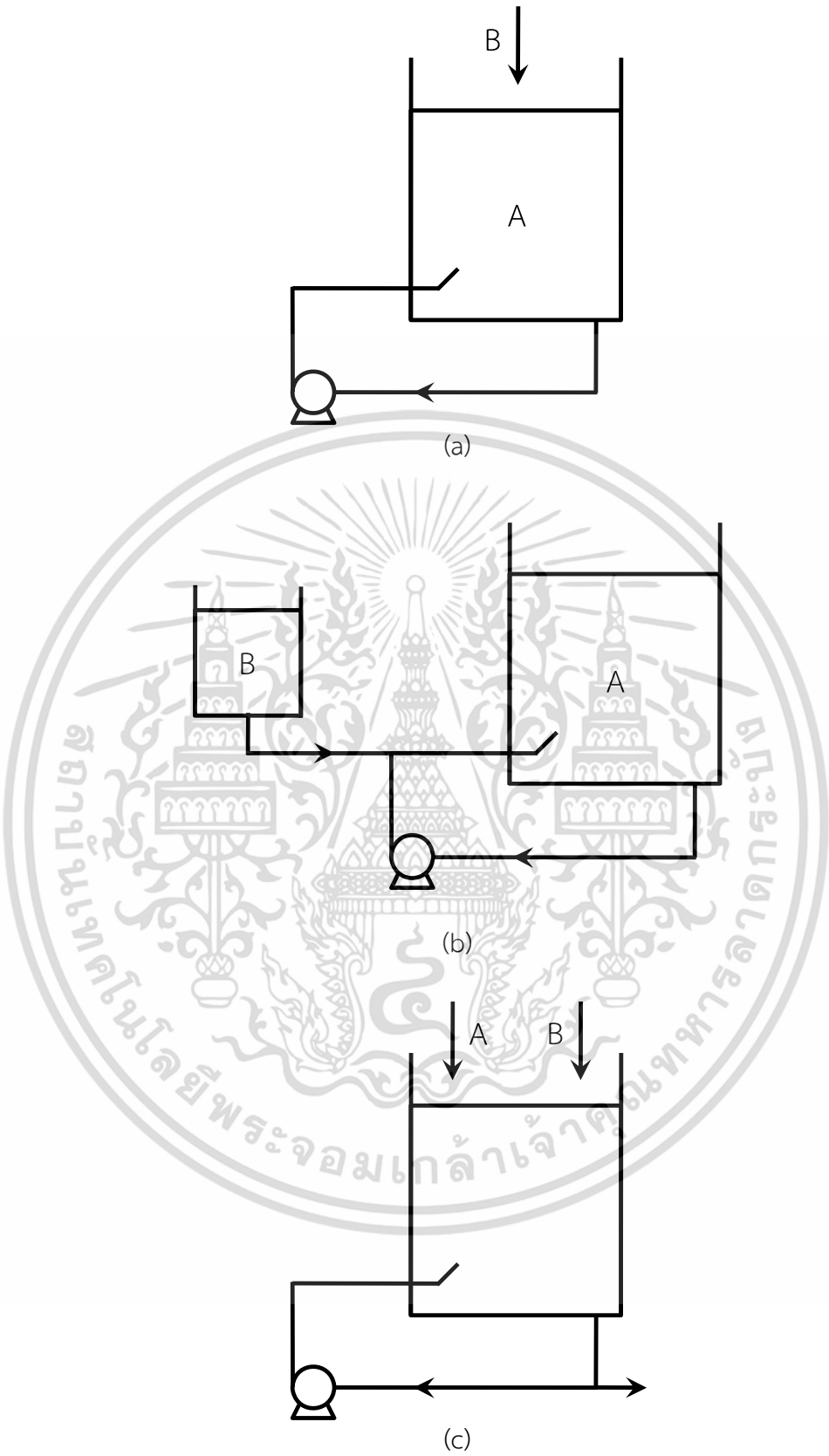

Figure 3.5 Schematics of (a) batch jet mixing tank (direct addition of liquid B) (b) batch jet mixing tank (addition of liquid B into recycle line) (c) continuous jet mixing tank [2, 33]

3.5 Fluid dynamics and fluid mixing of jet mixing tank

The jet mixing tanks can be classified by using jet nozzle installation, including side entry jet and axial jet. The flow patterns inside these two different jet mixing tanks are shown in Figure 3.6. The fluid flow inside the jet mixing tanks can be described as [33]:

- Radial spreading due to jet entrainment as the jet penetrates into the tank. The velocity and turbulence of the jet decrease because momentum of jet is spread over a steadily increasing area of the flow.

- Rollover of the jet flow when it impinge the tank boundaries, including tank wall, tank base, and liquid surface.

- After rollover, a very weak liquid motion driven by the jet flow along the tank boundaries.

- Liquid flow induced by jet entrainment from remote regions into the jet stream.

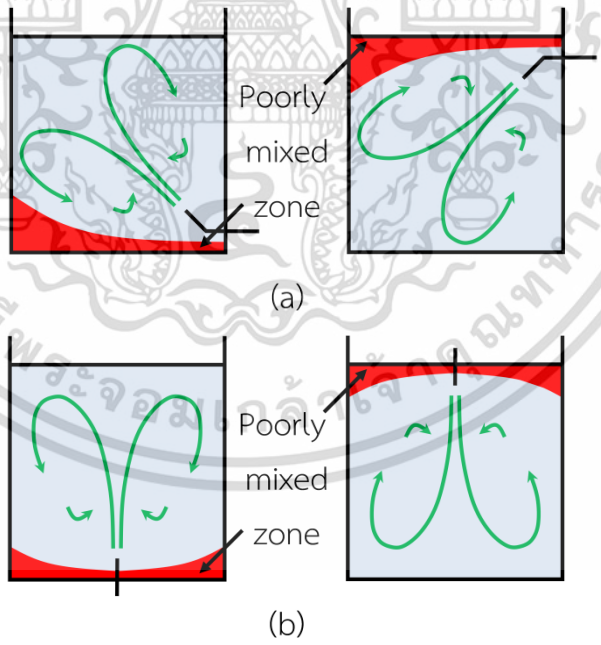

Figure 3.6 Schematics of (a) side entry jet mixing tanks (b) axial jet mixing tanks [2]

Furthermore, the mixing inside the jet mixing tanks can be achieved by the following processes [33]:

- Bulk transport of jet from jet nozzle exit to remote areas of the tank.

- Bulk transport of jet flow in remote areas of the tank.

- Bulk transport due to the entrainment of surrounding liquid into the jet stream.

- Mixing of jet and surrounding liquid inside the jet flow.

The mixing performance of jet mixing tank is limited by the poor mixing regions, which displayed in red color, as shown in Figure 3.6. The poor mixing zones are the last regions where the given degree of mixing is achieved. The poor mixing region size or mixing time is affected by jet nozzle position, recycle suction position, tank and jet sizes, jet protrusion, liquid height, and tank base shape [2]. The main objective of jet mixing design is to minimize these poor mixing regions. Further, the details of mixing time observations for experiments and CFD simulations are described as follows:

3.5.1 Experimental investigation of mixing time

Mixing time is an important key parameter for mixing devices. It can be typically obtained by two different methods, including tracer technique and visual observation technique. These techniques measure the macro mixing inside the tanks, meaning that the time taken to achieve a given degree of homogeneity in the whole tank is investigated.

For tracer technique, a tracer (electrolyte solution) is injected into the tank. Then, the time history of tracer concentration is investigated by using a single specific point or several specific points. Generally, the mixing time (t_m) is defined as a time at which the tracer concentration (c) has reached (or nearly reached) the final mean concentration of tracer ($\bar{c}$). If there is no tracer inside the vessel, a mixing time is the time from tracer injection to the time when

$$\frac{|c-\bar{c}|}{\bar{c}} = m \tag{3.9}$$

where m is the maximum acceptable absolute value of the relative deviation of the mix [65]. If the mixing inside the tank is completely mixed, m is equal to 0. In experiments, there are two criterions to identify mixing, including 99% mixing [66-68] and 95% mixing [69-71]. The values of m for 99% mixing and 95% mixing respectively are 0.01 and 0.05. The 99% mixing time ($t_{99\%}$) is about 1.5 times 95% mixing time ($t_{95\%}$) [33]. The tracer cannot only be concentration but also temperature [70-72]. For temperature, the 95% mixing is achieved when the temperature everywhere inside the tank is within the range of $\bar{T} \pm (\bar{T} - T) \times 0.05$, where $\bar{T}$ and T are the final mean temperature and initial bulk liquid temperature inside the vessel, respectively.

For visual observation, the liquid inside the tank is firstly made as a weakly acid. Further, the indicator is added to the tank. Later, the strong base is added to neutralize the acid. Finally, the mixing time is investigated as the time from the moment of strong base addition to the time at which the color of indicator disappears.

3.5.2 CFD investigation of mixing time

In CFD modeling, the tracer technique is commonly used to identify the mixing time inside jet mixing tank. The tracer can be concentration or temperature, which is similar to the experiments. For tracer concentration technique, in order to introduce the tracer for unsteady state simulation, the tracer may be patched inside the jet mixing tank domain [73-75] or directly injected into the tank [76-78]. Then, the time histories of tracer concentration for various specified probes are recorded and then used to determine the mixing time.

For temperature technique, a known fluid volume with a desired value of temperature is specified inside the computational domain. The time histories of temperature for different specified probes are then monitored and adopted to investigate the mixing time. This technique is successfully used in many CFD simulations of jet mixing tanks [70-72]. Further, for visual observation technique, it is not employed to determine the mixing time in CFD simulations.

3.6 Previous experimental studies of jet mixing tanks

Over 60 years or so, there are many extensive studies of jet mixing tanks. As mentioned earlier, the idea of liquid mixing driven by jet was firstly introduced by Fossett and Prosser [1]. They showed the mixing time correlation for inclined side entry jet mixing tank with the jet Reynolds number of 4,500 - 80,000 and exhibited that the mixing time of jet mixer was shorter than the impeller stirred tank. Further, Fossett [57] modified the mixing time correlation of Fossett and Prosser [1]. Fox and Gex [79] studied the jet mixing tanks for different ratios of liquid height (H) to tank diameter (D) and showed that the mixing time was dependent on momentum flux added to the vessel.

Furthermore, Van De Vusse [80] studied the inclined jet mixing tank and reanalyzed the experimental data of Fox and Gex [79] to obtain the mixing time correlation. Okita and Oyama [81] added the effect of liquid height into the mixing

time correlation, which showed more reliable than the previous correlations. Coldrey [82] presented the modified design of inclined side entry jet mixing tank and added the jet path length into the mixing time correlation. Hiby and Modigell [83] studied the axial jet mixing tank with flat base and found that the mixing time was independent on jet Reynolds number when the jet Reynolds number was higher than 1,000,000. Lehrer [84] investigated the mixing of miscible fluids with different densities and reported the mixing time correlation for axial jet mixing tank.

Lane and Rice [85] studied a vertical jet mixing tank with a hemispherical base and showed that the mixing time strongly depended on jet Reynolds number in laminar region. However, the mixing time slightly depended on jet Reynolds number in turbulent flow regime. They also extended their work and suggested that the mixing time is found to decrease with increasing the jet path length [66]. This suggestion is similar to the experimental work of Coldrey [82]. Maruyama et al. [86] showed that the mixing time depended on liquid depth, nozzle height, and nozzle angle. Further, Maruyama [87] showed that the jet nozzle angles of 25°-30° and 75° presented the local minimum mixing time. Simon and Fonade [62] and Orfaniotis et al. [88] proposed the mixing time correlations for steady and unsteady jets.

Grenville and Tilton [68] showed the mixing time correlation based on the turbulence kinetic energy dissipation rate at the jet path end, which was obtained by reanalyzing the previous data of Grenville et al. [67]. Further, they also proposed the mixing time correlation based on jet nozzle angle and compared their model with the circulation time model [89]. The results showed that these models were suitable to predict the mixing times for the tanks with H/D less than unity. Moreover, the mixing time was found to significantly increase when the jet nozzle angle below 15°. Grenville and Tilton [90] extended their work to study the mixing time for the tank with different H/D ($0.2 < H/D < 4$) and showed that their jet turbulence model fitted all data for H/D below 3.

Patwardhan and Gaikwad [91] studied the different effects on mixing time, including nozzle diameter, jet nozzle angle, and jet velocity. The results showed that the mixing time of horizontal side entry jet was higher than that obtained by inclined side entry jet. The tank with nozzle angle of 45° showed the minimum mixing time. Further, the mixing time was found to decrease with increasing the nozzle diameter and jet velocity. The jet mixing time correlations of previous works are summarized in Table 3.2 as reported by Bumrungthaichaichan [2].

Table 3.2 Summary of previous jet mixing time correlations [2]

Authors	Geometry	Dimension	Correlation
Fossett and Prosser (1949) [1]	Cylindrical tank with inclined side entry jet	D = 1.524 m H = 0.9144 m d_j = 1.9 mm d_o = 2.54 cm θ = 40° Re_j = 4,500-80,000	$t_m = 9\frac{D^2}{U_j d_j}$
Fossett (1951) [57]	Cylindrical tank with inclined side entry jet	D = 1.524 m H = 0.9144 m d_j = 1.9 mm d_o = 2.54 cm θ = 40°	$t_m = C_P\frac{D^2}{U_j d_j}$ $C_P = 9$ when $t_{inj} > t_m/2$ $C_P = 4.5$ when $t_{inj} < t_m/2$
Fox and Gex (1956) [79]	Cylindrical tank with side entry jet	D = 0.15-4.27 m H = 0.15-4.27 m d_j = 0.159-3.81 cm U_j = 0.6-11 m/s	$t_m = f\frac{H^{0.5}D}{\left(U_j d_j\right)^{4/6} g^{1/6}}$ $f = 95.638\mathrm{Re}_j^{-0.146}$
Van De Vusse (1959) [80]	Cylindrical tank with inclined side entry jet	-	$t_m = 3.68\frac{D^2}{U_j d_j}$
Okita and Oyama (1963) [81]	Cylindrical tank with inclined side entry jet	-	$t_m = 2.6\frac{D^{1.5}H^{0.5}}{U_j d_j}$
Coldrey (1978) [82]	Cylindrical tank with inclined side entry jet	-	$t_m = 4.507\frac{D^2 H}{L U_j d_j}$
Hiby and Modigell (1978) [83]	Cylindrical tank with axial jet	-	$t_m = T^*\frac{D^2}{U_j d_j}$ $T^* = 2.3$ when $\mathrm{Re}_t > 1{,}000{,}000$ $T^* \propto \mathrm{Re}$ when $\mathrm{Re}_t < 1{,}000{,}000$

Table 3.2 (Continued)

Authors	Geometry	Dimension	Correlation
Lehrer (1981) [84]	Axial jet	Free turbulent jet	$t_m = \frac{0.658}{U_j}\left(\frac{\rho_c}{\rho_d}\right)^{5/8} d_j^{0.25} \times \left(\frac{U_j}{N_j A}\right)^{3/4} \left[-\log\left(1-c^*\right)\right]$
Lane and Rice (1981) [85]	Cylindrical tank with axial jet	D = 0.31-0.57 m H/D = 0.5-3.0 Re_j = 250-60,000	$t_m = C_1 \frac{H^{0.5} D^{0.75}}{\mathrm{Re}_j^{1.3}\left(U_j d_j\right)^{0.5} g^{0.25}}$ $\mathrm{Re}_j < 1{,}800$ $t_m = C_2 \frac{H^{0.5} D^{0.75}}{\mathrm{Re}_j^{0.15}\left(U_j d_j\right)^{0.5} g^{0.25}}$ $\mathrm{Re}_j > 1{,}800$
Lane and Rice (1982) [66]	Cylindrical tank with side entry jet and axial jet	For side entry jets D = 0.31-0.57 m H/D = 0.9-1.1 For axial jets D = 0.31-0.57 m H/D = 0.5-3.0 Re_j = 250-60,000	$t_m = f \frac{H^{0.5} D}{\left(U_j d_j\right)^{0.667} g^{0.166}}$ $f = 113.133 \mathrm{Re}_j^{-0.146}$
Maruyama et al. (1982) [86]	Cylindrical tank with inclined side entry jet	D = 56, 104 cm H = 84, 125 cm h_i, h_o = 4.38, 20.5, 48.5 cm (D = 56 cm) h_i, h_o = 4, 14, 24, 44, 74, 94 cm (D = 104 cm) d_j = 0.5, 1, 1.8 cm θ = 7°, 15°, 30°, 45°, 54°, 60°, 73°	$\left(\frac{t_m}{t_r}\right)\left(\frac{L}{d_j}\right) = 2.5 - 8.0$ $\mathrm{Re}_j > 30{,}000$
Simon and Fonade (1993) [62]	Two jets at $H/2$ and $H/3$, horizontally located	D, H = 490 mm d_j =10 mm	$M = t_m (gH)^{0.5} D J_s^{2/3} \approx 1$ $J_s = \frac{J}{\rho U_j g}$, $J = \rho A U_j^2$

Table 3.2 (Continued)

Authors	Geometry	Dimension	Correlation
Orfaniotis et al. (1996) [88]	Two jets at $H/2$ and $H/3$, horizontally located	D, H = 500 mm d_j =9, 15 mm	$M = \left(\frac{t_m}{t_r}\right) J_s^{0.41} = 11.3$ $t_r = \frac{D}{(gH)^{0.5}}$, $J_s = \frac{J}{\rho U_j g}$, $J = \rho A U_j^2$
Grenville and Tilton (1996) [68]	Cylindrical tank	D = 0.61-36 m H/D = 0.2-1.0 d_j = 5.8-50 mm U_j = 2.2-24.8 m/s	$t_m = 3\frac{L^2}{U_j d_j}$
Grenville and Tilton (1997) [89]	Cylindrical tank	Same as Grenville and Tilton (1996)	$t_m = k\frac{D^2 H}{U_j d_j L}$ $k = 9.34$ when $\theta > 15°$ $k = 13.8$ when $\theta < 15°$
Grenville and Tilton (1998) [90]	Cylindrical tank	D = 0.61-36 m H/D = 0.2-4.0	$\frac{U_j t_m}{d_j}\left(\frac{d_j}{L}\right)^2 = 2.95$

According to previous experiments in jet mixing tanks, the only available information is the overall mixing time for the given parameters. The details of flow and mixing patterns inside the tank are not available. The shortfalls of experiments in jet mixing tanks can be presented and summarized as follows:

- As shown in Table 3.2, there are many mixing time correlations. However, the universal mixing time correlation is not available. That is, the mixing time correlations show the accurate results over the range of studied parameters, i.e. the correlations are case specific.

- The effect of liquid height is not taken into account the mixing time, meaning that the mixing times are identical regardless of the liquid height.

- The jet path length is only geometric parameter, which commonly defined as a distance between jet nozzle exit and opposite boundaries. So, this jet path length may not an actual jet path length, which directly affects on the mixing time estimation.

- The effects of liquid density, liquid viscosity and solid particles on mixing time are studied in a narrow range.

- The information of measuring probes is not reported. Furthermore, the measuring probes may be considered as the obstacles inside the vessel, which disturb the liquid flow.

3.7 Previous CFD studies of jet mixing tanks

According to the shortfalls of experiments in jet mixing tanks as mentioned in previous section, many researchers used the CFD technique to solve the limitations of experimental works. One of the earliest CFD studies has been carried out by Brooker [92]. He used only single measuring probe to determine the overall mixing time. Further, the predicted mixing time showed the maximum error about 15% as compared to experiment. Hoffman [59] reported the CFD modeling of jet mixing in large storage tank by simulating only one half of the tank (24,360 nodes). However, the validation of the model was unavailable. Ranade [73] simulated the alternating jet mixing tank by using standard k-epsilon model and revealed that the alternating jet did not always improve the mixing performance.

Jayanti [76] numerically studied the side entry and axial jet mixing tanks. The CFD results showed the good agreement with experimental data. The simulated results exhibited that the tank with a conical base reduced the mixing time by minimizing the poor mixed zone. Patwardhan [74] developed the in house CFD code to simulate the inclined side entry jet mixing tanks. He showed that the CFD code predicted the overall mixing time well. However, the concentration profiles were not in good agreement with experiments. Further, he also showed that these incorrect profiles can be improved by adjusting the turbulence model constants.

Zughbi and Rakib [71] and Zughbi and Ahmad [72] reported that the standard k-epsilon turbulence model was a suitable model for CFD simulations of inclined jet mixing tanks. Jaiklom et al. [93] studied the two different jet injections, including free jet and wall jet, by using CFD and showed that the free jet exhibited the better mixing as compared to the wall jet. Wasewar [94] reviewed the various parameters used in experimental and CFD studies to achieve the optimal design procedure. Later, Bumrungthaichaichan [2] reported the numerical setups of the previous jet mixing tank simulations as shown in Table 3.3.

Table 3.3 Numerical setup of the previous jet mixing simulations [2]

Authors	Geometry	Turbulence models	P-V coupling scheme[a] / Interpolation scheme	Temporal discretization scheme / Time step size	Convergence criteria
Ranade (1996) [73]	Cylindrical tank with side entry jet	SKE	Not mentioned / FOU	Not mentioned / 0.05 s	Normalized residue of species equation < 10^{-3}
Jayanti (2001) [76]	Cylindrical jet mixing tank	RNGKE	Not mentioned / Higher upwind scheme or CONDIF scheme	Not mentioned / 0.02 s (Gradually increased to 0.05 s or 0.1 s)	The equations were solved until the concentration at all points differed by less than 0.1% from the fully mixed value.
Patwardhan (2002) [74]	Cylindrical tank with inclined side entry jet	SKE	SIMPLER / Power law	Not mentioned / Dimensionless time step of 0.0025 (Gradually increased to 0.25)	Normalized mass residue < 0.005
Zughbi and Rakib (2002) [70]	Cylindrical tank with inclined side entry jet	SKE	PISO / Not mentioned	Not mentioned	Not mentioned
Thatte et al. (2004) [75]	Cylindrical tank with axial jet	Same as Patwardhan (2002)			

Table 3.3 (continued)

Authors	Geometry	Turbulence models	P-V coupling scheme[a] / Interpolation scheme	Temporal discretization scheme / Time step size	Convergence criteria
Zughbi and Rakib (2004) [71]	Cylindrical tank with inclined side entry jet	SKE and Reynolds Stress Model (RSM)	PISO / Not mentioned	Not mentioned / 1 s	Residual < 10^{-3} for all variables and < 10^{-6} for energy
Rahimi and Parvareh (2005) [77]	Cylindrical tank with inclined side entry jet	SKE, RNGKE, and RKE	SIMPLE / Standard for pressure and FOU for other quantities	Not mentioned	Residual < 10^{-3}
Zughbi and Ahmad (2005) [72]	Cylindrical tank with inclined side entry jet	SKE, RNGKE, RKE, and RSM	Not mentioned	Not mentioned / 1 s	Not mentioned
Marek et al. (2007) [95]	Cylindrical tank with inclined side entry jet	k-epsilon and k-omega	SIMPLE / First/second order hybrid scheme or second order HLPA scheme	Second order implicit (SOI) / Not mentioned	Not mentioned
Raja et al. (2007) [78]	Cylindrical tank with inclined side entry jet	SKE	Not mentioned / Power law	Not mentioned / 0.05 s (Gradually increased to 0.1 s)	The equations were solved until the concentration at all points differed by less than 0.1% from the fully mixed value.

Table 3.3 (continued)

Authors	Geometry	Turbulence models	P-V coupling scheme[a] / Interpolation scheme	Temporal discretization scheme / Time step size	Convergence criteria
Sendilkumar et al. (2007) [96]	Cylindrical tank with inclined side entry jet	RNGKE	Not mentioned / Higher order upwind scheme	Not mentioned / 0.1 s (Gradually increased to 1 s)	Residual < 10^{-3} for all variables and < 10^{-6} for energy
Wasewar and Sarathi (2008) [97]	Cylindrical tank with inclined side entry jet	SKE	SIMPLE for steady state and PISO for unsteady state / Power law for all variables and SOU for energy	Not mentioned / 0.1 s (Gradually increased to 0.5 s, 1 s, 2 s, 5 s, and 10 s)	Residual < 10^{-3} for all variables and < 10^{-6} for energy
Mathpati et al. (2009) [98]	Cylindrical tank with axial jet (jet loop reactor)	SKE, RSM, and LES	PISO / QUICK for RANS turbulence model and bounded central difference scheme for LES	SOI / 0.0005 s for LES	Residual < 10^{-4} for RANS turbulence model and 40,000 number of time steps for LES
Parvareh et al. (2009) [99]	Cubic vessel with a volume of 125 liters	RNGKE	SIMPLE / Standard for pressure and FOU for other quantities	Not mentioned / 0.01 s	Residual < 10^{-7}

Table 3.3 (continued)

Authors	Geometry	Turbulence models	P-V coupling scheme[a] / Interpolation scheme	Temporal discretization scheme / Time step size	Convergence criteria
Breisacher and Moder (2010) [100]	Axial jet mixing tank	k-epsilon	Not mentioned / Second order advection scheme	Not mentioned	Not mentioned
Furman and Stegowski (2011) [101]	Cylindrical tank with side entry jet	SKE, RNGKE, and RSM	Not mentioned	Not mentioned	Not mentioned
Lee and Armstrong (2011) [102]	Jet mixing tanks with and without cooling coils	SKE	Not mentioned	Not mentioned	The equations were solved until the acid species concentrations at all points in the tank reached the 95% mixing criteria.
Dautova et al. (2012) [103]	Cylindrical tank with symmetric axial jet and asymmetric axial jet	Spalart-Allmaras, RSM, SST k-omega, and k-omega transient model	Not mentioned	Not mentioned	Not mentioned

Table 3.3 (continued)

Authors	Geometry	Turbulence models	P-V coupling scheme[a] / Interpolation scheme	Temporal discretization scheme / Time step size	Convergence criteria
Leishear et al. (2012) [104]	Cylindrical tank with dual opposing jets	SKE	Not mentioned	Not mentioned	The equations were solved until the species concentrations at all points in the tank reached the 95% mixing criteria.
Muhammad and Kizito (2012) [105]	Cylindrical tank with single inclined jet and dual inclined jets	Not mentioned	Not mentioned	Not mentioned	Not mentioned
Rafiei et al. (2012) [106]	Cylindrical tank with axial jet and inclined top entry jet	RNGKE	Not mentioned	Not mentioned	Not mentioned
Jaiklom et al. (2013) [93]	Cylindrical tank with inclined side entry jet	SKE	SIMPLE / Standard for pressure, SOU for momentum and tracer, and FOU for turbulence quantities	Not mentioned	Not mentioned

Table 3.3 (continued)

Authors	Geometry	Turbulence models	P-V coupling scheme[a] / Interpolation scheme	Temporal discretization scheme / Time step size	Convergence criteria
Lee (2013) [107]	Jet mixing tanks with cooling coils	SKE	Not mentioned	Not mentioned	The equations were solved until the species concentrations of tank were reached at equilibrium concentration within 1% relative error.
Egedy et al. (2014) [108]	Jet mixer	k-epsilon	Not mentioned	Not mentioned	Not mentioned
Bumrungthaichai chan et al. (2016) [109]	Cylindrical tank with inclined side entry jet	SKE	SIMPLE / Standard for pressure, SOU for all variables	First order implicit (FOI) / 0.0025 s	Residual < 10^{-5}

[a] P-V coupling scheme denotes pressure-velocity coupling scheme.

Moreover, there are other previous works of different jet agitated systems, which used CFD to study circulating jet mixing tank [110, 111], water storage tank [112, 113], impinging jet mixer [114], service reservoir [115], in-line multi-jet in ozone contactors [116], lime slurry pond [117], large-scale crude-oil tank [118], and model anaerobic digester [119].

From the previous literatures, the summary for CFD simulations of jet mixing tanks can be drawn as follows:

- Most researchers used finite volume method, including in house CFD code and commercial CFD code, to simulate jet mixing tanks except Egedy et al. [108], who used the commercial finite element method CFD code to study the jet mixer.

- The various grid topologies, such as hexahedral grid, tetrahedral grid, etc., can be adopted to discrete the domain of jet mixing tanks.

- The SKE and RNGKE were the suitable turbulence models for inclined side entry jet mixing tank [71, 72] and side entry jet mixing tank [101] simulations, while the RSM and LES were appropriate to simulate axial jet mixing tanks [98].

- The SIMPLE algorithm was commonly used as the pressure-velocity coupling scheme for CFD modeling of jet mixing tanks. Further, some researchers also used PISO algorithm to simulate jet mixed tanks.

- To obtain the accurate results, the higher order spatial discretization schemes, such as SOU, QUICK, etc. are recommended to simulate the jet mixing tanks.

- For temporal discretization scheme, FOI and SOI schemes were suitable for SKE and LES, respectively.

- The previous CFD work reported that the time step sizes of jet mixing tank simulations were typically achieved by trial and error method. Further, the appropriate length and velocity scales approach or Courant-Friedrichs-Lewy (CFL) condition approach [120] can also be used to select the proper time step sizes for jet mixing tank simulations.

- Most of previous researches showed that the residual for all variables and for energy should be less than 10^{-3} and 10^{-6}, respectively. Furthermore, the other monitors, e.g. the species concentrations, were also used to consider the solution convergence.

- For validation, the predicted overall mixing time and concentration profiles were commonly adopted to compare with experimental data. Moreover, the velocity and temperature profiles can also be used to analyze the model.

Furthermore, the shortfalls and limitations of CFD simulations can be drawn as follows:

- The previous works suggested that the SKE and RNGKE were the proper turbulence models for CFD simulations of inclined side entry jet mixing tank [71, 72] and side entry jet mixing tank [101], respectively. However, these models are inadequate for the turbulent round jet simulations [28].

- The exact inlet turbulence conditions are unavailable. These inlet conditions generally affect on the flow and mixing behavior inside the vessels.

- Many CFD works considered the converged solutions when the residuals reached the specified criterions. These criterions may not be sufficient if the residuals were still change. Generally, to obtain the converged results, the simulations should be performed until the residuals and other convergence monitors are no longer change [2].

- The previous predicted concentration profiles were not in good agreement with experimental data. Up until today, there have been only a few attempts toward the accuracy improvement of concentration profile predictions. Further, the sources of this discrepancy are not clearly represented.

So, in this thesis, these shortfalls and limitations were addressed to obtain the more comprehensive CFD model of inclined side entry jet mixing tank. Further, the jet mixing tanks with different non-circular jet nozzles were also numerically studied.

CHAPTER IV

CFD MODELING OF JET MIXING TANKS

Chapter IV shows the considered pump-around jet mixing tank system. The descriptions of CFD modeling, including grid generation, model assumptions, numerical solution technique, governing equations, material properties, boundary conditions, numerical methods, and solution strategy, are also demonstrated. Further, the selected turbulence model and numerical methods are tested by comparing with the other CFD setups and previous experimental work to show fidelity of this model.

4.1 Considered jet mixing tank system

The primary considered jet mixing tank system of this thesis was an open 45° inclined side entry pump-around jet mixing tank reported by Patwardhan [74], which used concentration tracer technique to determine the mixing time by adding the dilute solution of sodium chloride (NaCl), because it exhibited the shortest mixing time as comparing with the other jet nozzle angles. Moreover, for CFD simulations, the concentration tracer technique is more reasonable than the temperature tracer technique to assume that the properties of primary liquid and tracer are identical because the difference in properties between these liquids for concentration technique is less than that obtained by the temperature tracer technique. For example, in concentration tracer technique, the kinematic viscosity of water and 0.1 molar NaCl solution at 25 °C respectively are 8.937×10^{-7} $m^2 \cdot s^{-1}$ [121] and 8.981×10^{-7} $m^2 \cdot s^{-1}$ [122], whereas, the kinematic viscosity of water at 25 °C and water at 80 °C (tracer) for temperature tracer technique are 8.937×10^{-7} $m^2 \cdot s^{-1}$ and 3.653×10^{-7} $m^2 \cdot s^{-1}$, respectively [121].

In experiment of Patwarhdhan [74], the flat bottom cylindrical tank with a diameter of 0.5 m was filled with the tap water to the height of 0.5 m (H/D =1). The dilute sodium chloride (NaCl) solution was used as a tracer, which was rapidly added at the center of the top liquid-surface with the help of a beaker. The conductivity was measured and recorded at four different locations by using four conductivity probes. Then, the mixing time was determined by considering the time taken for the

conductivity to reach the 95% of the fully mixed value. Moreover, the overall mixing time was evaluated by using the arithmetic average of the mixing times obtained by the four measuring probes. The geometrical dimensions and schematic of an open inclined side entry pump-around jet mixing tank are given in Table 4.1 and Figure 4.1, respectively.

Table 4.1 Geometrical dimensions of the tested jet mixing tank

Detail	Dimension	Dimension/D
Tank diameter (D)	0.5 m	1
Liquid height (H)	0.5 m	1
Outlet pipe diameter (d_o)	0.0381 m	0.0762
Outlet pipe height (h_o)	0.05 m	0.1
Nozzle diameter (d_j)	0.008 m	0.016
Nozzle angle (θ)	45°	-

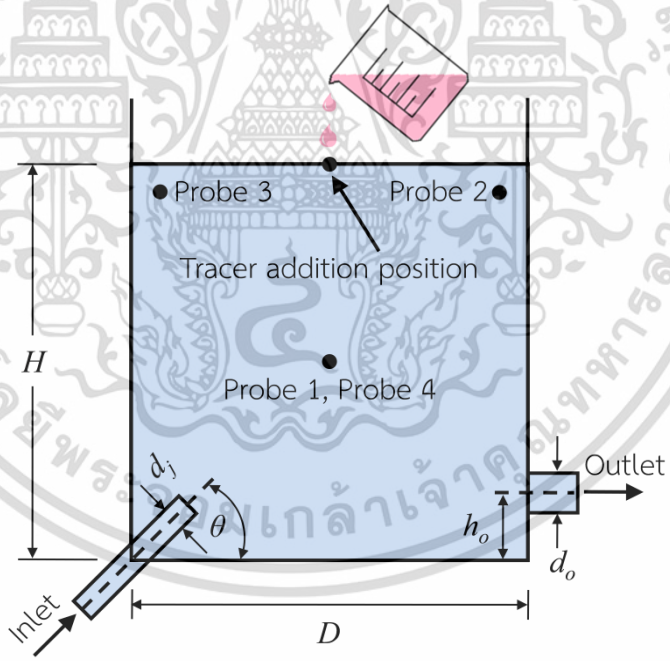

(a)

Figure 4.1 Schematics of (a) inclined side entry pump-around jet mixing tank (side view) (b) inclined side entry pump-around jet mixing tank (top view) (c) coordinate systems: x, y, z for tank coordinate system; x_j, y_j, z_j for jet nozzle coordinate system; r_1, r_2, s for jet streamwise coordinate system, Adapted from Bumrungthaichaichan et al. (J. Chin. Inst. Eng. 41(7) (2018) 612-621) with permission from Journal of the Chinese Institute of Engineers

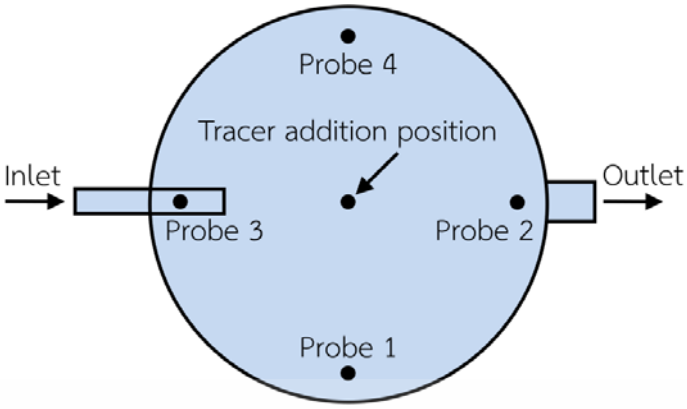

(b)

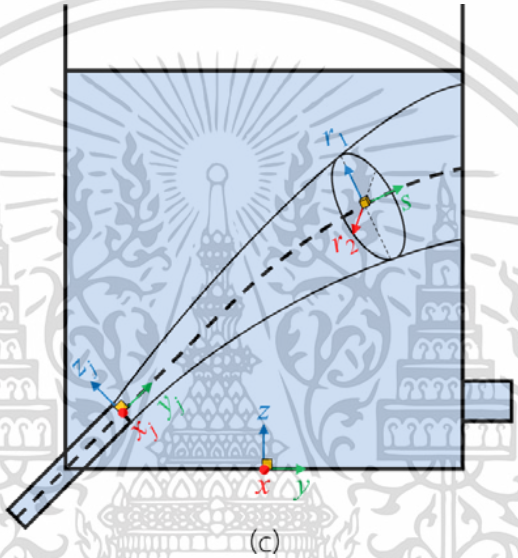

(c)

Figure 4.1 (continued)

4.2 Grid generation

As mentioned in section 3.7, the two different grid topologies, including tetrahedron [70-72, 77, 96, 97] and hexahedron [93, 95, 109, 123, 124], can be generated inside the inclined side entry jet mixing tanks. Generally, in order to obtain the high calculation stability and accurate results, the hexahedral grid topology is recommended [27]. However, this grid topology is loose its advantages when there is no dominant flow direction and/or the grid generation is not aligned to the flow direction. Hence, in order to retain the advantages of hexahedral grid, the researchers should be carefully performed grid generation.

In this thesis, the three-dimensional solid modeling and grid generation of inclined side entry pump-around jet mixing tanks were performed by using GAMBIT

2.4.6. The jet discharge velocity profile was uniform, so the computational domain was simplified by eliminating the jet nozzle pipe. Further, to achieve the accurate predicted results, the hexahedral grids were carefully generated inside the computational flow domain with the help of the domain decomposition concept, which is a method that splits the domain into the several blocks. However, the domain decomposition facility in GAMBIT is unavailable unlike the modern grid generators, e.g. ANSYS ICEM CFD, etc. In order to use this function in GAMBIT, the volume of the computational flow domain should be split by using the several faces, which are manually specified by user. The domain decomposition and grid generation of 45° inclined side entry pump-around jet mixing tank are shown in Figures 4.2 and 4.3, respectively.

Figure 4.2 Domain decomposition of an open 45° inclined side entry pump-around jet mixing tank (59 volumes)

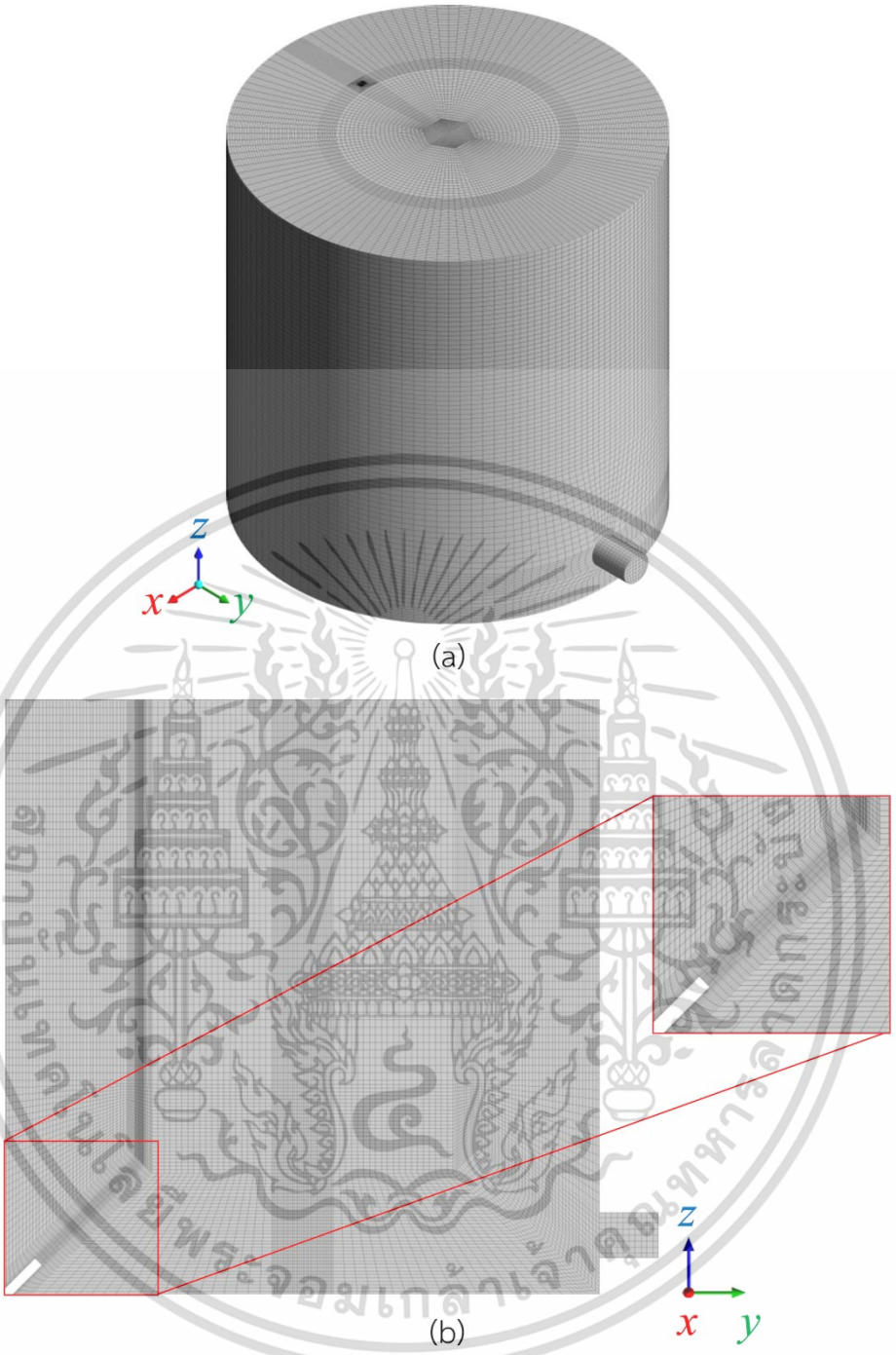

Figure 4.3 Grid generation of an open 45° inclined side entry pump-around jet mixing tank: (a) surface grid (b) grid at plane x=0, Adapted from Bumrungthaichaichan et al. (J. Chin. Inst. Eng. 41(7) (2018) 612-621) with permission from Journal of the Chinese Institute of Engineers

4.3 Model assumptions

In this thesis, the model was developed by using the assumptions as follows:

- The liquid flow inside the vessel was assumed to be steady state because the jet mixing time was investigated after the developed liquid flow pattern inside the vessel was achieved.

- The properties of water and tracer were identical because the concentration of tracer was dilute.

- The top liquid-surface was assumed to be flat because the bulk mixing was mainly considered. Moreover, the primary goal of this assumption were to reduce the number of grids for predicting the top liquid-surface shape and computational time.

- The turbulence inside the tank was estimated by using the turbulence model because the mean flow properties are sufficient to describe the considered processes for engineering applications. Further, the turbulence model requires the short computational time and low computer performance.

4.4 Numerical solution technique

From section 3.7, most of previous CFD works used the finite volume method to simulate jet mixing tanks. For this CFD work, the ANSYS FLUENT commercial finite volume CFD code was also conducted to study the inclined side entry jet mixing tanks because of low memory usage, low computational time for various flow situations, the physical quantities conserve even on the coarse grids, etc. [2]. Furthermore, the pressure-based solver with double precision option was selected to simulate fluid flow and mixing inside the jet mixing tanks because it is suitable for a wide range of flow regimes from low speed incompressible flow to high-speed compressible flow [125].

4.5 Governing equations for jet mixing tank simulation

In this thesis, the jet flow inside the mixing tank was turbulence because the jet Reynolds number was above about 1,000-2,000 [33] and the concentration tracer technique was adopted to investigate the mixing time. So, according to model assumptions, the governing equations of jet mixing tank simulation can be distinguished into three parts as follows:

4.5.1 Modeling of liquid flow

The liquid flow inside jet mixing tank is typically governed by the Reynolds-averaged equations for conservation of mass and momentum. For Cartesian coordinate, the Reynolds average equations for steady state incompressible fluid flow can be written as:

Continuity equation:

$$\frac{\partial \overline{u}}{\partial x}+\frac{\partial \overline{v}}{\partial y}+\frac{\partial \overline{w}}{\partial z}=0 \tag{4.1}$$

Reynolds equation in x-direction:

$$\rho\left(\frac{\partial \overline{u}^2}{\partial x}+\frac{\partial \overline{u}\overline{v}}{\partial y}+\frac{\partial \overline{u}\overline{w}}{\partial z}\right)=-\frac{\partial \overline{p}}{\partial x}+\mu_{eff}\left(\frac{\partial^2 \overline{u}}{\partial x^2}+\frac{\partial^2 \overline{u}}{\partial y^2}+\frac{\partial^2 \overline{u}}{\partial z^2}\right) \tag{4.2}$$

Reynolds equation in y-direction:

$$\rho\left(\frac{\partial \overline{v}\overline{u}}{\partial x}+\frac{\partial \overline{v}^2}{\partial y}+\frac{\partial \overline{v}\overline{w}}{\partial z}\right)=-\frac{\partial \overline{p}}{\partial y}+\mu_{eff}\left(\frac{\partial^2 \overline{v}}{\partial x^2}+\frac{\partial^2 \overline{v}}{\partial y^2}+\frac{\partial^2 \overline{v}}{\partial z^2}\right) \tag{4.3}$$

Reynolds equation in z-direction:

$$\rho\left(\frac{\partial \overline{w}\overline{u}}{\partial x}+\frac{\partial \overline{w}\overline{v}}{\partial y}+\frac{\partial \overline{w}^2}{\partial z}\right)=-\frac{\partial \overline{p}}{\partial z}+\mu_{eff}\left(\frac{\partial^2 \overline{w}}{\partial x^2}+\frac{\partial^2 \overline{w}}{\partial y^2}+\frac{\partial^2 \overline{w}}{\partial z^2}\right)+\rho g \tag{4.4}$$

4.5.2 Modeling of turbulence

As mentioned earlier, the standard k-epsilon model (SKE) was a suitable turbulence model to study the inclined side entry jet mixing tanks [71, 72]. However, there is an information that SKE is not suitable to study the turbulent round jet and the realizable k-epsilon model (RKE) is recommended to simulate this type of flow [28]. So, in this thesis, RKE was adopted to simulate the turbulence inside the inclined side entry pump-around jet mixing tanks. This model contains two extra transport equations, including transport equation of turbulence kinetic energy (k) and transport equation of dissipation rate of turbulence kinetic energy (ε). In general, k-transport equation and ε-transport equation of RKE for steady state flow can be written as shown in Equations (4.5) and (4.6), respectively [26]. Further, the model constants of RKE are represented in Table 4.2.

$$\frac{\partial(\rho\bar{u}_i k)}{\partial x_i} = \frac{\partial}{\partial x_j}\left[\left(\mu + \frac{\mu_t}{\sigma_k}\right)\frac{\partial k}{\partial x_j}\right] + G_k + G_b - \rho\varepsilon - Y_M \tag{4.5}$$

$$\begin{aligned}\frac{\partial(\rho\bar{u}_i \varepsilon)}{\partial x_i} &= \frac{\partial}{\partial x_j}\left[\left(\mu + \frac{\mu_t}{\sigma_\varepsilon}\right)\frac{\partial \varepsilon}{\partial x_j}\right] \\ &+ \rho C_1 S\varepsilon - \rho C_2 \frac{\varepsilon^2}{k + \sqrt{\nu\varepsilon}} + C_{1\varepsilon}\frac{\varepsilon}{k} C_{3\varepsilon} G_b\end{aligned} \tag{4.6}$$

Table 4.2 Model constants of RKE [26]

$C_{1\varepsilon}$	σ_k	σ_ε	C_1	C_2	C_μ
1.44	1.0	1.2	$\max\left[0.43, \frac{\eta}{\eta+5}\right]$	1.9	$\left[A_0 + A_S \frac{kU^*}{\varepsilon}\right]^{-1}$

4.5.3 Modeling of species transport

To obtain the tracer concentration distribution inside the jet mixing tanks, the species transport equations without chemical reaction was adopted. For this thesis, the species transport equations can be written as shown in Equation (4.7) [26].

$$\frac{\partial(\rho Y_i)}{\partial t} + \frac{\partial(\rho\bar{u}_i Y_i)}{\partial x_i} = \frac{\partial}{\partial x_j}\left(\left(\rho D_{i,m} + \frac{\mu_t}{\mathrm{Sc}_t}\right)\frac{\partial Y_i}{\partial x_j}\right) \tag{4.7}$$

where Y_i is the local mass fraction of species *i*, $D_{i,m}$ is the mass diffusion coefficient for species *i* in the mixture, Sc_t is the turbulent Schmidt number (ν_t/D_t where ν_t is the turbulent kinematic viscosity and D_t is the turbulent diffusivity), and μ_t is the turbulent viscosity.

4.6 Material properties

In this thesis, the working fluid and tracer were water and dilute solution of sodium chloride, respectively. The properties of tracer were assumed to be identical with the water properties because the sodium chloride solution was dilute. Hence, the self-diffusion coefficient of water, which is the average speed that a specific water molecule holds to diffuse in liquid water [126], was employed to simulate the jet mixing tanks. The necessary properties of these fluids can be summarized as shown in Table 4.3.

Table 4.3 Fluid properties used in simulations

Property	Value	Unit
Density	998.2	$kg \cdot m^{-3}$
Viscosity	0.001003	$kg \cdot m^{-1} \cdot s^{-1}$
Diffusion coefficient	2.3×10^{-9} [126-128]	$m^{2} \cdot s^{-1}$

4.7 Boundary conditions

For jet mixing tank simulations, there are four different boundaries, including inlet, outlet, top surface, and tank wall. The details of boundary conditions for these boundaries are described as follows:

4.7.1 Inlet

At inlet section, the velocity-inlet and recirculation-inlet boundary condition types were used to perform the steady state and unsteady state simulations, respectively. By default, in ANSYS FLUENT, the recirculation-inlet and recirculation-outlet boundary condition types are unavailable. However, these boundary condition types are enabled by respectively typing the two additional text commands in TUI [129], including (rpsetvar 'icepak? #t) and (models-changed). These boundary condition types are commonly used in the certain appliances which the fluid is recirculated into the domain from the outlet section, such as car HVAC systems, laboratory clean rooms, etc. In similar fashion, for pump-around jet mixing tank, the liquid flows through the outlet section and the pump, which is adopted to generate the high velocity liquid jet. Then, the high velocity liquid jet discharges through a nozzle into the tank. Finally, the high velocity jet entrains the surrounding liquid and creates the liquid circulation and mixing inside the vessel.

For inlet, all variables need to be imposed at the boundary. According to the previous work of Patwardhan [74], the jet discharge velocity of 4.4 $m \cdot s^{-1}$ was defined at inlet section. For turbulence boundary conditions, the k and epsilon specification method was adopted. Due to the absence of exact inlet turbulence conditions, the different turbulence estimation correlations were studied to achieve the appropriate conditions for pump-around jet mixing tank simulation. The descriptions of these turbulence conditions are demonstrated in chapter VI.

4.7.2 Outlet

At outlet boundary, the pressure-outlet boundary condition type was used for steady state simulation. The zero pressure gauge was specified. Moreover, the turbulence intensity and hydraulic diameter (D_h) specification method was adopted to specified turbulence boundary conditions (I = 5% and D_h = 0.0381 m).

In unsteady state simulation, the recirculation-outlet boundary condition type was adopted. Then, the mass flow rate, which corresponds to the inlet mass flow rate, was only specified (≈ 0.22 kg·s^{-1}).

4.7.3 Top surface

The top liquid-surface was assumed to be flat because the experiments showed that the liquid interface was flat for low jet velocities and low jet angles [74]. Further, this assumption was commonly used to study the bulk mixing processes inside the mixing tanks as reported by the previous CFD works of jet agitated tanks [95, 98] and stirred tanks [130, 131]. The main objective of this assumption was to obtain the computational convenience. A prediction of liquid-surface shape requires enormous number of grids and unsteady state simulation, that would be very time consuming.

For flat liquid-surface assumption, the symmetry boundary condition type was imposed at the top liquid-surface boundary. The normal velocity and normal gradient of all variables at symmetry boundary were zero.

4.7.4 Tank wall

At the tank walls, including side wall and tank base, the no-slip boundary condition was adopted. Generally, in viscous flow, the wall and tangential velocity of fluid are identical. Further, the normal fluid velocity is zero. For this considered system, there is no wall velocity. So, all velocity components were set to be zero.

4.8 Numerical methods

The pressure-velocity coupling scheme for this thesis was SIMPLE. The discretization scheme of pressure was standard. Further, the second order upwind (SOU) spatial discretization scheme was employed for all variables, including

momentum, turbulence quantities, and tracer. For unsteady state simulation, the temporal discretization scheme was first order implicit (FOI).

4.9 Mixing time investigation

In this thesis, the mixing time was evaluated by using the tracer concentration technique. The tracer with mass fraction of unity was patched at 0.03 m below the center of top liquid-surface to account the experimental observation that the tracer slightly moved downward during the tracer addition, which was added into the tank with the help of a beaker [74]. This tracer specification was an initial condition for unsteady state simulation. Then, Equation (4.7) was iteratively solved. During the unsteady state simulation, the time histories of tracer concentration for four different probes were monitored and recorded. The mixing times for four different probes were individually evaluated by considering the 95% mixing time ($t_{95\%}$), which can be considered as the time required for the concentration (c) to reach within 95% of the fully mixed concentration ($\bar{c}$). This 95% mixing time can be generally written as shown in Equation (4.8)

$$t_{95\%} = \text{time for} \left| \frac{c - \bar{c}}{\bar{c}} \right| \leq 0.05 \tag{4.8}$$

Then, the overall mixing time of the jet mixing tank was calculated by using arithmetic average of the 95% mixing times achieved by four different probes. Further, the locations of four different probes are summarized as shown in Table 4.4.

Table 4.4 Probe locations

Probe	Location in tank coordinate system [mm]		
	x	y	z
1	237.5	0	250
2	0	237.5	450
3	0	-237.5	450
4	-237.5	0	250

4.10 Solution strategy

The simulation was distinguished into two parts. First, the steady state simulation was adopted to achieve the steady state flow pattern of water jet. Second, the concentration distribution inside the vessel was obtained by using unsteady state simulation.

For steady state simulations of water jet flow pattern, the transport equations for flow and turbulence were calculated. The solution convergence was considered by monitoring the area weight average of velocity magnitude for two different planes, including outlet and plane x = 0. The converged solutions were achieved when the average values of the velocity magnitude for these planes were constant or exhibited the small variation.

Moreover, for unsteady state simulations of tracer distribution, the transport equation of tracer was only solved by using the segregated implicit solver (FOI). For implicit solver, there is no stability criterion (i.e. Courant number), which is used to evaluate the time step size (Δt) [132]. However, ANSYS FLUENT suggested that the time step size for transient simulation should be one order of magnitude less than the smallest time constant in the considered system [31]. For example, from previous CFD works of cyclone separator, the average residence time (cyclone volume/gas volumetric flow rate) was widely adopted to estimate the time step size [133-135]. In similar fashion, the average residence time, which was defined as the ratio of the mixing tank volume (V) to the volumetric flow rate of jet discharge (Q), was also employed to estimate the time step size for jet mixing tank simulations. In this work, the residence time of the simulated jet mixing tanks was 445 s and the used time step size was 0.0025 s. This specified time step size was five order of magnitude lower than the residence time. Moreover, this time step size was also lower than that calculated by the appropriate length and velocity scale approach (≈ 0.0074 s) [2]. Hence, this time step size was sufficient to achieve the accurate concentration distribution inside the jet mixing tank. For convergence criterion, the scaled residual of 10^{-5} was used.

4.11 Reliability of the present CFD model

In this thesis, the present jet mixing tank model was carefully constructed by considering the previous literatures and using the personal experience. Thus, in order to ensure that this CFD model was developed properly, the different k-epsilon turbulence models and numerical methods were simulated and compared with the present CFD model and previous experimental data of Patwardhan [74]. These CFD models were simulated by using jet discharge velocity of 4.4 $m \cdot s^{-1}$, turbulence kinetic energy of 0.2904 $m^2 \cdot s^{-2}$, and turbulence kinetic energy dissipation rate of 22.35614 $m^2 \cdot s^{-3}$. The details of these CFD models and their computational times are shown in Table 4.5.

Table 4.5 Details of turbulence model, numerical methods, and computational time for different simulations

Case	Turbulence model	P-V coupling scheme	Discretization scheme		Computational time [h][a]
			Spatial	Temporal	
PM1[b]	RKE	SIMPLE	SOU	FOI	39.77
TM1	SKE	SIMPLE	SOU	FOI	39.58
TM2	RNGKE	SIMPLE	SOU	FOI	43.23
NM1	RKE	PISO	SOU	FOI	39.85
NM2	RKE	SIMPLE	FOU	FOI	28.45
NM3	RKE	SIMPLE	QUICK	FOI	43.87
NM4	RKE	SIMPLE	SOU	SOI	39.83

[a] The computational time is the time required for performing the steady state and transient simulations.

[b] PM1 is a present CFD model.

Before analyzing the CFD results, the converged solutions should be achieved. Hence, the convergence histories should be firstly considered. So, the residuals and other convergence monitors of steady state simulation were recorded as shown in Figure 4.4. For transient simulation, the predicted normalized concentration profiles for different residuals, including 10^{-4}, 10^{-5}, and 10^{-6}, were compared as represented in Figure 4.5 to confirm that the residual of 10^{-5} presents the converged results.

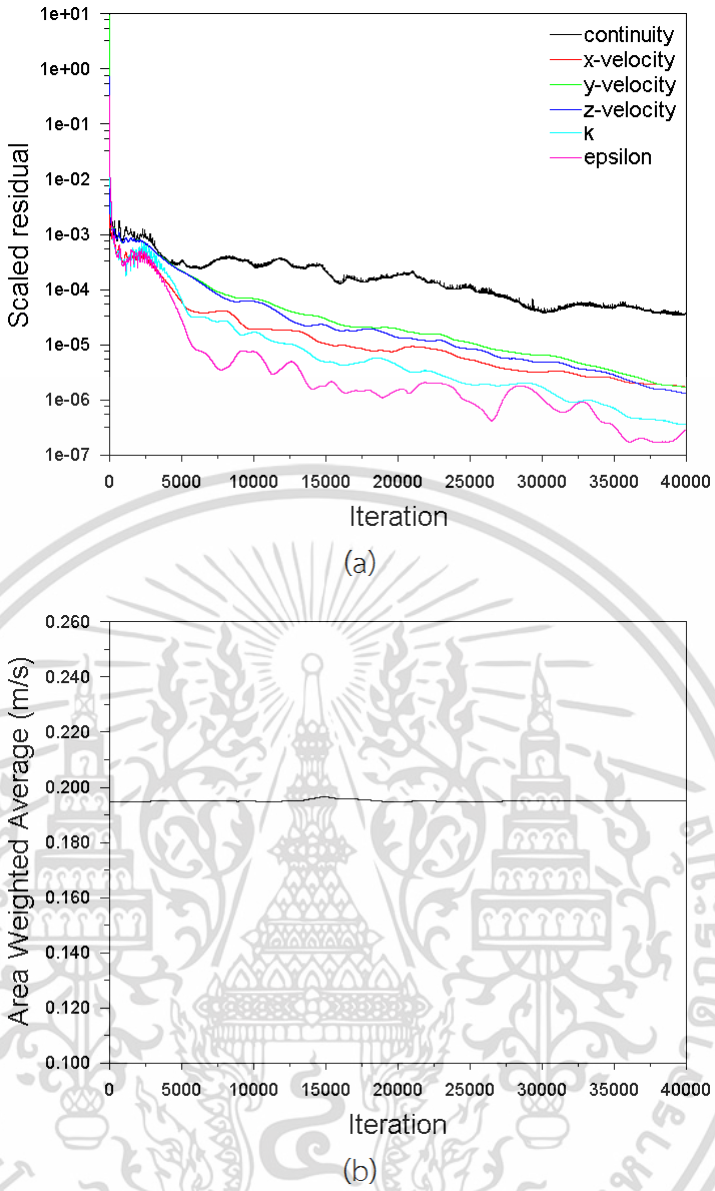

Figure 4.4 Convergence histories of steady state simulation for finest grid resolution of an open 45° inclined side entry jet mixing tank (U_j = 4.4 m·s^{-1} and I = 10%): (a) scaled residuals (b) area weighted average of velocity at outlet (c) area weighted average of velocity at plane x = 0

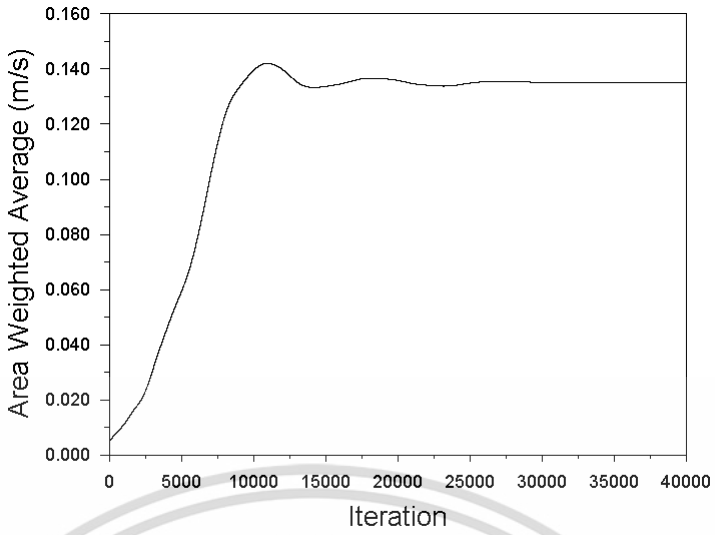

(c)

Figure 4.4 (continued)

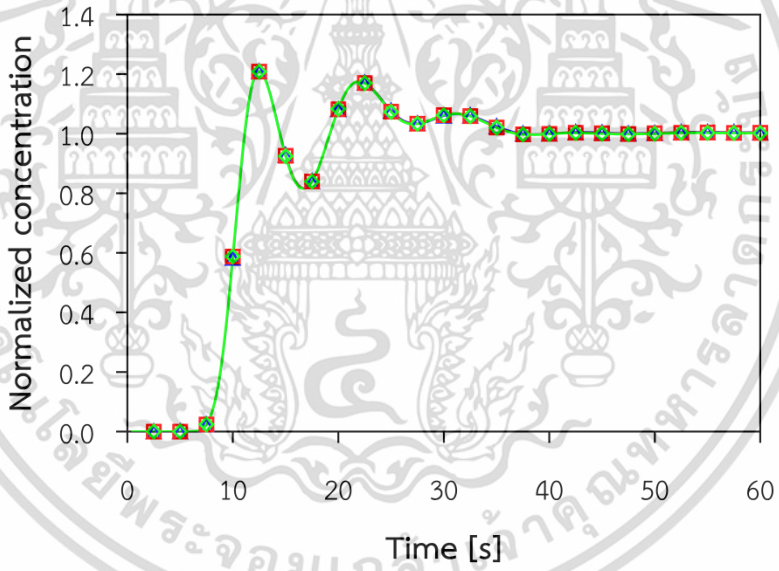

Figure 4.5 Normalized concentration profiles at probe 1 for different residuals: 10^{-4}; 10^{-5}; 10^{-6}

In Figure 4.4, it can be observed that the scaled residuals of all quantities rapidly fall down and reach the values of 10^{-3} within 2,900 iterations as depicted in Figure 4.4(a). Then, all scaled residuals are oscillatory decreasing and meet the values of 10^{-4} after 26,500 iterations. Furthermore, the area weight average values of velocity magnitude at outlet and plane x = 0 are constant after 30,000 iterations as shown in Figures 4.4(b) and 4.4(c), respectively. These observations indicate that the iterative convergence is achieved. Hence, the simulated solutions can be considered

as the converged results. This preliminary simulation indicates that the convergence criterion with a scaled residual of 10^{-3}, which was suggested by previous works, is insufficient to use as the criterion for steady state simulation. Thus, in order to consider and obtain the converged results, the simulations should be performed until the scaled residuals and other convergence monitors are no longer change.

Moreover, for unsteady state simulation, the results reveal that the predicted normalized concentration profiles of probe 1 for different residuals are similar as depicted in Figure 4.5. According to these results, it can be summarized that the suggested residual of 10^{-5} is sufficient to use as the convergence criterion and to achieve the converged results for mixing time investigation.

After the convergence criteria for steady state and transient simulations were confirmed, all simulations were performed by using these suggested criteria. Then, the overall mixing times and profiles of normalized concentration, which is defined as the ratio of the tracer concentration to the fully mixed value, predicted by different CFD models as expressed in Table 4.5 were compared to the experimental data of Patwardhan [74] as shown in Table 4.6 and Figure 4.6, respectively.

Table 4.6 Mixing times for different CFD models

Case	Mixing time [s]					% Error[a]
	Probe 1	Probe 2	Probe 3	Probe 4	Overall	
Experiment [74]	38.5000	37.7000	N/A	N/A	31.0000	-
PM1	33.1779	29.5401	27.3008	22.7423	28.1903	9.06
TM1	21.4033	22.8855	28.9077	21.4038	23.6501	23.71
TM2	29.3764	30.9891	29.6687	27.5838	29.4045	5.15
NM1	33.1779	29.5401	27.3008	22.7423	28.1903	9.06
NM2	31.9522	29.4013	26.3567	31.8529	29.8908	3.58
NM3	32.4339	29.4551	27.1993	22.6358	27.9310	9.90
NM4	33.2556	29.5879	27.3138	22.7207	28.2195	8.97

[a] The percentage error is a ratio of absolute difference between the predicted overall mixing time and experimental mixing time to the experimental value.

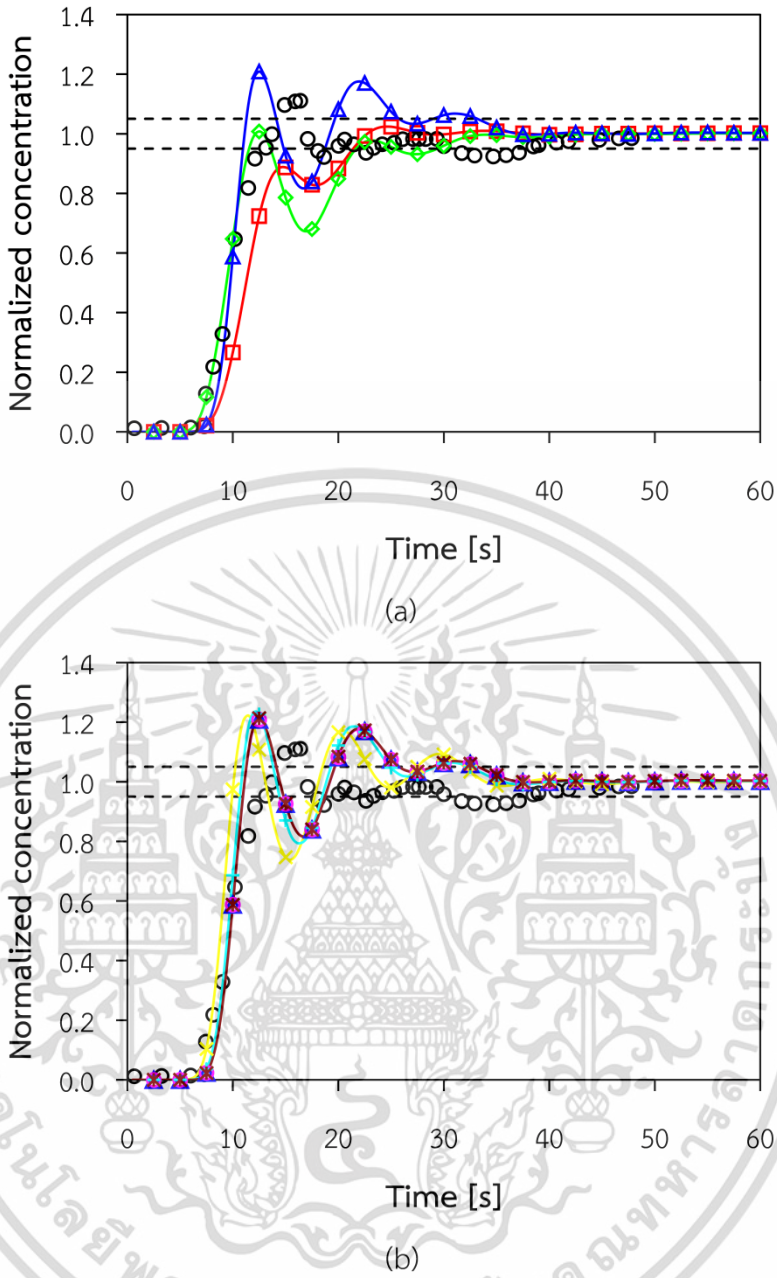

Figure 4.6 Comparison of normalized concentration profiles between present CFD simulations and previous work of Patwardhan [74] for (a) different k-epsilon turbulence models and (b) different numerical methods: PM1; TM1; TM2; NM1; NM2; NM3; NM4; Experiment [74], Adapted from Bumrungthaichaichan and Wattananusorn (J. Chin. Inst. Eng. 42(5) (2019) 428-437) with permission from Journal of the Chinese Institute of Engineers

From Table 4.6, the results showed that the predicted mixing times and overall mixing times of these CFD models are lower than the experimental data of Patwardhan [74]. The reasons of the underprediction in overall mixing times are

clearly described in Chapter VI. TM1 case predicts the shortest overall mixing time with the maximum percentage error of 23.71%. Whereas, NM2 case show the highest predicted overall mixing, which corresponds to the minimum percentage error of 3.58%. Moreover, the predicted overall mixing times of other cases are slightly different (percentage errors of about 5-10%).

Figure 4.6(a) shows the comparison of the normalized concentration profiles at probe 1 of three different k-epsilon models. It can be seen that the start of normalized concentration profiles of these models are slightly different. However, the first peak value of normalized concentration profile for PM1 case is highest, and followed by TM2 and TM1 cases, respectively. Meaning that, the decays of first peak values of predicted normalized concentration profiles for two latter cases are faster than those obtained by PM1 case and previous experimental data because TM1 and TM2 cases overpredict the turbulence dispersion levels. That is, TM1 case shows the highest volume-weighted average value of predicted turbulence diffusivity (3.97×10^{-4} $m^2 \cdot s^{-1}$) and respectively followed by TM2 (3.60×10^{-4} $m^2 \cdot s^{-1}$) and PM1 (2.87×10^{-4} $m^2 \cdot s^{-1}$). Finally, at the large times, all simulated normalized concentration profiles approach the measured data.

From Figure 4.6(b), the results show that the values of first peak of the predicted normalized concentration profiles for different numerical methods are slightly different and are higher than experimental data. Further, the start of normalized concentration profiles are slightly different, except the profile of NM2 case, which is slightly faster than other models. For the large times, all simulated profiles are in good agreement with the experimental data. Further, the jet streamwise velocity contours at plane x_j = 0 of all simulations were compared as depicted in Figure 4.7 to confirm that the present CFD model was properly selected.

In Figure 4.7, for comparison of three different k-epsilon turbulence models, the simulated results show that the TM2 case represents the widest jet spreading and respectively followed by TM1 and PM1 cases. The centerline velocity decay of TM2 case is faster than those predicted by PM1 and TM1 cases and the decay of centerline velocities of two latter cases are slightly different. Further, the decay of centerline velocity of PM1 case is in good agreement with experimental data of Fellouah et al. [40] as later reported in Chapter VI. It can be implied that the centerline velocity decay of TM1 case should be also similar to the experiment. Hence, the shortest overall mixing time obtained by TM1 case as shown in Table 4.6

is caused by the highest convective transport due to the wider jet spreading with normal decay of centerline velocity.

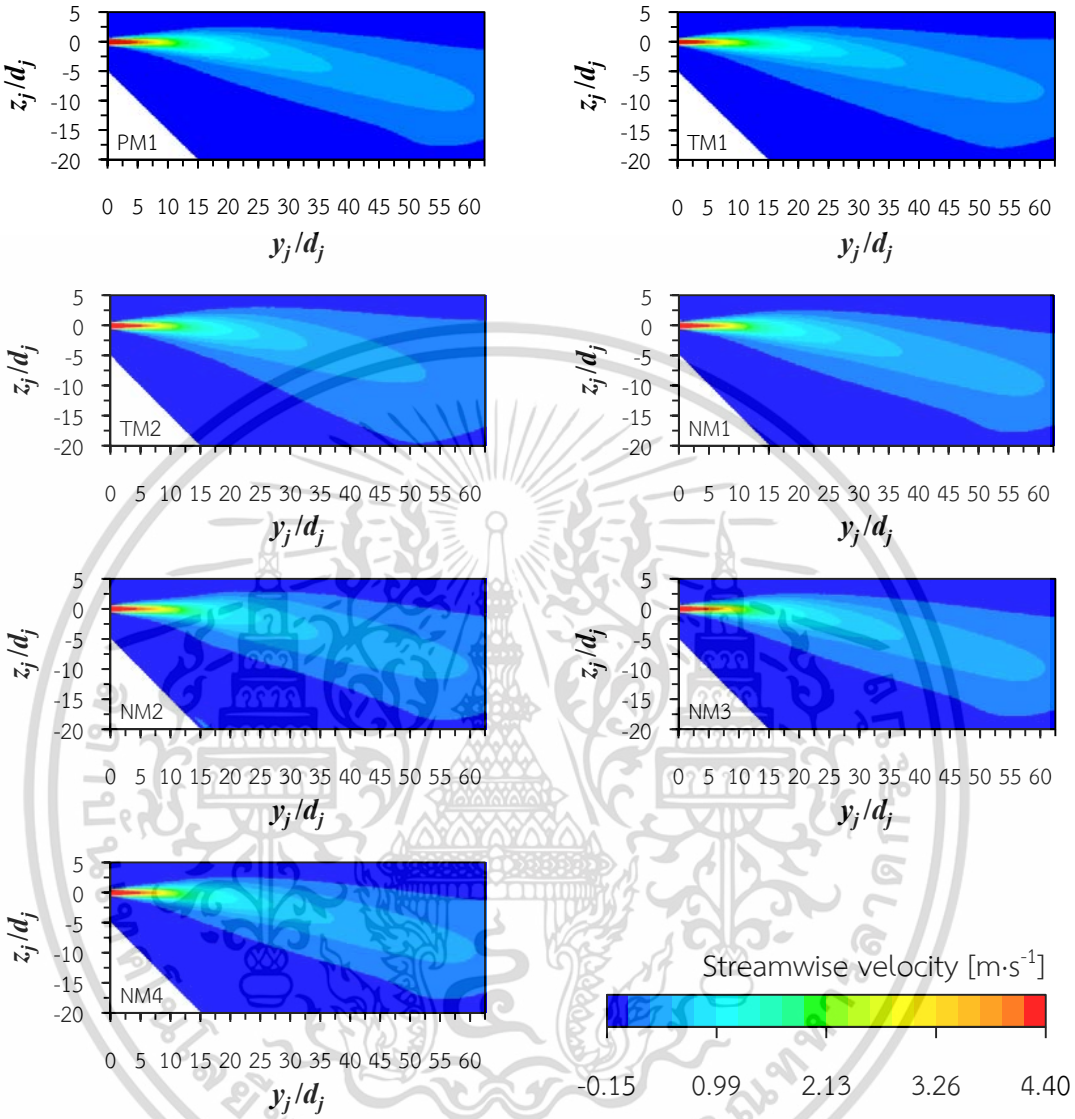

Figure 4.7 Jet streamwise velocity contours at plane x_j = 0 for different cases, Adapted from Bumrungthaichaichan and Wattananusorn (J. Chin. Inst. Eng. 42(5) (2019) 428-437) with permission from Journal of the Chinese Institute of Engineers

These results agree with the facts that the SKE overpredicts the spreading of round jet [136] and RNGKE is not suitable for simulating the turbulent round jet [28]. However, the present predicted results contradict the previous CFD works that SKE [71, 72] and RNGKE [77, 101] were suitable for predicting the jet mixing vessels. The discrepancy in results and suggestions between this thesis and other CFD works would be due to the reason that the smaller number of tetrahedral grids used in previous CFD works (< 1,000,000 cells) may not sufficient to obtain the correct

results. So, it can be seen that RKE is a suitable turbulence model for CFD simulation of pump-around jet mixing tank. Furthermore, the main reason for using the RKE for pump-around jet mixing tank simulation is that this model ensures the positivity of normal stresses and Schwarz's inequality [137, 138].

For comparison of different numerical methods, the results show that the streamwise velocity of NM2 case tends to be smeared out at y_j/d_j of about 12 as comparing with the other numerical setups because FOU shows the incorrect solutions when the flow is not aligned with the grids [3]. Although the NM1, NM3, and NM4 cases respectively employed the suitable pressure-velocity coupling scheme for unsteady state simulation (PISO), higher order spatial discretization scheme (QUICK), and higher temporal discretization scheme (SOI) to simulate jet mixing tanks, however, the results of these cases are similar to those obtained by PM1 case because the hexahedral grids were properly generated and aligned with the flow direction to minimize the numerical errors [27]. Furthermore, the computational time of NM1, NM3, and NM4 cases are higher than PM1 case as reported in Table 4.5.

When these results are viewed together, the results confirmed that the PM1 case is the suitable CFD model for simulating an open 45° inclined side entry pump-around jet mixing tank because of its accuracy and time efficiency.

CHAPTER V

PRELIMINARY CFD ANALYSIS OF JET MIXING TANKS

Chapter V represents the grid independency test and model validation of an open 45° inclined side entry pump-around jet mixing tank. In addition, the details of grid convergence index, which is commonly used to measure grid convergence, for jet mixing tank modeling are also demonstrated.

5.1 Grid independence study

In this thesis, the grid independence study of jet mixing tank model has been investigated with the help of grid adaption facility of ANSYS FLUENT. The grid adaption technique was adopted to reduce the computational requirements, e.g. number of grids, memory, computational time, etc. ANSYS FLUENT reported that the gradient adaption of velocity is appropriate for incompressible fluid flow [31]. The refine threshold for grid adaption should be 10% of the maximum gradient of the considered variable, e.g. velocity, temperature, etc. [139]. Thus, 10% of the maximum velocity magnitude gradient was used for grid adaption. Moreover, in order to ensure that the grids were properly adapted, the grid adaption was individually performed for different cases because the different conditions may produce the different phenomena, e.g. jet potential core, jet spreading, etc.

The grid independency of an open 45° inclined side entry pump-around jet mixing tank with jet discharge velocity of 4.4 $m \cdot s^{-1}$ was tested by comparing the simulated potential cores and overall mixing times of four different grid levels. The potential core and mixing time were employed as the key parameters for steady state and transient simulations, respectively. The results of grid independence study are represented in Table 5.1.

From Table 5.1, the values of percentage difference for potential core and mixing time are found to decrease with increasing the number of grids. The percentage difference achieved from the fine grid level (2-adapted-grid) and finest grid level (3-adapted-grid) is less than 1% for potential core and mixing time. These results indicate that the fine grid level sufficiently provides the grid independency.

However, for jet potential core, the coarsest grid level (0-adapted-grid) exhibits the highest percentage difference (40.14%). Thus, the grid convergence should be confirmed by using the concept of grid convergence index.

Table 5.1 Details of grid independence study of an open 45° inclined side entry jet mixing tank (U_j = 4.4 m·s^{-1} and I = 10%)

Grid	Number of cells	Potential core[a]		Mixing time [s]	
		s/d_j	% Difference[b]	Value	% Difference[b]
0-adapted-grid[c]	1,087,312	1.5042	40.14	29.6918	5.33
1-adapted-grid	1,184,437	2.0054	20.20	29.7257	5.45
2-adapted-grid	1,486,046	2.5065	0.26	28.3658	0.62
3-adapted-grid	1,739,978	2.5130	-	28.1903	-

[a] The potential core is a region where the mean centerline streamwise velocity is equal to jet discharge velocity, which is generally observed within $0 \leq s/d_j \leq 6$, where s is a longitudinal distance or jet streamwise distance from nozzle exit and d_j is a jet nozzle diameter.

[b] The percentage difference is a ratio of absolute difference between the values of potential core or mixing time for any grid and finest grid to the finest grid value.

[c] 0-adapted grid is an original grid generated by GAMBIT.

5.2 Grid convergence index

Grid convergence index (GCI) is a quantitative measurement of grid convergence suggested by Roache [140-142]. GCI can be evaluated by considering two different grid levels. However, three different grid levels or more are recommended. Three grid levels can also be employed to confirm that the solutions are within the asymptotic range of convergence [143]. The comprehensive procedure of GCI and GCI of 45° inclined side entry pump-around jet mixing tank simulation are represented as follows:

5.2.1 Procedure of GCI

The recommended procedure of GCI can be described below.

Step 1. Define a representative grid size (h), which is employed to determine the refinement factor in step 2. The representative grid size for two-

dimensional domain and three-dimensional domain can be calculated by using Equations (5.1) and (5.2), respectively.

$$h = \left[\frac{1}{N} \sum_{n=1}^{N} \left(\Delta A_n \right) \right]^{1/2} \tag{5.1}$$

$$h = \left[\frac{1}{N} \sum_{n=1}^{N} \left(\Delta V_n \right) \right]^{1/3} \tag{5.2}$$

where N is the total number of computational cells.

ΔA_n is the area of the *n*-th cell.

ΔV_n is the volume of the *n*-th cell.

Step 2. Evaluate the refinement factor (r) by using Equation (5.3).

$$r = \frac{h_{coarse}}{h_{fine}} \tag{5.3}$$

For complicated geometries, r is replaced by the ratio of the number of control volumes in the fine and coarse meshes. For example, for two-dimensional domains,

$$r = \left(\frac{N_{fine}}{N_{coarse}} \right)^{1/2} \quad \text{or} \quad r_{i+1,i} = \left(\frac{N_i}{N_{i+1}} \right)^{1/2} \tag{5.4}$$

For three-dimensional domains,

$$r = \left(\frac{N_{fine}}{N_{coarse}} \right)^{1/3} \quad \text{or} \quad r_{i+1,i} = \left(\frac{N_i}{N_{i+1}} \right)^{1/3} \tag{5.5}$$

where i indicates the finer grid level.

i+1 indicates the coarser grid level.

Step 3. Calculate the difference in numerical solutions (ε) and relative error of numerical solutions (e) by using Equations (5.6) and (5.7), respectively.

$$\varepsilon_{i+1,i} = f_{i+1} - f_i \tag{5.6}$$

$$e_{i+1,i} = \frac{f_{i+1} - f_i}{f_i} \tag{5.7}$$

where f is the value of key variable.

Step 4. Determine the order of the discretization method (p) by using Equation (5.8).

$$p = \frac{1}{\ln(r_{21})} \times \left| \ln\left[\left| \frac{\varepsilon_{32}}{\varepsilon_{21}} \right| \times \left(\frac{r_{21}^{p} - \mathrm{sgn}(\varepsilon_{32}/\varepsilon_{21})}{r_{32}^{p} - \mathrm{sgn}(\varepsilon_{32}/\varepsilon_{21})} \right) \right] \right| \tag{5.8}$$

where sgn is a sign function ($\mathrm{sgn}(x) = \begin{cases} -1 & \text{if } x < 0 \\ 0 & \text{if } x = 0 \\ 1 & \text{if } x > 0 \end{cases}$).

In order to achieve the value of p, the iterative method with relaxation factor as suggested by Roache [141, 142] is adopted. So, the value of p is computed by using Equation (5.9).

$$p = \omega\rho + (1-\omega)\frac{|\ln\beta|}{\ln(r_{21})} \tag{5.9}$$

where ω is a relaxation factor (ω = 0.5).

ρ is the previous iteration of p (The initial guess value is $\rho = \frac{1}{\ln(r_{21})}\left|\ln\left|\frac{\varepsilon_{32}}{\varepsilon_{21}}\right|\right|$).

$$\beta = \left| \frac{\varepsilon_{32}}{\varepsilon_{21}} \right| \times \left(\frac{r_{21}^{p} - \mathrm{sgn}(\varepsilon_{32}/\varepsilon_{21})}{r_{32}^{p} - \mathrm{sgn}(\varepsilon_{32}/\varepsilon_{21})} \right)$$

The iterative process of p value evaluation will stop when $\left|\frac{p-\rho}{p}\right| < 10^{-5}$.

Step 5. Calculate the GCI by using Equation (5.10).

$$\mathrm{GCI}_{i+1,i}^{fine} = \frac{F_s \left| e_{i+1,i} \right|}{r_{i+1,i}^{p} - 1} \tag{5.10}$$

where F_s is a safety factor (F_s = 3 for comparison of two grid levels and 1.25 for comparison of three grid levels or more)

Step 6. Identify the asymptotic range of convergence and evaluate the convergence ratio and exact value of key parameter. The descriptions of these parameters are represented as follows:

Asymptotic range of convergence can be determined by using Equation (5.11).

$$\alpha = \frac{r_{i+1,i}^{p}\mathrm{GCI}_{i+1,i}^{fine}}{\mathrm{GCI}_{i+2,i+1}^{fine}} \tag{5.11}$$

The solutions are in asymptotic range if the values of α are approximately unity.

The convergence ratio (R) is typically obtained by Equation (5.12).

$$R = \frac{e_{i+1,i}}{e_{i+2,i+1}} \tag{5.12}$$

This ratio is commonly used to indicate the convergence condition. Generally, there are three possible convergence conditions as reported by Ali et al. [144], which are represented as follows:

- Monotonic convergence ($0 < R < 1$)

- Oscillatory convergence ($R < 0$)

- Divergence ($R > 1$)

The exact value of key parameter (f_{exact}), which is the value of key parameter for zero grid space ($h \rightarrow 0$), can be obtained by using Richardson extrapolation [4] as shown in Equation (5.13) or Equation (5.14).

$$f_{exact} = f_1 + \frac{f_1 - f_2}{r_{21}^{p} - 1} \tag{5.13}$$

$$f_{exact} = \frac{r_{21}^{p} f_1 - f_2}{r_{21}^{p} - 1} \tag{5.14}$$

5.2.2 GCI for CFD modeling of jet mixing tanks

The GCI for CFD simulation of 45° inclined side entry pump-around jet mixing tank with jet discharge velocity of 4.4 m·s^{-1} is demonstrated in Table 5.2.

From Table 5.2, the results show the following conclusions:

- The grid refinement from medium to finest grid levels for potential core and overall mixing time are in the asymptotic range because the values of α are close to unity.

- For potential core (steady state simulation), the convergence conditions of all grid levels are monotonic convergence because the values of convergence

ratio are less than unity. Further, for unsteady state simulation of mixing time, the grid refinement from coarse to fine grids presents oscillatory convergence ($R < 0$). But, the grid refinement from medium to finest grid levels shows the monotonic convergence.

- The GCI values for potential core and mixing time are found to decrease from medium to finest grid levels ($GCI_{21} < GCI_{32}$). Thus, the grid independent solutions have been achieved, meaning that further grid refinement will not improve the accuracy of the simulated results. Moreover, the extrapolated values of potential core and mixing time are slightly different as comparing with those obtained by the finest grid level. Finally, it can be summarized that the solutions are converged with the refinement from medium to finest grid levels.

From above conclusions, in order to ensure that the grid convergence is obtained, the finest grid level is employed for all simulations. In this thesis, the grid adaption technique was used for grid refinement as mentioned earlier. So, the grids of different cases were adapted three times to achieve the finest grid resolution.

5.3 Model validation

In order to validate the model, the predicted overall mixing times of 45° inclined side entry pump-around jet mixing tank for different jet discharge velocities, including 2.2, 4.4, 6.6, 8.8, and 11 $m{\cdot}s^{-1}$, were compared to the measured data of Patwardhan [74] as shown in Figure 5.1. Further, for discharge velocity of 4.4 $m{\cdot}s^{-1}$, the predicted normalized concentration profiles at probe 1 and probe 2 were comparing with the experimental data as depicted in Figure 5.2.

Figure 5.1 represents that most of predicted overall mixing times are lower than those observed experimentally and close to the experiments, except the predicted overall mixing time for jet discharge velocity of 2.2 $m{\cdot}s^{-1}$. For jet velocity of 2.2 $m{\cdot}s^{-1}$, the mixing time is overpredicted with the maximum error of about 15% as comparing with the experiment because of the inadequacy of RKE that it is only suitable for high Reynolds number round jet. Furthermore, this result corresponds to the suggestion of Ghahremanian and Moshfegh [145] that the turbulence model with low Reynolds number correction is necessary to simulate the low Reynolds number turbulent round jet.

Table 5.2 GCI for an open 45° inclined side entry pump-around jet mixing tank with discharge velocity of 4.4 $m \cdot s^{-1}$

Key parameter	i[a]	N_i	f_i	$r_{i+1,i}$	$\varepsilon_{i+1,i}$	$e_{i+1,i}$	$GCI_{i+1,i}$ [%]	R	α
Potential core	0[b]		2.5133						
	1	1,739,978	2.5130						
				1.0540	-0.0065	-0.0026	0.0172		
	2	1,486,046	2.5065					0.0130	0.9974
				1.0785	-0.5011	-0.1999	0.3434		
	3	1,184,437	2.0054					0.7999	3.2954
				1.0289	-0.5012	-0.2499	7.6873		
	4	1,087,312	1.5042						
Mixing time	0[b]		28.1264						
	1	1,739,978	28.1903						
				1.0540	0.1755	0.0062	0.2834		
	2	1,486,046	28.3658					0.1299	1.0062
				1.0785	1.3599	0.0479	1.0550		
	3	1,184,437	29.7257					-42.0382	51.7529
				1.0289	-0.0339	-0.0011	0.1362		
	4	1,087,312	29.6918						

[a] i = 1, 2, 3, and 4 denote the calculations at the finest, fine, medium and coarse meshes, respectively.

[b] 0 indicates the exact value of key variable.

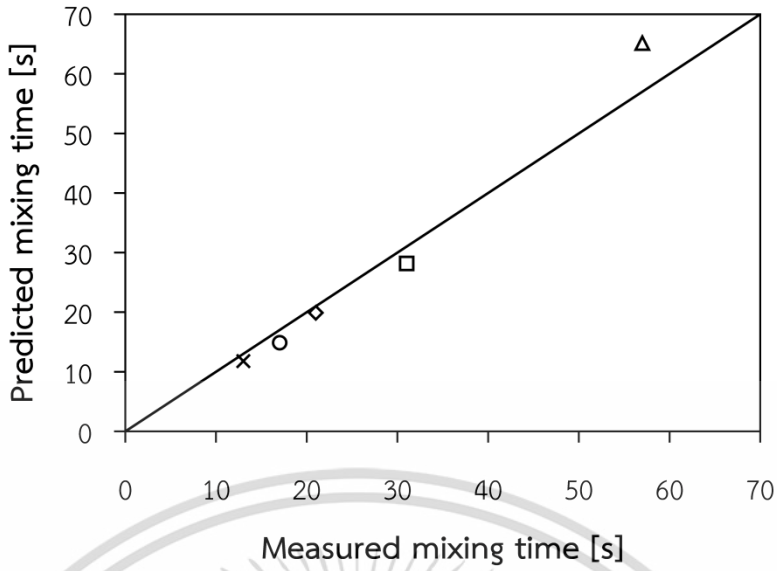

Figure 5.1 Comparison of overall mixing times between the present CFD predictions and the experimental data of Patwardhan [74] for different jet discharge velocities: △ 2.2 m·s^{-1}; □ 4.4 m·s^{-1}; ◇ 6.6 m·s^{-1}; ○ 8.8 m·s^{-1}; × 11 m·s^{-1}

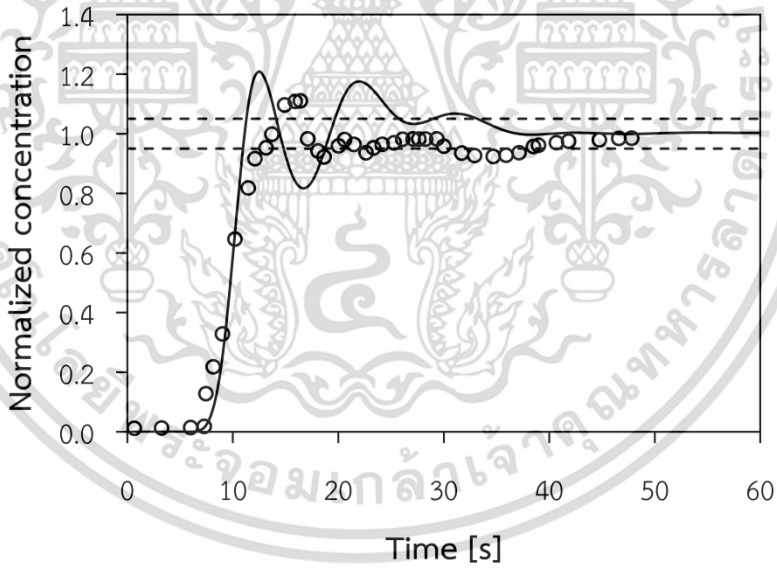

(a)

Figure 5.2 Comparison of normalized concentration profiles for jet discharge velocity of 4.4 m·s^{-1} between the present CFD simulations and the experimental data of Patwardhan [74] at (a) probe 1 (b) probe 2: —— CFD; ○ Experiment (Dash lines indicate the 95% mixing time criterion.)

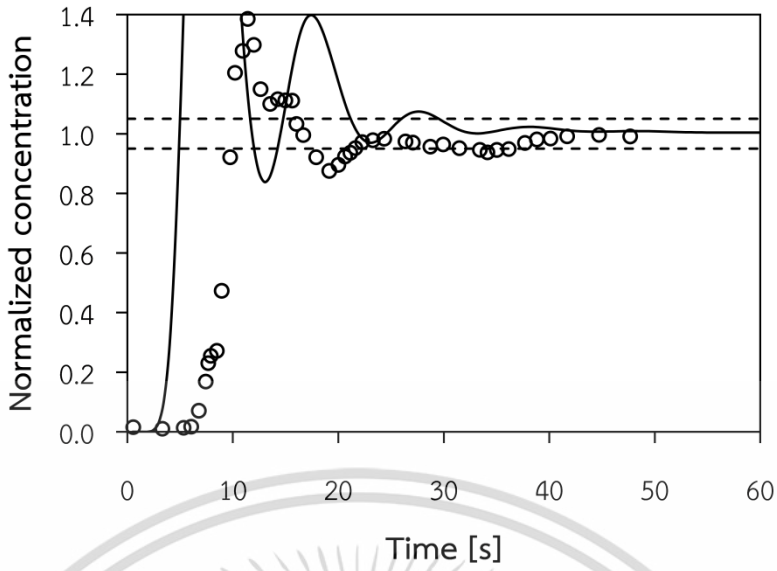

(b)

Figure 5.2 (continued)

From Figure 5.2(a), the good agreement between predicted normalized concentration profile and experimental data is observed for the time less than 10 s. After 10 s has elapsed, the predicted normalized concentration profile shows oscillatory curve and is not in good agreement with the experiment. The first peak value of normalized concentration is higher than actual observation. However, the predicted profile is found to reach the value of unity for the large value of time (≈ 40 s), which is similar to that achieved experimentally. For Figure 5.2(b), the predicted normalized concentration profile is not in good agreement with the experimental profile and the faster rise in predicted normalized concentration profile is investigated.

According to these results, it can be seen that the CFD model predicts the overall mixing time well. But, the normalized concentration profiles at different probe locations are not well predicted. However, in order to study the bulk mixing inside the jet mixing vessels, the present CFD model is acceptable. Meaning that, this CFD model can be adopted to determine the overall mixing time. So, in this thesis, the present CFD model was employed to study the pump-around jet mixing tanks. Moreover, the discrepancy in normalized concentration profiles between CFD simulation and experiment was investigated to improve the accuracy in concentration profile prediction and/or represent the possible reasons of this shortfall as represented in chapter VI.

CHAPTER VI

DISCREPANCY IN CONCENTRATION PROFILES BETWEEN CFD MODEL AND EXPERIMENT

Chapter VI presents the appropriate boundary conditions for inclined side entry pump-around jet mixing tank simulation. The possible reasons of the discrepancy in concentration profiles between CFD simulation and experimental data are also demonstrated.

6.1 Problem and its analysis

Although the CFD model of an open 45° inclined side entry pump-around jet mixing tank was carefully developed, however, a discrepancy in concentration profiles between CFD model and experiment was still observed as depicted in previous chapter. This discrepancy may be due to the inappropriate types of boundary conditions. The absence of exact turbulence conditions, which directly affect on the flow and mixing behaviors inside the tank, can also be considered as the possible cause of this shortfall. Thus, in this thesis, the two different sets of boundary condition types, including velocity-inlet and pressure-outlet for set I and recirculation-inlet and recirculation-outlet for set II, were tested to obtain the appropriate boundary condition types for this considered system. Further, the different inlet turbulence boundary conditions calculated by different estimation correlations, were simulated to examine the optimal conditions for predicting the concentration profiles and investigate the causes of the discrepancy in concentration profiles between CFD model and experiment. The details of turbulence boundary conditions for jet mixing tank simulations are described in section 6.2.

6.2 Specifications of turbulence boundary conditions

As mentioned in section 4.7, the turbulence kinetic energy (TKE or k) and turbulence kinetic energy dissipation rate (TDR or ε) were specified at inlet boundary. In this thesis, due to the absence of exact turbulence conditions, the two turbulence

quantities were estimated by using different correlations. The estimations of these turbulence quantities are represented as follows:

6.2.1 Turbulence kinetic energy

For turbulence kinetic energy, the jet discharge velocity and turbulence intensity are adopted to estimate this quantity as shown in Equation (6.1).

$$k = \frac{3}{2}\left(U_j I\right)^2 \tag{6.1}$$

For jet mixing tank simulations, the different values of turbulence intensity can be used. Patwardhan [74] reported that the proper turbulence intensity for inclined side entry jet mixing tank simulation was 10%, which corresponds to the information that the turbulence intensity in a jet is higher than 10% [146]. Further, Dautova et al. [103] specified the measured turbulence intensity of 4.7% at inlet section (Re_{D_h} = 15,083). This measured value is very close to that achieved by the correlation for fully developed pipe flow (4.8%) as shown in Equation (6.2) [147].

$$I = 0.16\,\mathrm{Re}_{D_h}^{-1/8} \tag{6.2}$$

where Re_{D_h} is the hydraulic diameter based Reynolds number ($\mathrm{Re}_{D_h} = \rho D_h v_{avg}/\mu$).

In this thesis, the 10% turbulence intensity and turbulence intensity estimated by Equation (6.2) were used to evaluate the turbulence kinetic energy at inlet section.

6.2.2 Turbulence kinetic energy dissipation rate

For turbulence kinetic energy dissipation rate, there are various correlations that use to estimate this quantity. White [148] showed the physical argument that the turbulence kinetic energy dissipation rate is proportional to the ratio of cube of velocity scale (u^3) to the length scale (l). Then, the square root of turbulence kinetic energy is used as a velocity scale. So, the correlation for estimating the turbulence kinetic energy dissipation rate can be written as depicted in Equation (6.3) [22].

$$\varepsilon = C_D \frac{k^{3/2}}{l} \tag{6.3}$$

where C_D is a constant of the correlation, which is 0.08. The length scale is approximately equal to $0.07D_h$ for fully developed internal flow.

ANSYS FLUENT also represents the correlation for turbulence kinetic energy dissipation rate estimation as shown in Equation (6.4) [31].

$$\varepsilon = C_{\mu}^{3/4} \frac{k^{3/2}}{l} \tag{6.4}$$

where C_{μ} is an empirical constant specified in the turbulence model (0.09).

Furthermore, ANSYS CFX shows that the turbulence kinetic energy dissipation rate is obtained by using Equation (6.5) [149].

$$\varepsilon = \frac{\rho C_{\mu} k^2}{1000 I \mu} \tag{6.5}$$

This equation was adopted to estimate the turbulence kinetic energy dissipation rate for turbulence round jet simulation as reported by Faghani et al. [150].

Thus, in this thesis, the three different correlations were employed to estimate the turbulence kinetic energy dissipation rate at inlet boundary.

6.2.3 Tested boundary conditions

From above correlations, the values of inlet turbulence kinetic energy and inlet turbulence kinetic energy dissipation rate were estimated and summarized as shown in Table 6.1.

Table 6.1 Details of tested boundary conditions

Case	Velocity [$m \cdot s^{-1}$]	Turbulence intensity	TKE [$m^2 \cdot s^{-2}$]		TDR [$m^2 \cdot s^{-3}$]	
			Equation	Value	Equation	Value
TC1	4.4	10%	(6.1)	0.2904	(6.3)	22.35614
TC2					(6.4)	45.91861
TC3					(6.5)	75.53572
TC4		4.33%		0.0543	(6.3)	1.809608
TC5					(6.4)	3.716862
TC6					(6.5)	6.114206

6.3 Boundary condition types

In order to obtain the appropriate boundary condition types for mixing time investigation of inclined side entry pump-around jet mixing tank, the two different

sets of boundary condition types, including velocity-inlet and pressure-outlet for set I and recirculation-inlet and recirculation-outlet for set II, were numerically studied by using conditions of TC1 case as reported in Table 6.1. The contours of normalized concentration for two different sets are represented in Figure 6.1. Further, the normalized concentration profiles at probe 1 of these sets are shown in Figure 6.2.

Figure 6.1 Contours of normalized concentration of plane x = 0 at t = 25 s for set I and set II, Adapted from Bumrungthaichaichan et al. (J. Chin. Inst. Eng. 41(7) (2018) 612-621) with permission from Journal of the Chinese Institute of Engineers

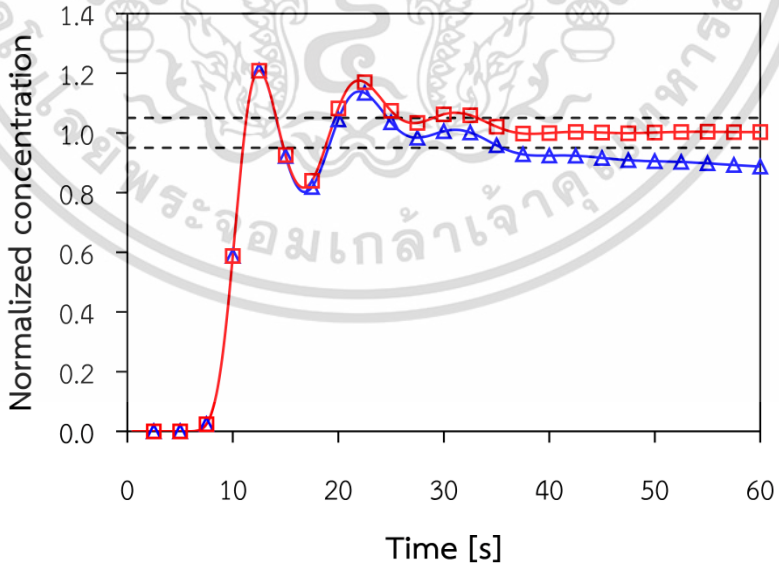

Figure 6.2 Normalized concentration profiles at probe 1 for two different sets of boundary condition types: Set I; Set II

In Figure 6.1, the results reveal that the contour of set I shows lower values of the normalized concentration as compared to those achieved by set II. At the region near the jet nozzle exit, the normalized concentration contour of set I presents zero value of normalized concentration, meaning that the mass of tracer from the outlet pipe exit does not return to the jet nozzle. For set II, the normalized concentration contour at the region near the nozzle exit exhibits the recirculation of tracer from outlet to inlet. Furthermore, from Figure 6.2, the normalized concentration profile at probe 1 predicted by set I is found to diminish after 31 s has elapsed because of the fact that the pressure-outlet boundary condition type only allows the tracer to flow pass the outlet boundary and does not permit the tracer to re-enter to the nozzle so the mass of tracer in the tank is decreased with increasing time. For set II, the values of normalized concentration are close to unity after 36 s has passed, meaning that the normalized concentration at probe 1 reaches the fully mixed value.

In this thesis, the normalized concentration profile was used to evaluate 95% mixing time with the help of Equation (4.8). For set I, the normalized concentration profile of probe 1 is reached the 95% mixing time criterion at t = 25 s. Later, the normalized concentration profile is found to deviate from this criteria. So, the 95% mixing time for set I cannot be investigated. In contrast, for set II, the normalized concentration profile of probe 1 meets the 95% mixing time criteria at t = 33.1779 s and is found to reach the value of unity as time increases. Hence, the 95% mixing time obtained by set II is 33.1779 s. From these results, it can be seen that the boundary condition types of set II are appropriate to simulate the mixing time for pump-around jet mixing tanks, whereas the boundary condition types of set I are suitable to evaluate the residence time distribution (RTD) inside the mixing tanks [101].

According to these results, it can be summarized that the jet mixing time investigation for pump-around jet mixing tank can be easily simulated by using the recirculation-inlet and recirculation-outlet (set II) because they allow the tracer to flow pass the outlet and return to the inlet section. Moreover, the mixing time of pump-around jet mixing systems can also be numerically investigated by simulating the complete jet mixing tank geometries with the help of the momentum source specification [70-72, 77] or using the user defined function (UDF) for the specification of the inlet tracer concentration (temperature), which obtained by the average value of outlet tracer concentration (temperature) [96, 97]. However, the present method is more suitable to simulate the mixing time in pump-around jet mixing tanks than the two latter approaches because it uses the smaller number of grids due to the absence of grids in the piping system between inlet and outlet, which directly

reduces the computational time, and the additional computer code (e.g. UDF) is not required.

6.4 Turbulence boundary conditions

Due to the absence of the exact inlet turbulence boundary conditions, the six different inlet conditions as depicted in Table 6.1 were numerically studied to obtain the appropriate inlet boundary conditions and describe the possible cause of the discrepancy in concentration profiles between simulation and experiment. The predicted overall mixing times and predicted normalized concentration profiles at probe 1 and probe 2 were compared with the measured and simulated data of Patwardhan [74] as shown in Table 6.2 and Figure 6.3, respectively. Further, the predicted jet flow patterns inside the inclined side entry pump-around jet mixing tanks were compared with the previous works of free turbulent round jet because the data of jet flow patterns inside the mixing tanks is unavailable.

Table 6.2 Overall mixing times for six different inlet turbulence conditions

Case	Mixing time [s]					% Error[a]
	Probe 1	Probe 2	Probe 3	Probe 4	Overall	
Experiment [74]	38.5	37.7	N/A	N/A	31.000	-
TC1	33.1779	29.5401	27.3008	22.7423	28.1903	9.06
TC2	33.8672	29.5534	27.4802	23.9380	28.7097	7.39
TC3	31.1278	29.4055	27.4505	24.0695	28.0133	9.63
TC4	33.1317	28.9753	27.5530	24.2202	28.4700	8.16
TC5	32.9547	29.0280	27.6818	24.4895	28.5385	7.94
TC6	32.5791	28.9529	27.7718	24.1286	28.3581	8.52

[a] The percentage error is a ratio of absolute difference between the predicted overall mixing time and experimental mixing time to the experimental value.

From Table 6.2, the simulated results reveal that the predicted overall mixing times are lower than the experimental data. Further, for probe 1 and probe 2, the predicted concentrations are faster to reach 95% mixing time criterion than those observed experimentally. For probe 1, the start of concentration profiles for 10% turbulence intensity are closer to the experiment and faster than those predicted by 4.33% turbulence intensity as depicted in Figure 6.3(a). The first peak values of

normalized concentration profiles for TC1 and TC2 cases are overpredicted and underpredicted, respectively. In contrast, the first peaks of normalized concentration profiles for other cases are not clearly represented.

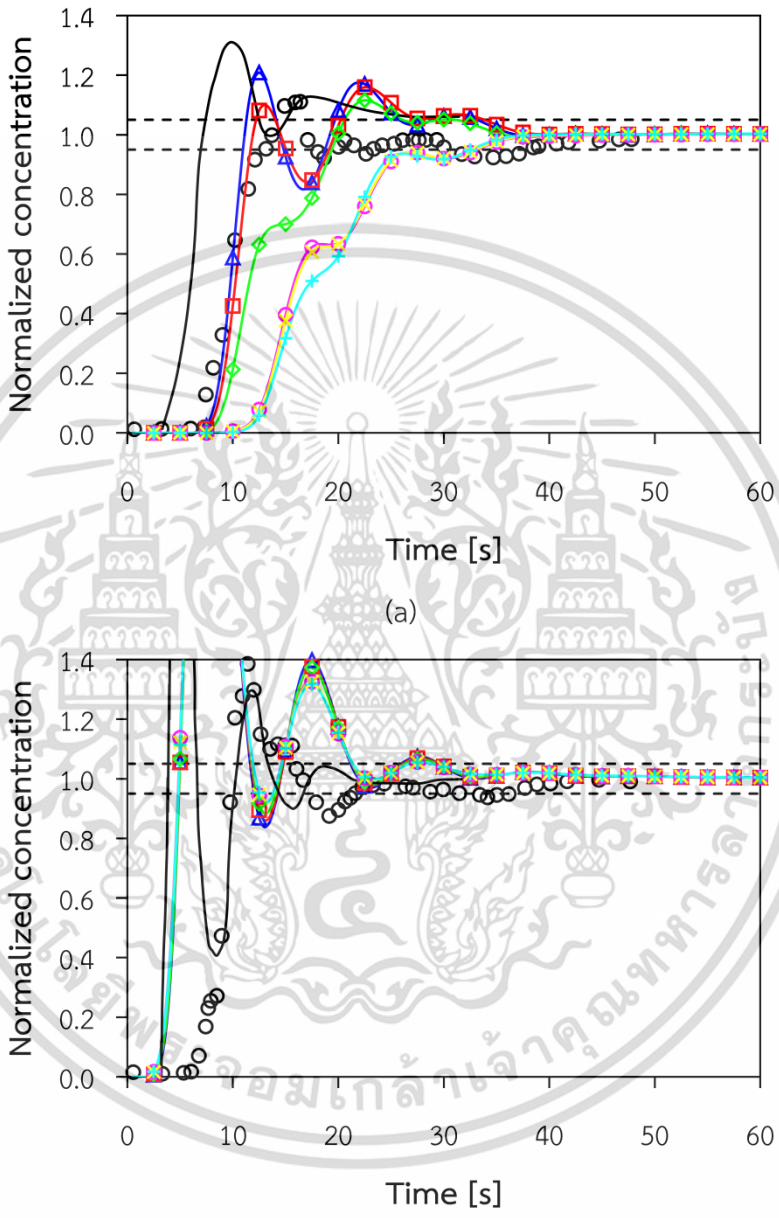

Figure 6.3 Comparison of normalized concentration profiles between present CFD simulations and previous work of Patwardhan [74] at (a) probe 1 and (b) probe 2: TC1; TC2; TC3; TC4; TC5; TC6; CFD [74]; Experiment [74], Adapted from Bumrungthaichaichan et al. (J. Chin. Inst. Eng. 41(7) (2018) 612-621) with permission from Journal of the Chinese Institute of Engineers

At probe 2, the start and first peak values of normalized concentration profiles predicted by six different cases are faster and higher than measured data as shown in Figure 6.3(b). However, all predicted normalized concentration profiles for probe 1 and probe 2 approach the value of unity for the large time values, which correspond to the experimental data. From these results, it can be implied that the difference in these profiles would be due to the different inlet turbulence conditions, which directly affect the extents of turbulent dispersion inside the tanks.

For jet flow behaviors inside the vessels, the contours of jet axial velocity of TC1 case were adopted to represent the general flow pattern inside the open 45° inclined side entry pump-around jet mixing tank as depicted in Figure 6.4. The radial profiles of jet streamwise velocities ($\overline{u}$) predicted by six different cases at different ratios of the jet streamwise distance to the jet nozzle diameter, including 2, 5, 10, and 15, were compared as shown in Figure 6.5. The streamwise velocity and radial distance were respectively scaled with jet discharge velocity and jet nozzle diameter. Further, the decay of centerline streamwise velocities ($\overline{u}_c$) and the spreading of jets (or the variation of jet half-velocity width) for turbulence intensities of 10% and 4.33% were represented by using the TC1 and TC4 cases as shown in Figures 6.6 and 6.7, respectively. Note that the jet half-velocity width is clearly defined in section 3.2.

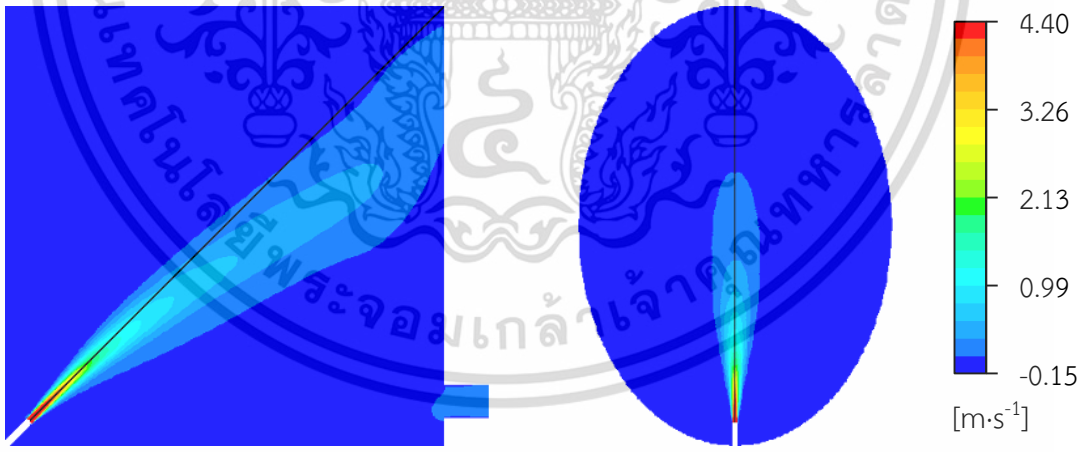

Figure 6.4 Contours of jet streamwise velocity of TC1 case at plane x_j = 0 (left) and plane z_j = 0 (right) (Black line indicates the jet centerline.)

In Figure 6.4, for plane x_j = 0, the jet axial velocity contour shows that the jet flows along the jet nozzle centerline at the region near the jet nozzle exit. Then, the jet flow is found to deviate from the jet nozzle centerline after about 10 times jet nozzle diameter distance downstream. Further, for plane z_j = 0, the contour of jet axial velocity reveals that the jet slightly shows asymmetry about the jet centerline.

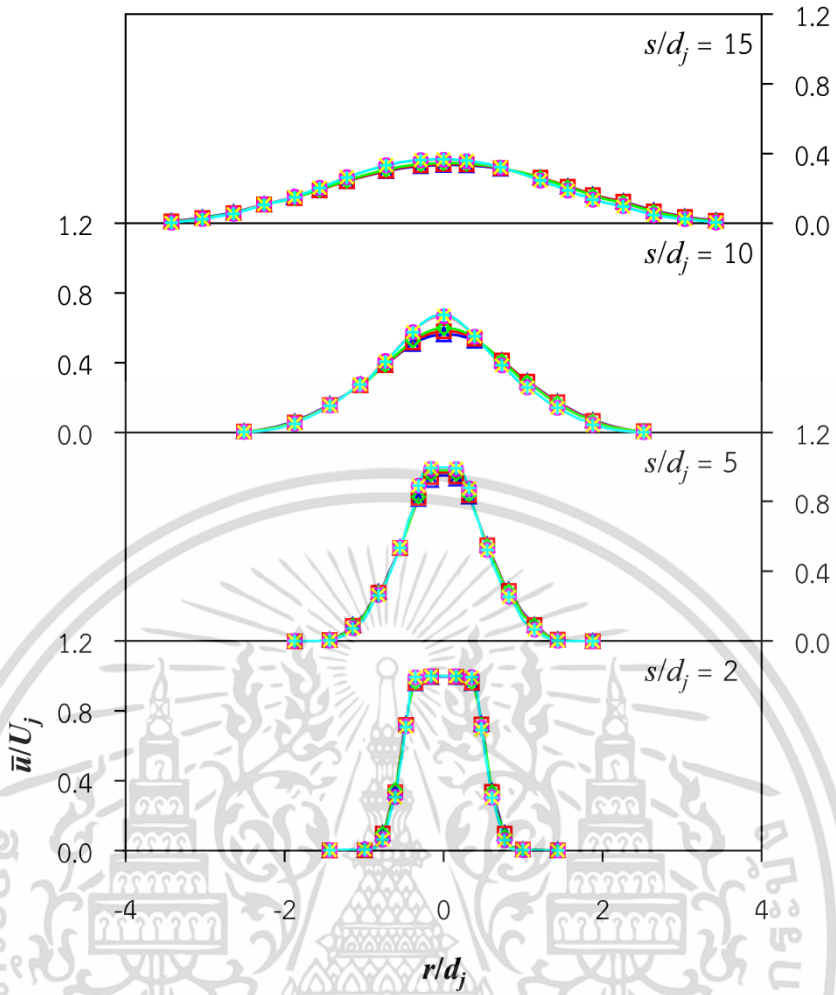

Figure 6.5 Predicted radial profiles of jet streamwise velocities for different s/d_j ratios:

Figure 6.5 reveals that the radial profiles of jet streamwise velocities for six different cases are slightly different and the jet flow behaviors of these cases are similar to the free turbulent round jet. That is, the streamwise velocities decrease with increasing the radial distances and their centerline velocities are found to decrease with increasing s/d_j ratios. Further, the decay of centerline streamwise velocities for 10% turbulence intensity cases are faster than those predicted by 4.33% turbulence intensity, which correspond to the experiments of Ashforth-Frost and Jambunathan [151] that the decay of centerline velocity for the jet with higher initial turbulence intensity was faster than the jet with lower turbulence intensity.

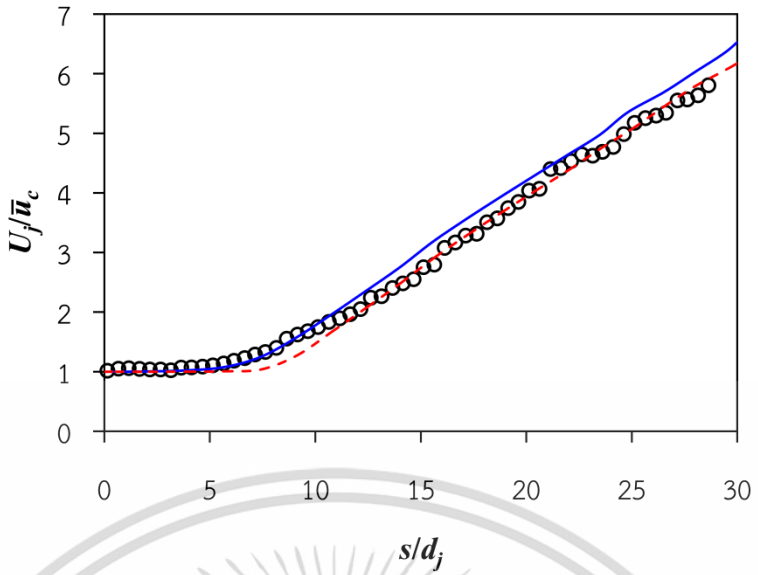

Figure 6.6 Comparison of decay of centerline streamwise velocities between the present jet mixing tank simulations and the previous experimental work of free turbulent jet: —— TC1; - - - TC4; o Experiment [40], Adapted from Bumrungthaichaichan et al. (J. Chin. Inst. Eng. 41(7) (2018) 612-621) with permission from Journal of the Chinese Institute of Engineers

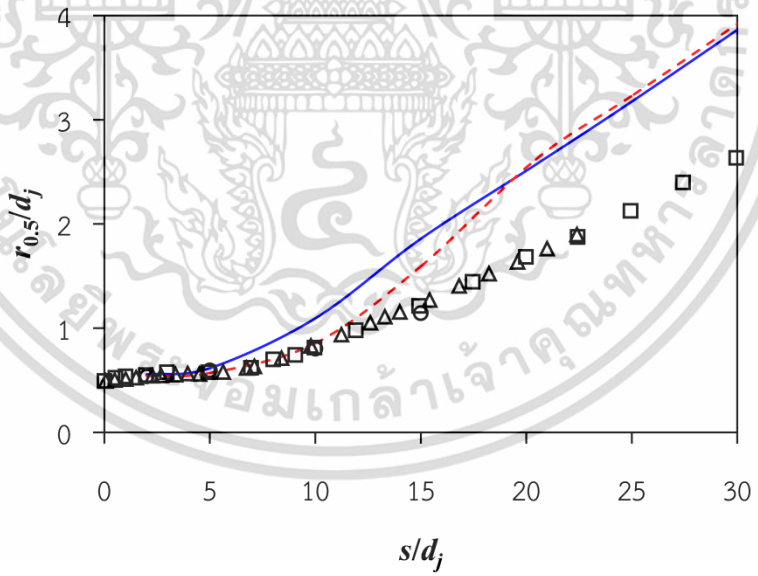

Figure 6.7 Comparison of jet spreading between present jet mixing tank simulations and the previous experimental works of free turbulent jets: —— TC1; - - - TC4; Δ Experiment [152]; □ Experiment [49]; o Experiment [40], Adapted from Bumrungthaichaichan et al. (J. Chin. Inst. Eng. 41(7) (2018) 612-621) with permission from Journal of the Chinese Institute of Engineers

In Figure 6.6, the results show that the decay of centerline velocity of TC1 and TC4 cases are in good agreement with the experiment of Fellouah et al. [40], especially for $s/d_j \leq 10$. For $s/d_j > 10$, the decay of centerline velocity of TC1 case is faster than experiment and the good agreement between the decay of centerline velocity for TC4 case and the experimental data is observed. Moreover, for Figure 6.7, the predicted jet half-velocity widths of TC1 and TC4 cases for $s/d_j < 5$ are in good agreement with the previous experimental data [40, 49, 152]. Then, for $5 < s/d_j < 15$ of TC1 case and $5 < s/d_j < 20$ of TC4 case, the non-linear spreading of jets are wider than those observed experimentally, which are similar to the previous work of jet loop reactor reported by Mathpati et al. [98]. Finally, for higher s/d_j ratios, the predicted spreading of jets are linearly wider than experiments.

According to these results, it can be seen that the tendencies of these jets are similar to the previous literatures, except the values of jet half-velocity widths for $s/d_j > 5$. Further, the discussion of these predicted results can be drawn as the follows:

- The results indicate that the mixing inside the vessels are dominated by convective transport because even when the inlet turbulence conditions, which directly result in the different turbulent dispersion levels, are varied, the predicted overall mixing times are slightly different.

- The underpredicted overall mixing times are caused by the overprediction in convective transport (or total momentum available for mixing) due to the fact that the top liquid-surface was assumed to be flat by using symmetry boundary condition.

- The overpredicted convective transport also results in the faster rise in simulated normalized concentration profiles. That is, the tracer is rapidly transported by jet recirculation from its initial position to the bulk of liquid within a short period of time. The values of predicted tracer concentration gradient would be lower than actual experiments (underprediction in dispersive transport). So, the first peak values of normalized concentration profiles would be higher than those observed experimentally. Meaning that, for jet mixing tanks with overpredicted Peclet number (Pe) – pronounced "Pay-clay" [153] – which is defined as a ratio of convective transport rate to diffusive transport rate, the overprediction in first peak values of normalized concentration profiles should be investigated. This discussion corresponds to the previous CFD work of Patwardhan [74] that the decay in peak value of concentration profiles was slower in simulations than experiments because of the underprediction in turbulent dispersion.

- Regarding to conservation of energy, the faster decay in predicted centerline streamwise velocities would be due to the fact that the jet kinetic energy is partly converted to the potential energy during the change in elevation of jet.

- The predicted jet half-velocity widths are wider than free turbulent round jet because the tank wall forces liquid to flow through the jet stream, which directly enhances the jet entrainment rate.

- When these results and above discussion are considered together, the proper conditions for jet mixing tank simulations would be the conditions of TC1 case. Hence, the appropriate estimation correlations for turbulence kinetic energy and turbulence kinetic energy dissipation rate and turbulence intensity for CFD modeling of inclined side entry pump-around jet mixing tank are Equation (6.1), Equation (6.3), and 10%, respectively. The main reason of using 10% turbulence intensity at jet discharge section is that the turbulence intensity profile is saddle-backed shape [49, 150], which provides the highest turbulence intensity value at jet edge. For example, Quinn [49] reported that the turbulence intensity at jet edge is about 10%, whereas, the centerline and average values of turbulence intensity were 0.5% and 2%, respectively.

From above discussion, it can be implied that the discrepancy in concentration profiles between CFD model and experiment may be due to the overprediction in convective transport. So, in order to test that the overpredicted convective transport is a reason of this shortfall, the jet mixing tanks with lower convective transport and higher convective transport were simulated by using jet discharge velocity of 4.4 $m \cdot s^{-1}$ with top solid wall (TC7 case) and jet discharge velocity of 6.6 $m \cdot s^{-1}$ (TC8 case), respectively. The normalized concentration profiles at probe 1 predicted by these two additional cases were compared with the predicted profile of TC1 case to represent the tendencies of normalized concentration profiles of different convective transport. These predicted profiles were also compared to the previous results of Patwardhan [74] as shown in Figure 6.8.

In Figure 6.8, the results show that the start and first peak value of normalized concentration profile predicted by TC1 case exhibit the better agreement with the experimental data than those simulated by Patwardhan [74] because the numerical diffusion of present model is eliminated by using the higher number of grids and SOU. These predicted results reveal that the normalized concentration profiles are faster rise with increasing the convective transport. The first peak values of normalized concentration profiles are found to decrease with decreasing the convective transport. Moreover, from previous work of Patwardhan [74], although the

predicted extent of turbulent dispersion inside the vessel was increased by using the modified k-epsilon model constants (C_μ = 0.135 and $C_{1\varepsilon}$ = 1.31) to compensate for the overpredicted convective transport, however, the faster rise and higher peak value of normalized concentration profile were still presented.

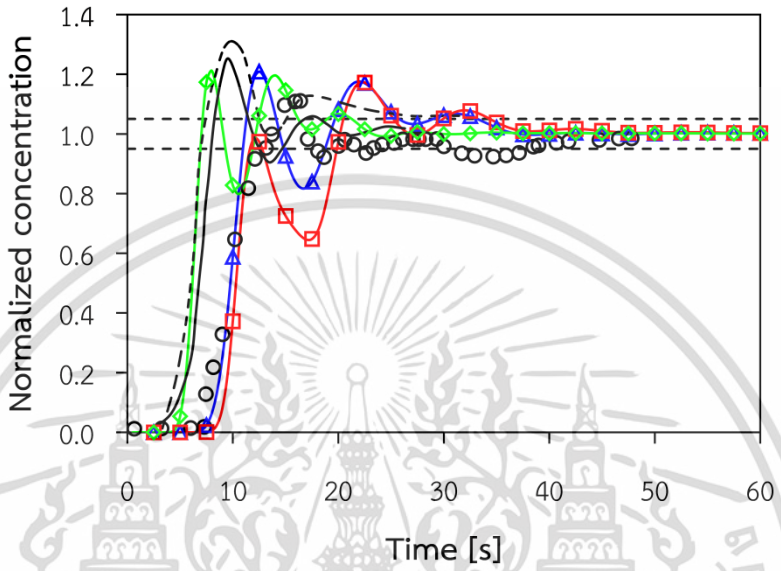

Figure 6.8 Comparison of normalized concentration profiles between present jet mixing tank simulations and previous works of Patwardhan [74]: —△— TC1; —□— TC7; —◇— TC8; - - - CFD with C_μ = 0.09 and $C_{1\varepsilon}$ = 1.42 (standard model constants) [74]; —— CFD with C_μ = 0.135 and $C_{1\varepsilon}$ = 1.31 (modified model constants) [74]; o Experiment [74], Adapted from Bumrungthaichaichan et al. (J. Chin. Inst. Eng. 41(7) (2018) 612-621) with permission from Journal of the Chinese Institute of Engineers

According to above evidence, it can be summarized that there are two possible reasons of discrepancy in concentration profiles between CFD simulation and experiment. The first reason is the improper inlet turbulence conditions, which mainly affect on the predicted extent of turbulent dispersion inside the jet mixing tank. The second cause is the flat top liquid-surface assumption, which overpredicts the total momentum available for mixing (convective transport). That is, there is no viscous dissipation due to the wave motion of liquid-surface, so, the convective transport would be overpredicted. Further, the simplified computational domain, such as jet mixing tank without measuring probes, simplified nozzle shape, etc., is another possible cause of this discrepancy.

CHAPTER VII

CFD PREDICTIONS OF PUMP-AROUND NON-CIRCULAR JET MIXING TANKS

Chapter VII describes the fundamentals of non-circular free jet flows. Further, the application of the present CFD model as described in Chapter IV for predictions of elliptic and square jet mixing tanks are also represented.

7.1 Non-circular jets

Jets are commonly used in various applications, especially the round jets (circular jets or axisymmetric jets) as mentioned in Chapter III. Moreover, the non-circular nozzles can also be adopted. The non-circular jets are generally known as the three-dimensional jets. These jets significantly improve the performance of various applications with inexpensive cost [154], such as improvement of large- and small-scales mixing in various flows, combustion performance enhancement by increasing efficiency of combustion and reducing instabilities and emissions, noise suppression, thrust vector control, etc.

Generally, the simple nozzle configurations are used to produce the non-circular jets, such as equilateral triangular nozzle, square nozzle, elliptic nozzle, rectangular nozzle, etc. The other nozzle shapes can also be employed, such as lobed nozzle, cross nozzle, star nozzle, etc.

For jet Reynolds number, the formula of non-circular jet is slightly different to that achieved by round jet. For Reynolds number of non-circular jet, the circular-equivalent diameter (D_e) is adopted as a characteristic length instead of the general jet nozzle diameter [154-156]. The circular-equivalent diameter is a diameter of an axisymmetric jet having the same jet discharge cross-sectional area of non-circular jet [154]. Hence, the jet Reynolds number of non-circular jet can be written as:

$$\mathrm{Re}_j = \frac{\rho D_e U_j}{\mu} \tag{7.1}$$

Note that the bulk mean velocity (U_b) is adopted as a jet discharge velocity.

7.2 Fluid dynamics of non-circular jet

The fluid dynamics of non-circular jets are different to those observed in turbulent round free jets as mentioned in section 3.2. The non-circular jet consists of four distinguished regions, including potential core (PC) region, characteristic decay (CD) region, axisymmetric type decay (AD) region, and fully axisymmetric region [157-159], as shown in Figure 7.1.

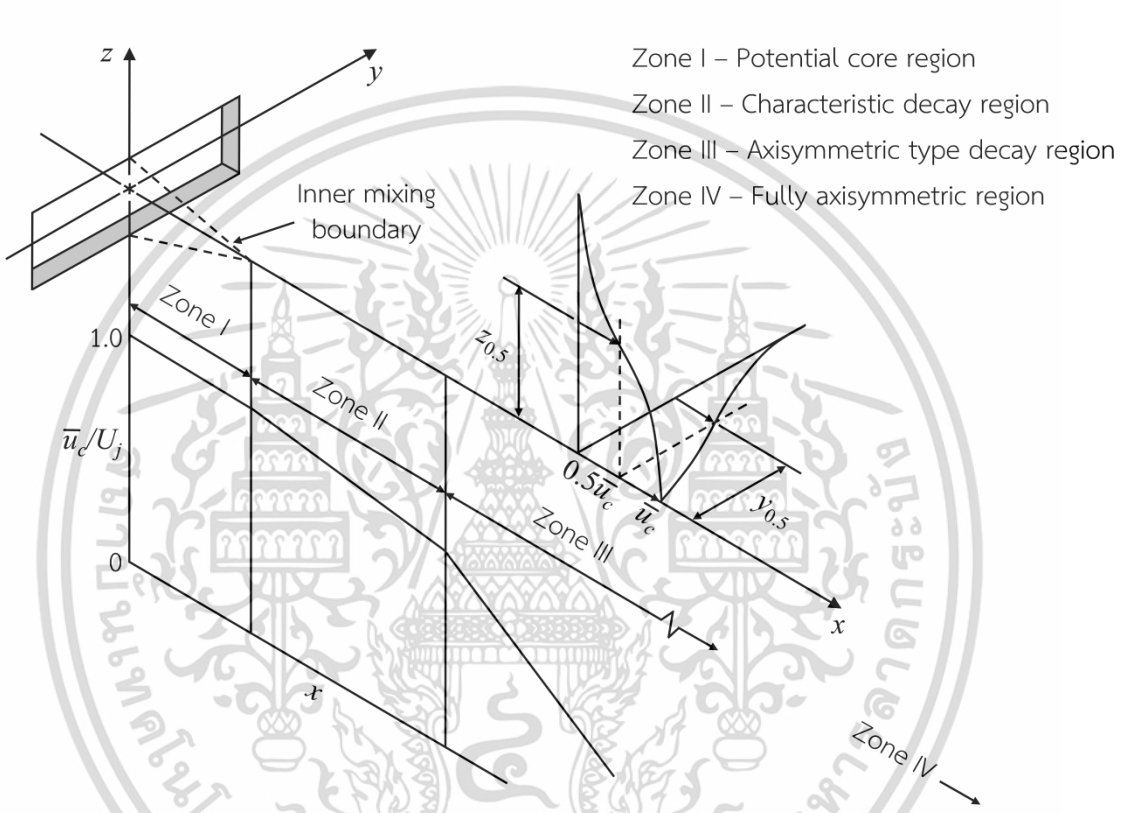

Figure 7.1 Flow field for non-circular jet [157-159]

Sforza et al. [157] and Trentacoste and Sforza [158] clearly described the details of these four distinguished regions. The phenomena of these regions can be represented and summarized as follows:

7.2.1 Potential core region

In the first region, the mixing occurs at jet boundaries and does not penetrate into the jet centerline. Hence, the mean centerline velocities of non-circular jets are constant and close to their jet discharge velocities. These phenomena are similar to those observed in turbulent round jets. Furthermore, the potential core lengths are dependent upon the nozzle configurations. The lengths of this zone are within 10 times characteristic dimension of the jets. For example, the

characteristic dimensions of rectangular and elliptic jets are minor axis lengths. Moreover, the height of equilateral triangular jet is adopted as characteristic dimension of this triangular jet [160].

7.2.2 Characteristic decay region

For the second zone of non-circular jets, the decay of axial velocities are dependent on orifice or nozzle geometries. The axial velocity profiles of minor axis planes are similar. But, the velocity distributions in major axis planes are non-similar.

7.2.3 Axisymmetric type decay region

In this region, the mean centerline velocity is inversely proportional to the longitudinal distance ($\overline{u}_c \sim x^{-1}$) and the jet is found to approach axisymmetry. Thus, the axial velocity profiles in the planes of major and minor axes are similar. Meaning that, the jet velocity distributions are oblivious to the nozzle geometries.

7.2.4 Fully axisymmetric region

For far downstream distance of jets, the non-circular jets become fully axisymmetric flow.

Moreover, from the previous experimental works of non-circular jets, the results showed that the vortex evolution, self-induction and interaction between azimuthal and axial vortices are complex [154]. These phenomena cause axis switching in the mean flow fields of non-circular jets. Further, the axis switching can enhance the entrainment properties of free non-circular jets. So, the entrainment rates of these jets are better than free turbulent round jets [161, 162].

7.3 CFD predictions of non-circular jet mixing tanks

For this section, the mixing performances of the open 45° inclined side entry pump-around non-circular jet mixing tanks were numerically predicted because of the reason that although the entrainment rates of free non-circular jets are greater than those achieved by free turbulent round jets which may improve the mixing performances, however, the round jet nozzles are modified to use in various mixing applications. So, it is interesting and necessary to study the performances of non-circular jet mixing tanks. The example of commercial round jet nozzle is shown in Figure 7.2.

Figure 7.2 Example of commercial nozzles and installation, Reproduced from http://www.samhwamix.com/product/in-tank-heater-jet-mixing-eductor/ with permission from SAMHWA Mixing Tech. Co., Ltd.

For CFD predictions of pump-around non-circular jet mixing tanks, the mixing performances of elliptic jet (EJ) and square jet (SJ) were numerically investigated. The tank geometries of these jet mixing tanks were similar to those reported in table 4.1, except the nozzle geometries. However, the discharge areas of non-circular jets were identical to circular jet discharge area. Further, the jet discharge velocities of non-circular jet mixing tanks were also 4.4 $m \cdot s^{-1}$. Hence, the jet Reynolds numbers calculated by Equation (7.1) and mass flow rates of these non-circular jet mixing tanks were also equal to those obtained by circular jet mixing tank.

From previous experimental data, the measurements revealed that the turbulence intensities of elliptic and square jets were higher than the turbulence intensity of round jet. For elliptic jet, the maximum streamwise turbulence intensity near the jet discharge plane was about 15% [161]. While, Quinn and Militzer [163] reported that the maximum streamwise turbulence intensity of square jet at a short distance downstream was about 12%. Hence, the specified values of turbulence kinetic energy and dissipation rate of turbulence kinetic energy for CFD predictions of these non-circular jet mixing tanks were different to those obtained by circular jet mixing tank. However, the estimation correlations for these turbulence quantities were similar to those suggested in chapter VI. That is, the specified turbulence kinetic energy and its dissipation rate were computed by Equations (6.1) and (6.3), respectively.

The turbulence model and numerical setups of these non-circular jet mixing tanks were also similar to those used in circular jet mixing tank as described in

chapter IV. The necessary details for these non-circular jet mixing tank simulations are summarized in Table 7.1

Table 7.1 Details of CFD predictions for non-circular jet mixing tanks

Detail	Elliptic jet mixing tank	Square jet mixing tank
Case	EJ	SJ
Schematic for cross-sectional shape of the jet	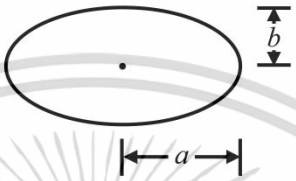	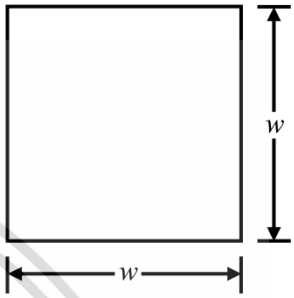
Dimensions	a = 5.656854 mm b = 2.828427 mm	w = 7.089815 mm
Grid topology	Hexahedral grid	Hexahedral grid
Discharge velocity [m·s^{-1}]	4.4	4.4
Turbulence intensity	15%	12%
TKE [m^{2}·s^{-2}]	0.6534	0.418176
TDR [m^{2}·s^{-3}]	75.45198	38.63142
Turbulence model	RKE	RKE
P-V coupling scheme	SIMPLE	SIMPLE
Spatial discretization scheme	SOU	SOU
Temporal discretization scheme	FOI	FOI
Time step size [s]	0.0025	0.0025
Steady state convergence criterion	All equations were solved until the area weight average of velocity magnitude at outlet and plane x = 0 were constant.	All equations were solved until the area weight average of velocity magnitude at outlet and plane x = 0 were constant.
Transient convergence criterion	Scaled residual of 10^{-5}	Scaled residual of 10^{-5}

7.4 Mixing performances

In this section, the predicted overall mixing time was adopted to indicate the mixing performance, which was similar to the circular jet mixing tank. The predicted overall mixing times for circular, elliptic, and square jet mixing tanks were compared as shown in Table 7.2. Moreover, in order to describe the mixing performances of these jet mixing tanks, the contours of streamwise velocity and velocity vector, line contours of normalized streamwise velocity, which is defined as a ratio of streamwise velocity to its centerline streamwise velocity ($\overline{u}/\overline{u}_c$),the decay of centerline streamwise velocities along jet streams, and turbulence kinetic energy profiles for three different jet mixing tanks are respectively represented in Figures 7.3-7.6. In addition, the contours of vorticity magnitude for these jet mixing tanks is shown in Figures 7.7.

Table 7.2 Overall mixing times for circular, elliptic, and square jet mixing tanks

Case	Mixing time [s]					% Difference[a]
	Probe 1	Probe 2	Probe 3	Probe 4	Overall	
CJ[b]	33.1779	29.5401	27.3008	22.7423	28.1903	-
EJ	30.3601	29.4807	26.7041	31.2199	29.4412	4.44
SJ	32.4218	29.3902	26.9298	32.3423	30.2710	7.38

[a] The percentage difference is a ratio of difference between the mixing time of non-circular jet and mixing time of circular jet to the circular jet mixing time.

[b] CJ stands for circular jet mixing tank case, which is similar to TC1 case.

In Table 7.2, the predicted results reveal that the circular jet mixing tank presents the shortest mixing time, respectively followed by elliptic and square jet mixing tanks. That is, the mixing performance of circular jet mixing tank is better than those obtained by non-circular jet mixing tanks, which contradicts the previous works of free jets that the mixing between jet and external fluid of non-circular jets were better than those obtained by circular jets as mentioned earlier. In order to explain this discrepancy, the flow patterns inside these jet mixing tanks were considered and analyzed.

Figure 7.3 shows that the flow patterns of three different jet mixing tanks have a similar tendency. That is, these jets gradually spread in lateral direction along the downstream distance until they impinge the opposite boundaries. After jet rollover, the recirculation regions below these jets are smaller than those observed above the jets because of the outlet pipe location, which allows water near the tank bottom to

partially flow out the tank. Moreover, after the larger recirculation zones, the water is induced by entrainment of jet from remote zones (above nozzles) into the jets.

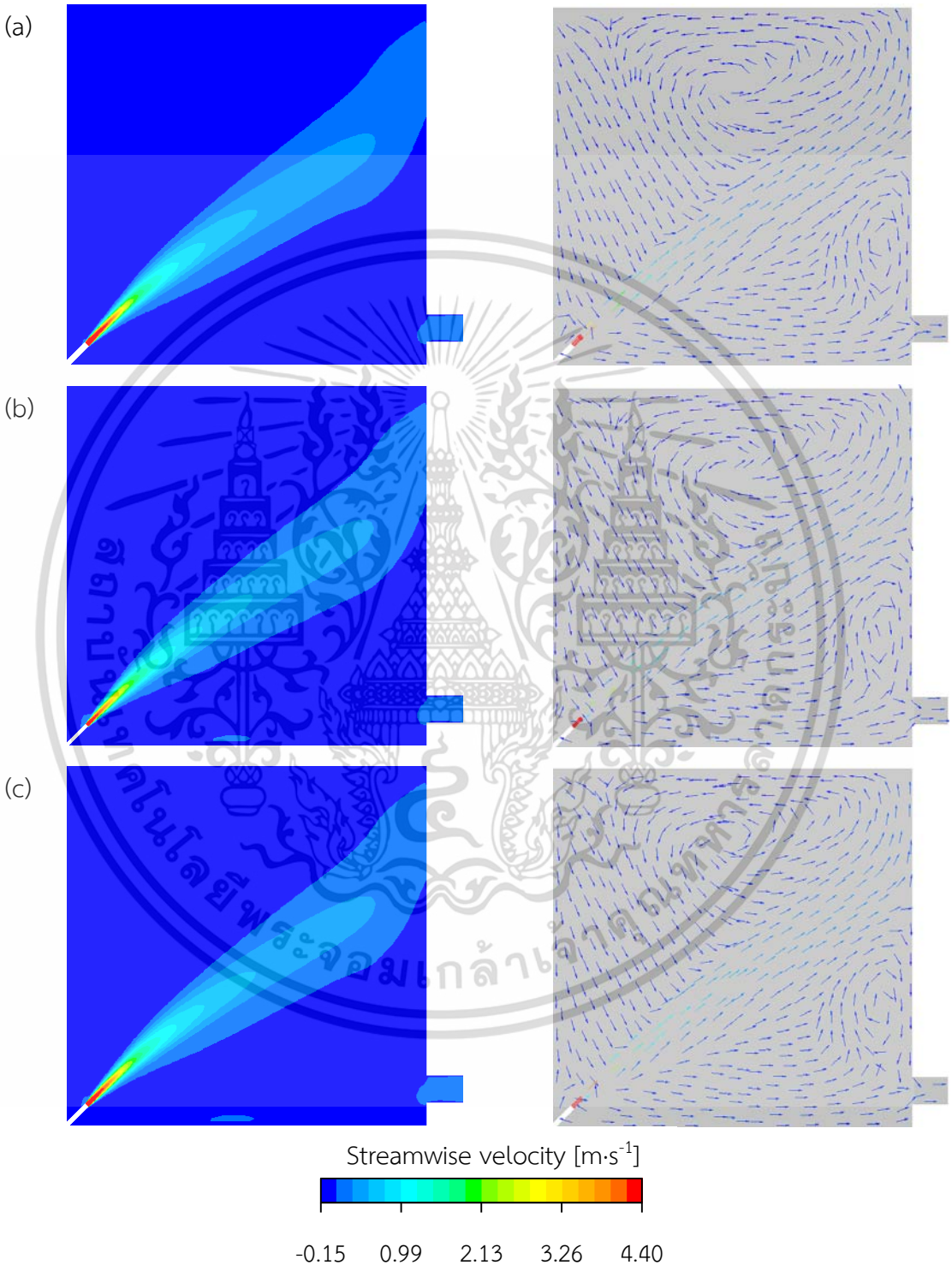

Figure 7.3 Contours of streamwise velocity (left) and velocity vector colored by streamwise velocity (right) at plane x = 0 for (a) circular jet, (b) elliptic jet, and (c) square jet

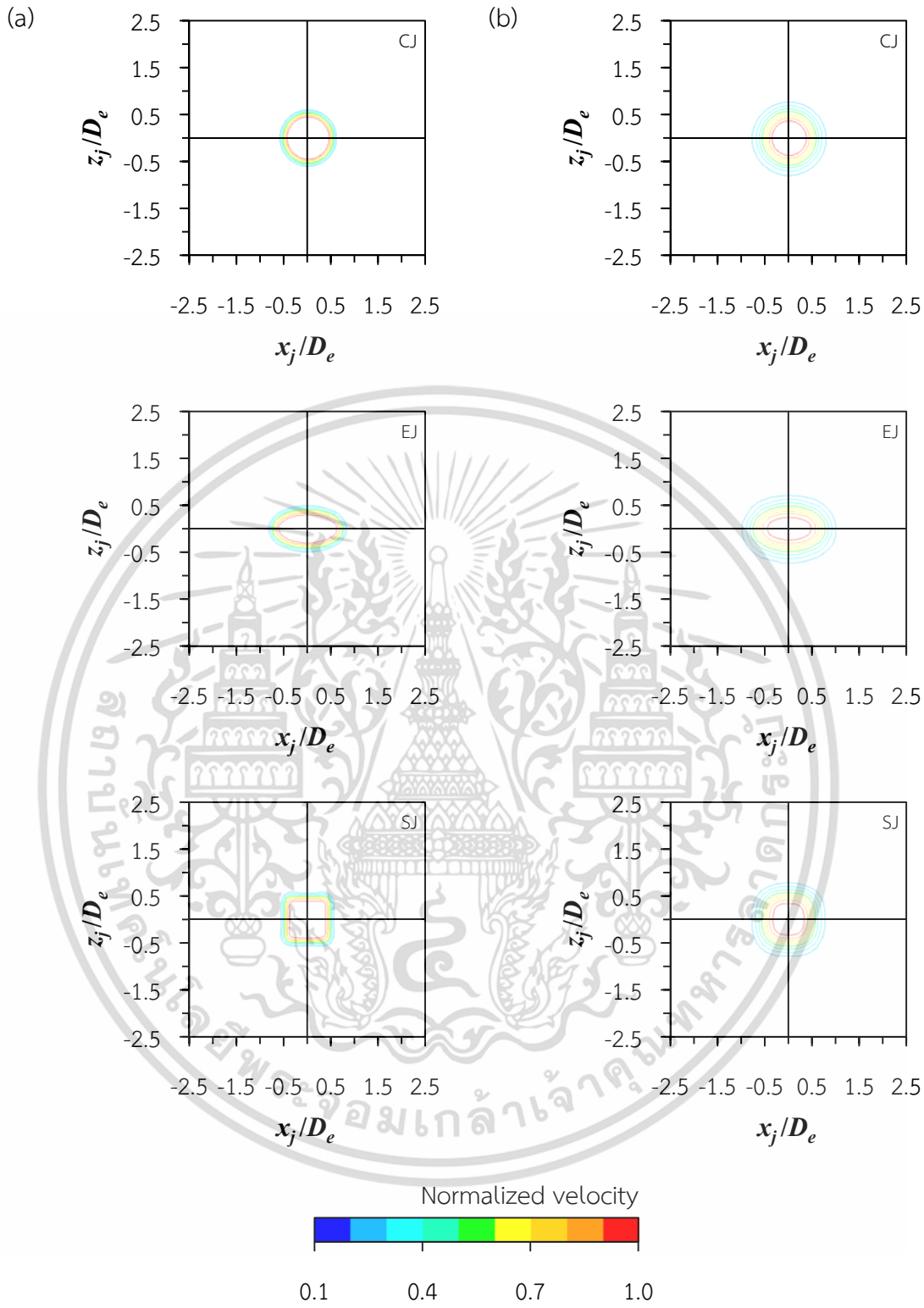

Figure 7.4 Line contours of normalized streamwise velocity for circular jet, elliptic jet, and square jet at (a) plane s/D_e = 1, (b) plane s/D_e = 3, (c) plane s/D_e = 5, and (d) plane s/D_e = 10

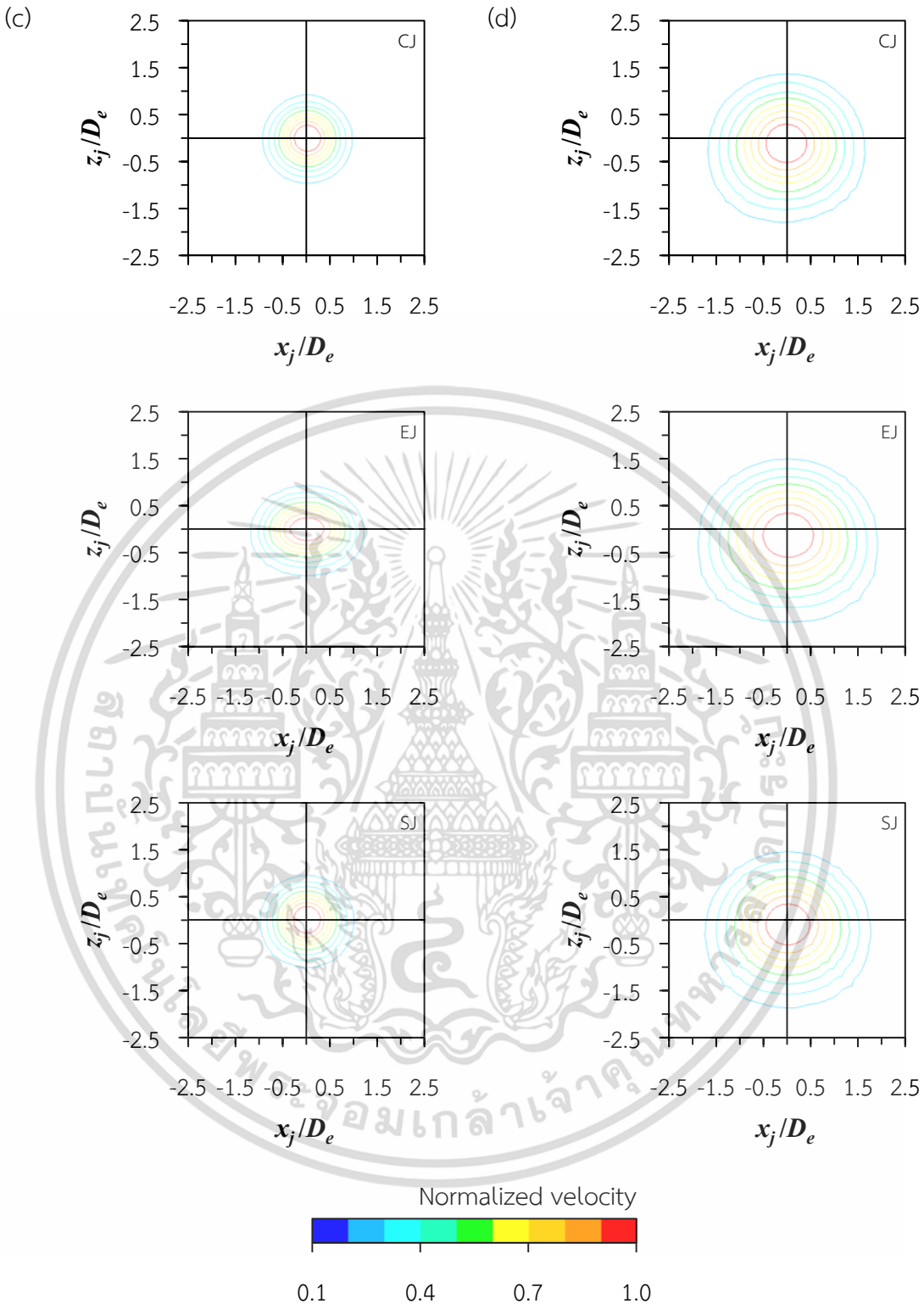

Figure 7.4 (continued)

In Figure 7.4, the line contours of normalized streamwise velocity exhibit the spreading of jets and their shapes for three different jet mixing tanks. For $s/D_e \leq 5$, these jets are gradually growth in lateral direction and retain their original nozzle shapes, except the square jet at $s/D_e = 5$. For $s/D_e > 5$, the shapes of these non-

circular jets are found to approach the shape of circular jet. Moreover, the spreading rates along the edges of non-circular jets are different because of non-uniform shear stresses along these jet boundaries. That is, the spreading rate along minor axis direction for elliptic jet is higher than that obtained in major axis direction. For square jet, the spreading rates of flat sides are greater than vertex sides. These non-circular jets provide high spreading rates to adjust their shapes to obtain uniform shear stresses along the jet edges. These results also indicate that the axis switching of non-circular jets are not investigated. The absences of axis switching for these non-circular jets are similar to the previous works of Schadow et al. [164] for elliptic pipe jet and Grinstein et al. [162] for square pipe jet.

At the regions near jet discharge planes ($s/D_e \leq 5$), the spreading rate (S) of elliptic jet shows the highest value of 0.035. While, the spreading rate of square and circular jets are 0.034 and 0.018, respectively. The spreading rates ($S = dr_{eq}/ds$) of these jets were computed by using equivalent jet half-width (r_{eq}), which is define as $r_{eq} = (r_{0.5,\text{major}} \times r_{0.5,\text{minor}})^{1/2}$ [165]. In general, for free jet, the wider jet spreading results in faster decay of jet centerline velocity. From Figure 7.5, the elliptic jet mixing tank provides the fastest decay of centerline streamwise velocity, respectively followed by square and circular jet mixing tanks, which are similar to the characteristics of free jets as reported by Mi et al. [155]. For $s/D_e > 15$, the decay of centerline velocity for these jets are slightly different.

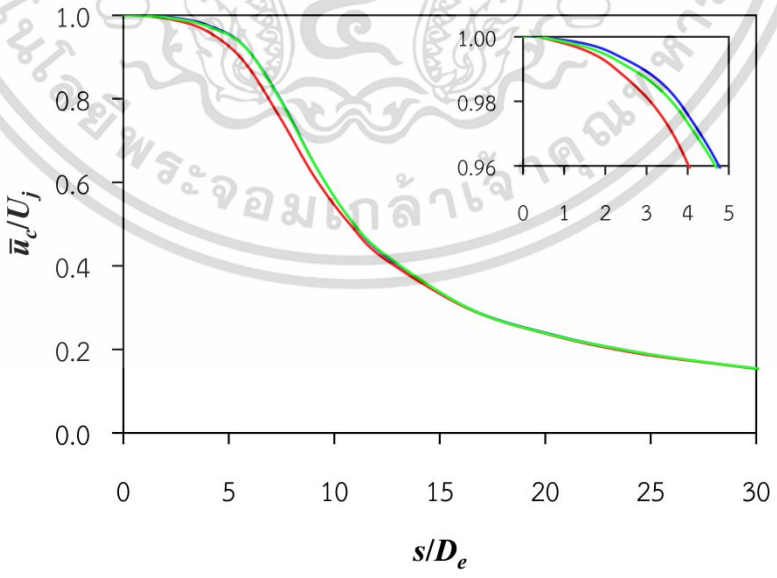

Figure 7.5 Decay of centerline streamwise velocities for three different jet mixing tanks: — CJ; — EJ; — SJ

In addition, the wider spreading of free jet generally provides the higher entrainment rate. Then, the mass flow rates and entrainment ratios, which is defined as $(Q\text{-}Q_0)/Q_0$ following Ho and Gutmark [161], of these jet mixing tanks are summarized in Table 7.3. In Table 7.3, it can be seen that the mass flow rate and entrainment ratio of elliptic jet mixing tank at different locations are greater than those achieved by other jet mixing tanks. According to these results, it seems logical to conclude that the best jet mixing performance should be obtained by elliptic jet mixing tank. However, the circular jet mixing tank presents the shortest predicted overall mixing time as previously reported in Table 7.2. Hence, it is possible to interpret that only high entrainment rate is not adequate to achieve the best mixing performance inside the jet mixing tank.

Table 7.3 Mass flow rates and entrainment ratios for circular, elliptic, and square jet mixing tanks

s/D_e	Mass flow rate[a] [kg·s^{-1}]			Entrainment ratio		
	CJ	EJ	SJ	CJ	EJ	SJ
0	0.2201	0.2201	0.2208	-	-	-
1	0.2565	0.2717	0.2625	0.1651	0.2346	0.1890
3	0.3286	0.3653	0.3387	0.4928	0.6597	0.5342
5	0.4142	0.4701	0.4277	0.8814	1.1359	0.9373
10	0.7156	0.8081	0.7481	2.2506	2.6718	2.3887

[a] These mass flow rates were computed within the areas of $\overline{u}/\overline{u}_c$ = 0.1.

Figure 7.6 illustrates the radial profiles of turbulence kinetic energy of three different jet mixing tanks. All turbulence kinetic energy distributions show saddle-backed profiles for $s/D_e \leq 5$ and bell-like profiles at s/D_e = 10. The elliptic jet provides the highest turbulence kinetic energy at $s/D_e \leq 3$ and also represents the fastest decay of turbulence kinetic energy. Then, at s/D_e = 10, the turbulence kinetic energy of elliptic jet is lower than other jets. For square jet, the turbulence kinetic energy and its decay are respectively greater (for s/D_e = 1) and faster than circular jet. The faster decay of turbulence kinetic energy for non-circular jets are caused by their high jet spreading rates during the shape adjustments. That is, the turbulence kinetic energy of non-circular jet highly transfers in lateral direction during jet spreading. Although the circular jet exhibits the lowest turbulence kinetic energy at s/D_e = 1, however, the decay of turbulence kinetic energy is slower than non-circular jets.

Finally, the circular jet shows the highest values of turbulence kinetic energy with slower decay of turbulence kinetic energy.

For RANS simulations, it is not possible to identify the velocity fluctuations. The best way to investigate the mixing due to the effect of turbulence velocity fluctuations is to determine the turbulence kinetic energy because the turbulence kinetic energy is a product of velocity fluctuations as shown in Equation (2.11). So, the turbulence kinetic energy is an indirect way to investigate the effect of velocity fluctuations. According to this interpretation, if it is correct, it can be implied that the mixing due to effect of velocity fluctuations for circular jet should be better than those obtained by non-circular jets for $s/D_e \geq 10$.

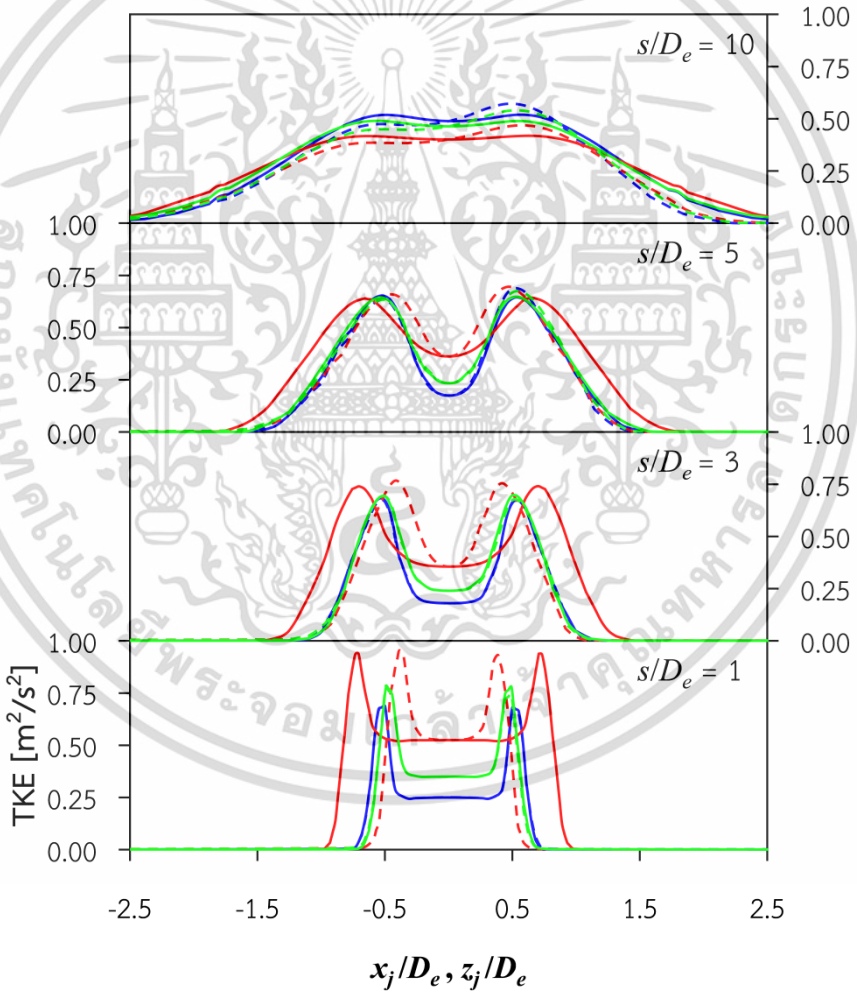

Figure 7.6 Predicted radial profiles of turbulence kinetic energy for different s/D_e ratios: —— CJ-Major axis; - - - CJ-Minor axis; —— EJ-Major axis; - - - EJ-Minor axis; —— SJ-Major axis; - - - SJ-Minor axis (Note: Major and minor axes respectively correspond to z_j and x_j axes as depicted in Figure 4.1)

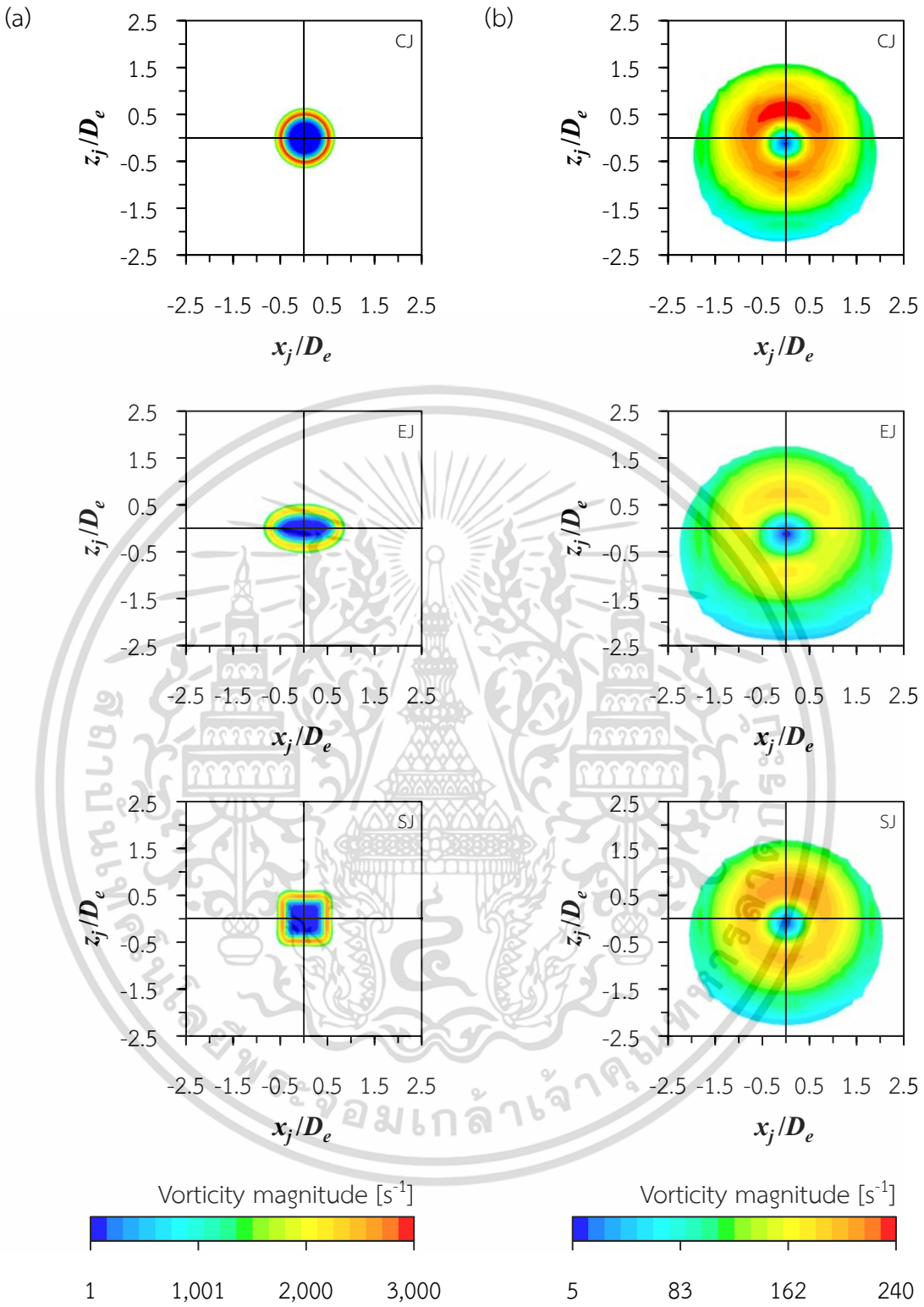

Figure 7.7 Contours of vorticity magnitude for circular jet, elliptic jet, and square jet at (a) plane s/D_e = 1 and (b) plane s/D_e = 10

Figure 7.7 represents the vorticity magnitude of three different jet mixing tanks at two different planes. The circular jet presents the highest values of vorticity magnitude for plane s/D_e = 1 and plane s/D_e = 10 because of the higher centerline streamwise

velocities, respectively followed by square and elliptic jets. Furthermore, the results reveal that the vorticity magnitude values are found to decrease with increasing the s/D_e ratios for three different jet configurations. Meaning that, the upstream vorticity magnitude values of three different jets are higher than those achieved downstream. The vorticity is a vector quantity and is twice of mean angular velocity. It is generally employed to measure the microscopic rotation (spin) of fluid at any point. The spin of fluid is a cause of fluid mixing. That is, the high value of vorticity provides the better mixing. In this case, the mixing of circular jet mixing tank should be better than those obtained by non-circular jet mixing tanks.

According to these predicted results, it can be seen that although the elliptic jet mixing tank shows the best entrainment, however, the mixing performance of circular jet mixing tank is the best because it provides higher values of upstream vorticity magnitude and downstream turbulence kinetic energy, which induce fluid to mix along the jet stream. These may be the reasons why the commercial designs of the nozzles inside jet mixing tanks are circular. Hence, it can be summarized that, for uniform jet discharge velocity profile, among three different jet nozzles considered, the circular jet mixing tank is suitable to achieve the best mixing performance (mixing without reaction). Moreover, the key parameters to achieve the best mixing performance of jet mixing tank are rotation of fluid and turbulence kinetic energy (velocity fluctuations).

CHAPTER VIII

CONCLUSIONS AND RECOMMENDATION

8.1 Conclusions

In this thesis, the comprehensive computational fluid dynamics (CFD) model for an open 45° inclined side entry pump-around jet mixing tank was properly developed with the help of grid convergence index (GCI). The discrepancy in concentration profiles between CFD model and experiment was also investigated. Further, the present CFD model was adopted to predict the mixing performances of non-circular jet mixing tanks.

The present CFD model was developed by using four assumptions including (i) The water flow inside jet mixing tank was steady state. (ii) The properties of water and tracer were identical. (iii) Top liquid-surface was assumed to be flat. (iv) The turbulence field was estimated by turbulence model. Hence, the Reynolds-averaged Navier-Stokes equations with appropriate turbulence model were adopted to solve flow and turbulence fields inside the jet mixing tanks. The tracer concentration distribution was achieved by using species transport equations without chemical reaction. Further, the predicted results were compared with reliable previous works to describe the phenomena inside the jet mixing vessel. Finally, the conclusions of the present research are summarized as follows:

8.1.1 Comprehensive CFD model

The CFD models with different k-epsilon turbulence models and numerical schemes were tested to obtain the comprehensive CFD model for simulating an open 45° inclined side entry pump-around jet mixing tank by considering the accuracy of predicted results and computational time. The concentration profiles predicted by the present model illustrated the better agreement with experimental data than previous CFD models. The necessary details of this comprehensive CFD model are summarized as shown in Table 8.1.

8.1.2 GCI analysis

GCI is generally used to measure grid convergence. In this work, the GCI was employed to confirm grid convergence of this CFD model because of high

percentage difference between potential cores predicted by coarsest and finest grid levels. Furthermore, the discretization error of this CFD model was successfully assessed by GCI analysis. The GCI results showed the discrerization error of this model of about 0.3%. The uncertainty in predicted overall mixing time was about ±0.08 s, which was three order of magnitude lower than the overall mixing time. So, this CFD model was a reliable model for overall mixing time prediction inside the jet mixing tank.

Table 8.1 Descriptions of CFD model for pump-around jet mixing tank

Detail	Steady state	Unsteady state
Grid	Hexahedral grids with appropriate arrangement	
Solver	Double precision pressure-based solver	
Turbulence model	RKE	
Boundary condition types	Inlet: velocity-inlet Outlet: pressure-outlet Wall: wall (no-slip) Top liquid-surface: symmetry	Inlet: recirculation-inlet Outlet: recirculation-outlet Wall: wall (no-slip) Top liquid-surface: symmetry
Discharge velocity [$m \cdot s^{-1}$]	4.4 - 11	
Turbulence intensity	10%	
TKE [$m^2 \cdot s^{-2}$]	$k = 1.5(U_j I)^2$	
TDR [$m^2 \cdot s^{-3}$]	$\varepsilon = C_D k^{3/2}/l$ where C_D = 0.08 and l = 0.07d_j	
P-V coupling scheme	SIMPLE	
Spatial discretization scheme	SOU	
Temporal discretization scheme	FOI	
Time step size [s]	-	0.0025
Convergence criterion	All equations were solved until the area weight average of velocity magnitude at outlet and plane x = 0 were constant.	Scaled residual of 10^{-5}

8.1.3 Model validation

In order to validate the present CFD model, the predicted overall mixing times for different jet discharge velocities were compared with experimental data of Patwardhan [74]. The results revealed that the present CFD model underpredicted the overall mixing times for jet discharge velocities of 4.4 - 11 $m \cdot s^{-1}$, which were in good agreement with experiments. These overpredicted mixing times were due to the flat top liquid-surface assumption. For jet discharge velocity of 2.2 $m \cdot s^{-1}$, this model showed the overpredicted overall mixing time with the maximum percentage error between CFD model and experiment of about 15% because of the limitation of RKE that it is valid only for high Reynolds number turbulent flow. However, for predicted concentration profiles, the differences between this CFD model and experiment were still observed, which were similar to the previous work of Patwardhan [74]. However, in order to study the bulk mixing of jet mixing tank, this model was acceptable.

8.1.4 Turbulence boundary conditions

Due to the absence of the exact inlet turbulence boundary conditions, the different turbulence intensities and correlations for estimating the turbulence kinetic energy and its dissipation rate were studied to obtain the accurate overall mixing time and concentration profiles, which corresponded to the model assumptions. From the results, the overall mixing times predicted by different conditions were slightly different. However, the predicted concentration profiles of 10% turbulence intensity showed the better agreement with experiments as comparing with the turbulence intensity estimated by the correlation of fully developed pipe flow. According to the higher convective transport due to top liquid-surface assumption, the concentration profiles simulated by turbulence kinetic energy obtained by Equation (6.1) with turbulence intensity of 10% and turbulence kinetic energy dissipation rate estimated by Equation (6.3) represented the acceptable agreement with experimental data.

8.1.5 Discrepancy in concentration profiles

Although the present comprehensive CFD model was adopted to predict the concentration profiles inside an open pump-around jet mixing tank, however, the discrepancy in concentration profiles between CFD simulation and experiment was still observed. From the present results, it can be concluded that there are two

possible causes of this discrepancy, including the improper extent of turbulent dispersion inside the vessel due to the inappropriate inlet turbulence conditions and the overpredicted convective transport due to flat top liquid-surface assumption. Further, the simplified computational domain is another possible cause of this discrepancy.

8.1.6 Pump-around non-circular jet mixing tanks

In this part, the pump-around elliptic and square jet mixing tanks with jet discharge velocity of 4.4 $m \cdot s^{-1}$ were simulated by using the present CFD model. The mixing performances and flow phenomena of these non-circular jet mixing tanks were compared to the circular jet mixing tank and can be summarized as depicted in Table 8.2.

Table 8.2 Mixing performances and flow phenomena of jet mixing tanks

Performance/Phenomena	Jet mixing tank		
	Circular	Elliptic	Square
Mixing time	●	◐	○
Spreading rate	○	●	◐
Entrainment	○	●	◐
Decay of centerline streamwise velocity	●	○	◐
Decay of turbulence kinetic energy	●	○	◐
Vorticity	●	○	◐

● Good; ◐ Fair; ○ Poor

From Table 8.2, it can be seen that although the entrainment of elliptic jet mixing tank was better than other jet mixing tanks, however, the circular jet mixing tank provided the best mixing performance. So, it can be concluded that, for uniform jet discharge velocity profile, the circular jet mixing tank showed the highest mixing performance because of high values of upstream vorticity and downstream turbulence kinetic energy due to the slowest decays of centerline streamwise velocity and turbulence kinetic energy, which induced liquid to mix in both near and far fields of jet. These may be the reasons why the circular nozzles are commonly used in commercial designs of jet mixing tanks. Further, the upstream vorticity and downstream turbulence kinetic energy can be considered as the key parameters to obtain the high jet mixing performance.

From above conclusions, it can be seen that this thesis represented the CFD modeling for overall mixing time prediction inside pump-around jet mixing tank, which was slightly different to the previous CFD models. However, this thesis showed the main contribution that the present CFD model was more reliable to predict the overall mixing time of jet mixing tank than the previous models because the GCI analysis confirmed that the discretization uncertainty in overall mixing time of the present model was three order of magnitude lower than the predicted mixing time. Further, the improvement and limitation of the present model for concentration profile prediction were clearly represented.

Hence, the present simulation procedures can be considered as the best practice guideline for predicting the overall mixing times of different jet mixing tanks. In order to predict the overall mixing times of different jet mixing tank geometries, this reliable CFD guideline is more suitable than non-universal mixing time correlations (i.e., correlations are case specific), especially for the complicate jet mixing tank geometries. That is, the present CFD model (or this CFD guideline) can be adopted to predict the overall jet mixing times instead of non-universal mixing time correlations. Moreover, for industrial applications, the predicted overall mixing times should be multiplied by safety factor of 1.2 to ensure that these estimated overall mixing times are sufficient to reach the mixing criteria. Note that, for special cases (e.g. stop runaway reactions), the present CFD guideline must be modified to obtain the more accurate overall mixing time and normalized concentration profiles.

8.2 Recommendation

Although the present comprehensive CFD model predicted overall mixing time accurately and fairly improved the simulated concentration profiles, however, the discrepancy between this model and experimental data was still observed. There are many possible routes to enhance an accuracy of concentration profile prediction. Some of possible ways for resolving this shortfall are suggested as follows:

- For the present CFD model, the flat top liquid-surface motion was assumed. In order to show the realistic behavior of liquid-surface motion, the multiphase model, e.g. volume of fluid (VOF) model, should be adopted. However, this multiphase model requires powerful computation facility due to a very large number

of small grids. If the computing facility is limited, at least, the effect of top liquid-surface motion should be modeled by specifying the shear stress at this surface.

- The turbulent flow phenomena of jet inside the mixing tank simulated by more accurate turbulence models, such as Reynolds stress model (RSM), large eddy simulation (LES), etc., may be improved the predicted extent of turbulent dispersion, which directly affects the distribution of concentration inside the tank.

- The actual jet nozzle geometry and exact inlet boundary conditions should be employed to predict the concentration profiles because the jet flow patterns are dependent on nozzle geometries and inlet conditions. Further, for turbulent flow, the upstream conditions significantly affect the downstream flow patterns [166, 167].

- The modification of near wall grids is necessary for improving the prediction accuracy of liquid flow along the tank wall, which may increase the accuracy of predicted concentration profiles.

Furthermore, there are a few experimental data of jet flow phenomena inside an inclined side entry jet mixing tank. Hence, the experimental work of jet flow inside the tank is necessary to understand the flow phenomena and to enhance the CFD simulation accuracy.

REFERENCES

[1] Fossett, H. and Prosser, L.E. "The Application of Free Jets to the Mixing of Fluids in Bulk" **Proceedings of the Institution of Mechanical Engineers**, vol. 160, 1949. pp. 224-232.

[2] Bumrungthaichaichan, E. "A review on numerical consideration for computational fluid dynamics modeling of jet mixing tanks" **Korean Journal of Chemical Engineering**, vol. 33, no. 11, 2016. pp. 3050-3068.

[3] Versteeg, H.K. and Malalasekera, W. **An introduction to computational fluid dynamics The finite volume method**. England : Addison Wesley Longman Limited. 1995.

[4] Richardson, L.F. "The Approximate Arithmetical Solution by Finite Differences of Physical Problems Involving Differential Equations, with an Application to the Stresses in a Masonry Dam" **Philosophical Transactions of the Royal Society of London. Series A**, vol. 210, January 1911. pp. 307-357.

[5] CFD Online. "History of CFD." [Online]. Available : http://www.cfd-online.com/Wiki/History_of_CFD. 2016.

[6] Fromm, J.E. and Harlow, F.H. "Numerical Solution of the Problem of Vortex Street Development" **Physics of Fluids**, vol. 6, no. 7, 1963. pp. 975-982.

[7] Harlow, F.H. and Fromm, J.E. "Computer Experiments in Fluid Dynamics" **Scientific American**, vol. 212, no. 3, March 1965. pp. 104-110.

[8] Thom, A. "The Flow Past Circular Cylinders at Low Speeds" **Proceedings of the Royal Society of London. Series A**, vol. 141, no. 845, September 1933. pp. 651-669.

[9] Dennis, B.H. and Kumar, R. "A least-squares/Galerkin split finite element method for incompressible Navier-Stokes problems" **Proceedings of the ASME 2008 International Design Engineering Technical Conferences & Computers and Information in Engineering Conference**, New York, USA, August, 2008. pp. 2-12.

[10] Bahhar, A., Baranger, J. and Sandri, D. "Galerkin discontinuous approximation of the transport equation and viscoelastic fluid flow on quadrilaterals" **Numerical Methods for Partial Differential Equations**, vol. 14, no. 1, January 1998. pp. 97-114.

[11] Evans, M.W. and Harlow, F.H. **THE PARTICLE-IN-CELL METHOD FOR HYDRODYNAMIC CALCULATIONS**. LA-2139. 1957.

[12] Bernoulli, D. **Hydrodynamica, sive De viribus et motibus fluidorum commentarii**. Strasbourg. 1738.

[13] Euler, L. "Principes généraux du mouvement des fluides" **Mémoires de l'Acad. des Sciences de Berlin**, vol. 11, 1757. pp. 274-315.

[14] Navier, C.-L. "Mémoire sur les lois du mouvement des fluides" **Mémoires de l'Acad. des Sciences de l'Institut de France**, vol. 6, 1827. pp. 389-440.

[15] Stokes, G.G. "On the theory of the internal friction of fluids in motion, and of the equilibrium and motion of elastic solids" **Transactions of the Cambridge Philosophical Society**, vol. 8, 1849. pp. 287-319.

[16] Stokes, G.G. "On the Effect of the Internal Friction of Fluids on the Motion of Pendulums" **Transactions of the Cambridge Philosophical Society**, vol. 9, 1851. pp. 8-106.

[17] Sommerfeld, A. "Ein Beitrag zur hydrodynamischen Erkläerung der turbulenten Flüssigkeitsbewegüngen" **International Congress of Mathematicians**, vol. 3, 1908. pp. 116-124.

[18] Reynolds, O. "An experimental investigation of the circumstances which determine whether the motion of water shall be direct or sinuous, and of the law of resistance in parallel channels" **Philosophical Transactions of the Royal Society of London**, vol. 174, 1883. pp. 935-982.

[19] Reynolds, O. "On the Dynamical Theory of Incompressible Viscous Fluids and the Determination of the Criterion" **Proceedings of the Royal Society of London. Series A**, vol. 186, 1895. pp. 123-164.

[20] Socolofsky, S. **Lecture note on Fluid Dynamics for Ocean and Environmental Engineering**. USA : TEXAS A&M UNIVERSITY. 2012.

[21] CFD Online. “Boussinesq eddy viscosity assumption.” [Online]. Available : http://www.cfd-online.com/Wiki/Boussinesq_eddy_viscosity_assumption. 2016.

[22] Celik, I.B. **Introductory Turbulence Modeling**. USA : West Virginia University. 1999.

[23] Harlow, F.H. and Nakayama, P.I. **Transport of Turbulence Energy Decay Rate**. LA-3854. 1968.

[24] Wikipedia. “K-epsilon turbulence model.” [Online]. Available : https://en.wikipedia.org/wiki/K-epsilon_turbulence_model. 2016.

[25] Launder, B.E. and Spalding, D.B. **Lectures in Mathematical Models of Turbulence**. England : Academic Press. 1972.

[26] ANSYS Inc. **ANSYS Fluent Theory Guide Release 15.0**. USA : ANSYS Inc. 2013.

[27] Kim, S.-E., Barbat, T., and Spicka, P. **Meshing and CFD Accuracy**. USA : FLUENT. 2005.

[28] Marshall, E.M. and Bakker, A. Computational Fluid Mixing. In : Paul, E.L., Atiemo-Obeng, V.A. and Kresta, S.M. (eds.) **HANDBOOK OF INDUSTRIAL MIXING SCIENCE AND PRACTICE**. Canada : John Wiley & Sons. 2004.

[29] Bakker, A. **Applied Computational Fluid Dynamics: Lecture 5 - Solution Methods**. USA : FLUENT. 2002.

[30] Patankar, S.V. and Spalding, D.B. “A Calculation Procedure for Heat, Mass and Momentum Transfer in Three-Dimensional Parabolic Flows” **International Journal of Heat and Mass Transfer**, vol. 15, 1972. pp. 1787-1806.

[31] ANSYS Inc. **ANSYS Fluent User's Guide Release 15.0**. USA : ANSYS Inc. 2014.

[32] AIAA. **Guide for the Verification and Validation of Computational Fluid Dynamics Simulations**. USA : AIAA. 1998.

[33] Revill, B.K. Jet mixing. In : Harnby, N., Edwards, M.F. and Nienow, A.W. (eds.) **Mixing in the Process Industries**. Oxford : Butterworth-Heinemann. 1992.

[34] Cushman-Roisin, B. “Environmental Fluid Mechanics.” [Online]. Available : https://engineering.dartmouth.edu/~d30345d/books/EFM.html. 2017.

[35] Lee, J.H.W. and Chu, V.H. **TURBULENT JETS AND PLUMES - A Lagrangian Approach**. New York : Kluwer Academic Publishers. 2003.

[36] Ball, C.G., Fellouah, H. and Pollard, A. "The flow field in turbulent round free jets" **Progress in Aerospace Sciences**, vol. 50, 2012. pp. 1-26.

[37] Wang, X. and Tan, S.K. "Environmental fluid dynamics-jet flow" **Journal of Hydrodynamics**, vol. 22, no. 5, 2012. pp. 1009-1014.

[38] Seok, J.K. and Il, W.S. "Reynolds number effects on the behavior of a non-buoyant round jet" **Experiments in Fluids**, vol. 38, 2005. pp. 801-812.

[39] Abdel-Rahman, A. "A review of effects of initial and boundary conditions on turbulent jets" **WSEAS transactions on Fluid Mechanics**, vol. 4, no. 5, 2010. pp. 257-275.

[40] Fellouah, H., Ball, C.G. and Pollard, A. "Reynolds number effects within the development region of a turbulent round free jet" **International Journal of Heat and Mass Transfer**, vol. 52, 2009. pp. 3943-3954.

[41] Gartshore, I.S. Self-preserving flows. In : VKI (ed.) **Lecture series 36 - Turbulent jet flows**. Rhode-Saint-Genèse : von Karman Institute for Fluid Dynamics. 1971.

[42] George, W.K. The self-preservation of turbulent flows and its relation to initial conditions and coherent structures. In : George, W.K. and Arndt, R.E.A. (eds.) **Advances in turbulence**. New York : Springer. 1989.

[43] Richards, C.D. and Pitts, W.M. "Global density effects on the self-preservation behaviour of turbulent free jets" **Journal of Fluid Mechanics**, vol. 254, 1993. pp. 417-435.

[44] Capone, A., Soldati, A. and Romano, G.P. "Mixing and entrainment in the near field of turbulent round jets" **Experiments in Fluids**, vol. 54, 2013. pp. 1434-1447.

[45] Wygnanski, I. and Fiedler, H. "Some measurements in the self-preserving jet" **Journal of Fluid Mechanics**, vol. 38, 1969. pp. 577-612.

[46] Papanicolaou, P.N. "**Mass and momentum transport in a turbulent buoyant vertical axisymmetric jet**" PhD thesis, California Institute of Technology, California, 1984.

[47] Hussein, H.J., Capp, S. and George, W.K. "Velocity measurements in a high-Reynolds-number, momentum-conserving, axisymmetric, turbulent jet" **Journal Fluid Mechanics**, vol. 258, 1994. pp. 31-75.

[48] Hongwei, W. "**Investigations of buoyant jet discharges using combined DPIV and PLIF**" PhD thesis, Nanyang Technological University, Singapore, 2000.

[49] Quinn, W.R. "Upstream nozzle shaping effects on near field flow in round turbulent free jets" **European Journal of Mechanics B - Fluids**, vol. 25, 2006. pp. 279-301.

[50] Yoder, D.A., DeBonis, J.R. and Georgiadis, N.J. "Modeling of Turbulent Free Shear Flows" **Proceedings of the 21st AIAA Computational Fluid Dynamics Conference**, San Diego, USA, June, 2013. AIAA 2013-2721.

[51] Pope, S.B. **Turbulent Flows**. New York : Cambridge University Press. 2000.

[52] Papanicolaou, P.N. and List, E.J. "Investigations of round vertical turbulent buoyant jets" **Journal of Fluid Mechanics**, vol. 195, 1988. pp. 341-391.

[53] Panchapakesan, N.R. and Lumley, J.L. "Turbulence measurements in axisymmetric jets of air and helium. Part 1. Air jet" **Journal of Fluid Mechanics**, vol. 246, 1993. pp. 197-223.

[54] Davies, J.T. **Turbulence phenomena**. New York : Academic Press. 1972.

[55] Schlichting, H. **Boundary Layer Theory**. New York : McGraw Hill. 1968.

[56] Albertson, M.L., Dai, Y.B., Jensen, R.A. and Rouse, H. "Diffusion of Submerged Jets" **Transactions of the American Society of Civil Engineers**, vol. 115, no. 1, 1950. pp. 639-664.

[57] Fossett, H. "The action of free jets in the mixing fluids" **Chemical Engineering Research and Design**, vol. 29a, 1951. pp. 322-332.

[58] Mewes, D. and Renz, R. "Jet mixing of liquids in storage tanks" **Proceedings of the 7th European Conference on Mixing**, Brugges, Belgium, 1991. pp. 131-137.

[59] Hoffman, P.D. "Mixing in a large storage tank" **AIChE Symposium Series**, vol. 286, no. 88, 1996. pp. 77-82.

[60] Schimetzek, R., Steiff, A. and Weinspach, P.M. "Examination of discontinuous jet mixing for designing emergency cooling systems of chemical reactors" **IChemE Symposium Series**, vol. 136, 1995. pp. 391-398.

[61] Sarsten, J.A. "LNG stratification and rollover" **Pipeline and Gas Journal**, September 1972. pp. 37-39.

[62] Simon, M. and Fonade, C. "Experimental study of mixing performances using steady and unsteady jets" **Canadian Journal of Chemical Engineering**, vol. 71, no. 4, 1993. pp. 507-513.

[63] Baldyga, J., Bourne, J.R. and Zimmermann, B. "Investigation of mixing in jet reactors using fast competitive–consecutive reactions" **Chemical Engineering Science**, vol. 49, no. 12, 1994. pp. 1937-1946.

[64] Sudhindra, N. and Sinha, S.N. "Paper C4" **Proceedings of the 4th European Conference on Mixing**, Leeuwenhors, Netherlands, 1982. Paper C4.

[65] Revill, B.K. "Paper to IChemE Course" University of Bradford, England, 1981.

[66] Lane, A.G.C. and Rice, P. "An investigation of liquid jet mixing employing an inclined side-entry jet" **Chemical Engineering Research Design**, vol. 60a, 1982. pp. 171-176.

[67] Grenville, R.K., Mak, A.T.C. and Ruszkowski, S.W. "Blending of fluids in mixing vessels by turbulent recirculating jets" **Proceedings of the 1992 IChemE Research Event**, University of Manchester Institute of Science and Technology, United Kingdom, 1992. pp. 128-130.

[68] Grenville, R.K. and Tilton, J.N. "A new theory improves the correlation of blend time data from turbulent jet mixed vessels" **Chemical Engineering Research and Design**, vol. 74a, 1996. pp. 390-396.

[69] Lane, A.G.C. "**Liquid Jet Mixing in Tanks**" PhD thesis, Loughborough University of Technology, United Kingdom, 1981.

[70] Zughbi, H.D. and Rakib, M.A. "Investigations of mixing in a fluid Jet agitated tank" **Chemical Engineering Communications**, vol. 189, no. 8, 2002. pp. 1038-1056.

[71] Zughbi, H.D. and Rakib, M.A. "Mixing in a fluid jet agitated tank: effects of jet angle and elevation and number of jets" **Chemical Engineering Science**, vol. 59, no. 4, 2004. pp. 829-842.

[72] Zughbi, H.D. and Ahmad, I. "Mixing in Liquid-Jet-Agitated Tanks: Effects of Jet Asymmetry" **Industrial & Engineering Chemistry Research**, vol. 44, no. 4, 2005. pp. 1052-1066.

[73] Ranade, V.V. "Towards better mixing protocols by designing spatially periodic flows: the case of a jet mixer" **Chemical Engineering Science**, vol. 51, no. 11, 1996. pp. 2637-2642.

[74] Patwardhan, A.W. "CFD modeling of jet mixed tanks" **Chemical Engineering Science**, vol. 57, no. 8, 2002. pp. 1307-1318.

[75] Thatte, A.R., Patwardhan, A.W., Pant, H.J., Sharma, V.K., Singh, G. and Berne, Ph. "Mixing and RTD in tanks: radiotracer experiments and CFD simulations" **Proceedings of the International Conference on Tracers and Tracing Methods**, Poland, 2004. pp. 43-47.

[76] Jayanti, S. "Hydrodynamics of jet mixing in vessels" **Chemical Engineering Science**, vol. 56, no. 1, 2001. pp. 193-210.

[77] Rahimi, M. and Parvareh, A. "Experimental and CFD investigation on mixing by a jet in a semi-industrial stirred tank" **Chemical Engineering Journal**, vol. 115, 2005. pp. 85-92.

[78] Raja, T., Kalaichelvi, P. and Anantharaman, N. "Development of CFD model for optimum mixing in jet mixed tanks" **Journal of Scientific & Industrial Research**, vol. 66, no. 7, 2007. pp. 522-527.

[79] Fox E.A. and Gex, V.E. "Single-phase blending of liquids" **AIChE Journal**, vol. 2, no. 4, 1956. pp. 539-544.

[80] Van De Vusse, J.G. "Vergleichende Rührversuche zum Mischen löslicher Flüssigkeiten in einem 12 000-m^3-Behälter" **Chemie Ingenieur Technik**, vol. 31, no. 9, 1959. pp. 583-587.

[81] Okita, N. and Oyama, Y. "Mixing characteristics in jet mixing" **Japanese Journal of Chemical Engineers**, vol. 27, no. 4, 1963. pp. 252-260.

[82] Coldrey, P.W. "Paper to IChemE Course" University of Bradford, England, 1978.

[83] Hiby J.W. and Modigell, M. "Experiments on jet agitation" **Proceedings of the 6th CHISA Congress**, Prague, 1978.

[84] Lehrer, I.H. "A new model for free turbulent jets of miscible fluids of different density and a jet mixing time criterion" **Chemical Engineering Research and Design**, vol. 59a, 1981. pp. 247-252.

[85] Lane, A.G.C. and Rice, P. "An experimental investigation of jet mixing employing a vertical submerged jet" **IChemE Symposium Series 64**, 1981. Paper K1.

[86] Maruyama, T., Ban, Y. and Mizushina, T. "Jet mixing of fluids in tanks" **Journal of Chemical Engineering of Japan**, vol. 15, no. 5, 1982. pp. 342-348.

[87] Maruyama, T. Jet mixing of fluids in vessels. In : Cheremisinoff, N.P. (ed.) **Encyclopedia of Fluid Mechanics Vol. 2. Houston** : Gulf Publishing Company. 1986.

[88] Orfaniotis, A., Fonade, C., Lalane, M. and Doubrovine, N. "Experimental study of the fluidic mixing in a cylindrical reactor" **Canadian Journal of Chemical Engineering**, vol. 74, no. 2, 1996. pp. 203-212.

[89] Grenville, R.K. and Tilton, J.N. "Turbulence or flow as a predictor of blend time in turbulent jet mixed vessels" **Proceedings of the 9th European Conference on Mixing**, France, 1997. pp. 67-74.

[90] Grenville, R.K. and Tilton, J.N. "Jet mixing in tall tanks: Comparison of methods for predicting blend times" **Chemical Engineering Research and Design**, vol. 89, no. 12, 2011. pp. 2501-2506.

[91] Patwardhan, A.W. and Gaikwad, S.G. "Mixing in tanks agitated by jets" **Chemical Engineering Research and Design**, vol. 81, no. 2, 2003. pp. 211-220.

[92] Brooker, L. "Mixing with the jet set" **Chemical Engineering**, vol. 30, 1993. pp. 16-25.

[93] Jaiklom, N., Bumrungthaichaichan, E. and Wattananusorn, S. "CFD Simulation of Turbulent Jet Mixing Tank" **Ladkrabang Engineering Journal**, vol. 30, no. 4, 2013. pp. 37-42.

[94] Wasewar, K.L. "A Design of Jet Mixed Tank" **Chemical and biochemical Engineering Quarterly**, vol. 20, no. 1, 2006. pp. 31-46.

[95] Marek, M., Stoesser, T., Roberts, P.J.W., Weitbrecht, V. and Jirka, G.H. "CFD modeling of turbulent jet mixing in a water storage tank" **Proceedings of the 32nd IAHR World Congress**, Italy, 2007.

[96] Sendilkumar, K., Kalaichelvi, P., Perumalsamy, M., Arunagiri, A. and Raja, T. "Computational Fluid Dynamic Analysis of Mixing Characteristics inside a Jet Mixer for Newtonian and Non Newtonian Fluids" **Proceedings of the World Congress on Engineering and Computer Science 2007**, USA, 2007.

[97] Wasewar, K.L. and Sarathi, J.V. "CFD Modelling and Simulation of Jet Mixed Tanks" **Engineering Applications of Computational Fluid Mechanics**, vol. 2, no. 2, 2008. pp. 155-171.

[98] Mathpati, C.S., Deshpande, S.S. and Joshi, J.B. "Computational and Experimental Fluid Dynamics of Jet Loop Reactor" **AIChE Journal**, vol. 55, no. 10, 2009. pp. 2526-2544.

[99] Parvareh, A., Rahimi, M. and Alsairafi, A.A. "Experimental and CFD Studies on the Effect of the Jet Position on Mixing Performance" **Iranian Journal of Chemical Engineering**, vol. 6, no. 3, 2009. pp. 3-12.

[100] Breisacher, K. and Moder, J. "Computational Fluid Dynamics (CFD) Simulations of Jet Mixing in Tanks of Different Scales" **NASA**, 2010. NASA/TM-2010-216749.

[101] Furman, L. and Stegowski, Z. "CFD models of jet mixing and their validation by tracer experiments" **Chemical Engineering and Processing**, vol. 50, no. 3, 2011. pp. 300-304.

[102] Lee, S.Y. and Armstrong, B.W. "SDI CFD Modeling Analysis" **Savannah River National Laboratory**, 2011. SRNS-STI-2011-00025.

[103] Dautova, L.S., Milanovic, I. and Hammad, K.J. "CFD Study of the Effect of Jet Placement on Flow Patterns Inside a Jet Stirred Tank" **Proceedings of 2012 ASEE Northeast Section Conference**, University of Massachusetts Lowell, 2012.

[104] Leishear, R.A., Lee, S.Y., Fowley, M.D., Poirier, M.R. and Steeper, T.J. "Comparison of Experiments to Computational Fluid Dynamics Models for Mixing Using Dual Opposing Jets in Tanks With and Without Internal

Obstructions" **Journal of Fluids Engineering**, vol. 134, no. 11, 2012. 111102-1–111102-21.

[105] Muhammad, I.R. and Kizito, J.P. "Mixing time determination of steady and pulse jet mixers" **ASME Early Career Technical Journal**, vol. 11, 2012. pp. 221-227.

[106] Rafiei, H., Janamiri, R., Sedaghat, M.H. and Hatampour, A. "Experimental and CFD Investigation of Nozzle Angle in Jet Mixer" **World Academy of Science, Engineering and Technology**, vol. 6, no. 12, 2012. pp. 1189-1191.

[107] Lee, S.Y. "Mixing Study for JT-71/72 Tanks" **Savannah River National Laboratory**, 2013. SRNL-STI-2013-00702.

[108] Egedy, A., Molnar, B., Varga, T. and Chován, T. "Optimization of Jet Mixer Geometry and Mixing Studies" **Proceedings of the 2014 COMSOL**, Cambridge, 2014.

[109] Bumrungthaichaichan, E., Jaiklom, N., Namkanisorn, A. and Wattananusorn, S. "On the computational fluid dynamics (CFD) analysis of the effect of jet nozzle angle on mixing time for various liquid heights" **Scientific Research and Essays**, vol. 11, no. 4, 2016. pp. 42-56.

[110] Meng, H.-B., Wang, W., Yu, Y.-F., Wu, J.-H., Wang, Y.-F. and Wang, Z.-Y. "Investigation of the Effect of Outlet Structures on the Jet Flow Characteristics in the Circulating Jet Tank" **International Journal of Chemical Reactor Engineering**, vol. 12, no. 1, 2014. pp. 35-45.

[111] Yu, Y.-F., Jiang, X.-H., Meng, H.-B., Wu, J.-H., Wang, Z.-Y. and Wang W. "Computational Simulation of Mixing Performance in the Circulating Jet Mixing Tank" **International Journal of Chemical Reactor Engineering**, vol. 14, no. 2, 2016. pp. 621-636.

[112] Moncho-Esteve, I.J., Palau-Salvador, G., Brevis, W., Vaas, M.O. and López-Jiménez, P.A. "Numerical simulation of the hydrodynamics and turbulent mixing process in a drinking water storage tank" **Journal of Hydraulic Research**, vol. 53, no. 2, 2015. pp. 207-217.

[113] Codina, R., Principe, J., Muñoz, C. and Baiges, J. "Numerical modeling of chlorine concentration in water storage tanks" **International Journal for Numerical Methods in Fluids**, vol. 79, no. 2, 2015. pp. 84-107.

[114] Wojtas, K., Orciuch, W. and Makowski, Ł. "Comparison of Large Eddy Simulations and k-ε Modelling of Fluid Velocity and Tracer Concentration in Impinging Jet Mixers" **Chemical and Process Engineering**, vol. 36, no. 2, 2015. pp. 251-262.

[115] Montoya-Pachongo, C., Laín-Beatove, S., Torres-Lozada, P., Cruz-Vélez, C.H. and Escobar-Rivera, J.C. "Effects of water inlet configuration in a service reservoir applying CFD modelling" **Ingenieria e Investigacion**, vol. 36, no. 1, 2016. pp. 31-40.

[116] Pathapati, S.S., Mazzei, A.L., Jackson, J.R., Overbeck, P.K., Bennett, J.P. and Cobar, C.M. "Optimization of Mixing and Mass Transfer in In-line Multi-Jet Ozone Contactors Using Computational Fluid Dynamics" **Ozone-Science & Engineering**, vol. 38, no. 4, 2016. pp. 245-252.

[117] Qu, Y., Zhou, C., Zhong, Y., Chen, S. and Wang, R. "A computational study on gas–liquid flow in a lime slurry pond equipped with a rotary jet mixing system" **Advances in Mechanical Engineering**, vol. 9, no. 2, 2017. pp. 1-9.

[118] Lotfi Neyestanak, A.A., Tarybakhsh, M.R. and Daneshmand, S. "Study on the Effect of Jet Velocity on Mixing Performance and Sludge Prevention in Large-Scale Crude-Oil Tanks by the CFD Technique" **Kemija u industriji-Journal of Chemists and Chemical Engineers**, vol. 66, no. 5-6, 2017. pp. 229-239.

[119] Low, S.C., Eshtiaghi, N., Shu, L., Parthasarathy, R. "Flow patterns in the mixing of sludge simulant with jet recirculation system" **Process Safety and Environmental Protection**, vol. 112, 2017. pp. 209-221.

[120] Courant, R. Friedrichs, K. and Lewy, H. "On the Partial Difference Equations of Mathematical Physics" **IBM Journal**, vol. 11, no. 2, 1967. pp. 215-234.

[121] Cimbala, J.M. and Çengel, Y.A. **Essentials of Fluid Mechanics: Fundamentals and Applications**. New York : McGraw Hill. 2008.

[122] Zhang, H.-J. and Han, S.-J. "Viscosity and Density of Water + Sodium Chloride + Potassium Chloride Solutions at 298.15 K" **Journal of Chemical & Engineering Data**, vol. 41, 1996. pp. 516-520.

[123] Dakshinamoorthy, D., Khopkar, A.R., Louvar, J.F. and Ranade, V.V. "CFD simulation of shortstopping runaway reactions in vessels agitated with impellers and

jets" **Journal of Loss Prevention in the Process Industries**, vol. 19, 2006. pp. 570-581.

[124] Dakshinamoorthy, D. and Louvar, J.F. "Shortstopping and jet mixers in preventing runaway reactions" **Chemical Engineering Science**, vol. 63, 2008. pp. 2283-2293.

[125] ANSYS, Inc. **Introduction to ANSYS FLUENT: Lecture 5 - Solver Settings**. USA : ANSYS, Inc. 2012.

[126] Spyrou, M. "The Diffusion Coefficient of Water: A Neutron Scattering Study using Molecular Dynamics Simulations" Master thesis, University of Surrey, Guildford, 2009.

[127] Krynicki, K., Green, C.D. and Sawyer, D.W. "Pressure and Temperature Dependence of Self-diffusion in Water" **Faraday Discussions of the Chemical Society**, vol. 66, 1978. pp. 199-208.

[128] Wu, Y., Tepper, H.L. and Voth, G.A. "Flexible simple point-charge water model with improved liquid-state properties" **Journal of Chemical Physics**, vol. 124, 2006. 024503.

[129] Dange, S. "Recirculation Boundary Conditions in ANSYS FLUENT." [Online]. Available : https://www.learncax.com/knowledge-base/blog/by-category/cfd/recirculation-boundary-conditions-in-ansys-fluent. 2016.

[130] Zhang, Q., Yang, C., Mao, Z.-S. and Mu, J. "Large Eddy Simulation of Turbulent Flow and Mixing Time in a Gas–Liquid Stirred Tank" **Industrial & Engineering Chemistry Research**, vol. 51, 2012. pp. 10124-10131.

[131] Yang, F.L., Zhou, S.J. and Zhang, C.X. "Turbulent flow and mixing performance of a novel six-blade grid disc impeller" **Korean Journal of Chemical Engineering**, vol. 32, no. 5, 2015. pp. 816-825.

[132] Elsayed, K. "Analysis and Optimization of Cyclone Separators Geometry Using RANS and LES Methodologies" PhD thesis, Vrije Universiteit Brussel, Belgium, 2011.

[133] Dirgo, J. and Leith, D. "Cyclone collection efficiency: Comparison of experimental results with theoretical predictions" **Aerosol Science and Technology**, vol. 4, 1985. pp. 401-415.

[134] Chuah, T.G., Gimbun, J. and Choong, T.S.Y. "A CFD study of the effect of cone dimensions on sampling aerocyclones performance and hydrodynamics" **Powder Technology**, vol. 162, 2006. pp. 126-132.

[135] Elsayed, K. and Lacor, C. "The effect of cyclone inlet dimensions on the flow pattern and performance" **Applied Mathematical Modelling**, vol. 35, no. 4, 2011. pp. 1952-1968.

[136] Pope, S.B. "An explanation of the turbulent round-jet/plane-jet anomaly" **AIAA Journal**, vol. 16, no. 3, 1978. pp. 279-281.

[137] Shih, T.-H., Liou, W.W., Shabbir, A., Yang, Z. and Zhu, J. "A new k-ε eddy viscosity model for high Reynolds number turbulent flows" **Computers & Fluids**, vol. 24, no. 3, 1995. pp. 227-238.

[138] Shih, T.-H. Constitutive relations and realizability of single-point turbulence closures. In : Hallbäck, M., Henningson, D.S., Johanssan, A.V. and Alfredsson, P.H. (eds.) **Turbulence and Transition Modelling**. Dordrecht : Springer. 1996.

[139] ANSYS Inc. **ANSYS Fluent Tutorial Guide Release 15.0**. USA : ANSYS Inc. 2013.

[140] Roache, P.J. "Perspective: A Method for Uniform Reporting of Grid Refinement Studies" **Journal of Fluids Engineering**, vol. 116, 1994. pp. 405-413.

[141] Roache, P.J. "Quantification of Uncertainty in Computational Fluid Dynamics" **Annual Review of Fluid Mechanics**, vol. 29, 1997. pp. 123-160.

[142] Roache, P.J. "Verification of Codes and Calculations" **AIAA Journal**, vol. 36, no. 5, 1998. pp. 696-702.

[143] Slater, J.W. "Examining spatial (grid) convergence." [Online]. Available : https:// www.grc.nasa.gov/WWW/wind/valid/tutorial/spatconv.html. 2008.

[144] Ali, M.S.M., Doolan, C.J. and Wheatley, V. "Grid convergence study for a two-dimensional simulation of flow around a square cylinder at a low Reynolds number" **Proceedings of the Seventh International Conference on CFD in the Minerals and Process Industries CSIRO**, Melbourne, Australia, December, 2009. pp. 1-6.

[145] Ghahremanian, S. and Moshfegh, B. "Evaluation of RANS Models in Predicting Low Reynolds, Free, Turbulent Round Jet" **Journal of Fluids Engineering**, vol. 136, no. 1, 2013. pp. 011201-1-011201-13.

[146] Reynolds, A.J. **Turbulent Flows in Engineering**. New York : Wiley. 1974.

[147] Fluent Inc. **FLUENT 6.3 User's Guide**. Lebanon : Fluent Inc. 2006.

[148] White, F.M. **Viscous Fluid Flow**. New York : McGraw Hill. 2006.

[149] ANSYS Inc. **ANSYS CFX-Solver Theory Guide Release 15.0**. USA : ANSYS Inc. 2013.

[150] Faghani, E., Saemi, S.D., Maddahian, R. and Farhanieh, B. "On the effect of inflow conditions in simulation of a turbulent round jet" **Archive of Applied Mechanics**, vol. 81, 2011. pp. 1439-1453.

[151] Ashforth-Frost, S. and Jambunathan, K. "Effect of nozzle geometry and semi-confinement on the potential core of a turbulent axisymmetric free jet" **International Communications in Heat and Mass Transfer**, vol. 23, no. 2, 1996. pp. 155-162.

[152] Quinn, W.R. and Militzer, J. "Effects of nonparallel exit flow on round turbulent free jets" **International Journal of Heat and Fluid Flow**, vol. 10, no. 2, 1989. pp. 139-145.

[153] Bird, R.B., Stewart, W.E., and Lightfoot, E.N. **Transport phenomena**. 2nd edition. New York : John Wiley and Sons, Inc. 2007.

[154] Gutmark, E.J. and Grinstein, F.F. "Flow control with noncircular jets[1]" **Annual Review of Fluid Mechanics**, vol. 31, 1999. pp. 239-272.

[155] Mi, J. Nathan, G.J., and Luxton, R.E. "Centreline mixing characteristics of jets from nine differently shaped nozzles" **Experiments in Fluids**, vol. 28, no. 1, 2000. pp. 93-94.

[156] Mi, J. and Nathan, G.J. "Statistical properties of turbulent free jets issuing from nine differently-shaped nozzles" **Flow, Turbulence and Combustion**, vol. 84, no. 4, 2010. pp. 583-606.

[157] Sforza, P.M., Steiger, M.H., and Trentacoste, N. "Studies on three-dimensional viscous jets" **AIAA Journal**, vol. 4, no. 5, 1966. pp. 800-806.

[158] Trentacoste, N. and Sforza, P. "Further experimental results for three-dimensional free jets" **AIAA Journal**, vol. 5, no. 5, 1967. pp. 885-891.

[159] Sforza, P. "A quasi-axisymmetric approximation for turbulent, three-dimensional jets and wakes" **AIAA Journal**, vol. 7, no. 7, 1969. pp. 1380-1383.

[160] Rajaratnum, N. and Subramanya, K. "Three-Dimensional Free Jets" **Aeronautical Journal**, vol. 71, no. 684, 1967. pp. 858-859.

[161] Ho, C.M. and Gutmark, E.J. "Vortex induction and mass entrainment in a small-aspect ratio elliptic jet" **Journal of Fluid Mechanics**, vol. 179, 1987. pp. 383-405.

[162] Grinstein, F.F., Gutmark, E.J., and Parr, T. "Near field dynamics of subsonic free square jets. A computational and experimental study" **Physics of Fluids**, vol. 7, no. 6, 1995. pp. 1483-1497.

[163] Quinn, W.R. and Militzer, J. "Experimental and numerical study of a turbulent free square jet" **Physics of Fluids**, vol. 31, no. 5, 1988. pp. 1017-1025.

[164] Schadow, K.C., Wilson, K.J., and Lee, M.J. "Enhancement of Mixing in Reacting Fuel-Rich Plumes Issued from Elliptical Nozzles" **Journal of Propulsion and Power**, vol. 3, no. 2, 1987. pp. 145-149.

[165] Hussain, F. and Husain, H.S. "Elliptic jets. Part 1. Characteristics of unexcited and excited jets" **Journal of Fluid Mechanics**, vol. 208, 1987. pp. 257-320.

[166] Bradshaw, P. **An Introduction to Turbulence and its Measurement**. England : Pergamon Press Ltd. 1971.

[167] Bradshaw, P. **Turbulence**. Germany : Springer-Verlag Berlin Heidelberg. 1976.

[168] Celik, I.B., Ghia, U., Roache, P.J., Freitas, C.J., Coleman, H., and Raad, P.E. "Procedure for Estimation and Reporting of Uncertainty Due to Discretization in CFD Applications" **Journal of Fluids Engineering**, vol. 130, no. 7, 2008. pp. 078001-1–078001-4.

Appendices

Appendix A

DOMAIN DECOMPOSITION TECHNIQUE

The domain decomposition technique is a computational domain preparation before grid generation by dividing the whole domain into various faces for two-dimensional domain or various volumes for three-dimensional domain. Generally, this technique is very important for quadrilateral grid generation in two-dimensional domain or hexahedral grid generation in three-dimensional domain. However, for complicated geometry, the domain decomposition may not suitable, so, the other techniques should be employed to achieve accurate solutions.

For GAMBIT, the domain decomposition facility is unavailable. However, the computational domain can manually split by using various specified faces. For two-dimensional domain, the domain is split into various quadrilateral faces to store quadrilateral grids. While, the three-dimensional domain is divided into various hexahedral volumes to contain hexahedral grids. Moreover, the edges and faces of two- and three-dimensional sub-domains must be linked by sharing their edges and faces, respectively. The examples of shared edges of two-dimensional domain and shared faces of three-dimensional domain are presented in Figure A.1.

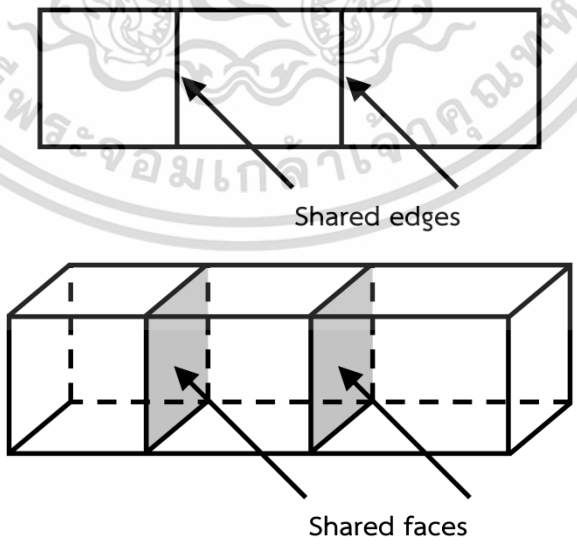

Figure A.1 Examples of two- and three-dimensional decomposed computational domains

In Figure A.1, from domain decomposition technique, the three faces of two-dimensional domain show ten edges, including eight boundary edges and two shared edges. Moreover, for three-dimensional domain, three volumes provide fourteen boundary faces and two shared faces. These shared parts are very important in simulation because they allow the CFD program to solve fluid flow through these boundaries. Meaning that, if there are no shared boundaries, the correct solutions of fluid flow inside the computational domain are impossible.

Nowadays, the technologies used in grid generator programs are successfully developed. However, the concept of domain decomposition for GAMBIT grid generator program as described above can also apply to the modern grid generator programs, e.g. ANSYS ICEM CFD.

Appendix B

EXAMPLE OF GCI CALCULATION

In this part, an example of GCI calculation is represented. The key parameter of this example is overall mixing time. The predicted overall mixing times for three different grids of this example are shown in Table B.1.

Table B.1 Predicted overall mixing times for GCI calculation example

i[a]	Number of cells (N_i)	Overall mixing time [s] (f_i)
1	1,739,978	28.1903
2	1,486,046	28.3658
3	1,184,437	29.7257

[a] i = 1, 2, and 3 denote the calculations at the fine, medium and coarse meshes, respectively.

According to GCI procedure as mentioned in section 5.2.1, the main GCI procedure can be summarized as shown in Figure B.1. The calculations of this example can be represented as follows:

- Determine the refinement factor (r):

$$r_{21} = \left(\frac{N_1}{N_2}\right)^{1/3} = \left(\frac{1{,}739{,}978}{1{,}486{,}046}\right)^{1/3} = 1.0540$$

$$r_{32} = \left(\frac{N_2}{N_3}\right)^{1/3} = \left(\frac{1{,}486{,}046}{1{,}184{,}437}\right)^{1/3} = 1.0785$$

- Calculate the difference in numerical solutions (ε):

$$\varepsilon_{21} = f_2 - f_1 = 28.3658 - 28.1903 = 0.1755$$

$$\varepsilon_{32} = f_3 - f_2 = 29.7257 - 28.3658 = 1.3599$$

- Calculate the relative error of numerical solutinos (e):

$$e_{21} = \frac{f_2 - f_1}{f_1} = \frac{28.3658 - 28.1903}{28.1903} = 0.0062$$

$$e_{32} = \frac{f_3 - f_2}{f_2} = \frac{29.7257 - 28.3658}{28.3658} = 0.0479$$

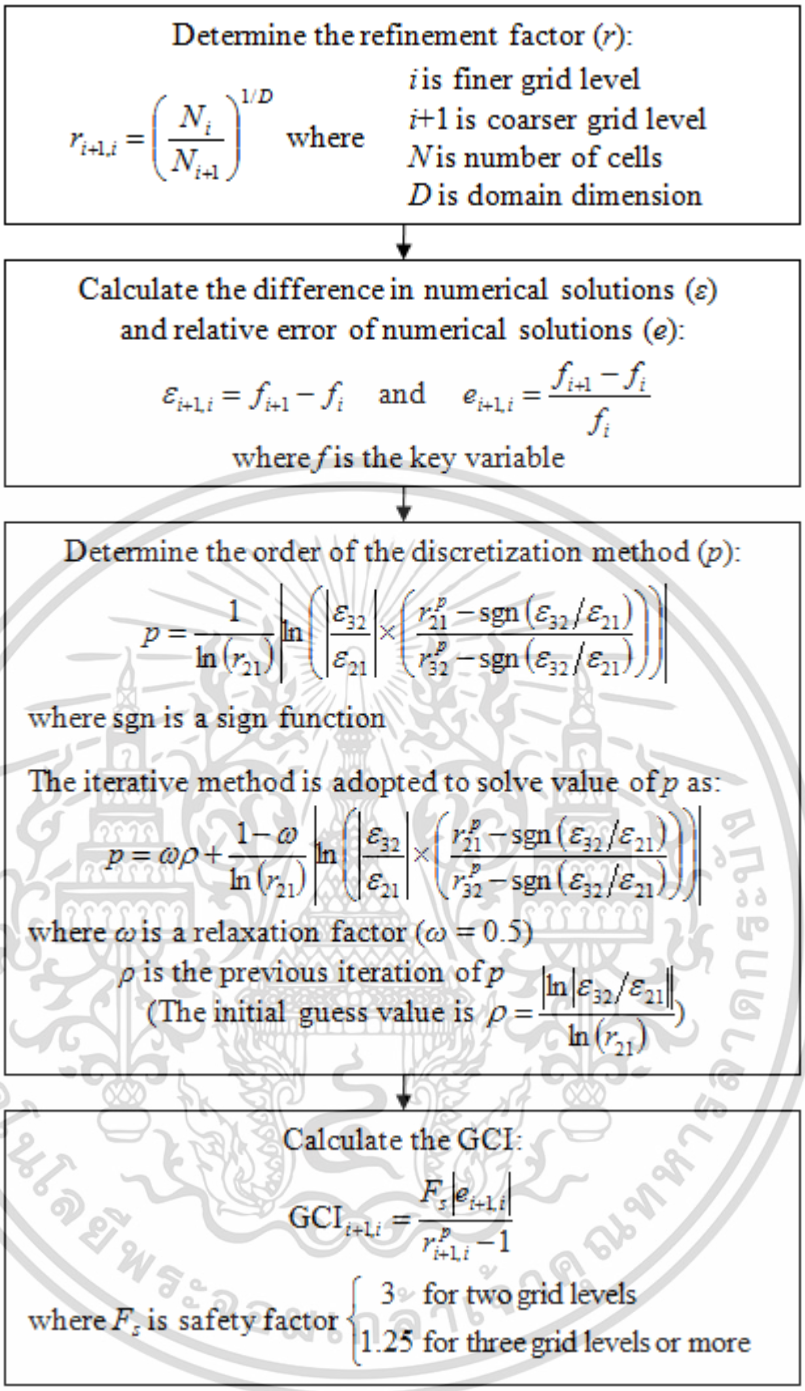

Figure B.1 Recommended GCI procedure, Reproduced from Bumrungthaichaichan and Wattananusorn (J. Chin. Inst. Eng. 42(5) (2019) 428-437) with permission from Journal of the Chinese Institute of Engineers

- Determine the order of the discretization method (p):

From Figure B.1, the value of p is solved by using iterative method. In this example, in order to solve the value of p, the iterative calculation facility of Microsoft Office Excel (MS Excel) is employed. The setup of iterative calculation of MS Excel is shown in Figure B.2.

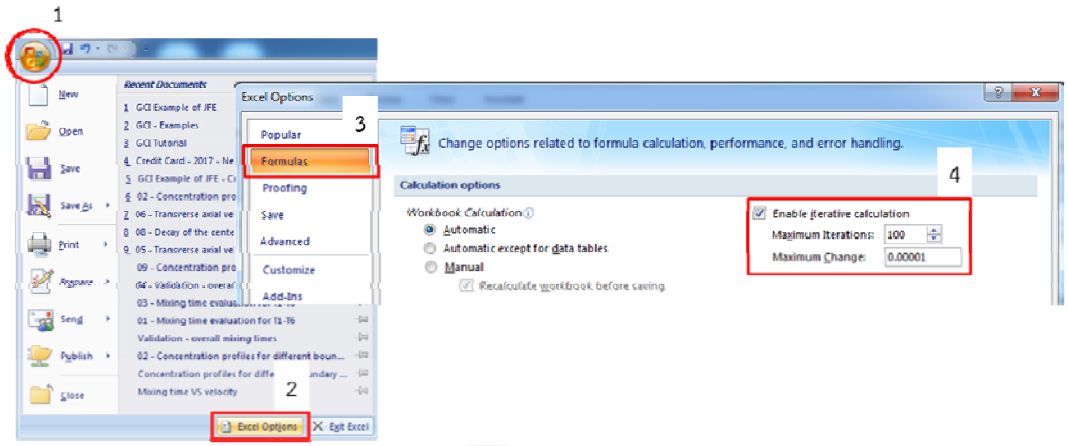

Figure B.2 Setup of iterative calculation facility of MS Excel

Calculate the initial guess value (ρ):

$$\rho = \frac{\left|\ln\left|\varepsilon_{32}/\varepsilon_{21}\right|\right|}{\ln(r_{21})} = \frac{\left|\ln\left|1.3599/0.1755\right|\right|}{\ln(1.0540)} = 38.9320\,.$$

Fill all necessary data in MS Excel sheet as shown in Figure B.3.

	A	B	C	D	E	F	G	H	I	J	K	L	M
1	r_{21}	r_{32}	$\ln(r_{21})$	$1/\ln(r_{21})$	ε_{21}	ε_{32}	$\varepsilon_{32}/\varepsilon_{21}$	$ABS(\varepsilon_{32}/\varepsilon_{21})$	$SGN(\varepsilon_{32}/\varepsilon_{21})$	*Guess p*	β	*f(p)*	*p*
2	1.0540	1.0785	0.0526	19.0141	0.1755	1.3599	7.7487	7.7487	1	38.9320	2.9123	29.6285	38.9320
3													

I2	=SIGN(G2)
K2	=H2*(((A2^J2)-I2)/((B2^J2)-I2))
L2	=(0.5*J2)+((1-0.5)*(ABS(LN(K2)))*D2)
M2	=J2

Figure B.3 Excel sheet for iterative calculation of p and descriptions of all necessary functions (see section 5.2.1 for details of β and $f(p)$ is a function for iterative calculation of p as shown in Figure B.1)

Enter =L2 in cell J2 to calculate the value of p as shown in Figure B.4. From iterative calculation, the value of p for this case is 25.1357.

J2 =L2

	A	B	C	D	E	F	G	H	I	J	K	L	M
1	r_{21}	r_{32}	$\ln(r_{21})$	$1/\ln(r_{21})$	ε_{21}	ε_{32}	$\varepsilon_{32}/\varepsilon_{21}$	$ABS(\varepsilon_{32}/\varepsilon_{21})$	$SGN(\varepsilon_{32}/\varepsilon_{21})$	*Guess p*	β	*f(p)*	*p*
2	1.0540	1.0785	0.0526	19.0141	0.1755	1.3599	7.7487	7.7487	1	25.1357	3.7507	25.1357	25.1357

Figure B.4 Computation for value of p

- Calculate the GCI:

$$\mathrm{GCI}_{21} = \frac{F_s|e_{21}|}{r_{21}^{p}-1}\times 100 = \frac{1.25|0.0062|}{1.0540^{25.1357}-1}\times 100 = 0.2817$$

$$\mathrm{GCI}_{32} = \frac{F_s|e_{32}|}{r_{32}^{p}-1}\times 100 = \frac{1.25|0.0479|}{1.0785^{25.1357}-1}\times 100 = 1.0536$$

This example only shows the calculation of GCI. However, for CFD study, the other parameters should be investigated, including asymptotic range of convergence, convergence ratio, and exact value of key parameter. In addition, the GCI can be used to determine the discretization error bars of the simulated results [168].

Appendix C

PUBLICATIONS

C.1 CFD modelling of pump-around jet mixing tanks: a discrepancy in concentration profiles

Taylor & Francis
Taylor & Francis Group

Journal of the Chinese Institute of Engineers

ISSN: 0253-3839 (Print) 2158-7299 (Online) Journal homepage: http://www.tandfonline.com/loi/tcie20

CFD modelling of pump-around jet mixing tanks: a discrepancy in concentration profiles

Eakarach Bumrungthaichaichan, Apinan Namkanisorn & Santi Wattananusorn

To cite this article: Eakarach Bumrungthaichaichan, Apinan Namkanisorn & Santi Wattananusorn (2018) CFD modelling of pump-around jet mixing tanks: a discrepancy in concentration profiles, Journal of the Chinese Institute of Engineers, 41:7, 612-621, DOI: 10.1080/02533839.2018.1530956

To link to this article: https://doi.org/10.1080/02533839.2018.1530956

Published online: 08 Nov 2018.

JOURNAL OF THE CHINESE INSTITUTE OF ENGINEERS
2018, VOL. 41, NO. 7, 612–621
https://doi.org/10.1080/02533839.2018.1530956

CFD modelling of pump-around jet mixing tanks: a discrepancy in concentration profiles

Eakarach Bumrungthaichaichan, Apinan Namkanisorn and Santi Wattananusorn

Department of Chemical Engineering, Faculty of Engineering, King Mongkut's Institute of Technology Ladkrabang, Bangkok, Thailand

ABSTRACT

Jet mixing tanks are important in chemical processes. Over the past two decades or so, computational fluid dynamics (CFD) has been employed to study jet mixers. The shortfalls of the previous CFD models were the discrepancy in concentration profiles between simulation and experiment and the absence of exact inlet turbulence conditions. So, in our present work, the CFD model was developed to investigate the proper conditions for jet mixing tank simulation and improve the accuracy of concentration profile prediction by using an appropriate grid arrangement, a realizable k-epsilon model, and a second-order upwind discretization scheme. The results revealed that the CFD model with proper inlet conditions predicted the overall mixing time well and somewhat improved the predicted concentration profiles. Further, the reasons for discrepancies in concentration profiles were inappropriate inlet turbulence conditions and overprediction in total momentum available for mixing due to the flat top liquid surface assumption. In addition, this discrepancy may be caused by the dynamic response of concentration measuring device.

ARTICLE HISTORY
Received 3 October 2017
Accepted 28 September 2018

KEYWORDS
CFD; jet; mixing; boundary conditions

1. Introduction

The jet mixing tank is one of the important mixing devices in many chemical processes. This device uses a high velocity liquid jet produced by a pump to create liquid recirculation and entrainment inside a vessel. Finally, the different compositions inside the tank are mixed. The idea of jet mixing was first introduced by Fossett and Prosser (1949). The first jet mixer was adopted to mix tetraethyl-lead fluid in a 4,000-t underground petroleum storage tank. This device has been adopted in various mixing applications due to its advantages, including simple design, low operating cost, no moving parts, and easy installation and maintenance.

Over the past 20 years or so, computational fluid dynamics (CFD) has been employed to address the shortfalls in experimental studies of jet mixing tanks, including case-specific overall jet mixing time correlations (Bumrungthaichaichan 2016), but the details of fluid flow and mixing inside this device are not presented. The earliest CFD study of a jet mixing tank was carried out by Brooker (1993). He showed that his CFD model predicted the overall mixing time with maximum error of about 15% as comparing with experimental results. Later, the effects of tank configurations and operating conditions, such as jet elevation (Ranade 1996), jet angle (Patwardhan 2002; Zughbi and Rakib 2004; Zughbi and Ahmad 2005), tank shape (Raja, Kalaichelvi, and Anantharaman 2007), liquid height (Bumrungthaichaichan et al. 2016), jet injection rate (Zughbi and Rakib 2002), fluid types (Sendilkumar et al. 2007), and others, on jet mixing behavior, were numerically studied.

The previous CFD models of jet mixing tanks well predicted the overall mixing times. However, the predicted concentration profiles were not in good agreement with the measured data. Up until today, there have been only a few attempts toward accuracy improvement of concentration profile predictions. Patwardhan (2002) improved the concentration profile predictions by modifying the constants of standard k-epsilon model. The better predicted concentration profiles were observed by using 10% turbulence intensity with modified constants (C_μ = 0.135 and $C_{1\varepsilon}$ = 1.31).

Furthermore, the accuracy of concentration profile predictions can also be increased by using a large number of grids and a higher discretization scheme as reported by Marek et al. (2007) and Bumrungthaichaichan et al. (2016). Although the improvement of simulated concentration profiles has been studied by previous researchers, the concentration profiles were still not in good agreement with experiments. Moreover, the reasons for this discrepancy have not been clearly presented. Hence, the improvement of concentration profile prediction is still a challenging issue worth farther study.

Further, another shortfall of jet mixing tank simulations is the absence of exact inlet turbulence conditions. This problem can be considered as the possible source of the discrepancy in concentration profiles. So, in this paper, the effects of inlet conditions on pump-around jet mixing tank simulation were studied to investigate the suitable conditions for predicting the concentration profiles and describe the cause of the discrepancy in concentration profiles between CFD model and experiment.

CONTACT Eakarach Bumrungthaichaichan b_eakarach@hotmail.com Department of Chemical Engineering, Faculty of Engineering, King Mongkut's Institute of Technology Ladkrabang, Bangkok, Thailand

2. Description of CFD modeling

2.1. Consideration of jet mixing tank system

In our present work, the considered system was an open 45° inclined side entry pump-around jet mixing tank following Patwardhan (2002), which used the concentration tracer technique to investigate the mixing time. For CFD modeling, this tracer technique is more reasonable than the temperature tracer technique which assumes that the properties of primary liquid and tracer are identical because the difference in their properties of concentration technique is less than in the latter method. For example, in concentration tracer technique, the kinematic viscosity of water and 0.1 M NaCl solution at 25°C respectively are 8.937×10^{-7} (Cimbala and Çengel 2008) and 8.981×10^{-7} m^2 s^{-1} (Zhang and Han 1996), whereas for temperature tracer technique, the kinematic viscosity of water at 25°C and water at 80°C (tracer) are 8.937×10^{-7} and 3.653×10^{-7} m^2 s^{-1}, respectively (Cimbala and Çengel 2008).

In experiments of Patwardhan (2002), the 0.5-m diameter cylindrical tank with flat bottom was filled with water to the height of 0.5 m ($H/D = 1$). The dilute NaCl solution was rapidly added into the tank at the center of the top water surface with the help of a beaker. The conductivity was measured and recorded by using four conductivity probes. Then, the mixing time was determined by using the time taken for the conductivity to reach 95% of fully mixed value. The overall mixing time was determined by finding the mean of the mixing times obtained by these measuring probes. The schematic and coordinate systems of this jet mixing tank are shown in Figure 1.

2.2. Grid generation

The three-dimensional solid modeling and grid generation of jet mixing tank were determined by using GAMBIT 2.4.6 program. In order to obtain accurate results, the hexahedral grid generation should be aligned to the flow direction. So, the domain was manually decomposed into several blocks by using the specified faces to control the grid generation. The grid generation of this work is shown in Figure 2.

2.3. Numerical solution technique

In this work, the ANSYS FLUENT finite volume CFD code was adopted to simulate the jet mixing tanks because of low memory usage and computational time, the fact that physical quantities are conserved even on coarse grids, and other reasons (Bumrungthaichaichan 2016). In addition, the double precision pressure-based solver was selected.

2.4. Governing equations

For CFD simulations of jet mixing tanks, the Reynolds average equations for conservation of mass and momentum together with realizable k-epsilon model (RKE) were employed to obtain the mean velocity and turbulence inside the tanks. The compact form of steady-state Reynolds average equation is generally obtained by eliminating the unsteady state term in the general Reynolds average equation reported by Bumrungthaichaichan et al. (2016) and can be written as

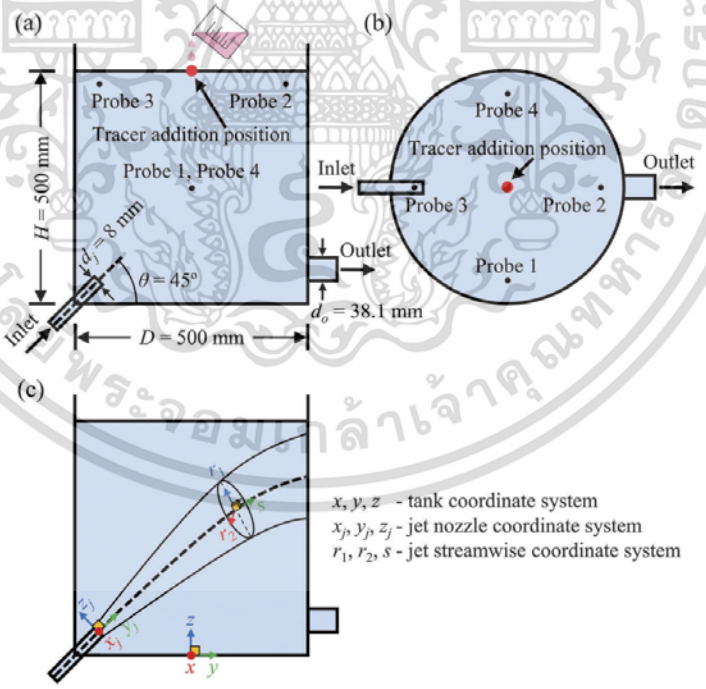

Figure 1. Schematics of (a) jet mixing tank (side view) and (b) jet mixing tank (top view) (c) coordinate systems.

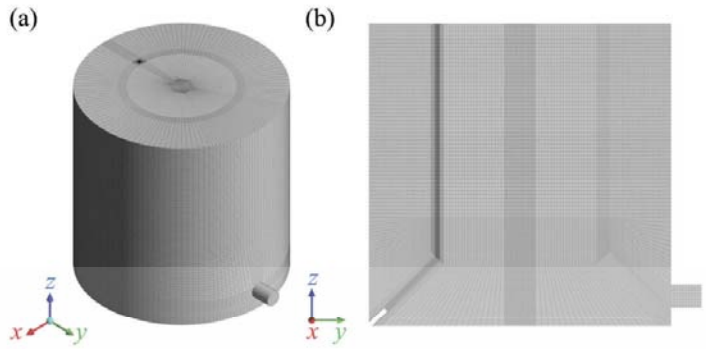

Figure 2. Grid generation of jet mixing tank (a) isometric view and (b) plane $x = 0$.

$$\frac{\partial(\rho U\varphi)}{\partial x_j} = \frac{\partial}{\partial x_j}\left[\Gamma_\phi \frac{\partial \varphi}{\partial x_j}\right] + S_\phi \quad (1)$$

where ρ is fluid density, $\boldsymbol{U}$ is mean velocity vector, ϕ is a universal dependent variable, Γ_φ is the diffusivity, and S_φ is the source term. Further, the details of the variables for continuity equation, momentum equations, and RKE (ANSYS Inc 2013b) are shown in Table 1.

For tracer concentration distribution inside the vessel, the unsteady-state species transport equations without chemical reaction (ANSYS Inc 2013b) were solved and can be written as

$$\frac{\partial(\rho Y_i)}{\partial t} + \frac{\partial(\rho U Y_i)}{\partial x_j} = \frac{\partial}{\partial x_j}\left(\left(\rho D_{i,m} + \frac{\mu_t}{Sc_t}\right)\frac{\partial Y_i}{\partial x_j}\right) + S_i \quad (2)$$

where Y_i is the local mass fraction of species i, $D_{i,m}$ is the mass diffusion coefficient for species i in the mixture, Sc_t is the turbulent Schmidt number (ν_t/D_t where ν_t is the turbulent kinematic viscosity and D_t is the turbulent diffusivity), μ_t is the turbulent viscosity, and S_i is the source term for species transport equations.

Equation (2) is valid for turbulent mixing without chemical reaction. In turbulent flow, the turbulent diffusion overwhelms the laminar diffusion (ANSYS Inc 2013b). So, the specification of laminar mass diffusion coefficient is unnecessary. However, in this research, the self-diffusion coefficient of liquid water was specified to obtain accurate results.

2.5. Material properties

The water and tracer properties were assumed to be identical because the NaCl solution was dilute. The density, viscosity, and mass diffusivity of these fluids respectively were 998.2 kg m^{-3}, 0.001003 kg m^{-1} s^{-1}, and 2.3×10^{-9} m^2 s^{-1} (Spyrou 2009).

2.6. Boundary conditions

In the present work, the inlet and outlet boundary condition types for steady-state simulations were velocity-inlet and pressure-outlet, respectively. For unsteady-state simulations, the two different sets of inlet and outlet boundary condition types, including velocity-inlet and pressure-outlet for set I and recirculation-inlet and recirculation-outlet for set II, were studied. For set II, these extra boundary condition types were manually enabled by respectively typing the two additional text commands in TUI (Dange 2016), including (rpsetvar 'icepak? #t) and (models-changed).

The no-slip boundary condition and standard wall functions were applied at the wall boundaries, including tank wall and tank base. The flat top water surface was assumed by using symmetry boundary condition, e.g. the normal velocity and normal gradient of all variables are zero, because the bulk mixing in the vessel was mainly considered and the liquid interface remained flat for low jet velocities and jet angles as observed by the experiments (Patwardhan 2002). Further, this boundary condition type was adopted to reduce the computational cost for liquid interface shape simulation.

The uniform jet discharge velocity (U_j) of 4.4 m s^{-1} from the experiment of Patwardhan (2002) was adopted at the jet nozzle exit. For turbulence conditions, the turbulence kinetic energy (TKE or k) and TKE dissipation rate (TDR or ε) were directly imposed at inlet. Due to the absence of exact

Table 1. Details of the variables for continuity equation, momentum equations, and transport equations of k and ε for RKE.

Equation	ϕ	Γ_φ	S_φ	Constants
Continuity	1	0	0	–
Momentum	U_i	μ	$-\frac{\partial P}{\partial x_i} + \frac{\partial}{\partial x_j}\left[\mu_t \frac{\partial U_i}{\partial x_j}\right] + S_{M,i}$	–
k-Transport	k	$\mu + \frac{\mu_t}{\sigma_k}$	$G_k + G_b - \rho\varepsilon - Y_M + S_k$	$\sigma_k = 1.0$
ε-Transport	ε	$\mu + \frac{\mu_t}{\sigma_\varepsilon}$	$\rho C_1 S\varepsilon - \rho C_2 \frac{\varepsilon^2}{k+\sqrt{\nu\varepsilon}} + C_{1\varepsilon}\frac{\varepsilon}{k} C_{3\varepsilon} G_b + S_\varepsilon$	$\sigma_\varepsilon = 1.2$ $C_1 = \max\left[0.43, \frac{\eta}{\eta+5}\right]$ $C_2 = 1.9$ $C_{1\varepsilon} = 1.44$

Table 2. Boundary conditions for jet mixing tank simulations.

Case	Velocity ($m\ s^{-1}$)	Turbulence intensity	TKE ($m^2\ s^{-2}$) Formula	TKE Value	TDR ($m^2\ s^{-3}$) Formula	TDR Value
T1	4.4	10%	$\frac{3}{2}(U_j I)^2$	0.2904	$C_D \frac{k^{3/2}}{l}$	22.35614
T2					$C_\mu^{3/4} \frac{k^{3/2}}{l}$	45.91861
T3					$\frac{\rho C_\mu k^2}{1000\mu}$	75.53572
T4		4.33%		0.0543	$C_D \frac{k^{3/2}}{l}$	1.809608
T5					$C_\mu^{3/4} \frac{k^{3/2}}{l}$	3.716862
T6					$\frac{\rho C_\mu k^2}{1000\mu}$	6.114206

turbulence conditions, these turbulence quantities were estimated by using different correlations.

The value of TKE can be calculated as $k = \frac{3}{2}(U_j I)^2$, where I is turbulence intensity. The suitable turbulence intensity for CFD modeling of jet mixing tanks was 10% (Patwardhan 2002). Fluent Inc (2006) represented the correlation for turbulence intensity estimation as $I = 0.16\mathrm{Re}_{D_h}^{-1/8}$, where Re_{D_h} is Reynolds number based on hydraulic diameter (D_h). These turbulence intensities were adopted to compute the TKE.

For TDR, three different formulas were used to calculate this quantity, including $\varepsilon = C_D \frac{k^{3/2}}{l}$ (Celik 1999), $\varepsilon = C_\mu^{3/4} \frac{k^{3/2}}{l}$ (ANSYS Inc 2013d), and $\varepsilon = \frac{\rho C_\mu k^2}{1000\mu}$ (ANSYS Inc 2013a), where C_D is a constant approximately equal to 0.08 (Wilcox 1994), C_μ is an empirical constant equal to 0.09 (ANSYS Inc 2013b), and l is a length scale, which is approximately equal to $0.07 d_j$ (ANSYS Inc 2013d). The boundary conditions for this work are summarized in Table 2.

2.7. Numerical methods

The SIMPLE algorithm was employed as a pressure–velocity coupling scheme. The spatial discretization schemes of momentum, turbulence quantities, and tracer were second-order upwind. For transient simulation, the temporal discretization scheme was first-order implicit.

2.8. Mixing time simulation

In this CFD work, the tracer with a mass fraction of unity was patched at 0.03 m below the center of top liquid surface to account for the experimental observation that the tracer slightly moved downward because the tracer was added by using a beaker (Patwardhan 2002). Then, Equation (2) was solved with this initial condition. During the transient simulation, the time histories of tracer distributions for four different probes were recorded. The mixing times for these probes were individually computed by considering the time required for the concentration (c) to reach 95% of the fully mixed concentration ($\bar{c}$). Generally, the 95% mixing time ($t_{95\%}$) can be written as

$$t_{95\%} = \text{time for} \left| \frac{c - \bar{c}}{\bar{c}} \right| \leq 0.05 \tag{3}$$

Finally, the overall mixing time of jet mixing tank was determined by finding the mean of the mixing times obtained by four different probes.

Generally, Equation (3) is used for the concentration tracer technique. The constant of 0.05 can be changed to 0.01 for 99% mixing time ($t_{99\%}$). The value of $t_{99\%}$ is about 1.5 times $t_{95\%}$. For temperature tracer technique, the different correlation is employed as suggested by Zughbi and Rakib (2004). Moreover, the details of mixing time investigation are clearly described by Bumrungthaichaichan (2016).

2.9. Solution strategy

The liquid flow and tracer distribution inside the jet mixing tanks have been carried out by using the steady and unsteady simulations, respectively. For steady simulations, the scaled residuals were primarily used to identify the solution convergence. Further, the area weighted average value of the velocity magnitude at plane $x = 0$ (see the tank coordinate system in Figure 1(c)) was monitored until it was constant to obtain the converged solutions. For transient simulations, the scaled residual of 10^{-5} for tracer was adopted as the convergence criteria.

The selected transient formulation of this study was implicit. Hence, the Courant–Friedrichs–Lewy (CFL) condition (Courant, Friedrichs, and Lewy 1967) was not necessarily taken into account for the time step size. However, in order to model transient phenomena properly, the time step size should be one order of magnitude smaller than the time constant of the considered system (ANSYS Inc 2013d), e.g. residence time (jet mixing tank volume/inlet volumetric flow rate). For this case, the residence time of the jet mixing tank and fixed time step size were 445 and 0.0025 s (Bumrungthaichaichan et al. 2016), respectively. The selected time step size was lower than the residence time, time step size estimated by the appropriate length and velocity scale approach (≈0.0074 s) (Bumrungthaichaichan 2016), and previous CFD works. Hence, this time step size was sufficient to investigate the mixing time.

2.10. Grid independence study

In this work, the grid independence study was investigated with the help of gradient adaption technique to reduce the computational requirements, e.g. computational time, memory, etc. ANSYS FLUENT suggested that the gradient adaption of mean velocity is suitable for incompressible fluid flow (ANSYS Inc 2013d). So, for grid adaptation of jet mixing tank models, the velocity gradient adaption with the refine threshold of 10% of the maximum value (ANSYS Inc 2013c) was employed. In order to ensure that the grids were refined correctly, the grid adaptation was performed individually for different cases because the different conditions may produce different results, e.g. jet spreading rate. The descriptions of grid independence study for T1 case are shown in Table 3.

In Table 3, the results reveal that the percentage difference for potential core and mixing time for different grid levels are found to decrease when increasing the number of grids. Further, the percentage difference of potential core for the coarsest grid level exhibits the highest value (40.15%). Due to this high percentage difference, the grid convergence index (GCI) was employed to ensure that converged solutions were obtained.

Table 3. The details of the grid independence study for case *T*1.

Grid	Number of cells	Potential core[a] s/d_j	Potential core % Difference[b]	Mixing time (s) Value	Mixing time (s) % Difference[b]
0-Adapted grid[c]	1,087,312	1.504	40.15	30.000	5.26
1-Adapted grid	1,184,437	2.005	20.21	30.125	5.70
2-Adapted grid	1,486,046	2.506	0.28	28.625	0.44
3-Adapted grid	1,739,978	2.513	–	28.500	–

[a]The potential core is a region where the mean centerline axial velocity is equal to jet discharge velocity, which is generally observed within $0 \le s/d_j \le 6$, where s is a streamwise distance from nozzle exit and d_j is a jet nozzle diameter.
[b]The percentage difference is a ratio of absolute difference between the values of potential core or mixing time for any grid and finest grid to the finest grid value.
[c]0-adapted grid is an original grid obtained by GAMBIT.

3. GCI and model validation

GCI is a quantitative measurement of the grid convergence, which was suggested by Roache (1994, 1997, 1998). The GCI procedure has been clearly described by previous literature (Celik et al. 2008; Elsayed 2011) and can be summarized as depicted in Figure 3. In this work, the GCI calculations of four different grid levels of *T*1 case are shown in Table 4.

From Table 4, the GCI analysis shows the following conclusions:

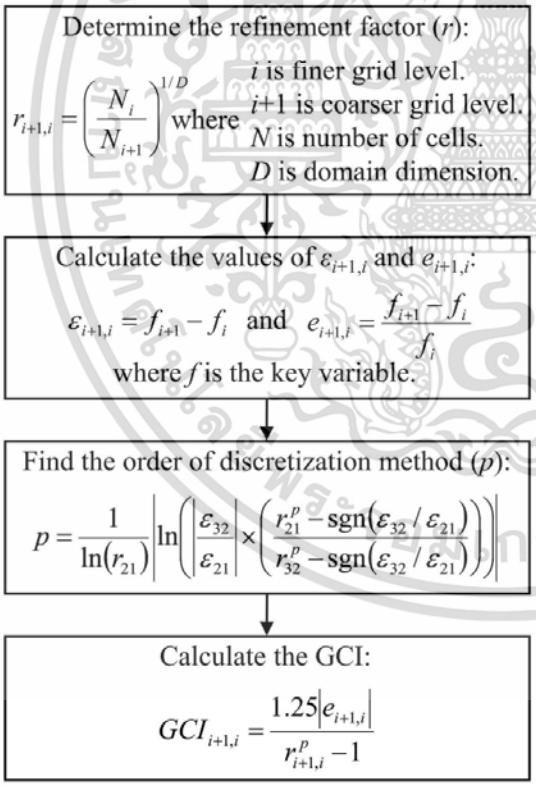

Figure 3. Recommended GCI procedure.

(1) The results obtained by the grid refinement from medium to finest grid levels are in the asymptotic range because the values of a are close to unity.
(2) For potential core, the convergence ratios (R) are less than unity, which show the monotonic convergence for all grid levels. Further, for mixing time, the oscillatory convergence ($R < 0$) is found in the grid refinement from coarse to fine grids. However, for the grid refinement from medium to finest grid levels, the monotonic convergence is observed.
(3) The results show that GCI_{21} is less than GCI_{32} for potential core and mixing time, which indicate that the grid independent solution has been achieved. Meaning that, further grid refinement will not much improve the simulated results. Moreover, the potential core and mixing time of the finest grid level are close to their extrapolated values. Hence, the solutions are converged with the refinement from medium to finest grid resolutions.

According to the above conclusions, in order to ensure that the grid convergence is achieved, the finest grid level should be adopted for all simulations. For this research, the final grid should be adapted three times to achieve the finest grid resolution.

For model validation, four different jet discharge velocities were simulated. The predicted overall mixing times were compared with the experimental data of Patwardhan (2002) as shown in Figure 4. From Figure 4, the overall mixing times are underpredicted and are in good agreement with experiments. Thus, this simulation methodology is reasonably adopted to study the pump-around jet mixing tank.

4. Results and discussion

4.1. *Boundary condition types*

As mentioned earlier, the two different sets of boundary condition types, including velocity-inlet and pressure-outlet for set I and recirculation-inlet and recirculation-outlet for set II, were tested by using conditions of *T*1 case as depicted in Table 2 to achieve the appropriate method for pump-around jet mixing time investigation. The contours of normalized concentration, which was defined as a ratio of the concentration to the fully mixed value, for two different sets are presented in Figure 5.

From Figure 5, at the region near the nozzle exit, the contour of set I presents zero normalized concentration, whereas the contour of set II indicates the recirculation of the tracer from outlet pipe to jet nozzle inlet. From these results, it can be summarized that the jet mixing time simulation for pump-around jet mixing tank is successfully predicted by using boundary condition types of set II because they allow the tracer to flow past the outlet and return to the inlet section.

Further, this mixing time investigation method is more advantageous than the other approaches because it reduces the computational time due to the absence of grids in the piping system between inlet and outlet for momentum source

Table 4. Grid convergence index analysis of case *T*1.

Variable	i[a]	N_i	f_i	$r_{i+1,i}$	$\varepsilon_{i+1,i}$	$e_{i+1,i}$	$GCI_{i+1,i}$ (%)	R[b]	a[c]
Potential core	0[d]		2.5133						
	1	1,739,978	2.5130						
				1.0540	−0.0065	−0.0026	0.0172		
	2	1,486,046	2.5065					0.0130	0.9974
				1.0785	−0.5011	−0.1999	0.3434		
	3	1,184,437	2.0054					0.7999	3.2954
				1.0289	−0.5012	−0.2499	7.6873		
	4	1,087,312	1.5042						
Mixing time	0[d]		28.470						
	1	1,739,978	28.500						
				1.0540	0.1250	0.0044	0.1307		
	2	1,486,046	28.625					0.0837	1.0044
				1.0785	1.5000	0.0524	0.6760		
	3	1,184,437	30.125					−12.6288	20.1168
				1.0289	−0.1250	−0.0041	0.3592		
	4	1,087,312	30.000						

[a] i = 1, 2, 3, and 4 denote the calculations at the finest, fine, medium, and coarse mesh, respectively.
[b] $R = e_{i+1,i}/e_{i+2,i+1}$: monotonic convergence for $0 < R < 1$, oscillatory convergence for $R < 0$, and divergence for $R > 1$.
[c] $a = \left(r_{i+1,i}^{p} GCI_{i+1,i}\right)/GCI_{i+2,i+1}$: The solution is in the asymptotic range if $a \approx 1$.
[d] $f_{exact} = f_1 + (f_1 - f_2)/(r_{12}^{p} - 1)$: The value at zero grid space (i = 0).

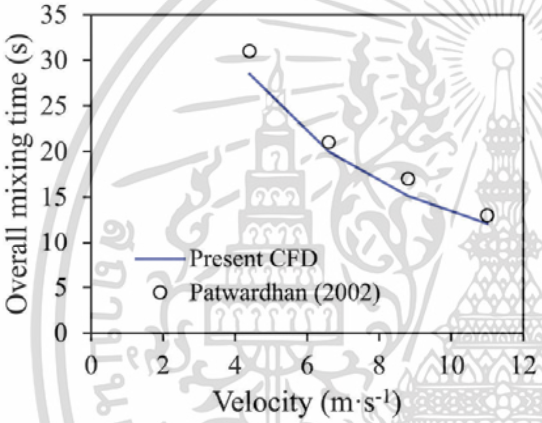

Figure 4. Comparison of overall mixing times.

specification method (Zughbi and Rakib 2002, 2004; Zughbi and Ahmad 2005) and the additional computer code for specifying the inlet tracer concentration or temperature (Sendilkumar et al. 2007; Wasewar and Sarathi 2008), which obtained from the average of outlet values, is not required.

4.2. Turbulence boundary conditions

The inlet turbulence conditions can be considered as the possible cause of the discrepancy in concentration profiles between simulation and experiment. Hence, the different conditions as depicted in Table 2 were tested. The predicted overall mixing times and concentration profiles were compared with the experimental data of Patwardhan (2002) as shown in Table 5 and Figure 6, respectively. The jet flow behaviors of 10% and 4.33% turbulence intensities were respectively compared and demonstrated by *T*1 and *T*4 cases. The predicted flow patterns, including decay of centerline streamwise velocity and jet spreading, were also compared with previous works of turbulent round jet as respectively shown in Figures 7 and 8 because the measured data for jet mixing tanks were unavailable.

From Table 5, the results show that the predicted mixing times are slightly different and lower than those obtained experimentally. Further, for probe 1 and probe 2, all predicted concentration values reach the 95% mixing time criterion faster than the experiment. For probe 1, the start of normalized concentration profiles predicted by 10% turbulence intensity cases are faster than those achieved by 4.33% turbulence intensity and close to the experimental data (Patwardhan 2002) as shown in Figure 6(a). The first peak values of

Figure 5. Contours of normalized concentration at t = 25 s for set I and set II.

Table 5. Mixing times for different inlet turbulence boundary conditions.

Case	Mixing time (s)					
	Probe 1	Probe 2	Probe 3	Probe 4	Overall	% Error[a]
Patwardhan (2002)	38.5	37.7	N/A	N/A	31.000	–
*T*1	33.5	30.0	27.5	23.0	28.500	8.06
*T*2	34.0	30.0	27.5	24.0	28.875	6.85
*T*3	31.5	29.5	27.5	24.5	28.250	8.87
*T*4	33.5	29.0	28.0	24.5	28.750	7.26
*T*5	33.0	29.5	28.0	24.5	28.750	7.26
*T*6	33.0	29.0	28.0	24.5	28.625	7.66

[a]The percentage error is a ratio of absolute difference between the predicted overall mixing time and experimental mixing time to the experimental value.

normalized concentration profiles are respectively overpredicted and underpredicted by *T*1 and *T*2 cases as compared with the experiment, whereas the other cases do not clearly represent the peaks of normalized concentration profiles.

For probe 2, the start and peak values of the normalized concentration profiles respectively are faster and higher than the experiment as depicted in Figure 6(b). However, for both probe locations, all simulated profiles approach the experimental values. From these results, it can be implied that the cause of the difference in normalized concentration profiles would be due to the different inlet turbulence conditions, which affect the predicted turbulent dispersion levels inside the tanks.

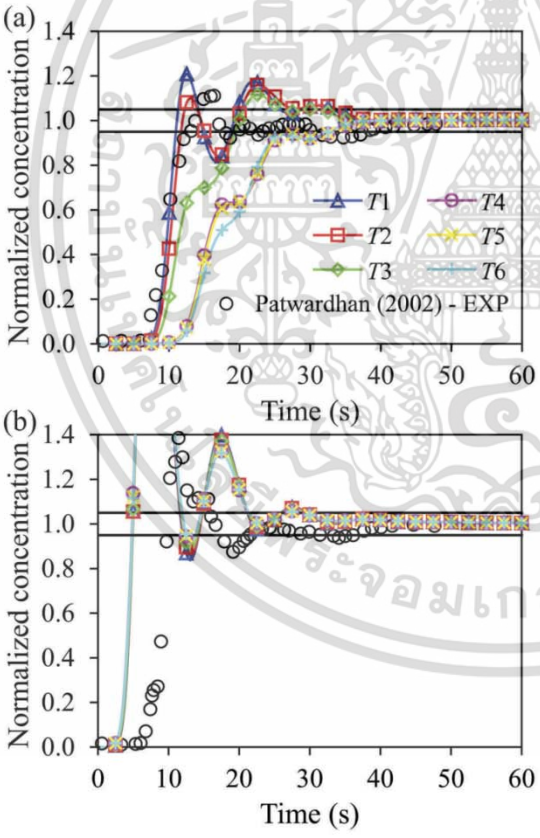

Figure 6. Comparison of normalized concentration profiles at (a) probe 1 and (b) probe 2.

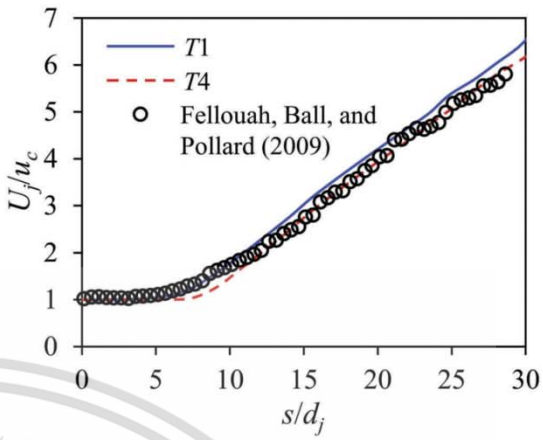

Figure 7. Decay of centerline streamwise velocity.

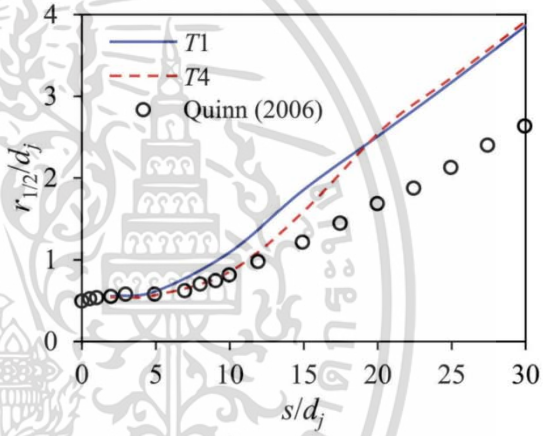

Figure 8. Jet spreading.

In Figure 7, the predicted decay of centerline streamwise velocity (u_c) is compared with the experimental data of Fellouah, Ball, and Pollard (2009). The results show that the decay of centerline velocity of *T*1 case is faster than that obtained by *T*4 case and measured data, especially for $s/d_j > 10$. Further, the decay of centerline velocity of *T*1 and *T*4 cases shows good agreement with the experiment for $s/d_j \leq 10$ and $s/d_j > 10$, respectively.

Figure 8 shows the jet spreading or the variation of jet half-velocity width ($r_{1/2}$), which is defined as a radial distance where the streamwise velocity equals half of the centerline value. The predicted jet half-velocity widths are in good agreement with the experimental data of Quinn (2006), especially $s/d_j \leq 5$ for *T*1 case and $s/d_j \leq 10$ for *T*4 case. Then, for $5 < s/d_j < 15$ of *T*1 case and $10 < s/d_j < 20$ of *T*4 case, the predicted spreading of jets is nonlinearly wider than measured data,

which are similar to the previous work of Mathpati, Deshpande, and Joshi (2009). Finally, for higher s/d_j ratios, the predicted higher jet half-velocity widths are linear. From these results, it can be summarized that the tendencies of simulated jets are similar to those in previous studies, except for the values of jet half-velocity widths.

From these results, even when the inlet turbulence boundary conditions are varied, the predicted overall mixing times are slightly different and lower than the experimental data. It can be inferred that the mixing is dominated by convective transport. Further, these underpredicted overall mixing times are caused by the overprediction in total momentum available for mixing (convective transport) because of the flat top liquid surface assumption. This cause also results in the faster rise of predicted normalized concentration profiles. That is, the tracer is rapidly transported by jet rollover from the addition position to the bulk of liquid within a short time period. So, the predicted tracer concentration gradient would be lower than the actual experiment (underprediction in dispersive transport). Then, overprediction in peak value of normalized concentration profile should be observed.

Furthermore, for jet characteristics of this considered system, the jet kinetic energy should be partly converted to the potential energy during the change in elevation because of the energy conservation. Hence, the decay of centerline streamwise velocity should be faster than the free turbulent round jet. Moreover, the larger jet half-velocity width should be observed because the tank wall forces the liquid to circulate inside the vessel, which directly increases the rate of jet entrainment.

Hence, the appropriate conditions that correspond to the above discussion would be the conditions of *T1* case. That is, the suitable turbulence intensity for jet mixing tank simulations is 10% because the measured turbulence intensity profile of round jet is saddle-backed shape, which exhibits that the turbulence intensity at the jet half-width is higher than the centerline and average values. For example, Quinn (2006) revealed that the turbulence intensities at jet half width and jet centerline and average turbulence intensity for the region near jet nozzle exit were 10%, 0.5%, and 2%, respectively.

Further, in order to investigate the cause of the discrepancy in concentration profiles between CFD model and experiment, the jet mixing tank with jet discharge velocity of 4.4 m s^{-1} and top solid wall (*T7* case) and the jet mixing tank with jet discharge velocity of 6.6 m s^{-1} (*T8* case) were simulated to represent the lower and higher total momentum available for mixing, respectively. The normalized concentration profiles at probe 1 of these cases were compared with the results of *T1* case and the previous work of Patwardhan (2002) as shown in Figure 9.

From Figure 9, it can be seen that the normalized concentration profile of *T1* case shows better agreement with the experimental data as compared to the CFD models of Patwardhan (2002), especially the start and first peak value of concentration profile, because the numerical diffusion is eliminated by using the large number of grids and second order upwind scheme. These results also show the tendency and confirm that the normalized concentration profiles rise faster when increasing the convective transport. The first peak

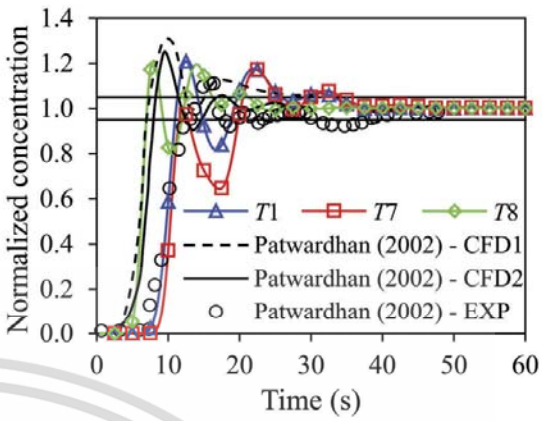

Figure 9. Normalized concentration profiles at probe 1 of present models and previous work of Patwardhan (2002) (C_μ = 0.09 and $C_{1\varepsilon}$ = 1.42 for CFD1 and C_μ = 0.135 and $C_{1\varepsilon}$ = 1.31 for CFD2).

values are found to decrease as the momentum available for mixing decreases. Further, although the level of turbulent dispersion was increased by modifying the model constants (C_μ = 0.135 and $C_{1\varepsilon}$ = 1.31) to compensate for the overprediction in convective transport due to the flat top liquid surface assumption, however, the faster rise and higher peak value of normalized concentration profile were still observed as reported by Patwardhan (2002).

According to above evidence, it can be summarized that the main cause of the discrepancy in concentration profiles between simulation and experiment for jet mixing tank would be due to the inappropriate inlet turbulence conditions, which affect the turbulent dispersion level inside the vessel, and the flat top liquid surface assumption, which provides the overprediction in total momentum available for mixing. That is, for the latter reason, the viscous dissipation is lower than the experiment because the energy is not lost to the viscous dissipation due to the wave motion of liquid surface.

Further, another possible reason for this discrepancy would be the problem in dynamic response of conductivity probe for mixing time investigation of jet mixing tank, which indicates how rapidly it is able to track changes in conductivity. That is, the output of measured conductivities may be shifted from their input values. So, when the simulated results and experimental data are compared, the difference between these data may be observed. Generally, the dynamic response can also be found in various engineering applications, such as flow rate measurement (Wiklund and Peluso 2002), and pumped-storage hydropower plants (Zhang et al. 2018).

5. Conclusions

In this work, the comprehensive CFD model was carefully developed to predict the mixing inside the open 45° inclined side entry pump-around jet mixing tank. The CFD model with the suitable inlet turbulence conditions, obtained by 10% turbulence intensity and the correlations used in *T1* case,

well predicted the overall mixing time with an error of about 8% as compared to the previous literature. Further, this model fairly showed the accuracy improvement of concentration profile prediction as compared with previous CFD models, especially the start and first peak value of the normalized concentration profile. However, the discrepancy in concentration profiles between CFD and experiment was still presented. The possible reasons for this shortfall were the inappropriate inlet turbulence conditions, which directly result in the improper extent of turbulent dispersion inside the tank, and the overprediction in convective transport due to the flat top liquid surface assumption. In addition, the dynamic response of conductivity probe can be considered as another possible cause of this discrepancy.

Although the present model with RKE gave acceptable results for a wide range of high jet Reynolds numbers, the turbulence model with low Reynolds number correction is recommended to achieve accurate results for low jet Reynolds numbers. For future work, the liquid surface simulation with suitable inlet turbulence conditions should be employed to achieve the accurate concentration profiles. Moreover, the fractional calculus, which is generally adopted in various chaotic systems (Chen et al. 2012; Xu et al. 2015), is another possible method that can be used to study the jet mixing behavior inside the tank.

Nomenclature

c	concentration
$\bar{c}$	fully mixed concentration
C_1, C_2, $C_{1\varepsilon}$, $C_{3\varepsilon}$	constants for RKE turbulence model
C_D	constant for turbulence kinetic energy dissipation rate correlation
C_μ	empirical constant for turbulence model
d_j	jet nozzle diameter
d_o	tank outlet diameter
D	tank diameter
$D_{i,m}$	mass diffusion coefficient for species i in the mixture
D_h	hydraulic diameter
D_t	turbulent diffusivity
e	relative error of numerical solutions
f_i	numerical solution of key variable for i grid level
G_b	generation of k due to buoyancy
G_k	production of turbulence kinetic energy
H	height of liquid
I	turbulence intensity
k	turbulence kinetic energy
l	length scale
N_i	number of grids for i grid level
p	order of the discretization method
P	mean pressure
r	refinement factor
$r_{1/2}$	jet half-velocity width
Re_{D_h}	Reynolds number based on hydraulic diameter
s	jet streamwise distance
S	modulus of the mean rate-of-strain tensor
S_i	source term for species transport equations
S_k	source term for k-transport equation
$S_{M,I}$	source term for momentum equation in i direction
S_ε	source term for ε-transport equation
S_φ	source term
Sc_t	turbulent Schmidt number
t	time
$t_{95\%}$, $t_{99\%}$	95% mixing time and 99% mixing time
u	streamwise velocity
u_c	centerline streamwise velocity
$\boldsymbol{U}$	mean velocity vector
U_j	jet discharge velocity
U_i	mean velocity in i direction
Y_i	local mass fraction of species i
Y_M	dilatation dissipation
Γ_φ	diffusivity
ε	turbulence kinetic energy dissipation rate or difference in numerical solutions
θ	jet nozzle angle
μ	fluid viscosity
μ_t	turbulent viscosity or eddy viscosity
ν_t	turbulent kinematic viscosity
ρ	fluid density
σ_k	turbulent Prandtl numbers for k
σ_ε	turbulent Prandtl numbers for ε
ϕ	universal independent variable

Acknowledgments

The authors would like to express their appreciation to professor emeritus Dr ès sc. techn. Horst Stoff, Department of Mechanical Engineering, Ruhr-Universität Bochum, Germany, for his valuable and constructive suggestions during the course of this research. Further, the ANSYS FLUENT software was supplied by College of Advanced Manufacturing Innovation, King Mongkut's Institute of Technology Ladkrabang, Thailand.

Disclosure statement

No potential conflict of interest was reported by the authors.

ORCID

Eakarach Bumrungthaichaichan http://orcid.org/0000-0003-1969-3110

References

ANSYS Inc. 2013a. *ANSYS CFX-Solver Theory Guide*. USA: ANSYS.
ANSYS Inc. 2013b. *ANSYS Fluent Theory Guide*. USA: ANSYS.
ANSYS Inc. 2013c. *ANSYS Fluent Tutorial Guide*. USA: ANSYS.
ANSYS Inc. 2013d. *ANSYS Fluent User's Guide*. USA: ANSYS.
Brooker, L. 1993. "Mixing with the Jet Set." *Chemical Engineering* 30: 16–25.
Bumrungthaichaichan, E. 2016. "A Review on Numerical Consideration for Computational Fluid Dynamics Modeling of Jet Mixing Tanks." *Korean Journal of Chemical Engineering* 33 (11): 3050–3068. doi:10.1007/s11814-016-0236-x.
Bumrungthaichaichan, E., N. Jaiklom, A. Namkanisorn, and S. Wattananusorn. 2016. "On the Computational Fluid Dynamics (CFD) Analysis of the Effect of Jet Nozzle Angle on Mixing Time for Various Liquid Heights." *Scientific Research and Essays* 11 (4): 42–56.
Celik, I. B. 1999. *Introductory Turbulence Modeling*. USA: West Virginia University.
Celik, I. B., U. Ghia, P. J. Roache, C. J. Freitas, H. Coleman, and P. E. Raad. 2008. ""Procedure for Estimation and Reporting of Uncertainty Due to Discretization in CFD Applications." *Journal of Fluids Engineering* 130 (7): 078001-1–078001-4. doi:10.1115/1.2960953.
Chen, D., Y. Liu, X. Ma, and R. Zhang. 2012. "Control of A Class of Fractional-Order Chaotic Systems via Sliding Mode." *Nonlinear Dynamics* 67 (1): 893–901. doi:10.1007/s11071-011-0002-x.
Cimbala, J. M., and Y. A. Çengel. 2008. *Essentials of Fluid Mechanics: Fundamentals and Applications*. New York: McGraw-Hill.
Courant, R., K. Friedrichs, and H. Lewy. 1967. "On the Partial Difference Equations of Mathematical Physics."." *IBM Journal of Research and Development* 11 (2): 215–234. doi:10.1147/rd.112.0215.
Dange, S. 2016. "Recirculation Boundary Conditions in ANSYS FLUENT."Accessed 1 March. https://www.learncax.com/knowledge-

base/blog/by-category/cfd/recirculation-boundary-conditions-in-ansys-fluent

Elsayed, K. 2011. "Analysis and Optimization of Cyclone Separators Geometry Using RANS and LES Methodologies." PhD thesis, Vrije Universiteit Brussel.

Fellouah, H., C. G. Ball, and A. Pollard. 2009. "Reynolds Number Effects within the Development Region of A Turbulent Round Free Jet." *International Journal of Heat and Mass Transfer* 52: 3943–3954. doi:10.1016/j.ijheatmasstransfer.2009.03.029.

Fluent Inc. 2006. *FLUENT 6.3 User's Guide*. Lebanon: Fluent.

Fossett, H., and L. E. Prosser. 1949. "The Application of Free Jets to the Mixing of Fluids in Bulk." *Proceedings of the Institution of Mechanical Engineers* 160: 224–232. doi:10.1243/PIME_PROC_1949_160_024_02.

Marek, M., T. Stoesser, P. J. W. Roberts, V. Weitbrecht, and G. H. Jirka. 2007. "CFD Modeling of Turbulent Jet Mixing in A Water Storage Tank." Proceedings of the 32nd IAHR World Congress, Venice, Italy, 1–6 July 2007, 1–10. Spain: IAHR.

Mathpati, C. S., S. S. Deshpande, and J. B. Joshi. 2009. "Computational and Experimental Fluid Dynamics of Jet Loop Reactor." *AIChE Journal* 55 (10): 2526–2544. doi:10.1002/aic.11853.

Patwardhan, A. W. 2002. "CFD Modeling of Jet Mixed Tanks." *Chemical Engineering Science* 57 (8): 1307–1318. doi:10.1016/S0009-2509(02)00049-0.

Quinn, W. 2006. "Upstream Nozzle Shaping Effects on near Field Flow in Round Turbulent Free Jets." *European Journal of Mechanics B/Fluids* 25 (3): 279–301. doi:10.1016/j.euromechflu.2005.10.002.

Raja, T., P. Kalaichelvi, and N. Anantharaman. 2007. "Development of CFD Model for Optimum Mixing in Jet Mixed Tanks." *Journal of Scientific & Industrial Research* 66 (7): 522–527.

Ranade, V. V. 1996. "Towards Better Mixing Protocols by Designing Spatially Periodic Flows: The Case of A Jet Mixer.." *Chemical Engineering Science* 51 (11): 2637–2642. doi:10.1016/0009-2509(96)00129-7.

Roache, P. J. 1994. "Perspective: A Method for Uniform Reporting of Grid Refinement Studies." *Journal of Fluids Engineering* 116 (3): 405–413. doi:10.1115/1.2910291.

Roache, P. J. 1997. "Quantification of Uncertainty in Computational Fluid Dynamics." *Annual Review of Fluid Mechanics* 29: 123–160. doi:10.1146/annurev.fluid.29.1.123.

Roache, P. J. 1998. "Verification of Codes and Calculations." *AIAA Journal* 36 (5): 696–702. doi:10.2514/2.457.

Sendilkumar, K. K., P. Kalaichelvi, M. Perumalsamy, A. Arunagiri, and T. Raja. 2007. "Computational Fluid Dynamic Analysis of Mixing Characteristics inside a Jet Mixer for Newtonian and Non Newtonian Fluids." Proceedings of the World Congress on Engineering and Computer Science 2007, San Francisco, USA, 24–26 October 2007, 120–128. Hong Kong: IAENG.

Spyrou, M. 2009. "The Diffusion Coefficient of Water: A Neutron Scattering Study Using Molecular Dynamics Simulations." Master thesis, University of Surrey.

Wasewar, K. L., and J. V. Sarathi. 2008. "CFD Modelling and Simulation of Jet Mixed Tanks." *Engineering Applications of Computational Fluid Mechanics* 2 (2): 155–171. doi:10.1080/19942060.2008.11015218.

Wiklund, D., and M. Peluso. 2002. "Quantifying and Specifying the Dynamic Response of Flowmeters." Proceedings of ISA 2002 Technical Conference (TECHNICAL PAPERS - ISA), Chicago, USA, 21–24 October 2002, 463–476. USA: ISA. doi: 10.1044/1059-0889(2002/er01).

Wilcox, D. C. 1994. *Turbulence Modeling for CFD*. California: DCW Industries.

Xu, B., D. Chen, H. Zhang, and F. Wang. 2015. "The Modeling of the Fractional-Order Shafting System for A Water Jet Mixed-Flow Pump during the Startup Process." *Communications in Nonlinear Science and Numerical Simulation* 29: 12–24. doi:10.1016/j.cnsns.2015.04.018.

Zhang, H., D. Chen, B. Xu, E. Patelli, and S. Tolo. 2018. "Dynamic Analysis of A Pumped-Storage Hydropower Plant with Random Power Load." *Mechanical Systems and Signal Processing* 100: 524–533. doi:10.1016/j.ymssp.2017.07.052.

Zhang, H.-L., and S.-J. Han. 1996. "Viscosity and Density of Water + Sodium Chloride + Potassium Chloride Solutions at 298.15 K." *Journal of Chemical & Engineering Data* 41 (3): 516–520. doi:10.1021/je9501402.

Zughbi, H. D., and I. Ahmad. 2005. "Mixing in Liquid-Jet-Agitated Tanks: Effects of Jet Asymmetry." *Industrial & Engineering Chemistry Research* 44 (4): 1052–1066. doi:10.1021/ie0496683.

Zughbi, H. D., and M. A. Rakib. 2002. "Investigations of Mixing in A Fluid Jet Agitated Tank." *Chemical Engineering Communications* 189 (8): 1038–1056. doi:10.1080/00986440213878.

Zughbi, H. D., and M. A. Rakib. 2004. "Mixing in A Fluid Jet Agitated Tank: Effects of Jet Angle and Elevation and Number of Jets." *Chemical Engineering Science* 59 (4): 829–842. doi:10.1016/j.ces.2003.09.044.

C.2 CFD modelling of pump-around jet mixing tanks: a reliable model for overall mixing time prediction

Taylor & Francis
Taylor & Francis Group

Journal of the Chinese Institute of Engineers

ISSN: 0253-3839 (Print) 2158-7299 (Online) Journal homepage: https://www.tandfonline.com/loi/tcie20

CFD modelling of pump-around jet mixing tanks: a reliable model for overall mixing time prediction

Eakarach Bumrungthaichaichan & Santi Wattananusorn

To cite this article: Eakarach Bumrungthaichaichan & Santi Wattananusorn (2019) CFD modelling of pump-around jet mixing tanks: a reliable model for overall mixing time prediction, Journal of the Chinese Institute of Engineers, 42:5, 428-437, DOI: 10.1080/02533839.2019.1598287

To link to this article: https://doi.org/10.1080/02533839.2019.1598287

Published online: 19 Apr 2019.

Submit your article to this journal

Article views: 64

View Crossmark data

JOURNAL OF THE CHINESE INSTITUTE OF ENGINEERS
2019, VOL. 42, NO. 5, 428–437
https://doi.org/10.1080/02533839.2019.1598287

CFD modelling of pump-around jet mixing tanks: a reliable model for overall mixing time prediction

Eakarach Bumrungthaichaichan and Santi Wattananusorn

Department of Chemical Engineering, Faculty of Engineering, King Mongkut's Institute of Technology Ladkrabang, Bangkok, Thailand

ABSTRACT

Over the past two decades or so, computational fluid dynamics (CFD) has been employed to predict overall mixing times inside jet mixing tanks instead of non-universal mixing time correlations obtained by experiments. However, the numerical methods for jet mixing tank simulations were not clearly tested and the discretization errors of the previous CFD models were not assessed. So, in this paper, the suitable turbulence model and numerical methods for pump-around jet mixing tank simulations were investigated. Further, the discretization errors of the present CFD models were estimated with the help of grid convergence index (GCI). The results revealed that the realizable k-epsilon model, SIMPLE, second order upwind, and first order implicit were proper turbulence model and numerical methods for pump-around jet mixing tank simulations. From GCI analyses, the maximum discretization uncertainty in overall mixing time of the present CFD models was about ±0.08 s.

ARTICLE HISTORY
Received 2 March 2018
Accepted 26 February 2019

KEYWORDS
CFD; jet; mixing; discretization error

1. Introduction

The jet mixing tank is a mixing device used in many chemical processes, which was firstly proposed by Fossett and Prosser (1949). The liquid recirculation and entrainment inside the tank are driven by a high-velocity liquid jet generated by the pump. Then, the different components inside the vessel are mixed. The jet mixing tank has become an important mixing device because of its advantages, including simple design with non-moving parts, low operating cost, and easy installation and maintenance.

Over the past 60 years or so, jet mixing tanks were experimentally studied by many researchers. Most of these works end up in different overall mixing time correlations (Patwardhan 2002; Wasewar 2006). That is, these mixing time correlations were individually developed by considering the studied parameters of those researches. However, these correlations are case specific (Bumrungthaichaichan 2016). Further, the fluid flow and mixing behaviors inside this device were not presented. So, computational fluid dynamics (CFD) is adopted to address these experimental problems.

One of the earliest CFD studies on a jet mixing tank was carried out by Brooker (1993). He successfully showed that the maximum error between predicted overall mixing time and experiment was about 15%. Later, the effects of jet arrangement (Ranade 1996; Patwardhan 2002; Zughbi and Rakib 2004; Zughbi and Ahmad 2005; Jaiklom, Bumrungthaichaichan, and Wattananusorn 2013), tank shape (Raja, Kalaichelvi, and Anantharaman 2007), liquid height (Bumrungthaichaichan et al. 2016), jet injection rate (Zughbi and Rakib 2002), and fluid types (Sendilkumar et al. 2007) on mixing behavior were investigated by CFD. In addition, the effect of turbulence models (Rahimi and Parvareh 2005; Marek et al. 2007; Mathpati, Deshpande, and Joshi 2009; Furman and Stegowski 2011) on jet mixing behavior was also studied.

Over the past two decades or so, although the CFD models of jet mixing tanks were properly developed, the discrepancies in concentration profiles between CFD models and experiments were still present. Up until today, the accuracy improvement of concentration profile predictions has been investigated by a few researchers (Patwardhan 2002; Marek et al. 2007; Bumrungthaichaichan et al. 2016). However, this discrepancy was still observed. Later, Bumrungthaichaichan, Namkanisorn, and Wattananusorn (2018) revealed that the possible reasons for the discrepancy in concentration profiles between CFD model and experiment were improper inlet turbulence conditions, overprediction in total momentum due to the flat top liquid surface assumption, and dynamic response of concentration measuring device.

According to the previous works, it can be seen that the CFD models can be used to predict the overall mixing times instead of the mixing time correlations obtained by experiments. However, the numerical errors of these CFD models were not assessed. Generally, there are three different components of numerical error, including round-off error, iterative error, and discretization error (Roache 2009). Eça and Hoekstra (2009, 2014) stated that the contribution of round-off and iterative errors to the numerical error is negligible as compared to the discretization error. Furthermore, the suitable numerical methods for pump-around jet mixing tank simulation were not clearly studied and represented.

So, in order to obtain the suitable turbulence model and numerical methods for pump-around jet mixing tank simulation, the different CFD models were simulated by using jet

CONTACT Eakarach Bumrungthaichaichan b_eakarach@hotmail.com Department of Chemical Engineering, Faculty of Engineering, King Mongkut's Institute of Technology Ladkrabang, Bangkok 10520, Thailand

This article has been republished with minor changes. These changes do not impact the academic content of the article.

Table 1. Details of turbulence model and numerical setups for different cases.

Case	Turbulence model	P-V coupling scheme	Discretization scheme	
			Spatial	Temporal
SM1[a]	RKE	SIMPLE	SOU	FOI
TM1	SKE	SIMPLE	SOU	FOI
TM2	RNGKE	SIMPLE	SOU	FOI
NM1[b]	RKE	PISO	SOU	FOI
NM2	RKE	SIMPLE	FOU	FOI
NM3	RKE	SIMPLE	QUICK	FOI
NM4	RKE	SIMPLE	SOU	SOI

[a]*SM1* case is a standard setup case.
[b]For *NM1* case, the SIMPLE and PISO were employed for steady state and transient simulations, respectively.

discharge velocity (U_j) of 4.4 m·s^{-1}. For turbulence model, the three different k-epsilon models, including standard k-epsilon (SKE), renormalization k-epsilon (RNGKE), and realizable k-epsilon (RKE) models, were employed. Generally, these k-epsilon models contain two transport equations, including turbulence kinetic energy (k) and turbulence kinetic energy dissipation rate (ε) transport equations. SKE represents acceptable results for a wide range of industrial and non-industrial application areas. However, it is not suitable for predicting complex flows, such as swirling flows, flows with strong separation, axisymmetric jets, etc. So, the other complex k-epsilon models are developed to address these problems.

For RNGKE, the turbulent viscosity is modified by adding the effects of swirl (or rotation) and Reynolds number (ANSYS Inc. 2013a). Further, ε-transport equation is also modified by considering interaction between turbulence dissipation and mean shear. RNGKE is commonly used for various swirl flows, for example cyclone separator, stirred tank, etc. For RKE, improved ε-transport equation and alternative formulation for turbulent viscosity are developed (ANSYS Inc. 2013a). The advantage of this model is that it ensures the positivity of normal stresses and Schwarz's inequality (Shih et al. 1995; Shih 1996). This model is recommended for simulating turbulent round and planar jets.

For numerical methods, the different pressure-velocity coupling schemes (Semi-Implicit Method for Pressure-Linked Equations (SIMPLE) and Pressure Implicit with Splitting of Operators (PISO)), spatial discretization schemes (first-order upwind (FOU), second-order upwind (SOU), and quadratic upwind interpolation for convective kinetics (QUICK)), and temporal discretization schemes (first-order implicit (FOI) and second-order implicit (SOI)) were adopted. The details of tested turbulence models and numerical methods for different CFD models are summarized in Table 1. Further, the discretization errors of pump-around jet mixing tank simulations for different jet discharge velocities, including 4.4, 6.6, 8.8, and 11 m·s^{-1}, were also studied with the help of grid convergence index to show the reliability of present CFD model for predicting the overall mixing time.

2. Description of CFD modelling

2.1. Consideration of jet mixing tank system

In our present work, the considered system was an open 45° inclined side entry pump-around jet mixing tank following Patwardhan (2002). The flat bottom cylindrical tank with a diameter (D) of 0.5 m was filled with water to the height (H) of 0.5 m (H/D = 1). The 45° nozzle with a jet diameter (d_j) of 0.008 m was located at tank base. The outlet pipe diameter (d_o) was 0.0381 m. Further, in experiments of Patwardhan (2002), the dilute NaCl solution was rapidly added into the tank at the center of the top water surface with the help of a beaker. The conductivity was measured and recorded by using four conductivity probes. Then, the mixing time was determined by using the time taken for the conductivity to reach 95% of fully mixed value. The overall mixing time was determined by finding the mean of the mixing times obtained by these measuring probes. The schematic of this jet mixing tank and coordinate systems are shown in Figure 1.

2.2. Grid generation

The three-dimensional jet mixing tank model and grids were created by using GAMBIT 2.4.6 program. Typically, in order to achieve accurate predicted results for turbulent flows, the hexahedral grid generation should be designed to align to flow direction (Kim, Barbat, and Spicka 2005). Further, the fine grids should be created in upstream and viscous-dominated regions, for example shear layer region, near wall region (boundary layer region), high-velocity gradient region, etc. Hence, the hexahedral grids were carefully generated inside the flow domain with the help of domain decomposition technique, similar to the previous work of Bumrungthaichaichan, Namkanisorn, and Wattananusorn (2018). The grid generation of pump-around jet mixing tank is shown in Figure 2.

2.3. Governing equations

For present CFD simulations of jet mixing tanks, the simulations were distinguished into two parts. First, the steady state mean velocity and turbulence were achieved by solving the Reynolds average equations for conservation of mass and momentum together with turbulence model. Second, the unsteady state species transport equations without chemical reaction were solved to obtain the tracer concentration distribution inside the vessel. So, the compact form of steady state Reynolds average equations can be written as:

$$\frac{\partial(\rho \boldsymbol{U}\phi)}{\partial x_j} = \frac{\partial}{\partial x_j}\left[\Gamma_\varphi \frac{\partial \phi}{\partial x_j}\right] + S_\varphi, \tag{1}$$

where ρ is fluid density, $\boldsymbol{U}$ is mean velocity vector, ϕ is a universal dependent variable, Γ_φ is the diffusivity, and S_φ is the source term. Further, the details of the variables for continuity equation, momentum equations, and turbulence models (ANSYS Inc. 2013a) are shown in Table 2.

Further, the unsteady state species transport equations without chemical reaction (ANSYS Inc. 2013a) can be written as:

$$\frac{\partial(\rho Y_i)}{\partial t} + \frac{\partial(\rho \boldsymbol{U} Y_i)}{\partial x_j} = \frac{\partial}{\partial x_j}\left(\left(\rho D_{i,m} + \frac{\mu_t}{\mathrm{Sc}_t}\right)\frac{\partial Y_i}{\partial x_j}\right) + S_i, \tag{2}$$

where Y_i is the local mass fraction of species i, $D_{i,m}$ is the mass diffusion coefficient for species i in the mixture, Sc_t is the turbulent Schmidt number (ν_t/D_t where ν_t is the turbulent kinematic viscosity and D_t is the turbulent diffusivity), μ_t is

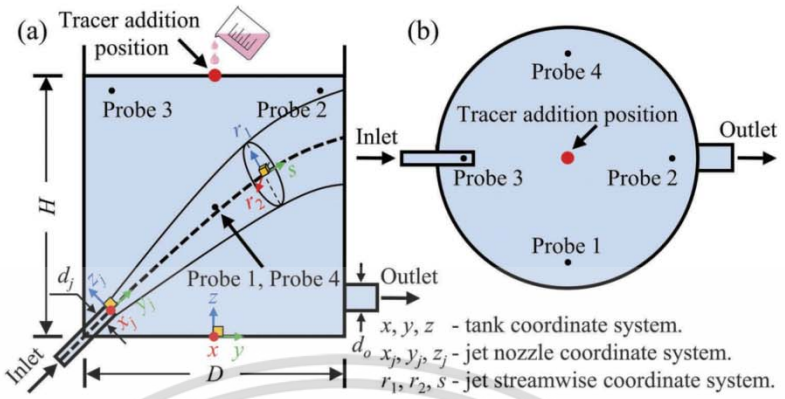

Figure 1. Schematic of jet mixing tank and coordinate systems that are necessary to describe flow and mixing phenomena inside the vessel (a) side view and (b) top view. (Adapted from Bumrungthaichaichan, Namkanisorn, and Wattananusorn (2018))

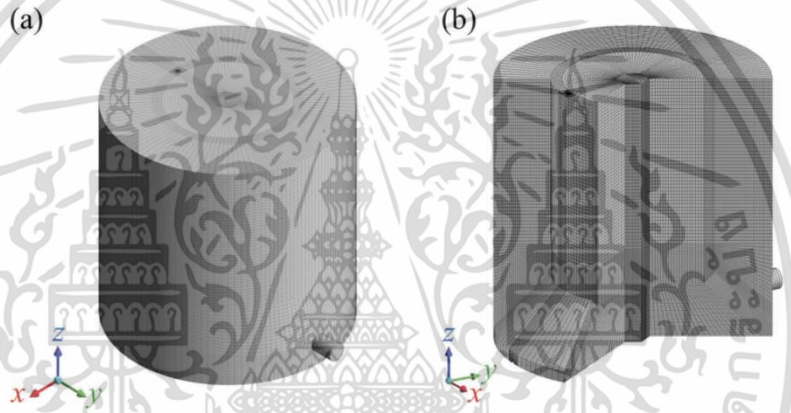

Figure 2. Grid generation of jet mixing tank (a) isometric view and (b) inside view. (Adapted from Bumrungthaichaichan, Namkanisorn, and Wattananusorn (2018))

Table 2. Details of the variables for continuity equation, momentum equations, and transport equations of k and ε for three different k-epsilon turbulence models.

Equation		ϕ	Γ_φ	S_φ	Constants
Continuity		1	0	0	-
Momentum		U_i	μ	$-\frac{\partial P}{\partial x_i}+\frac{\partial}{\partial x_j}\left[\mu_t\frac{\partial U_i}{\partial x_j}\right]+S_{M,i}$	-
SKE	k-transport	k	$\mu+\frac{\mu_t}{\sigma_k}$	$G_k+G_b-\rho\varepsilon-Y_M+S_k$	$\sigma_k=1.0$
	ε-transport	ε	$\mu+\frac{\mu_t}{\sigma_\varepsilon}$	$C_{1\varepsilon}\frac{\varepsilon}{k}(G_k+C_{3\varepsilon}G_b)-C_{2\varepsilon}\rho\frac{\varepsilon^2}{k}+S_\varepsilon$	$\sigma_\varepsilon=1.3$ $C_{1\varepsilon}=1.44$ $C_{2\varepsilon}=1.92$
RNGKE	k-transport	k	$\alpha_k(\mu+\mu_t)$	$G_k+G_b-\rho\varepsilon-Y_M+S_k$	-
	ε-transport	ε	$\alpha_\varepsilon(\mu+\mu_t)$	$C_{1\varepsilon}\frac{\varepsilon}{k}(G_k+C_{3\varepsilon}G_b)-C_{2\varepsilon}\rho\frac{\varepsilon^2}{k}-R_\varepsilon+S_\varepsilon$	$C_{1\varepsilon}=1.42$ $C_{2\varepsilon}=1.68$
RKE	k-transport	k	$\mu+\frac{\mu_t}{\sigma_k}$	$G_k+G_b-\rho\varepsilon-Y_M+S_k$	$\sigma_k=1.0$
	ε-transport	ε	$\mu+\frac{\mu_t}{\sigma_\varepsilon}$	$\rho C_1 S\varepsilon-\rho C_2\frac{\varepsilon^2}{k+\sqrt{\nu\varepsilon}}+C_{1\varepsilon}\frac{\varepsilon}{k}C_{3\varepsilon}G_b+S_\varepsilon$	$\sigma_\varepsilon=1.2$ $C_1=\max\left[0.43,\frac{\eta}{\eta+5}\right]$ $C_2=1.9$ $C_{1\varepsilon}=1.44$

the turbulent viscosity, and S_i is the source term for species transport equations.

2.4. Physical and numerical setups

For standard pump-around jet mixing tank simulations, the details of physical and numerical setups, including solver, material properties, boundary conditions, pressure-velocity coupling scheme, spatial discretization scheme, temporal discretization scheme, time step size, and convergence criteria were similar to the previous CFD work of Bumrungthaichaichan, Namkanisorn, and Wattananusorn (2018) as shown in Table 3.

2.5. Mixing time investigation

For mixing time simulation, the tracer with mass fraction of unity was initially patched at 0.03 m below the top liquid surface center to account for the experimental observation that the tracer slightly moved downward because the tracer was added by using a beaker (Patwardhan 2002). Then, Equation (2) was iteratively solved. During the calculation, the time histories of tracer concentrations for four different probes were monitored and recorded. The mixing times of these probes were individually evaluated by considering the 95% mixing time ($t_{95\%}$), which is the time required for the concentration (c) to reach 95% of the fully mixed concentration ($\bar{c}$) and can be written in compact form as:

$$t_{95\%} = \text{time for} \left| \frac{c - \bar{c}}{\bar{c}} \right| \leq 0.05 \quad (3)$$

Table 4. The details of the grid independence study of *SM1* case.

Grid	Number of cells	Mixing time (s)	% difference[a]
0-adapted grid[b]	1,087,312	29.6918	5.33
1-adapted grid	1,184,437	29.7257	5.45
2-adapted grid	1,486,046	28.3658	0.62
3-adapted grid	1,739,978	28.1903	-

[a]The percentage difference is a ratio of absolute difference between the mixing times for any grid and finest grid to the finest grid value.
[b]0-adapted grid is an original grid obtained by GAMBIT.

Finally, the overall jet mixing time was determined by finding the mean of the mixing times obtained by four different probes.

2.6. Grid independence study

In this paper, the grid independence study has been performed with the help of grid adaptation technique. In order to ensure that the grids were properly refined, the velocity gradient adaptation with the refinement threshold of 10% of its maximum value (ANSYS Inc. 2013b, 2013c) was performed individually for different cases because the different setups may present different jet spreading rates. The simulated overall mixing times of *SM1* cases for different grid resolutions are represented in Table 4.

In Table 4, the results showed that the maximum percentage difference of mixing time is less than 6%. This means that the grid independency is sufficiently achieved by using the original grid obtained by GAMBIT. However, to eliminate any uncertainty and to ensure that the grid convergence was achieved, the finest grid level obtained by adapting an original grid three times was adopted for all simulations.

Table 3. Standard setup for pump-around jet mixing tank simulation.

Setup	Description	Comment
Solver	Double precision pressure-based solver	Round-off error is omitted by this selected solver.
Turbulence model	RKE	RKE ensures the positivity of normal stresses and Schwarz's inequality (Shih et al. 1995; Shih 1996).
Material properties	ρ = 998.2 kg·m^{-3} μ = 0.001003 kg·m^{-1}·s^{-1} D = 2.3 × 10^{-9} m^2·s^{-1} (Spyrou 2009)	The properties of water and tracer were assumed to be identical because the NaCl solution was dilute.
Boundary condition types	Inlet (Steady state): velocity-inlet Outlet (Steady state): pressure-outlet Inlet (Transient): recirculation-inlet Outlet (Transient): recirculation-outlet Wall and base: wall (no-slip boundary condition) Top water surface: symmetry	The recirculation-inlet and recirculation outlet were enable by respectively typing the additional text commands in TUI (Dange 2016), including (rpsetvar 'icepak? #t) and (models-changed).
Boundary conditions	U_j = 4.4, 6.6, 8.8, and 11 m·s^{-1} $k = 1.5(U_j I)^2$ where I = 10% (Patwardhan 2002) $\varepsilon = C_D k^{3/2}/l$ (Celik 1999) where C_D = 0.08 (Wilcox 1994) and $l = 0.07 d_j$ (ANSYS Inc. 2013c)	The uniform jet discharge velocity was specified.
Pressure-velocity coupling scheme	SIMPLE	This scheme is widely used in various CFD studies.
Spatial discretization scheme	SOU	This scheme was applied for all quantities.
Temporal discretization scheme	FOI	For FOI, the large time step size can be used.
Time step size	0.0025 s	This time step size was lower than residence time.
Convergence criterion (Steady state)	The area weighted average of velocity magnitude at plane x = 0 was monitored until it was constant.	This criterion was used to ensure that the iterative convergence was achieved.
Convergence criterion (Transient)	The tracer scaled residual of 10^{-5} was used.	The lower residuals did not improve the results.

3. Grid convergence index and model validation

Roache (1994) suggested the qualitative measurement of grid convergence, which is known as grid convergence index (GCI). The GCI is not only able to determine the grid convergence but also to assess the discretization error in CFD studies (Celik et al. 2008). The GCI can be computed by considering two grid levels. However, in order to check the convergence condition and asymptotic range of convergence, three or more grid levels are recommended. From previous studies (Celik et al. 2008; Elsayed 2011), the comprehensive procedure of GCI can be drawn as shown in Figure 3. In this paper, the GCI analysis for overall mixing time and model validation of standard model (*SM*1 case) are represented in Table 5.

From Table 5, for GCI analysis, the results reveal that GCI_{21} is less than GCI_{32}, which indicates and confirms that the grid independent solution has been achieved. This means further grid refinement is unnecessary. In addition, the overall mixing time predicted by finest grid level is close to its extrapolated value. So, the solutions are converged with the refinement from medium to finest grid resolutions. Further, for model validation, the overall mixing time of finest grid level is an underprediction and is in good agreement with experimental data. The error between simulation and experiment is about 9%. So, it can be inferred that this CFD model is reasonably adopted to study the pump-around jet mixing tank.

4. Results and discussion

4.1. Suitable turbulence model and numerical methods

As mentioned earlier, the different k-epsilon turbulence models and numerical methods as depicted in Table 1 were tested by using the jet discharge velocity of 4.4 $m{\cdot}s^{-1}$ with inlet turbulence conditions ($k = 0.2904\ m^2{\cdot}s^{-2}$ and $\varepsilon = 22.35614\ m^2{\cdot}s^{-3}$) suggested

Determine the refinement factor (r):

$$r_{i+1,i} = \left(\frac{N_i}{N_{i+1}}\right)^{1/D}$$ where

i is finer grid level.
i+1 is coarser grid level.
N is number of cells.
D is domain dimension.

Calculate the difference in numerical solutions (ε) and relative error of numerical solutions (e):

$$\varepsilon_{i+1,i} = f_{i+1} - f_i \quad \text{and} \quad e_{i+1,i} = \frac{f_{i+1} - f_i}{f_i}$$

where f is the key variable.

Determine the order of the discretization method (p):

$$p = \frac{1}{\ln(r_{21})}\left|\ln\left(\left|\frac{\varepsilon_{32}}{\varepsilon_{21}}\right| \times \left(\frac{r_{21}^p - \mathrm{sgn}(\varepsilon_{32}/\varepsilon_{21})}{r_{32}^p - \mathrm{sgn}(\varepsilon_{32}/\varepsilon_{21})}\right)\right)\right|$$

where sgn is a sign function

The iterative method is adopted to solve value of p as:

$$p = \omega\rho + (1-\omega)\frac{1}{\ln(r_{21})}\left|\ln\left(\left|\frac{\varepsilon_{32}}{\varepsilon_{21}}\right| \times \left(\frac{r_{21}^p - \mathrm{sgn}(\varepsilon_{32}/\varepsilon_{21})}{r_{32}^p - \mathrm{sgn}(\varepsilon_{32}/\varepsilon_{21})}\right)\right)\right|$$

where ω is a relaxation factor ($\omega = 0.5$)

ρ is the previous iteration of p

(The initial guess value is $\rho = \frac{\left|\ln\left|\varepsilon_{32}/\varepsilon_{21}\right|\right|}{\ln(r_{21})}$)

Calculate the GCI:

$$GCI_{i+1,i} = \frac{F_s\left|e_{i+1,i}\right|}{r_{i+1,i}^p - 1}$$ where F_s is safety factor

$$\left(F_s = \begin{cases} 3 & \text{for two grid levels} \\ 1.25 & \text{for three grid levels or more} \end{cases}\right)$$

Figure 3. GCI procedure. (Adapted from Bumrungthaichaichan, Namkanisorn, and Wattananusorn (2018))

Table 5. Grid convergence index and model validation of *SM*1 case.

i [a]	N_i	f_i	$GCI_{i+1,i}$ (%)	% Error[b]
Patwardhan (2002)	-	31.0000	-	-
0[c]	-	28.1264	-	-
1	1,739,978	28.1903		9.06
			0.2834	
2	1,486,046	28.3658		8.50
			1.0550	
3	1,184,437	29.7257		4.11
			0.1362	
4	1,087,312	29.6918		4.22

[a] i = 1, 2, 3, and 4 denote the finest, fine, medium and coarse mesh, respectively.
[b] The percentage error is a ratio of absolute difference between the predicted overall mixing time and experimental mixing time to the experimental value.
[c] $f_{exact} = f_1 + (f_1 - f_2)/(r_{12}^p - 1)$: The value at zero grid space.

by Bumrungthaichaichan, Namkanisorn, and Wattananusorn (2018) to obtain the suitable CFD model for pump-around jet mixing tank. The predicted overall mixing times and profiles of normalized concentration, which is defined as the ratio of the tracer concentration to the fully mixed value, for different models were compared to the experimental data of Patwardhan (2002) as shown in Table 6 and Figure 4, respectively.

From Table 6, the results reveal that the mixing times and overall mixing times predicted by different cases are lower than those observed experimentally because of the overprediction in convective transport due to flat top liquid surface assumption as reported by Bumrungthaichaichan, Namkanisorn, and Wattananusorn (2018). *TM*1 and *NM*2 cases respectively show the lowest and highest predicted overall mixing times, which correspond to the maximum and minimum percentage errors of 23.71% and 3.58%. Further, the overall mixing times predicted by other cases are slightly different with percentage errors between 5 and 10%.

For turbulence models, in Figure 4(a), the results show that the rise in predicted normalized concentration profiles of three k-epsilon models are slightly different. But, the *SM*1 case presents the highest first peak value of normalized concentration profile, respectively followed by *TM*2 and *TM*1 cases. The decays of first peak values of simulated normalized concentration profiles of *TM*1 and *TM*2 cases are faster than *SM*1 case and experimental data because these CFD simulations overpredict the turbulence dispersion levels inside the tanks. That is, the *TM*1 case provides the highest predicted turbulence diffusivity inside the tank with a value of 3.97×10^{-4} $m^2 \cdot s^{-1}$ and followed by *TM*2 (3.60×10^{-4} $m^2 \cdot s^{-1}$)

Table 6. Mixing times and calculation times for different CFD models.

Case	Mixing time (s) Probe 1	Probe 2	Probe 3	Probe 4	Overall	% Error	Calculation time (h)[a]
EXP[b]	38.5000	37.7000	N/A	N/A	31.0000	-	-
*SM*1	33.1779	29.5401	27.3008	22.7423	28.1903	9.06	39.77
*TM*1	21.4033	22.8855	28.9077	21.4038	23.6501	23.71	39.58
*TM*2	29.3764	30.9891	29.6687	27.5838	29.4045	5.15	43.23
*NM*1	33.1779	29.5401	27.3008	22.7423	28.1903	9.06	39.85
*NM*2	31.9522	29.4013	26.3567	31.8529	29.8908	3.58	28.45
*NM*3	32.4339	29.4551	27.1993	22.6358	27.9310	9.90	43.87
*NM*4	33.2556	29.5879	27.3138	22.7207	28.2195	8.97	39.83

[a] Calculation time is the time required for performing the steady state and transient simulations of final grid resolution.
[b] EXP is the experimental data of Patwardhan (2002).

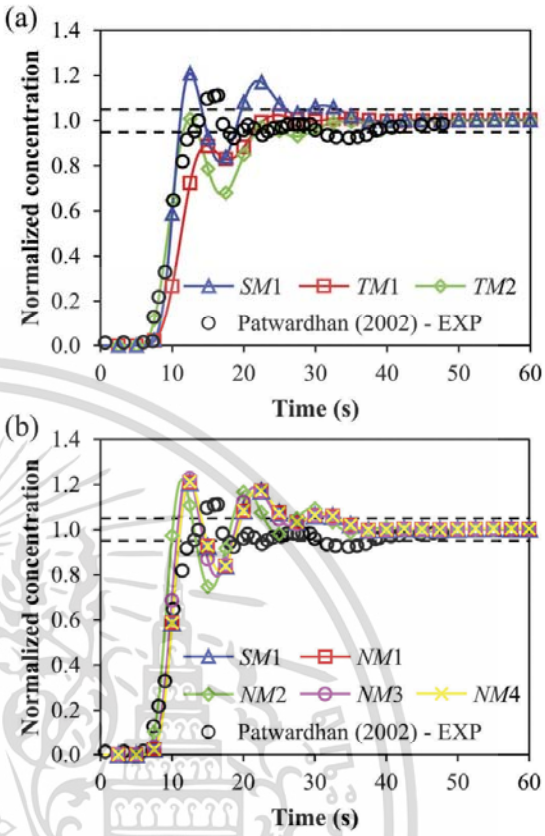

Figure 4. Comparison of normalized concentration profiles at probe 1 for (a) different turbulence models and (b) different numerical methods.

and *SM*1 (2.87×10^{-4} $m^2 \cdot s^{-1}$), respectively. However, all predicted profiles approach the measured profile, most times.

In Figure 4(b), the results reveal that the first peak values of the predicted normalized concentration profiles for different numerical methods are slightly different and are higher than those observed experimentally. The start of normalized concentration profile for *NM*2 case is slightly faster than other CFD models. Mostly, all simulated profiles are in good agreement with the experimental data. The reasons for the discrepancy in concentration profiles between CFD model and experiment were clearly described by Bumrungthaichaichan, Namkanisorn, and Wattananusorn (2018). Further, in order to select the appropriate turbulence model and numerical methods for CFD simulation of pump-around jet mixing tank, the jet axial velocity contours at plane $x_j = 0$ for these cases were also compared as depicted in Figure 5.

From Figure 5, the results show that the jet spreading of *TM*1 and *TM*2 cases are wider than that obtained in the *SM*1 case. The decays of centerline velocity predicted by *SM*1 and *TM*1 cases are slightly different and are slower than that achieved by *TM*2 case. Regarding to the previous work of Bumrungthaichaichan, Namkanisorn, and Wattananusorn

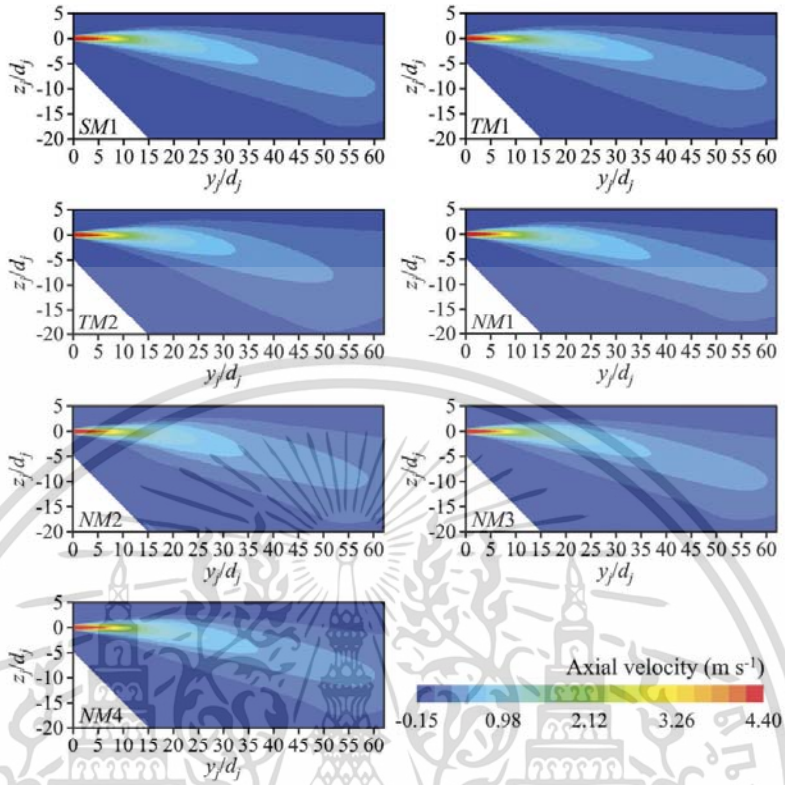

Figure 5. Contours of jet axial velocity at plane $x_j = 0$ (y_jz_j – plane) for different cases.

(2018), the decay of centerline velocity for CFD model with the same physical and numerical setups of *SM*1 case is in good agreement with the experimental data. This means the decay of centerline velocity of *TM*1 case should be also similar to the experiment. Moreover, for *TM*2 case, the centerline velocity decay is faster than the measured data. So, the wider jet spreading with normal decay of centerline velocity of *TM*1 case results in higher convective transport, which can be considered as another possible reason for the shortest predicted overall mixing time.

These results correspond to the fact that the SKE overpredicts the round jet spreading (Pope 1978) and RNGKE is not suitable for predicting the round jet (Marshall and Bakker 2004). However, the present results contradict the suggestions of previous CFD works that SKE (Zughbi and Rakib 2004; Zughbi and Ahmad 2005) and RNGKE (Rahimi and Parvareh 2005; Furman and Stegowski 2011) were suitable for simulating the jet mixing tanks. The discrepancy in results and suggestions between present and previous CFD works may be due to the fact that the previous works used a smaller number of grids to simulate the jet mixing tanks, which may not be sufficient to represent the correct solutions.

For *NM*2 case, the axial velocity tends to be smeared out at y_j/d_j of about 12 as compared to the other cases because FOU produces incorrect results when the flow is not aligned with grids (Versteeg and Malalasekera 1995). Although the recommended pressure-velocity coupling scheme for transient simulation (PISO), higher order spatial discretization scheme (QUICK), and higher temporal discretization scheme (SOI) were respectively adopted in *NM*1, *NM*3, and *NM*4 cases to simulate the pump-around jet mixing tanks, the results are very similar to that predicted by *SM*1 case because the hexahedral grids were controlled and aligned with the flow direction to minimize the truncation error and numerical diffusion (Kim, Barbat, and Spicka 2005). Further, the computational time of *SM*1 is shorter than *NM*1, *NM*3, and *NM*4 cases as depicted in Table 6.

Hence, when these results are viewed together, it can be seen that the turbulence model (RKE), pressure-velocity coupling scheme (SIMPLE), spatial discretization scheme (SOU), and temporal discretization scheme (FOI) of *SM*1 case are suitable for simulating the pump-around jet mixing tank because of accuracy and time efficiency.

4.2. Discretization error

As mentioned earlier, the CFD was adopted to address the experimental problem that the universal jet mixing time correlation is unavailable (Bumrungthaichaichan 2016). However, even when the appropriate simulation setups were employed,

the discrepancy in concentration profiles between CFD model and experiment was still present as shown previously. So, in order to show that the present CFD model is a reliable model for predicting overall mixing time, the discretization errors of pump-around jet mixing tank simulations for different jet discharge velocities, including 4.4, 6.6, 8.8, and 11 $m{\cdot}s^{-1}$, were assessed with the help of GCI. From the recommended GCI procedure, the GCI analyses of these pump-around jet mixing tank simulations are shown in Table 7.

From Table 7, for jet discharge velocities of 4.4 and 11 $m{\cdot}s^{-1}$, the monotonic convergences ($0 < R < 1$) of the grid refinement from medium to finest grid levels are observed. The oscillatory convergences ($R < 0$) are found in the grid refinement from medium to finest grids for other jet discharge velocities. The overall mixing times predicted by finest grid levels are close to their extrapolated values; this confirms that the solutions are converged with the refinement from medium to finest grid resolutions. The results also show that the predicted overall mixing times are found to decrease with increasing the jet discharge velocities. Based on the predicted overall mixing times of the finest grid levels, the minimum and maximum percentage errors between CFD models and experimental data for these jet discharge velocities are 5.64% and 12.35%, respectively.

From Celik et al. (2008), it is recommended that the numerical uncertainty can be identified by using GCI_{21}. Based on this suggestion, the discretization errors for pump-around jet mixing tank simulations with jet discharge velocities of 4.4, 6.6, 8.8, and 11 $m{\cdot}s^{-1}$ are 0.2834%, 0.0134%, 0.0032%, and 0.0213%, respectively. These discretization errors correspond to the uncertainties in predicted overall mixing times of ±0.0799 s, ±0.0027 s, ±0.0005 s, and ±0.0025 s. The maximum uncertainty in predicted overall mixing time is three orders of magnitude smaller than the predicted results. The small values of discretization errors or uncertainties in predicted overall mixing times may be due to the appropriate grid arrangement and numerical methods. So, the difference in overall mixing times between simulation and experiment may be due to the model assumptions, for example turbulence model, flat top liquid surface, etc.

According to these results, it can be seen that the present CFD models successfully predict the overall mixing times of pump-around jet mixing tanks with circular nozzle for jet discharge velocities of 4.4, 6.6, 8.8, and 11 $m{\cdot}s^{-1}$ (jet Reynolds numbers ($Re_j = \rho d_j U_j/\mu$) of about 35,000–87,500) with the maximum percentage error between CFD simulation and experiment of about 12.5% and the maximum uncertainty in predicted overall mixing time of about ±0.08 s. Therefore, it can be stated that the present CFD models for pump-around

Table 7. Grid convergence index analyses for different jet discharge velocities.

Velocity ($m{\cdot}s^{-1}$)	i	N_i	f_i	% Error	$GCI_{i+1,i}$ (%)	R^a
4.4	EXP[b]	-	31.0000	-	-	-
	0	-	28.1264	-	-	-
	1	1,739,978	28.1903	9.06		
					0.2834	
	2	1,486,046	28.3658	8.50		0.1299
					1.0550	
	3	1,184,437	29.7257	4.11		−42.0382
					0.1362	
	4	1,087,312	29.6918	4.22		
6.6	EXP[b]	-	21.0000	-	-	-
	0	-	19.8132	-	-	-
	1	1,744,115	19.8153	5.64		
					0.0134	
	2	1,521,347	19.8208	5.62		−0.1168
					0.0332	
	3	1,189,897	19.7737	5.84		2.3974
					0.0936	
	4	1,087,312	19.7541	5.93		
8.8	EXP[b]	-	17.0000	-	-	-
	0	-	14.8994	-	-	-
	1	1,740,804	14.8998	12.35		
					0.0032	
	2	1,544,223	14.9011	12.35		−0.0473
					0.0096	
	3	1,191,941	14.8736	12.51		1.1631
					0.0931	
	4	1,087,312	14.8500	12.65		
11	EXP[b]	-	13.0000	-	-	-
	0	-	11.8688	-	-	-
	1	1,747,930	11.8708	8.69		
					0.0213	
	2	1,557,838	11.8729	8.67		0.1207
					0.0434	
	3	1,192,676	11.8903	8.54		−0.2723
					0.8710	
	4	1,087,312	11.8263	9.03		

[a] $R = e_{i+1,i}/e_{i+2,i+1}$: monotonic convergence for $0 < R < 1$, oscillatory convergence for $R < 0$, and divergence for $R > 1$.
[b] EXP is the experimental data of Patwardhan (2002).

jet mixing tank are reliable to predict the overall mixing times for these tested conditions. Further, the present CFD model can also be used to predict the overall mixing time for higher jet Reynolds numbers because RKE is developed for high Reynolds number turbulent flows.

However, for lower jet Reynolds numbers, the present CFD model should be modified by using low Reynolds number k-epsilon model as suggested by Phapatarinan, Bumrungthaichaichan, and Wattananusorn (2018). Moreover, for pump-around jet mixing tanks with non-circular nozzles, the grid generation idea and numerical setups of this work can be employed. But, the appropriate turbulence model and turbulence conditions for non-circular pump-around jet mixing tanks must be investigated.

5. Conclusions

In this work, the appropriate turbulence model and numerical methods for CFD model of an open 45° inclined side entry pump-around jet mixing tank were properly investigated. The suitable turbulence model for this system was RKE. Further, the proper pressure-velocity coupling scheme, spatial discretization scheme, and temporal discretization scheme of the present CFD model respectively were SIMPLE, SOU, and FOI because these setups accurately predicted the overall mixing time with reasonable computational time. Although the appropriate CFD setups were adopted to simulate the jet mixing tank, discrepancy in concentration profiles between CFD simulation and experiment was still observed because the flat top liquid surface assumption was employed as reported by Bumrungthaichaichan, Namkanisorn, and Wattananusorn (2018).

From GCI analyses, the discretization errors of jet mixing tank simulations for different jet discharge velocities, including 4.4, 6.6, 8.8, and 11 $m{\cdot}s^{-1}$, were successfully assessed. The maximum discretization error of these CFD models was about 0.3%, which corresponded to the maximum uncertainty in predicted overall mixing time of about ±0.08 s. Further, this maximum uncertainty was three orders of magnitude lower than the predicted overall mixing times. Hence, it can be concluded that the present CFD model provided high reliability for predicting the overall mixing times of pump-around jet mixing tanks over a wide range of jet Reynolds numbers ($Re_j \approx$ 35,000–87,500). However, for lower jet Reynolds numbers, the low Reynolds number k-epsilon model was recommended to predict the overall mixing time of pump-around jet mixed tank (Phapatarinan, Bumrungthaichaichan, and Wattananusorn 2018). Further, for non-circular jet mixing tank, the present CFD model should be modified. In future work, the universal CFD model that can be used to predict the overall mixing times for all jet Reynolds numbers and nozzle geometries should be investigated. Furthermore, the fractional calculus and other mathematical techniques, which are successfully employed to describe the nonlinear behaviors, physics, mechanics, and so on (Xu et al. 2015; Li et al. 2017), can be adopted to study the pump-around jet mixing tank.

Nomenclature

c	concentration
$\bar{c}$	fully mixed concentration
C_1, C_2, $C_{1\varepsilon}$, $C_{2\varepsilon}$, $C_{3\varepsilon}$	constants for k-epsilon turbulence models
C_D	constant for turbulence kinetic energy dissipation rate correlation
d_j	jet nozzle diameter
d_o	tank outlet diameter
D	tank diameter
$D_{i,m}$	mass diffusion coefficient for species i in the mixture
D_t	turbulent diffusivity
e	relative error of numerical solutions
f_i	numerical solution of key variable for i grid level
G_b	generation of k due to buoyancy
G_k	production of turbulence kinetic energy
H	height of liquid
I	turbulence intensity
k	turbulence kinetic energy
l	length scale
N_i	number of grids for i grid level
p	order of the discretization method
P	mean pressure
r	refinement factor
R_ε	additional term due to interaction between turbulence dissipation and mean shear in ε-transport equation of RNGKE
S	modulus of the mean rate-of-strain tensor
S_i	source term for species transport equations
S_k	source term for k-transport equation
$S_{M,i}$	source term for momentum equation in i direction
S_ε	source term for ε-transport equation
S_φ	source term
Sc_t	turbulent Schmidt number
t	time
$t_{95\%}$	95% mixing time
$\boldsymbol{U}$	mean velocity vector
U_j	jet discharge velocity
U_i	mean velocity in i direction
Y_i	local mass fraction of species i
Y_M	dilatation dissipation
α_k	inverse effective Prandtl number for turbulence kinetic energy
α_ε	inverse effective Prandtl number for turbulence kinetic energy dissipation rate
Γ_φ	diffusivity
ε	turbulence kinetic energy dissipation rate or difference in numerical solutions
μ	fluid viscosity
μ_t	turbulent viscosity or eddy viscosity
ν_t	turbulent kinematic viscosity
ρ	fluid density
σ_k	turbulent Prandtl numbers for k
σ_ε	turbulent Prandtl numbers for ε
ϕ	universal independent variable

Acknowledgments

The authors would like to express their gratitude to Professor emeritus Dr ès sc. techn. Horst Stoff, Department of Mechanical Engineering, Ruhr-Universität Bochum, Germany, for his valuable suggestions and discussion during the course of this research. Furthermore, the ANSYS FLUENT software was supplied by College of Advanced Manufacturing Innovation, King Mongkut's Institute of Technology Ladkrabang, Thailand.

Disclosure statement

No potential conflict of interest was reported by the authors.

ORCID

Eakarach Bumrungthaichaichan http://orcid.org/0000-0003-1969-3110

References

ANSYS Inc. 2013a. *ANSYS Fluent Theory Guide*. Pennsylvania: ANSYS.

ANSYS Inc. 2013b. *ANSYS Fluent Tutorial Guide*. Pennsylvania: ANSYS.

ANSYS Inc. 2013c. *ANSYS Fluent User's Guide*. Pennsylvania: ANSYS.

Brooker, L. 1993. "Mixing with the Jet Set." *Chemical Engineer* 30 (550): 16–25.

Bumrungthaichaichan, E. 2016. "A Review on Numerical Consideration for Computational Fluid Dynamics Modeling of Jet Mixing Tanks." *Korean Journal of Chemical Engineering* 33 (11): 3050–3068. doi:10.1007/s11814-016-0236-x.

Bumrungthaichaichan, E., N. Jaiklom, A. Namkanisorn, and S. Wattananusorn. 2016. "On the Computational Fluid Dynamics (CFD) Analysis of the Effect of Jet Nozzle Angle on Mixing Time for Various Liquid Heights." *Scientific Research and Essays* 11 (4): 42–56. doi:10.5897/SRE2015.6353.

Bumrungthaichaichan, E., A. Namkanisorn, and S. Wattananusorn. 2018. "CFD Modelling of Pump-Around Jet Mixing Tanks: A Discrepancy in Concentration Profiles." *Journal of the Chinese Institute of Engineers* 41 (7): 612–621. doi:10.1080/02533839.2018.1530956.

Celik, I. B. 1999. *Introductory Turbulence Modeling*. USA: West Virginia University.

Celik, I. B., U. Ghia, P. J. Roache, C. J. Freitas, H. Coleman, and P. E. Raad. 2008. "Procedure for Estimation and Reporting of Uncertainty Due to Discretization in CFD Applications." *Journal of Fluids Engineering* 130 (7): 078001-1–078001-4. doi:10.1115/1.2960953.

Dange, S. 2016. "Recirculation Boundary Conditions in ANSYS FLUENT." LearnCAx. Accessed March 1. https://www.learncax.com/knowledge-base/blog/by-category/cfd/recirculation-boundary-conditions-in-ansys-fluent.

Eça, L., and M. Hoekstra. 2009. "Evaluation of Numerical Error Estimation Based on Grid Refinement Studies with the Method of the Manufactured Solutions." *Computers & Fluids* 38 (8): 1580–1591. doi:10.1016/j.compfluid.2009.01.003.

Eça, L., and M. Hoekstra. 2014. "A Procedure for the Estimation of the Numerical Uncertainty of CFD Calculations Based on Grid Refinement Studies." *Journal of Computational Physics* 262: 104–130. doi:10.1016/j.jcp.2014.01.006.

Elsayed, K. 2011. "Analysis and Optimization of Cyclone Separators Geometry Using RANS and LES Methodologies." PhD thesis, Vrije Universiteit Brussel.

Fossett, H., and L. E. Prosser. 1949. "The Application of Free Jets to the Mixing of Fluids in Bulk." *Proceedings of the Institution of Mechanical Engineers* 160 (1): 224–232. doi:10.1243/PIME_PROC_1949_160_024_02.

Furman, L., and Z. Stegowski. 2011. "CFD Models of Jet Mixing and Their Validation by Tracer Experiments." *Chemical Engineering and Processing: Process Intensification* 50 (3): 300–304. doi:10.1016/j.cep.2011.01.007.

Jaiklom, N., E. Bumrungthaichaichan, and S. Wattananusorn. 2013. "CFD Simulation of Turbulent Jet Mixing Tank." *Ladkrabang Engineering Journal* 30 (4): 37–42.

Kim, S.-E., T. Barbat, and P. Spicka. 2005. *Meshing and CFD Accuracy*. Lebanon: Fluent.

Li, H., D. Chen, B. Xu, S. Tolo, and E. Patelli. 2017. "Dynamic Analysis of Multi-Unit Hydropower Systems in Transient Process." *Nonlinear Dynamics* 90 (1): 535–548. doi:10.1007/s11071-017-3679-7.

Marek, M., T. Stoesser, P. J. W. Roberts, V. Weitbrecht, and G. H. Jirka. 2007. "CFD Modeling of Turbulent Jet Mixing in A Water Storage Tank." In *Proceedings of the 32nd IAHR World Congress*, Venice, Italy, 1–6 July 2007: 1–10. Spain: IAHR.

Marshall, E. M., and A. Bakker. 2004. "Computational Fluid Mixing." In *Handbook of Industrial Mixing: Science and Practice*, edited by E. L. Paul, V. A. Atiemo-Obeng, and S. M. Kresta, 257–343. New Jersey: John Wiley & Sons.

Mathpati, C. S., S. S. Deshpande, and J. B. Joshi. 2009. "Computational and Experimental Fluid Dynamics of Jet Loop Reactor." *AIChE Journal* 55 (10): 2526–2544. doi:10.1002/aic.11853.

Patwardhan, A. W. 2002. "CFD Modeling of Jet Mixed Tanks." *Chemical Engineering Science* 57 (8): 1307–1318. doi:10.1016/S0009-2509(02)00049-0.

Phapatarinan, S., E. Bumrungthaichaichan, and S. Wattananusorn. 2018. "A Suitable K-Epsilon Model for CFD Simulation of Pump-Around Jet Mixing Tank with Moderate Jet Reynolds Number." *MATEC Web of Conferences* 192: 03010. doi:10.1051/matecconf/201819203010.

Pope, S. B. 1978. "An Explanation of the Turbulent Round-jet/Plane-jet Anomaly." *AIAA Journal* 16 (3): 279–281. doi:10.2514/3.7521.

Rahimi, M., and A. Parvareh. 2005. "Experimental and CFD Investigation on Mixing by A Jet in A Semi-Industrial Stirred Tank." *Chemical Engineering Journal* 115 (1–2): 85–92. doi:10.1016/j.cej.2005.09.021.

Raja, T., P. Kalaichelvi, and N. Anantharaman. 2007. "Development of CFD Model for Optimum Mixing in Jet Mixed Tanks." *Journal of Scientific & Industrial Research* 66 (7): 522–527.

Ranade, V. V. 1996. "Towards Better Mixing Protocols by Designing Spatially Periodic Flows: The Case of A Jet Mixer." *Chemical Engineering Science* 51 (11): 2637–2642. doi:10.1016/0009-2509(96)00129-7.

Roache, P. J. 1994. "Perspective: A Method for Uniform Reporting of Grid Refinement Studies." *Journal of Fluids Engineering* 116 (3): 405–413. doi:10.1115/1.2910291.

Roache, P. J. 2009. *Fundamentals of Verification and Validation*. New Mexico: Hermosa Publishers.

Sendilkumar, K. K., P. Kalaichelvi, M. Perumalsamy, A. Arunagiri, and T. Raja. 2007. "Computational Fluid Dynamic Analysis of Mixing Characteristics inside a Jet Mixer for Newtonian and Non Newtonian Fluids." In *Proceedings of the World Congress on Engineering and Computer Science 2007*, San Francisco, USA, 24–26 October 2007: 120–128. Hong Kong: IAENG.

Shih, T.-H. 1996. "Constitutive Relations and Realizability of Single-Point Turbulence Closures." In *Turbulence and Transition Modelling*, edited by M. Hallbäck, D. S. Henningson, A. V. Johanssan, and P. H. Alfredsson, 155–192. Netherlands: Springer.

Shih, T.-H., W. W. Liou, A. Shabbir, Z. Yang, and J. Zhu. 1995. "A New k-ε Eddy Viscosity Model for High Reynolds Number Turbulent Flows." *Computers & Fluids* 24 (3): 227–238. doi:10.1016/0045-7930(94)00032-T.

Spyrou, M. 2009. "The Diffusion Coefficient of Water: A Neutron Scattering Study Using Molecular Dynamics Simulations." Master thesis, University of Surrey.

Versteeg, H. K., and W. Malalasekera. 1995. *An Introduction to Computational Fluid Dynamics: The Finite Volume Method*. England: Pearson Education.

Wasewar, K. L. 2006. "A Design of Jet Mixed Tank." *Chemical and Biochemical Engineering Quarterly* 20 (1): 31–46.

Wilcox, D. C. 1994. *Turbulence Modeling for CFD*. California: DCW Industries.

Xu, B., D. Chen, H. Zhang, and R. Zhou. 2015. "Dynamic Analysis and Modeling of A Novel Fractional-Order Hydro-Turbine-Generator Unit." *Nonlinear Dynamics* 81 (3): 1263–1274. doi:10.1007/s11071-015-2066-5.

Zughbi, H. D., and I. Ahmad. 2005. "Mixing in Liquid-Jet-Agitated Tanks: Effects of Jet Asymmetry." *Industrial & Engineering Chemistry Research* 44 (4): 1052–1066. doi:10.1021/ie0496683.

Zughbi, H. D., and M. A. Rakib. 2002. "Investigations of Mixing in A Fluid Jet Agitated Tank." *Chemical Engineering Communications* 189 (8): 1038–1056. doi:10.1080/00986440213878.

Zughbi, H. D., and M. A. Rakib. 2004. "Mixing in A Fluid Jet Agitated Tank: Effects of Jet Angle and Elevation and Number of Jets." *Chemical Engineering Science* 59 (4): 829–842. doi:10.1016/j.ces.2003.09.044.

Author biography

Name	Eakarach Bumrungthaichaichan
Date of birth	30 July 1987
Address	99/327 Sisa Chorakhe Noi, Bang Sao Thong, Samut Prakan 10540
Education	2010, Bachelor degree of Engineering in Chemical Engineering, Faculty of Engineering, King Mongkut's Institute of Technology Ladkrabang, Thailand 2013, Master degree of Engineering in Chemical Engineering, Faculty of Engineering, Chulalongkorn University, Thailand
Proficiencies	Computational Fluid Dynamics Transport phenomena Fluid Mechanics
Work experience	2014-Present Researcher at Department of Chemical Engineering, Faculty of Engineering, King Mongkut's Institute of Technology Ladkrabang, Thailand
Publications	1. Eakarach Bumrungthaichaichan and Santi Wattananusorn (2019) CFD modelling of pump-around jet mixing tanks: a reliable model for overall mixing time prediction. *Journal of the Chinese Institute of Engineers*, 42(5), 428-437. 2. Eakarach Bumrungthaichaichan, Apinan Namkanisorn and Santi Wattananusorn (2018) CFD modelling of pump-around jet mixing tanks: a discrepancy in concentration profiles. *Journal of the Chinese Institute of Engineers*, 41(7), 612-621. 3. Thanwa Jorakit, Natthanon Phaiboonsilpa, Apinan Namkanisorn, Phisan Ponpo, Eakarach Bumrungthaichaichan and Santi Wattananusorn (2018). Influence of jet discharge velocity profile on CFD simulation of pump-around jet mixing tank. *MATEC Web of Conferences*, 192, 03019.

4. Satapan Phapatarinan, Eakarach Bumrungthaichaichan and Santi Wattananusorn (2018) A suitable k-epsilon model for CFD simulation of pump-around jet mixing tank with moderate jet reynolds number. *MATEC Web of Conferences*, 192, 03010.

5. Natthawut Ruangtrakoon and Eakarach Bumrungthaichaichan (2018) Influence of grid distribution on CFD model of compressible flow inside the primary nozzle and mixing chamber used in refrigeration application. *MATEC Web of Conferences*, 192, 02045.

6. Eakarach Bumrungthaichaichan (2016) A review on numerical consideration for computational fluid dynamics modeling of jet mixing tanks. *Korean Journal of Chemical Engineering*, 33(11), 3050-3068.

7. Kasamawan Taorat, Eakarach Bumrungthaichaichan and Santi Wattananusorn (2016) Influence of Packing Limit on Gas-Solid Fluidized Bed Flow Pattern by Computational Fluid Dynamics. *Ladkrabang Engineering Journal*, 33(1), 30-35.

8. Eakarach Bumrungthaichaichan, Nattawat Jaiklom, Apinan Namkanisorn and Santi Wattananusorn (2016) On the computational fluid dynamics (CFD) analysis of the effect of jet nozzle angle on mixing time for various liquid heights. *Scientific Research and Essays*, 11(4), 42-56.

9. Awanee Wongnui, Charkorn Akavipat, Eakarach Bumrungthaichaichan and Santi Wattananusorn (2015) CFD Simulation of Disc Radius and Blade Height Effects on Mixing Performance in the Unbaffled Tank Covered by a Lid. *Ladkrabang Engineering Journal*, 32(4), 49-54.

10. Siripan Murathathunyaluk, Nitika Srisakwattana, Treenuch Saksawad and Eakarach Bumrungthaichaichan (2015) Development of Rotating Tray Dryer and Study of the Hot Air Flow Pattern with Computational Fluid Dynamics. *Chemical Engineering Transactions*, 43, 1669-1674.

11. Pimpun Tongpun, Eakarach Bumrungthaichaichan and Santi Wattananusorn (2014) Investigation of entrance length in circular and noncircular conduits by computational fluid dynamics simulation. *Songklanakarin Journal of Science and Technology*, 36(4), 471-475.

12. Tupthai Seethao, Eakarach Bumrungthaichaichan and Santi Wattananusorn (2014) Simulation of Secondary Flows in Newtonian and Viscoelastic Fluids through Various Shaped Conduits. *Ladkrabang Engineering Journal*, 31(1), 55-60.

13. Duangkamol Onprom, Eakarach Bumrungthaichaichan and Santi Wattananusorn (2014) Investigation of the Effects of Fin Heights and Swept Fins on the Performance of Plate-fin Heat Sink. *Ladkrabang Engineering Journal*, 31(1), 49-54.

14. Passaporn Mahaphonsirigul, Eakarach Bumrungthaichaichan, Santi Wattananusorn, Tawatchai Charinpanitkul and Pimporn Ponpesh (2014) 2D CFD Simulation of ZnO Nanoparticle Synthesis using Modified French Method in Tubular Reactor. The 5th Research Symposium on Petrochemical and Materials Technology and The 20th PPC Symposium on Petroleum, Petrochemicals, and Polymers, Bangkok, Thailand, April 22, 2014, pp. 494-500.

15. Kritsana Saiyood, Eakarach Bumrungthaichaichan, Santi Wattananusorn and Walairat Chandra-ambhorn (2013) CFD Modeling of Microfiltration Membrane with Seven Star-shape Channels. *Ladkrabang Engineering Journal*, 30(4), 43-48.

16. Nattawat Jaiklom, Eakarach Bumrungthaichaichan and Santi Wattananusorn (2013) CFD Simulation of Turbulent Jet Mixing Tank. *Ladkrabang Engineering Journal*, 30(4), 37-42.

17. Eakarach Bumrungthaichaichan, Charkorn Akavipat, Urkarn Kajonrungsilp and Santi Wattananusorn (2013) Influence of Injection Position on Water Jet Propulsion under the Royal Development Project Initiated by His Majesty the King. *Ladkrabang Engineering Journal*, 30(3), 31-36.

18. Nantikan Lamaipan, Seeroong Prichanont, Kijchai Kanjanapaprakul, Eakarach Bumrungthaichaichan and Pimporn Ponpesh (2013) Computational Fluid Dynamics Modeling of a Mixing Tank for the Production of Shellac-Carnauba Wax Fruit Coating Solution. The 4th Research Symposium on Petrochemical and Materials Technology and The 19th PPC Symposium on Petroleum, Petrochemicals, and Polymers, Bangkok, Thailand, April 23, 2013, pp. 23-29.

19. Eakarach Bumrungthaichaichan, Varong Pavarajarn, Pimporn Ponpesh, Santi Wattananusorn and Tawatchai Charinpanitkul (2012) CFD simulation of zinc oxide synthesis using pulse injection with thermal oxidation. The 2nd TIChE International Conference 2012 (TIChE 2012), Nakornratchasima, Thailand, October 25-26, 2012, pp. 1-8.

20. Supawadee Wanthamanee, Eakarach Bumrungthaichaichan and Santi Wattananusorn (2012) Influence of Turbulence Promoter Geometry on Flow Pattern in Cross-Flow Membrane Ultrafiltration. *Ladkrabang Engineering Journal*, 29(2), 48-53.